

**AN EXPERIMENTAL AND THEORETICAL STUDY
ON THE IMPROVEMENT OF ADSORPTION HEAT
PUMP PERFORMANCE**

A Thesis Submitted to
The Graduate School of Engineering and Sciences of
İzmir Institute of Technology
in Partial Fulfillment of the Requirements for the Degree of
DOCTOR OF PHILOSOPHY
in Chemical Engineering

by
Hasan DEMİR

December 2008
İZMİR

We approve the thesis of **Hasan DEMİR**

Prof. Dr. Semra ÜLKÜ
Supervisor

Assist. Prof. Dr. Moghtada MOBEDİ
Co-Supervisor

Prof. Dr. Barış ÖZERDEM
Committee Member

Prof. Dr. Sacide ALSOY ALTINKAYA
Committee Member

Prof. Dr. Şerife Ş. HELVACI
Committee Member

Assoc. Prof. Dr. Fehime ÖZKAN
Committee Member

19 December 2008

Prof. Dr. Devrim BALKÖSE
Head of Chemical Engineering Department

Prof. Dr. Hasan BÖKE
Dean of the Graduate School of
Engineering and Sciences

ACKNOWLEDGEMENTS

I would like to thank to my advisors, Prof. Dr. Semra ÜLKÜ and Assist. Prof. Dr. Moghtada MOBEDİ for their supervision, guidance, support and encouragement during my PhD studies. I am also grateful to Prof. Dr. Barış ÖZERDEM and Assoc.Prof.Dr. Fehime ÖZKAN for their valuable recommendations during progression of the study. I would also like to thank to State Planning Organization of Turkey for their great financial supports to this project.

I would like to express my sincere gratitude to Research Specialist Burcu ALP for her kind help during the microcalorimetry study, Ersin YAZGAN and his co-workers for the construction of AHPs and Dr. Tuncay GÜNHAN for his valuable guidance on data acquisition system. I would like to appreciate deeply to the Research Assistants: Dildare METİN, Alev G. YERKESİKLİ, Yasemin ERTEN and Dilek D. KAVAK Research Specialist Didem B. ALYANAK for their friendship and encouragement during my studies. I also thank to Ulaş ATIKLER and Gözde G. ATIKLER for their valuable helps.

Finally, I am deeply indebted to my wife for her encouragement, helpfulness and patience during PhD graduate. I would also like to thank to Demir and Gençkal families.

ABSTRACT

AN EXPERIMENTAL AND THEORETICAL STUDY ON THE IMPROVEMENT OF ADSORPTION HEAT PUMP PERFORMANCE

Adsorption heat pumps, which have considerably sparked attentions in recent years, have the advantage of being environmentally friendly and operating with heat sources such as waste heat, solar and geothermal energies as well as storing the energy. The present investigation covers working principle of adsorption heat pumps, a detailed literature survey on the performed studies, information about adsorption phenomena, experimental results of two differently designed and constructed systems, numerical simulation of heat and mass transfer in an annular adsorbent bed, and microcalorimetric study for obtaining isosteric heat of adsorption for water vapor-silica gel pair. The two intermittent adsorption heat pumps can operate without any leakage. The silica gel-water was employed as the adsorbent-adsorbate pair in both of the systems. The temperature and pressure in the evaporator, condenser and adsorbent bed were measured and the coefficients of performance, total entropy generation, the second law efficiency, specific heating and cooling power values were calculated based on these measured values for all of the representative cycles. The heat transfer area of the second designed adsorption heat pump is 550% greater than the first designed adsorption heat pump and this increase resulted in 170% and 200% of improvements in specific heating power (SHP) and specific cooling power (SCP) values respectively. The silica gel granules were mixed with small size metal pieces in order to accelerate heat transfer in the bed. Experiments were performed to measure the thermal diffusivity through the adsorbent bed in which adsorbent is mixed with metal pieces. It was observed that the mixing of silica gel grains with 10wt% of small size aluminum pieces increases the SHP and SCP values of the second heat pump by 250%.

ÖZET

ADSORPSİYONLU ISI POMPASININ PERFORMANSININ GELİŞTİRİLMESİ ÜZERİNE DENEYSEL VE TEORİK ÇALIŞMA

Günümüzde, enerji ihtiyacının hızla artması ve buna bağlı olarak sınırlı olan fosil yakıtların tüketilmesi, gelecekte bir enerji dar boğazı oluşacağını sinyallerini vermektedir. Bu sebeple sürdürülebilir ve yenilenebilir enerji kaynaklarının, özellikle ısıtma ve soğutma alanlarında kullanımı büyük önem taşımaktadır. Adsorpsiyonlu ısı pompası, sürdürülebilir ve yenilenebilir enerji kaynaklarının ısıtma ve soğutma amaçlı kullanımını sağlaması açısından son yıllarda dikkatleri üzerine çekmiştir.

Bu çalışmada adsorpsiyonlu ısı pompalarının çalışma prensipleri, detaylı bir literatür taraması, adsorpsiyon üzerine genel bilgiler, tasarlanan ve üretilen iki farklı sistemin deneysel sonuçları, sistemlerin modellenmesi için nümerik analiz ve su buharı-silika jel ikilisinin izosterik adsorpsiyon ısını elde etmek için mikroklorimetrik çalışma gibi konular anlatılmıştır. Her iki kesikli adsorpsiyonlu ısı pompası da herhangi bir kaçak olmaksızın, çevrimin defalarca tekrar edilebilmesini sağlamıştır. Her iki sistem için de adsorbent-adsorbat ikilisi olarak silika jel-su kullanılmıştır. Söz konusu sistem için ayrıca, performans katsayıları, toplam entropi üretimi, ikinci yasa verimliliği, özgül ısıtma ve soğutma gücü değerleri hesaplamaları yapılmıştır. İkinci adsorpsiyonlu ısı pompasında, yataktaki ısı transfer alanı birinci adsorpsiyonlu ısı pompasına (AHP) göre %550 arttırılarak, sistemin SHP ve SCP değerleri sırasıyla %170 ve %200 geliştirilmiştir. Ayrıca yatak içinde ısı iletimi, yeni bir yaklaşımla alüminyum metal parçaları silika jel ile karıştırılarak arttırılmıştır. Böylece, sistemin tam bir çevrim için gereken zaman kayda değer bir oranda azaltılmış ve sistemin SHP ve SCP değerleri %250 geliştirilmiştir. Adsorbent yatağı için ısı ve kütle iletim denklikleri ve adsorbent parçacıkları için ise kütle iletimi denklikleri nümerik olarak çözülmüştür.

TABLE OF CONTENTS

LIST OF FIGURES.....	IX
LIST OF TABLES	XIV
NOMENCLATURE.....	XV
CHAPTER 1. INTRODUCTION	1
CHAPTER 2. ADSORPTION HEAT PUMP	5
2.1 Fundamental of Adsorption Heat Pump Cycle.....	5
2.2. Performance Analysis.....	9
2.2.1 Coefficient of Performance.....	9
2.2.2 Second Law Performance	9
2.2.3 Specific Cooling and Heating Powers	11
2.3 Comparison of Heat Pumps	12
2.4. Adsorption Heat Pump; Problems and Solutions	13
2.4.1 Advanced Adsorption Heat Pump Cycles	14
2.4.1.1 Uniform Temperature Adsorber Process.....	14
2.4.1.2 Thermal Wave Process	15
2.5 Adsorbent-Adsorbate Pairs	16
2.6. Adsorbent Bed Design.....	18
2.6.1 Coated Adsorbers	19
2.6.2 Unconsolidated Adsorbers.....	19
2.6.3 Consolidated Adsorbers.....	20
CHAPTER 3. ADSORPTION.....	24
3.1- Types of Adsorption Isotherms	24
3.2- Adsorbent (Porous and Non-Porous Adsorbent).....	26
3.2.1 Silica Gel.....	26
3.3 Mass Transfer around Adsorbents	28
3.4 Mass Transfer through the Porous Adsorbents (Diffusion).....	30
3.4.1 Molecular Diffusion	31

3.4.2-Surface Diffusion	31
3.4.3-Knudsen Diffusion	31
3.4.4 Poiseuille Flow	32
3.4.5 Effective Diffusivity for Microporous Single Particle	32
3.5- Heat of Adsorption	33
3.5.1- Differential Heat of Adsorption.....	34
3.5.2- Integral Heat of Adsorption.....	34
3.5.3- Isosteric Heat of Adsorption.....	35
3.6- Calorimetric Techniques for Measuring Differential Heat of Adsorption.....	36
3.6.1- Tian-Calvet Type Microcalorimeter.....	36
3.6.2- Survey of Measurement of Heat of Adsorption	37
 CHAPTER 4. EXPERIMENTAL STUDIES	 40
4.1 Materials	40
4.2 Experimental Setups and Procedures.....	41
4.2.1 Adsorption Heat Pump-1	41
4.2.2 Experimental Procedure for AHP-1	44
4.2.3 Adsorption Heat Pump-2	45
4.2.4 Experimental Procedure for AHP-2.....	47
4.2.5 Microcalorimetry	47
4.2.5.1 Operation Principle of Microcalorimetry	48
4.2.6 Experimental Procedure for Microcalorimetry	49
4.2.7 Measurement of Thermal Diffusivity	50
4.2.7.1 Determination of Bed Thermal Diffusivity	51
 CHAPTER 5. RESULTS OF EXPERIMENTAL STUDIES ON AHP	 54
5.1 Results of Adsorption Heat Pump-1	54
5.2 Results of Adsorption Heat Pump-2	62
5.2.1 Effect of Heating Rate in Regeneration.....	70
5.2.2 Effect of Condenser Design.....	72
5.3 Heat Transfer Enhancement with Metal Additives	73
5.4 Additive Loaded AHP-2	81

CHAPTER 6. RESULTS OF MICROCALORIMETRIC STUDY.....	88
6.1 Water Vapor Isotherms.....	88
6.2 Differential Heat of Adsorption.....	88
6.3 Isosteric Heat of Adsorption.....	90
6.4 Water Vapor Diffusivity.....	94
6.5 Diffusion in Porous Silica Gel.....	98
CHAPTER 7. SIMULATION OF HEAT AND MASS TRANSPORT IN BED.....	100
7.1 Mechanism of Heat and Mass Transfer in Adsorbent Bed.....	100
7.2 Fluid Flow in Porous Bed.....	102
7.3 The Considered Annular Adsorbent Bed.....	104
7.3.1 Governing Equations.....	104
7.3.2 Initial and Boundary Conditions for Case 1.....	106
7.3.3 Initial and Boundary Conditions for Case 2.....	106
7.3.4 Details of Solution Procedure.....	108
7.4 Results and Discussions of Case 1.....	109
7.5 Results and Discussions of Case 2.....	116
7.5.1 Comparison of Experimental and Numerical Cycles.....	127
CHAPTER 8. CONCLUSIONS.....	129
REFERENCES.....	134
APPENDICES	
APPENDIX A. LITERATURE SURVEY FOR ADSORPTION HEAT PUMP	15447
APPENDIX B. REPRESENTATIVE RAW DATA OF INTERMITTENT AHP	159
APPENDIX C. OBTAINED CYCLES FOR INTERMITTENT AHP.....	159
APPENDIX D. PHYSICAL PROPERTIES OF MATERIALS.....	159
APPENDIX E. RAW DATA OF MICROCALORIMETRY STUDY.....	159
APPENDIX F. LITERATURE SURVEY FOR NUMERICAL STUDY.....	159
APPENDIX G. GOVERNING EQUATIONS.....	171

LIST OF FIGURES

<u>Figure</u>	<u>Page</u>
Figure 2.1. Heat transfer configuration of an ideal adsorption heat pump cycle	6
Figure 2.2. Thermodynamic cycle of a basic adsorption heat pump	7
Figure 2.3. Sub-systems of an adsorption heat pump and heat transfer between components and heat reservoirs	10
Figure 2.4. Working principle of an adsorption cycle with uniform temperature adsorbers	15
Figure 2.5. Working principle of an adsorption heat pump cycle with thermal wave process	16
Figure 2.6. Ideal cycle of the system on isosteric graphs for single and binary working fluid.....	19
Figure 2.7. Photograph of coated type of adsorbent bed designs	20
Figure 2.8. Photograph of unconsolidated type of adsorbent bed designs	21
Figure 2.9. Photograph of a) structure of adsorber and CaCl ₂ -expanded graphite composite b) simple design AHP and CaCl ₂ -expanded graphite composite c) cross-section and top view of CaCl ₂ -activated carbon composite d) zeolite 4A brick.....	22
Figure 3.1. Types of adsorption isotherms	25
Figure 3.2. Bidisperse ideal spherical particle.....	26
Figure 3.3. Hydroxyl group on surface of silica	27
Figure 3.4. Adsorption isotherms of water vapor for Type A and Type B silica gels....	27
Figure 3.5. Three basic types of silanol groups	27
Figure 3.6. Schematic illustration of concentration profile due to external and internal mass transfer resistance	28
Figure 3.7. Isotherm data for type A silica gel water pair	36
Figure 3.8. Schematically illustration of Tian-Calvet type calorimeter	37
Figure 3.9. Differential heat of CO adsorption at 298K	38
Figure 3.10. Heat of water vapor adsorption on a) BaY at 298K, b) BaX at 298K, c) BaY at 423K and d) BaX at 423K	38

Figure 3.11. Differential heat of adsorption of water vapor on zeolite and CaCl_2 at 313K.....	39
Figure 4.1. A photograph of used metal pieces a) Copper b) Aluminum c) Stainless steel d) Brass.....	41
Figure 4.2. Schematic view of the designed intermittent adsorption heat pump.....	42
Figure 4.3. Photographs of the intermittent adsorption heat pump a) front view, b) top view of adsorbent bed.....	43
Figure 4.4. Location of thermocouples and pressure sensors in the AHP-1.....	43
Figure 4.5. Schematic view of AHP-2.....	46
Figure 4.6. Schematic view of designed bed, top view of bed, fins configuration and thermocouple inside the bed of AHP-2.....	46
Figure 4.7. Photograph of the intermittent adsorption heat pump and top view of adsorbent bed of AHP-2	47
Figure 4.8. Configuration of microcalorimetry a) before modification b) after modification.....	48
Figure 4.9. Illustration of thermopile.....	49
Figure 4.10. Generated voltage versus time	49
Figure 4.11. Schematically illustration of test apparatus.....	51
Figure 4.12. Photograph of test apparatus and water bath during experiment	51
Figure 4.13. Change of temperature of experimental and theoretical model in dimensionless form.....	53
Figure 5.1. The variations of pressure with temperature in the adsorbent bed a) cycle 1 b) cycle 2	56
Figure 5.2. The variations of adsorbent bed and adsorber surface temperatures during cycle a) cycle 1 b) cycle 2.	57
Figure 5.3. The variations of adsorbent bed temperature and pressure during the cycle a) cycle 1 b) cycle 2.....	58
Figure 5.4. The changes of evaporator temperature and pressure during the adsorption process a) cycle 1 b) cycle 2.	59
Figure 5.5. The amount of adsorbed water during the adsorption process for two cycles.	60
Figure 5.6. Experimental and theoretical cycles of intermittent AHP for 80°C and 110°C.	63

Figure 5.7. Change of pressure and temperature of adsorbent bed with time a) 80°C and b)110°C	64
Figure 5.8. Pressure and temperature variations in the evaporator during isobaric adsorption a) 80°C and b) 110°C.	65
Figure 5.9. The variation of inlet and outlet temperatures of heat exchanger fluid in evaporator during isobaric adsorption process a) 80°C and b)110°C.	66
Figure 5.10. The variation of heat transfer from heat exchanger fluid to adsorptive during isobaric adsorption process.	67
Figure 5.11. Change of amount of evaporated adsorptive with time.....	68
Figure 5.12. Change of amount of desorbed water with time during isobaric desorption.....	68
Figure 5.13. Effect of heating rate on cycle during isobaric desorption process.....	71
Figure 5.14. Effect of cooling surface area of condenser on cycle.....	73
Figure 5.15. Variations of temperature of metal pieces according to dimensions.....	75
Figure 5.16. Variations of temperature of Si-Al mixture, silica gel and aluminum	76
Figure 5.17. Variations of temperature of Si-Cu mixture, silica gel and copper.....	77
Figure 5.18. Variations of temperature of Si-Brass mixture, silica gel and brass	77
Figure 5.19. Variations of temperature of Si-St-St mixture, silica gel and stainless steel.....	78
Figure 5.20. Comparison of temperature profile of silica gel-metal pieces mixture and pure silica gel	79
Figure 5.21. Amount of adsorbate and thermal diffusivity of silica gel – Al mixture with respect to aluminum concentration in mixture	81
Figure 5.22. Temperature and pressure profile of Al-loaded second setup (dots) and ideal cycle (dashed line)	82
Figure 5.23. Change of temperature and pressure of adsorbent bed during the cycle (a) without and (b) with metal additives.....	83
Figure 5.24. The variation of inlet and outlet temperatures of heat exchanger fluid in evaporator during isobaric adsorption process, (a) setup without metal additives and (b) metal loaded setup.....	84
Figure 5.25. The amount of evaporated adsorptive during adsorption process for both cycles.	85
Figure 5.26. Variations of transferred heat from heat exchanger fluid to adsorptive during adsorption process for with and without metal loaded setup	86

Figure 6.1. Isotherms of water vapor adsorption on silica gel.....	89
Figure 6.2. Heat flow versus time curve of water vapor – silica gel pair at 35°C	89
Figure 6.3. Heat of adsorption versus water vapor loading curve at 35, 40, and 60°C. .	90
Figure 6.4. Calculation of isosteric heat of adsorption	91
Figure 6.5. Representative graph of Langmuir model	92
Figure 6.6. Classius – Clapeyron diagram of water vapor on silica gel	93
Figure 6.7. The variations of intercept and slope of $\ln P$ versus $-1/T$ with constant amount of adsorbate (a) intercept (b) slope.....	94
Figure 6.8. Kinetics of water adsorption on silica gel	95
Figure 6.9. Variations of water vapor diffusivity on silica gel with temperatures a) short range period and b) long range period.....	96
Figure 6.9. Variations of water vapor diffusivity on silica gel with temperatures a) short range period and b) long range period	97
Figure 6.10. Experimental and theoretical amount of adsorbate fractions a) 35°C and b) 90°C	98
Figure 7.1. a) Porous packed bed having cylindrical shape b) tube bundle model	103
Figure 7.2. A schematic view of the adsorbent bed.....	104
Figure 7.3. Variations of temperature, adsorbate concentration, adsorptive density and pressure in radial direction of adsorbent bed with time, a) temperature, b) adsorbate concentration, c) adsorptive density, d) pressure.....	112
Figure 7.4. The comparisons of averages of temperature, adsorbate concentration, adsorptive density and pressure during the adsorption process for three different adsorbent beds, (a) average temperature, (b) average adsorbate concentration, (c) average adsorptive density, (d) average pressure.	115
Figure 7.5. $\ln P$ vs $-1/T$ diagram of simulated a) startup cycle b) cycle 2 and c) cycle3	117
Figure 7.6. The distribution of bed temperature in the adsorbent bed a) isobaric adsorption process, b) isosteric heating process, c) isobaric desorption process, d) isosteric cooling process.....	119
Figure 7.7. The variation of adsorbate concentration in the adsorbent bed for a) isobaric adsorption process b) isosteric heating process c) isobaric desorption process d) isosteric cooling process.....	122

Figure 7.8. Pressure variation in the adsorbent bed a) isobaric adsorption process b) isosteric heating process c) isobaric desorption process d) isosteric cooling process.....	124
Figure 7.9. The variation of the adsorbent bed average temperature for a cycle.....	125
Figure 7.10. The change of average adsorbate concentration during a cycle.....	126
Figure 7.11. The variation of average bed pressure during a cycle.....	126
Figure 7.12. The variations of average bed temperature for experimental and numerical cycles.....	127
Figure 7.13. The variations of average bed pressure for experimental and numerical cycles.....	128

LIST OF TABLES

<u>Table</u>	<u>Page</u>
Table 2.1. Coefficients of performance of heat pump systems for cooling.....	12
Table 2.2. Comparisons of adsorbent-adsorbate pairs.....	18
Table 2.3. Types of adsorbent and physical properties.....	23
Table 3.1. Experimental kinetic parameter of water vapor adsorption on Fuji RD silica gel.....	34
Table 5.1. The operation conditions for two cycles.....	55
Table 5.2. The amounts of heat transfer between cycle and heat reservoirs for two cycles.....	61
Table 5.3. Performance indicators for two cycles.....	61
Table 5.4. The operation conditions for two cycles.....	62
Table 5.5. The amounts of heat transfer between adsorption heat pump and heat reservoirs for two cycles.....	69
Table 5.6. Performance indicators for two cycles.....	70
Table 5.7. The thermal diffusivity and thermal conductivity of the metal pieces.....	75
Table 5.8. Thermal properties of mixtures of silica gel – metal (1.0-2.8mm) and improvements.....	76
Table 5.9. Effective thermal conductivity of silica gel – metal (1.0-2.8mm) mixtures..	80
Table 5.10. The operation conditions for two cycles.....	83
Table 5.11. The amounts of heat transfer between adsorption heat pump and heat reservoirs for two cycles.....	86
Table 5.12. Performance indicators for two cycles.....	87
Table 6.1. Water vapor diffusivities against temperature.....	95
Table 6.2. Biot mass number for silica gel – water pair at different temperatures.....	99
Table 6.3. Lewis number for silica gel – water pair at different temperatures.....	99
Table 7.1. Initial and boundary conditions for the problem.....	106
Table 7.2. Initial and boundary conditions for the problem.....	107
Table 7.3. The amounts of heat transfer for cycle processes.....	128

NOMENCLATURE

A	cross sectional area of the bed, m^2
Bi_m	Biot number for mass transfer
b	Langmuir constant
C	adsorptive concentration in bulk phase, kg m^{-3}
C_1	Seebeck coefficient, μVK^{-1}
C_0	initial concentration, kg m^{-3}
C_∞	equilibrium concentration, kg m^{-3}
C_p	specific heat, $\text{kJ kg}^{-1} \text{K}^{-1}$
COP	coefficient of performance
D_{ap}	apparent micropore diffusivity, m^2s^{-1}
D_e	effective pore diffusivity, m^2s^{-1}
D_{eff}	effective diffusivity, m^2s^{-1}
D_{Kn}	Knudsen diffusivity, m^2s^{-1}
D_m	molecular diffusivity, m^2s^{-1}
D_{bed}	effective diffusivity of adsorptive in adsorbent bed, m^2s^{-1}
D_0	reference diffusivity, m^2s^{-1}
E	diffusional activation energy, J mol^{-1}
G	specific Gibbs free energy, J kg^{-1}
g_j	shape factor
g	mass of substance, kg
k	Boltzmann constant, $\text{J K}^{-1}\text{molecule}^{-1}$
k_f	linearized mass transfer coefficient, m s^{-1}
K	inherent permeability of adsorbent bed, m^2
K_{app}	apparent permeability of adsorbent bed, m^2
Le	Lewis number
M	molecular weight of adsorptive, kg mol^{-1}
m	mass of dry adsorbent, kg
n	Eigen value
n_a	amount of adsorbate, mol kg_s^{-1}
P	pressure, kPa
Pr	Dimensionless Prandtl number

Q	heat transferred, W kg_s^{-1}
Q_{ab}	heat of isosteric heating process, kJ kg_s^{-1}
Q_{bc}	heat of isobaric desorption process, kJ kg_s^{-1}
Q_{cd}	heat of isosteric cooling process, kJ kg_s^{-1}
Q_{da}	heat of isobaric adsorption process, kJ kg_s^{-1}
Q_m	volumetric flow rate $\text{m}^3 \text{s}^{-1}$
r	pore radius, m
r_p	radius of adsorbent granule, m
R	radius of bed, m; ideal gas constant, $\text{J mol}^{-1} \text{K}^{-1}$
r^*	dimensionless radius variable, (r/R)
Re	Reynolds number
Sh	Dimensionless Sherwood number
Sc	Dimensionless Schmidt number
S	entropy, kJ K^{-1}
SCP	specific cooling power, W kg^{-1}
SHP	specific heating power, W kg^{-1}
t	time (s)
T	temperature, K
T_i	initial temperature, K
u	adsorptive velocity, m s^{-1}
V	volume of system, m^3
V_t	voltage, μV
W	average adsorbate concentration, $\text{kg}_w \text{kg}_s^{-1}$
W_{init}	initial adsorbate concentration, $\text{kg}_w \text{kg}_s^{-1}$
W_m	monolayer adsorption coverage, $\text{kg}_w \text{kg}_s^{-1}$
\bar{W}_t	average adsorption coverage at time t, $\text{kg}_w \text{kg}_s^{-1}$
W_∞	adsorbate concentration in equilibrium, $\text{kg}_w \text{kg}_s^{-1}$
W_0	limiting adsorbate capacity of adsorbent, $\text{kg}_w \text{kg}_s^{-1}$
X	mass fraction of adsorbed adsorbate per dry adsorbent, $\text{kg}_w \text{kg}_s^{-1}$

Greek letters

α	thermal diffusivity, $\text{m}^2 \text{s}^{-1}$
β	correlation factor for thermal conductivity
$\Delta_a h$	differential enthalpy in adsorbed phase, J mol_w^{-1}

$\Delta_a H$	integral enthalpy of adsorbed phase, $J kg_w^{-1}$
ΔH_a	heat of adsorption, $kJ kg_w^{-1}$
ΔH_v	heat of vaporization, $kJ kg_w^{-1}$
ΔH_{st}	heat of vaporization, $kJ kg_w^{-1}$
ΔS	entropy, $kJ K^{-1}$
ε	porosity
ϕ	volume fraction
φ	a dependent variable
λ_{eff}	effective thermal conductivity, $W m^{-1} K^{-1}$
λ_1	thermal conductivity of metal pieces, $W m^{-1} K^{-1}$
λ_0	thermal conductivity of silica gel, $W m^{-1} K^{-1}$
μ	adsorptive viscosity, Nsm^{-2}
η_{II}	second law efficiency
Ω	collision integral
ρ	density, $kg m^{-3}$
σ	collision diameter for Lennard-Jones potential, A^0
θ	dimensionless temperature variable, $(T-T_\infty) / (T_{init} - T_\infty)$
τ	dimensionless time variable, $(\alpha t/R^2)$
τ	tortuosity
τ_{cyc}	period of cycle

Subscripts

ads	adsorption
bed	adsorbent bed
C	Carnot
c	intermediate temperature source
cell	microcalorimetry sample cell
cond	condenser
cyc	cycle
dose	water vapor dose
eff	effective
ev	evaporation or evaporator
exp	expected
g	gas phase
h	heating

i	inner
init	initial
L	low temperature source
o	outer
ref	cooling
reg	regeneration
s	adsorbent or solid phase
sat	saturation
sys	system
w	adsorbate
Z	high temperature source
∞	equilibrium

CHAPTER 1

INTRODUCTION

Heating and cooling systems are widely used in industry as well as they have been an essential part of daily life. The share of the energy for heating and cooling purposes in total energy consumption gradually increases in time. Due to the economical benefits resulting from high coefficient of performance (COP) values, mechanical heat pump systems become convenient devices for heating and cooling purposes. However, in the past two decades, it is found out that the mechanical heat pumps and traditional refrigeration systems play an important role in the depletion of the ozone layer and global warming.

For the protection of the ozone layer, refrigeration technology should continue with the developing refrigeration systems without ecological damages. Chlorofluorocarbons and HCFC hydrochlorofluorocarbons have been prohibited for the protection of ozone layer considering new environmental regulations which have been accepted first in Montreal in 1988 and in Kyoto in 1998. As a consequence of new regulations, the conventional vapor compression systems are currently worked by using hydrofluorocarbons as refrigerant. However, the use of these new refrigerants has also been restricted due to limitation of the emission of some greenhouse gases (CO₂, CH₄, N₂O, Hydrofluorocarbons, PFC, and SF₆) by Kyoto protocol. Considering the increasing consciousness and precautions offered against global warming, strict restrictions on greenhouse gases might be expected in the following decades.

Due to the limitation of conventional energy sources, recent researches on heat pumps commonly focus on developing more environmental friendly new systems that have high primary energy efficiencies and are able to employ various kinds of energies from waste heat to the solar energy. The primary energy efficiency has gained critical importance besides the traditional definitions of the efficiency or performance of devices. Since the mechanical heat pumps work by electrical power, their primary energy efficiency is less than their COP. Ülkü et al. (1987) reported the primary energy

efficiency of traditional heat pumps as 90-100%, while the primary energy efficiency of thermal driven heat pumps was determined around 130-180%.

Moreover, the thermal driven heat pumps that have the advantage of using in heating and cooling systems and operating by natural thermal energy sources such as solar and geothermal energies or waste heat from industrial processes provide obvious benefits both for economical and environmental aspects. Mainly, there are two types of thermal driven heat pump which are absorption and adsorption heat pumps. Adsorption heat pumps (AHP), which have gained remarkable attention in recent years, have some significant advantages compared to the absorption or the mechanical heat pumps. The adsorption heat pumps are environmental friendly since they do not contain any hazardous materials for environment and no moving parts are involved. They can operate without noise and vibration.

A simple adsorption heat pump consists of an adsorbent bed, an evaporator, a condenser and an expansion valve. The adsorbent bed is a container filled with an adsorbent such as zeolite, active carbon, silica gel etc. The most common working fluids for adsorption heat pump are water, methanol and ammonia. Basically, adsorption heat pump operates by cycling adsorbate between adsorber, condenser and evaporator. In the adsorption heat pump cycle, adsorption and desorption phenomena provide the circulation of working fluid in the cycle without any mechanical power. Hence, interactions between adsorbent and adsorbate, physical or chemical properties and types of the adsorbent – adsorbate pairs are important factors for adsorption heat pumps. In general, adsorbate should have high latent heat, non-corrosive, non-toxic and good thermal and chemical stability within the working conditions (temperature and pressure ranges). On the other hand, adsorbents should have the features of high adsorption capacity, high thermal conductivity, low cost and also high thermal stability.

The adsorption heat pumps have some drawbacks such as low COP, intermittent working principle for basic construction, requirement of high technology, high heat and mass transfer resistances in the adsorbent bed and special designs to maintain high vacuum etc. The studies on the adsorption heat pumps focus on developing an adsorption heat pump system which can technically and economically be a serious alternative to the conventional systems. For optimization or development of any system, the factors that affect performance of system should certainly be investigated and described. Hence any attained development has gained remarkable attention; researches on heat pumps concentrate more and more on these issues currently. In Chapter 2,

definition of the adsorption heat pump, recent researches, difficulties which influence performance of system and their solution on adsorption heat pumps are reviewed in detail.

In the present study, theoretical and experimental investigations were performed on adsorption heat pump. Two different intermittent adsorption heat pumps were designed and constructed for performing experiments in laboratory environment. Both of the systems were operated without any leakage problem by using an appropriate construction method and vacuum tight connections. The cycle period of AHP-1 was very long. The second intermittent adsorption heat pump was designed and constructed in order to improve heat and mass transfer in the adsorbent bed and performance criteria. The heat transfer in the adsorbent bed of AHP-2 was enhanced by the fins and the heat transfer area was increased from 0.74m^2 to 4.1m^2 . The mass transfer rate was also increased in the adsorbent bed of AHP-2 by leaving some space between the fin blocks and at the middle of adsorbent bed. The configurations of designed adsorption heat pumps are explained in detail in Chapter 4. In Chapter 5, the thermodynamic analyses of two intermittent adsorption heat pumps were introduced and all relations for determination of the first and second law efficiencies and specific heating and cooling powers were stated.

Although the application of fins is a proper method for improving heat transfer rate through the adsorbent bed, it does not reduce discontinuity and thermal resistance between the granules and granules with the bed casing. In order to increase the thermal diffusivity in the adsorbent bed, an innovative approach which is mixing the metal pieces with adsorbent granules was decided to be used. For this reason, a thermal diffusivity test which was explained in section 4.2.7 in Chapter 4 was performed for pure silica gel grains, pure four different metal pieces (aluminum, copper, brass and stainless steel -AISI-304) and silica gel – metal pieces mixtures. The metal pieces were separated into two fractions; 1 – 2.8mm and 2.8 – 4.75mm. In Chapter 5, the thermal conductivities of the pure and mixed adsorbent beds were determined by comparison of the experimental results with the solution of conduction heat transfer equation and Maxwell relation. In Chapter 5, the thermodynamic analyses and performance criteria of metal loaded AHP-2 were introduced and experimental results were discussed. Transient behavior of adsorbent bed, evaporator and condenser were plotted to support discussions on the performance of the equipments designed.

Isosteric chart of the adsorbent – adsorbate pair is important for the adsorption heat pumps since the ideal coefficient of performance and operating conditions of AHP can be described by using isosteric chart of the adsorbent – adsorbate pair. The isosteric behavior of the studied adsorbent – adsorbate pair, which is silica gel – water, was investigated by performing a detailed microcalorimetric study given in section 4.2.5 of Chapter 4. The results of microcalorimetric study including; the isosteric chart of silica gel – water pair, the effective diffusivities of water through silica gel particle and the water adsorption capacity of silica gel were revealed and discussed in Chapter 6.

The numerical study on heat and mass transfer in the adsorbent bed was presented in Chapter 7. The mechanism of heat and mass transfer in an annular adsorbent bed of an AHP was studied. The governing equations, which were heat and mass transfer equations of the bed and mass balance equation for the granules, were derived and solved. The results were evaluated and discussed via graphics that have depicted the variation of temperature, pressure, adsorbate concentration and adsorptive density in the radial direction of the bed during an adsorption process. Two cases were investigated in the concept of the numerical study. In the first case, the influence of porosity on the variations of temperature, pressure, adsorbate concentration and adsorptive density profiles in a thick granular silica gel bed during adsorption process were studied. In the second case, the variations of temperature, pressure and adsorbate concentration in annular adsorbent bed were simulated for cycle processes which are isobaric adsorption, isosteric heating, isobaric desorption and isosteric cooling processes. The designed AHP cycle was also compared with numerically simulated cycle.

The aim of this study is to develop an innovative intermittent adsorption heat pump which has high performance criteria. In order to design and construct AHP, adsorption capacity, heat of adsorption and isotherms behavior of silica gel – water pair were described. The numerical simulation of AHP was performed to investigate the heat and mass transfer in the adsorbent bed and investigate the influence of porosity on heat and mass transfer in the adsorbent bed.

CHAPTER 2

ADSORPTION HEAT PUMP

Thermal energy storage can be performed in various ways based on storage of sensible and latent heats. The adsorption heat pump is a promising thermal energy storage method as storage of latent heat and sensible heat. The thermal energy can be stored in the adsorbent during desorption stage at high temperature level from any source (peak electricity, solar energy, industrial waste heat, geothermal energy, etc.) and it is possible to use during adsorption. Adsorption is associated with formation of heat where the heat of adsorption is usually 30% to 100% higher than heat of evaporation (condensation) of adsorbate (Suzuki 1990).

Close and Duncle (in 1977) utilized the adsorption-desorption cycle as energy recovery system by passing humid air through a silica gel adsorbent. A solar refrigerator, operating on the same principle of the adsorption heat pump using zeolite – water pair, was constructed and demonstrated by Tchernev in 1978 (Ülkü 1986).

2.1 Fundamental of Adsorption Heat Pump Cycle

A basic adsorption heat pump cycle consists of four main parts: an adsorber, which is a container filled with an adsorbent (such as zeolite, active carbon, silica gel etc.), a condenser, an evaporator and an expansion valve. Basically, adsorption heat pump operates by cycling adsorbate between adsorber, condenser and evaporator (Ülkü 1986, Ülkü 1987, Meunier 2002). In the adsorption heat pump cycle, adsorption phenomena have the similar role of mechanical power, so that the working fluid can be circulated in the cycle without any mechanical power. The adsorption heat pump cycle works between four temperatures levels (Figure 2.1), whereas a vapor compression cycle works between two temperatures levels and needs a mechanical power.

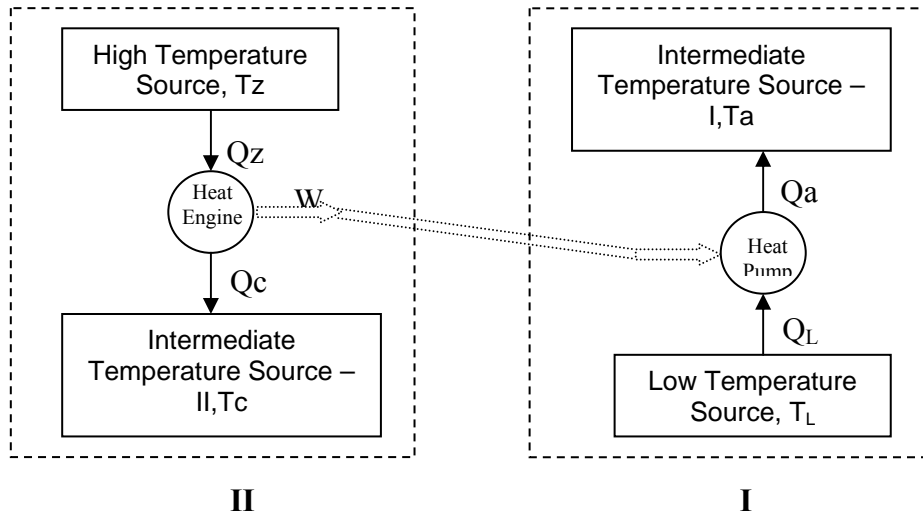


Figure 2.1. Heat transfer configuration of an ideal adsorption heat pump cycle (Source: Ülkü 1986)

The adsorption heat pump cycle can be considered as two separate cycles. The first cycle is a heat pump in which the working fluid is vaporized in evaporator by taking the heat (Q_L) from the low level temperature source and releasing the heat (Q_a) to the first intermediate temperature source. This cycle represents the adsorption process. The second cycle is a heat engine which receives heat (Q_Z) from the high temperature source and releases heat (Q_C) to the second intermediate temperature source. The transfer of heat (Q_C) to the second intermediate temperature source occurs during the condensation of working fluid in condenser. This cycle represents the desorption process. It is assumed that the work obtained in the heat engine is employed to run the heat pump. The temperatures of intermediate sources (T_c and T_a) are generally close to each other. Thus, three temperature levels can be considered for an adsorption heat pump and the ideal coefficient of performance of an adsorption heat pump cycle for cooling can be obtained as (Ülkü 1986, Meunier, et al. 1996, Alefeld, et al. 1992, Kodama, et al. 2000, Spinner, et al. 2001, Pons and Kodama 2000):

$$COP_{ref} = \frac{Q_L}{Q_Z} = \frac{1 - \frac{T_c}{T_Z}}{\frac{T_a}{T_L} - 1} \quad (2.1)$$

For heating, the coefficient of performance can be written as:

$$COP_h = \frac{Q_c}{Q_z} = 1 + \frac{1 - \frac{T_c}{T_z}}{\frac{T_a}{T_L} - 1} \quad (2.2)$$

Figure 2.2 illustrates the thermodynamic cycle of a basic adsorption heat pump on an isoster of an adsorbent-adsorbate pair. An isoster of an adsorbent-adsorbate pair indicates the change of the constant amount of adsorbate pressure with temperature. The isosters of the adsorbent-adsorbate pairs are helpful diagrams for determination of thermodynamical cycle of adsorption heat pump and calculation of COP theoretically.

An adsorption heat pump cycle consists of four processes which are isosteric heating (a-b), isobaric desorption (b-c), isosteric cooling (c-d) and isobaric adsorption (d-a) as shown in Figure 2.2.

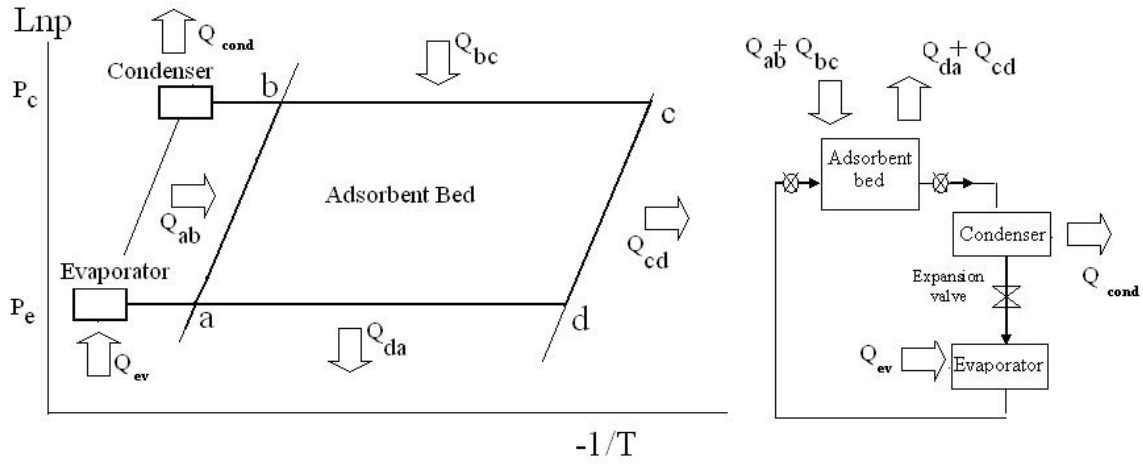


Figure 2.2. Thermodynamic cycle of a basic adsorption heat pump

Isosteric heating (a-b): The valves between the adsorbent bed and the condenser and evaporator are closed. The temperature of adsorbent bed is increased from T_a to T_b by heating the adsorbent bed while desorption is avoided. The amount of heat which should be transferred to the adsorbent bed to increase temperature of the bed from T_a to T_b can be calculated by the following relation:

$$Q_{ab} = \int_{T_a}^{T_b} [m.(C_{p,s} + W.C_{p,w}) + m_{bed}.C_{p,bed}] dT \quad (2.3)$$

Isobaric desorption (b-c): After the isosteric heating of adsorbent bed, the heating process is continued. The valve between the adsorbent bed and condenser is opened

when the adsorbent bed pressure reaches to the condenser pressure. The desorption process starts and water vapor is condensed in the condenser. The pressure of the cycle remains constant. As it is seen from Equation 2.4, a portion of the heat which is transferred to the adsorbent bed increases the temperature of adsorbate-adsorbent pair and adsorbent bed while the other portion causes the desorption process:

$$Q_{bc} = \int_{T_b}^{T_c} [m(C_{p,s} + WC_{p,w}) + m_{bed}C_{p,bed}]dT + \int_b^c m\Delta H_a dW \quad (2.4)$$

Isosteric cooling (c-d): When the valve between the condenser and adsorbent bed is closed, the temperature of adsorbent bed (T_c), which is the maximum temperature of the cycle, is decreased to T_d . During this process both the pressure and temperature of the adsorbent bed are decreased to the evaporator values:

$$Q_{cd} = \int_{T_c}^{T_d} [m(C_{p,s} + WC_{p,w}) + m_{bed}C_{p,bed}]dT \quad (2.5)$$

Isobaric adsorption (d-a): The valve between the adsorbent bed and evaporator is opened and vaporization of the adsorbate in the evaporator is started. During adsorbing of the adsorbate in the adsorbent, heat is released due to heat of adsorption. This generated heat should be removed from the adsorbent bed and the temperature of adsorbate-adsorbent pair and container should be decreased to T_a :

$$Q_{da} = \int_{T_d}^{T_a} [m(C_{p,s} + WC_{p,w}) + m_{bed}C_{p,bed}]dT + \int_d^a m\Delta H_a dW \quad (2.6)$$

The heat of evaporation which causes cooling effect and heat of condensation which can be employed for heating purposes can be determined by the following relations:

$$Q_{ev} = m\Delta W\Delta H_v + \int_{T_{cond}}^{T_{ev}} m\Delta WC_{p,w}dT \quad (2.7)$$

$$Q_{cond} = m\Delta W\Delta H_v \quad (2.8)$$

2.2. Performance Analysis

The effectiveness of an AHP can be evaluated by three criteria; a) coefficient of performance b) second law efficiency c) specific cooling and heating powers. For an AHP which operates between four temperature levels; the increments of the coefficient of performance, second law efficiencies and specific cooling/heating power can be provided by improvement of heat transfer from the lowest to the highest temperature level heat reservoirs, reduction of irreversibilities and enhancement of heat transfer powers between the heat reservoirs. The definitions and relations for determination of these effectiveness indicators are presented in the following subtitles.

2.2.1 Coefficient of Performance

The cooling and heating COP of an intermittent AHP can be determined by Equations 2.9 and 2.10 (Ülkü 1986, Pons, et al.1999, Pons and Kodama 2000).

$$COP_{ref} = \frac{Q_{ev}}{Q_{ab} + Q_{bc}} \quad (2.9)$$

$$COP_h = \frac{Q_{cond} + Q_{cd} + Q_{da}}{Q_{ab} + Q_{bc}} \quad (2.10)$$

2.2.2 Second Law Performance

For an AHP cycle, the following equations according to the first and second laws of thermodynamic can be written:

$$Q_{reg} + Q_{ev} + Q_{cond} + Q_{ads} = 0 \quad (2.11)$$

$$\frac{Q_{reg}}{T_{reg}} + \frac{Q_{ev}}{T_{ev}} + \frac{Q_{cond}}{T_{cond}} + \frac{Q_{ads}}{T_{ads}} = -\Delta S; \quad \Delta S \geq 0 \quad (2.12)$$

The heats (Q_{ev} and Q_{reg}) transferred from low and high temperature level heat reservoirs to the evaporator and adsorbent bed are positive while the heat transfer from condenser and adsorbent bed to the intermediate temperature level heat reservoirs (Q_{cond} and Q_{ads}) are negative. The temperatures of intermediate heat reservoirs (T_{cond} and T_{ads}) are different since four temperature levels are considered. Hence, the Carnot performance for cooling can be written as (Meunier 1985, Meunier, et al. 1996, Meunier, et al. 1997, Pons and Kodama 2000):

$$COP_c = \frac{\frac{1}{T_{ads}} - \frac{1}{T_{reg}}}{\frac{1}{T_{ev}} - \frac{1}{T_{cond}}} \quad (2.13)$$

The AHP system can be divided into two sub-systems as shown in Figure 2.3. The following relations are valid for each sub-system:

$$Q_{ev} + Q_{cond} + \Delta H_1 = 0 \quad (2.14)$$

$$\frac{Q_{ev}}{T_{ev}} + \frac{Q_{cond}}{T_{cond}} + \Delta S_1 = 0 \quad (2.15)$$

The symbols ΔH_1 and ΔS_1 refer to enthalpy and entropy transfer between sub-system I and its surroundings in Equations 2.14 and 2.15. The same relations can also be written for the sub-system II as presented in Equations 2.16 and 2.17.

$$Q_{ads} + Q_{reg} + \Delta H_2 = 0 \quad (2.16)$$

$$\frac{Q_{ads}}{T_{ads}} + \frac{Q_{reg}}{T_{reg}} + \Delta S_2 = 0 \quad (2.17)$$

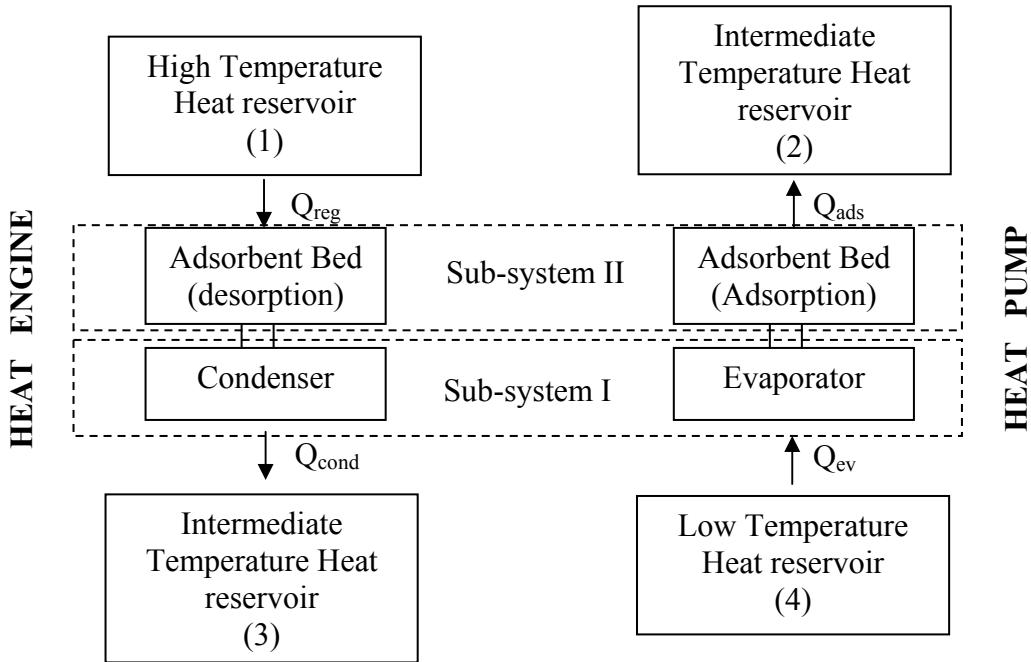


Figure 2.3. Sub-systems of an adsorption heat pump and heat transfer between components and heat reservoirs

The Equations 2.18 and 2.19 are valid for the entire system:

$$\Delta H_1 + \Delta H_2 = 0 \quad (2.18)$$

$$\Delta S_1 + \Delta S_2 = \Delta S \quad (2.19)$$

The combination of Equations 2.14 and 2.15 yields the following relation:

$$Q_{ev} \left(\frac{T_{cond}}{T_{ev}} - 1 \right) = \Delta H_1 - T_{cond} \Delta S_1 \quad (2.20)$$

Similarly, the following relation can be derived for sub-system II:

$$Q_{reg} \left(\frac{T_{ads}}{T_{reg}} - 1 \right) = -\Delta H_1 - T_{ads} \Delta S_2 \quad (2.21)$$

The expected COP can be calculated by using Equations 2.11 to 2.21 :

$$COP_{exp} = \frac{Q_{ev}}{Q_{reg}} = \frac{1 - \frac{T_{ads}}{T_{reg}}}{\frac{T_{cond}}{T_{ev}} - 1} - \frac{T_{cond} \Delta S_1 + T_{ads} \Delta S_2}{Q_{reg} \left(\frac{T_{cond}}{T_{ev}} - 1 \right)} \quad (2.22)$$

It might be useful to mention that the definitions of COP_{exp} (Equation 2.22) and COP_{ref} (Equation 2.9) are same; however COP_{exp} defines the cooling performance in terms of operation temperatures and generated entropy. The second law efficiency for cooling purpose which is the ratio of COP_{exp} to COP_C can be defined by Equation 2.23 (Meunier 1985, Pons and Kodama 2000, Kodama, et al. 2000, Gui, et al. 2002):

$$\eta_{II} = \frac{COP_{exp}}{COP_C} = 1 - \frac{\Delta_i S}{Q_{reg} \left(\frac{1}{T_{ads}} - \frac{1}{T_{reg}} \right)} \quad (2.23)$$

2.2.3 Specific Cooling and Heating Powers

Specific cooling or heating power (SCP/SHP) value is another expression that describes the effectiveness of the system. The SCP/SHP is the ratio of cooling/heating power per mass of adsorbent per cycle time. In some studies, SCP/SHP is determined according to cooling/heating power per cycle time and per mass of reactor which consists of mass of adsorbent, mass of working fluid in the adsorbent bed, mass of heat transfer fluid (HTF) and mass of container. According to the authors, the meaningful definition for SCP/SHP is the ratio of cooling/heating power to the mass of adsorbent and cycle time. The definition of SCP/SHP involves the period of cycle and contributes

the comparison of various adsorption heat pump designs (Poyelle, et al. 1999, Chahbani, et al. 2002, Pons, et al. 1999).

$$SCP = \frac{Q_{ev}}{m\tau_{cyc}} \quad (2.24)$$

$$SHP = \frac{Q_{cond} + Q_{cd} + Q_{da}}{m\tau_{cyc}} \quad (2.25)$$

2.3 Comparison of Heat Pumps

The comparison of the adsorption heat pump with the conventional heat pumps which are mechanical and absorption heat pumps contributes understanding of the present position and future of adsorption heat pumps. Table 2.1 illustrates the comparison of COP values of adsorption heat pump systems with absorption and mechanical heat pump systems.

Table 2.1. Coefficients of performance of heat pump systems for cooling

Types of Heat Pumps and Working Pairs		Coefficient of Performance (COP _{ref})
Adsorption	Carbon-Methanol	0.43
	Zeolite-Water	0.8
	Silica gel-Water	0.3-0.6
Absorption	Methanol-Water	0.7-1.1
	Lithium Bromide-Water	
Vapor compression		3-4

As it is seen, the COP value of the vapor compression heat pumps is higher than thermal driven pumps with incomparable huge difference. This is the major advantage of the mechanical driven heat pumps. However, thermal driven heat pumps have many other advantages which force industry to employ them. Thermal driven heat pumps operate with waste heat or any kind of thermal energy source. The use of waste heat as a driving energy in adsorption heat pump does not only recover the energy which is thrown away but also offer a zero operational cost system. The sustainable energy sources such as solar and geothermal energies can be employed in thermal driven heat pumps. This feature is the other advantage for this kind of heat pumps. It should be kept in mind that the vapor compression heat pumps operate with electrical power which is generally produced by the heat of fossil fuels. Thus, the primary energy efficiency of

mechanical heat pumps is around 90-100% while the primary energy efficiency of thermal driven heat pumps is about 130-180% (Ülkü, et al. 1987).

From the practical application point of view, the major advantage of the adsorption heat pumps is that they do not need maintenance for long periods since they do not contain any moving parts and in advanced systems they have a few simple moving parts. The life time of adsorption heat pump is shorter than adsorption one due to problem of salt corrosion. Moreover, the adsorbent used in adsorption system should be changed every 4 to 5 years. In the adsorption heat pump, the system does not require exchanging of the adsorbent-adsorbate pairs for a long period of time. No corrosive chemical materials are employed in the adsorption heat pump systems. As it was mentioned before, the vapor compression heat pumps use toxic and greenhouse gases. Some of refrigerants have been banned and others will be prohibited in future. These problems of mechanical heat pumps increase attractions on adsorption heat pump systems and make them comparative even to the adsorption heat pumps which are another kind of thermal driven heat pumps.

2.4. Adsorption Heat Pump; Problems and Solutions

The application of adsorption heat pumps has their own difficulties and problems. An intermitted principle of working, high technology for working under high vacuum and design of adsorbent bed are some of these difficulties. The studies on the adsorption heat pumps are focused on developing an adsorption heat pump system which can technically and economically be a serious alternative to the conventional systems.

The aim of researchers is to develop an adsorption heat pump which:

- has continuous cooling or heating process,
- has high COP values,
- can operate with lower temperature driving heat source,
- has practical design for construction and application

A detailed list of the performed adsorption heat pumps studies are shown in Table A.1 in Appendix A. The employed adsorbent-adsorbate pair, condensation and evaporation temperatures, desorption temperature of the studies are given in the table. The COP values for the studies in which the cycle is theoretically or experimentally

achieved are also presented. Some studies have been focused on bed design or solution of heat and mass transfer equations. Thus, no COP value is given for those studies. The aim or result of studies is explained in the remarks column. Thus, the reader can easily follow the performed studies from this table.

Based on a detailed literature survey, the performed studies on the adsorption heat pumps can be categorized into three areas. The studies are performed on:

- advanced adsorption cycles in order to increase COP, operate with lower temperature driving heat source and provide continuous cooling or heating process
- new adsorbent-adsorbate pairs or promoting the existence pairs in order to increase adsorption rate, enhance COP and decrease the temperature of driving heat source
- design of an adsorbent bed for appropriate heat and mass transfer

2.4.1 Advanced Adsorption Heat Pump Cycles

Literature survey has shown that many studies on adsorption heat pump have been performed in order to increase the COP values and provide a continuous cooling or heating process. In the most of papers, the developed systems have been called as advanced adsorption heat pump cycles. The continuity of cooling and heating processes is generally provided by increasing the number of adsorbers. The increase of COP is obtained by recovering and utilizing heat which is transferred during isosteric cooling (c-d) and isobaric adsorption (d-a) in another adsorption cycle. This increases the COP of cycle since the amount of external heat supplied to the cycle is reduced. The advanced cycles can be categorized into two groups which are briefly explained in this section (Meunier 2002, Dous and Meunier 1989).

2.4.1.1 Uniform Temperature Adsorber Process

These systems consist of two or more adsorbers, operating with the same refrigerant, a single evaporator and a single condenser. A general view of the uniform temperature adsorber cycle is shown in Figure 2.4. In this system, one of the adsorbers is preheated with rejection heat of another adsorber which is under the cooling process.

The transfer of heat between the adsorbers is performed by a heat transfer fluid. The process continues until both adsorbers reach to the same temperature (G and H). After this period of heat recovery, one adsorber is heated by the external heat source (GD) while the other one is cooled by the external heat sink (HA) (Chahbani, et al. 2002). Although each adsorber follows exactly the same cycle as the basic adsorption heat pump cycle, the heat which is supplied to the total system decreases. This type of advanced cycle improves the COP up to 50% (Meunier 2002, Dous and Meunier 1989, Szarzynski, et al. 1997).

Douss and Meunier (1989) have proposed and made another alternative adsorption cycle. The proposed adsorption cycle consists of two cycles, a zeolite-water cycle for high temperature stage and an active carbon-methanol cycle for low temperature stage. The heat which should be transferred to the active carbon-methanol cycle for isosteric heating and isobaric desorption processes is completely obtained from the zeolite-water cycle. The driving heat source for zeolite-water cycle is supplied from an external heat source. The experimental COP for cooling was found as 1.06.

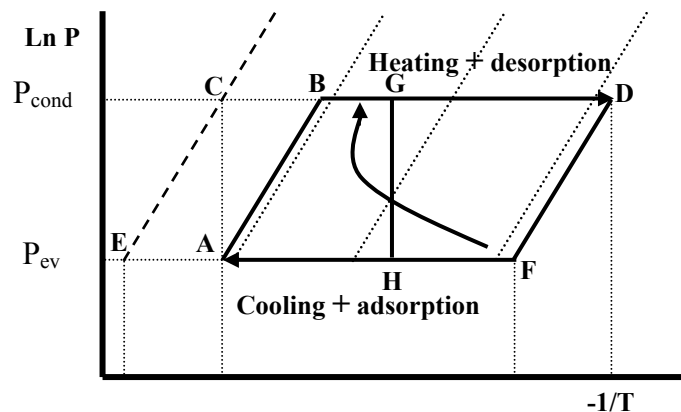


Figure 2.4. Working principle of an adsorption cycle with uniform temperature adsorbers (Source: Szarzynski, et al. 1997)

2.4.1.2 Thermal Wave Process

The system is composed of two or more adsorbers, a condenser and an evaporator. The working principle of a thermal wave process is shown in Figure 2.5. The cycle consists of two adsorbers which are called as adsorber 1 and 2. A heat transfer fluid is circulated between the two adsorbers. While adsorber 1 is under cooling, the adsorber 2 is under heating process and vice versa. For the case shown in Figure 2.5, the heat which is recovered from the adsorbent 1 is transferred to the heat

transfer fluid. The heating of fluid is continued to desorption temperature by a heating system and then it is fed to adsorber 2 for the isobaric desorption process. After leaving of heat transfer fluid from adsorber 2, it is cooled by a cooler to be fed into the adsorber 1. Hence, the heat transfer fluid completes a cycle in the system. A reversible pump is used to change flow direction of heat transfer fluid for the reverse process, when the adsorber 2 is under cooling and adsorber 1 is under heating stage (Meunier 2002, Dous and Meunier 1989, Szarzynski, et al. 1997, Pons and Szarzynski 2000, Chahbani, et al. 2004).

As it was mentioned before, many studies which have been performed to increase the COP of the adsorption heat pumps can be found in literature. Among those studies, the system of Saha et al. (1997) and Hamamoto et al. (2005) is remarkable. They worked on an advanced two stages adsorption heat pump cycle and improved the thermal wave process by employing two additional adsorbers in cycle. They found that the cooling capacity of two stages adsorption heat pump can be improved by allocating required adsorbent mass between adsorbers. The main advantage of the improved two stages adsorption heat pump is being capable to utilize low temperature solar/waste heat (40-95°C) as driven heat source (Saha, et al. 1997, Hamamoto, et al. 2005, Saha, et al. 2006b, Khan, et al. 2005).

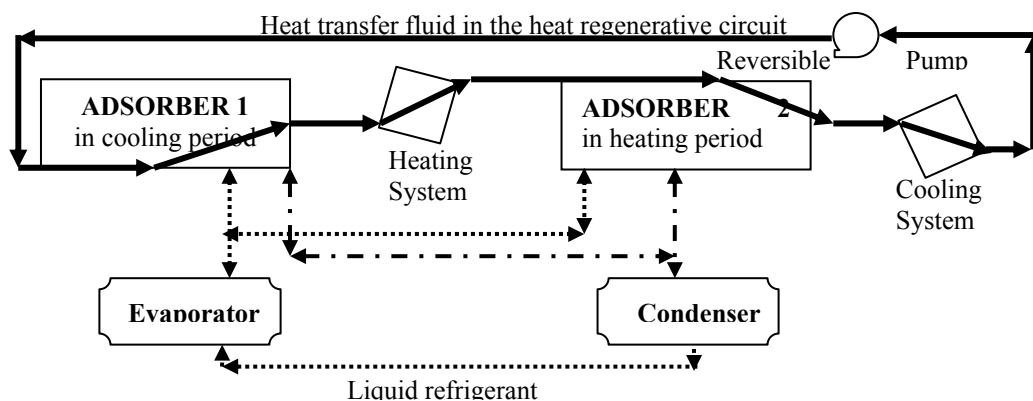


Figure 2.5. Working principle of an adsorption heat pump cycle with thermal wave process (Source: Pons and Szarzynski 2000)

2.5 Adsorbent-Adsorbate Pairs

The adsorbent-adsorbate pair, which must be compatible with the environment, is one of the important parts of adsorption heat pump system. Main requirements of the

adsorbate are high latent heat, non-corrosive, non-toxicity and good thermal and chemical stability within the working conditions (temperature and pressure ranges). On the other hand, adsorbents should have high adsorption capacity, high thermal conductivity, low cost and also thermal stability. Zeolite-water, active carbon-methanol, silica gel-water, activated alumina-water and carbon-ammonia are some of the common adsorbent-adsorbate pairs used in adsorption heat pump systems (Ülkü and Mobedi 1989, Srivastava and Eames 1998, Wang, et al. 2005, Cerkvénik, et al. 2001).

Another important criterion for the selection of appropriate adsorbent-adsorbate pair is the type of interaction between solid adsorbent and vapor adsorbate. There are two types of adsorption which are called as physical and chemical adsorptions. The physical adsorption or physisorption is caused by Van der Waals forces and chemical adsorption or chemisorption involves valence forces. In adsorption heat pumps, the adsorption and desorption processes have to be reversible to provide repetition of the cycle. Therefore, the interaction between adsorbent and adsorbate must be a physical adsorption type. Detail information about adsorption is given in Chapter 3.

Table 2.2 illustrates the comparison of adsorbent-adsorbate pairs for considering maximum adsorbate capacity, heat of adsorption values, adsorbent specific heat, energy density and operating temperature range (Ülkü and Mobedi 1989). For the selection of a convenient adsorbent adsorbate pair not only the adsorption capacity, which may seem the most important parameter, but also the other properties such as operating temperature range, reversibility of adsorption and cost must also be considered.

For many adsorbent-adsorbate pairs, the adsorption heat pump cycle operates under high vacuum. It is difficult to maintain the operation pressure in a high vacuum for a long time. This requires high vacuum technology, special materials and gaskets which increase the cost of adsorption heat pump and cause the use of heavier containers. Some studies have been performed to obtain systems that can operate at high evaporation or condensation pressure. Wang and Zhu (2002) have proposed an innovative adsorption heat pump cycle which operates with binary working fluid NH_3 and H_2O . The differences between the cyclic behaviors of the single and binary working fluid systems are shown in Figure 2.6. The operation pressure of the water-zeolite system is low and requires high vacuum in the cycle (Figure 2.6-A), however, the NH_3 -zeolite cycle operates at higher pressure which is 4 to 11 times higher than the ambient pressure (Figure 2.6-B). With an appropriate mixing of ammonia and water, a cycle which operates with a pressure close to ambient pressure can be obtained as shown in

Figure 2.6-C. Although, this improvement may solve one of the main problems of the adsorption heat pumps which is working under high vacuum, the corrosion problem can be faced by using ammonia-water working fluid in the system (Wang and Zhu 2002).

Table 2.2. Comparisons of adsorbent-adsorbate pairs
(Source: Ülkü and Mobedi 1989)

Adsorbate-Adsorbent	Max. Adsorbate capacity (kg/kg)*	Avg. Heat of Adsorption (kJ/kg _s)*	Adsorbent Sp. Heat (kJ/kg)*	Energy density (kJ/kg _s)	Temperature Range (°C)
Water-Zeolite 4A	0.22	4400	1.05	1250	30-350
Water-Zeolite 5A	0.22	4180	1.05	1200	30-350
Water-Zeolite MgA	0.29	3400	1.06	800	60-250
Water-Zeolite 13X	0.30	4400	0.92	1290	30-350
Water-Zeolite 13X	0.27		0.84	930	20-300
Water-Zeolite 10A	0.20	4000		897	50-250
Water-Zeolite 13X	0.27	3400	1.06	1200	30-350
Water-Clinoptilolite	0.12	3000	1.11	480	20-240
Water-Mordenite	0.11	4000		419	30-350
Water-Chabazite	0.17	3000	1.08	700	30-250
Water-Charcoal	0.40	2320	1.09	1200	30-250
Water-Ac. Alumina	0.19	2480	1.00	660	30-250
Water-Silica gel	0.37	2560	0.88	1000	30-150
Water-Silica gel	0.20	2500	1.045	600	20-130
Methanol-Zeolite 13X	0.20	2400	1.07		
Methanol-Zeolite 4A	0.16	2300	1.07		
Methanol-Zeolite 5A	0.17	2300	1.07		
Methanol-Zeolite 5A	0.17	2300	1.07		
Methanol-Ac. Carbon	0.32	1400	0.9	590	20-140

* Energy densities were calculated using the data given in the reference for possible max. Load

2.6. Adsorbent Bed Design

The main drawback of the adsorbent that used in adsorption heat pump is poor thermal conductivity. The poor thermal conductivity of adsorbents influences directly heat transfer and indirectly mass transfer in the bed. Thus cycle time, coefficient of performance (COP) etc of the adsorption heat pumps are also affected by thermal conductivity of adsorbent bed. For these reasons, the poor thermal conductivity of adsorbent is observed as another main problem for the application or commercialization of adsorption heat pump (AHP). In order to achieve high COP and short period of cycle of AHP, heat and mass transfer in the adsorbent bed should be enhanced. In the literature survey shows that, the researchers enhanced the heat and mass transfer in the adsorbent bed with three different ways (Ülkü and Mobedi 1989, Critoph and Zhong 2004, Wang, et al. 2004).

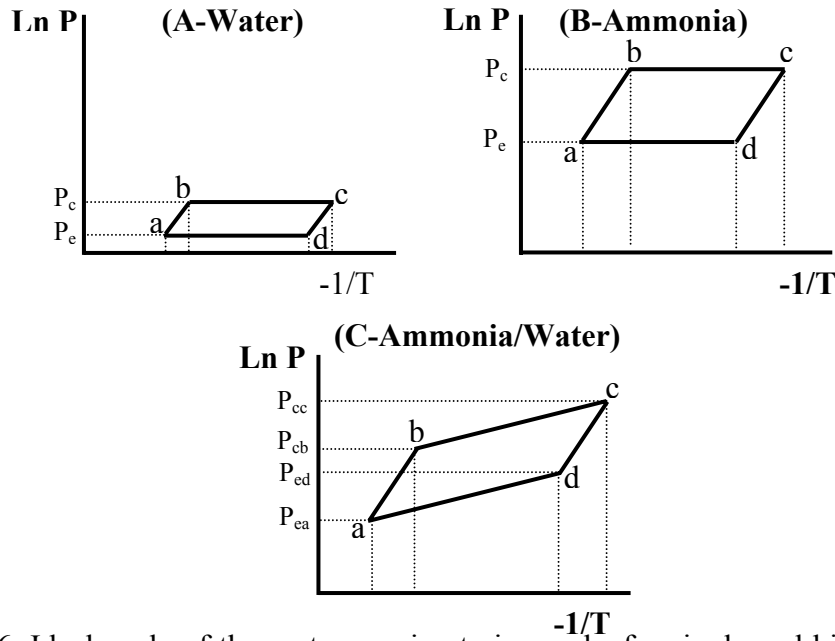


Figure 2.6. Ideal cycle of the system on isosteric graphs for single and binary working fluid (Source: Wang and Zhu 2002)

2.6.1 Coated Adsorbers

In this type of adsorber, adsorbent is coated around a pipe, fin or in metal foam. This type of adsorbent bed results high speed heat and mass transfer. Diffusion in the adsorbent is accepted as the main mechanisms of mass transfer since there is no void in the coated adsorbents. Figure 2.7a shows a coated stainless steel tube with adsorbent for improving heat and mass transfer rate in bed. This method allows obtaining high specific power adsorption heat pump (Restuccia, et al. 2002). Restuccia et al. (2005) designed an adsorbent bed which is made of finned tubes covered with SWS-1L (CaCl_2 in mesoporous silica gel) adsorbent as shown in Figure 2.7b. The optimal cycle time of system is 20-40 minutes and a cooling COP varies between 0.17 and 0.48. Bonaccorsi et al. (2006) prepared open-cell copper foam as metal support for adsorbent bed as shown in Figure 2.7c. The zeolite adsorbent is grown by hydrothermal synthesis on this metal support as shown in Figure 2.7d.

2.6.2 Unconsolidated Adsorbers

In this type of adsorbent bed, pellet, granule or fiber adsorbent is generally employed. Adsorbent is not treated and used as it is received from manufacturer.

However, the heat transfer in the adsorbent bed is enhanced by fin, metal additives, metallic foams and adsorbent-additive (having high thermal conductivity) composites. Some examples of unconsolidated type adsorbers are shown in Figure 2.8. Figure 2.8a depicts slim thin wall shell tube adsorber designed for improving heat transfer rate by Gui et al. (2002). The activated carbon used as adsorbent which is placed among the tubes that are used for heating and cooling. The rib pieces on tubes increase heat transfer rate from the tubes to the activated carbon, since the surface of heat transfer is increased. Critoph et al. (2000) developed prototype of a fast cycle adsorption refrigerator that is composed of laminate of monolithic carbon discs and aluminum fins as shown in figure 2.8b. The monolithic carbon is mixed with organic binder, compressed and fired. Saha et al. (2006a) employed activated carbon fiber as adsorbent. Activated carbon fibers have higher total pore volume, surface area and adsorption capacity than silica gel particles. Moreover, adsorption/desorption isotherm shows that activated carbon fibers do not have adsorption/desorption hysteresis. Activated carbon fibers are packed tightly inside oxygen-free copper fins as shown in Figure 2.8c.

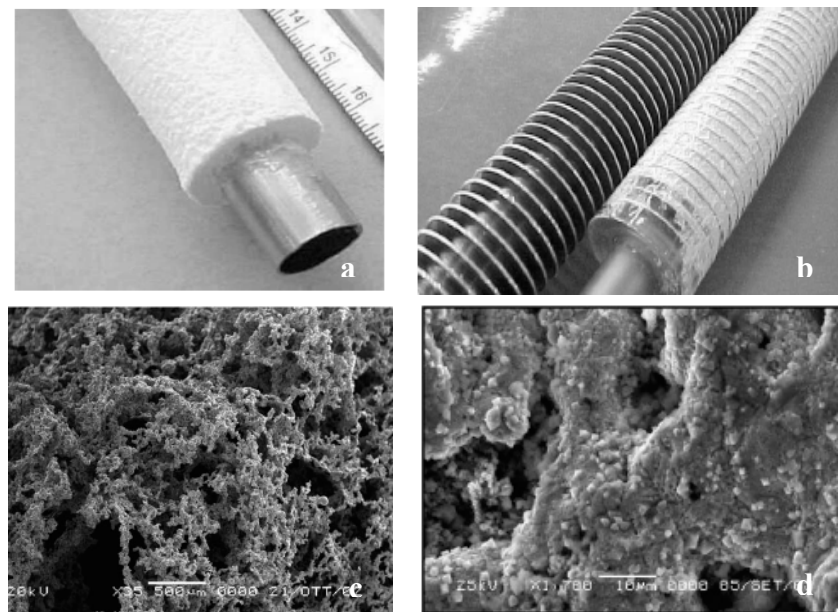


Figure 2.7. Photograph of coated type of adsorbent bed designs
(Source: Restuccia, et al. 2002, Restuccia, et al. 2005, Bonaccorsi, et al. 2006)

2.6.3 Consolidated Adsorbers

When granular adsorbent and additive which has high thermal conductivity properties mixed without any binder, there is still have low thermal conductivity due to

contact resistance. To eliminate contact resistance between granular adsorbent and additives, binder is used during preparation of composites. Wang et al. (2006a) prepared expanded graphite-CaCl₂ composite with using binder. The effective thermal conductivity of composite (Figure 2.9a) is enhanced from 0.3-0.4 W m⁻¹ K⁻¹ to 7.05-9.2 W m⁻¹ K⁻¹. Oliveira and Wang (2007) prepared composite from expanded graphite powder impregnated with CaCl₂ under 10 MPa to enhanced heat transfer properties as shown in Figure 2.9b. They used prepared composite with simple design adsorption heat pump and investigated SCP values as 415 W kg⁻¹ and 255 W kg⁻¹ at the average evaporation temperature -2.7°C and 18.3°C. The COP values changed between 0.36 and 0.46.

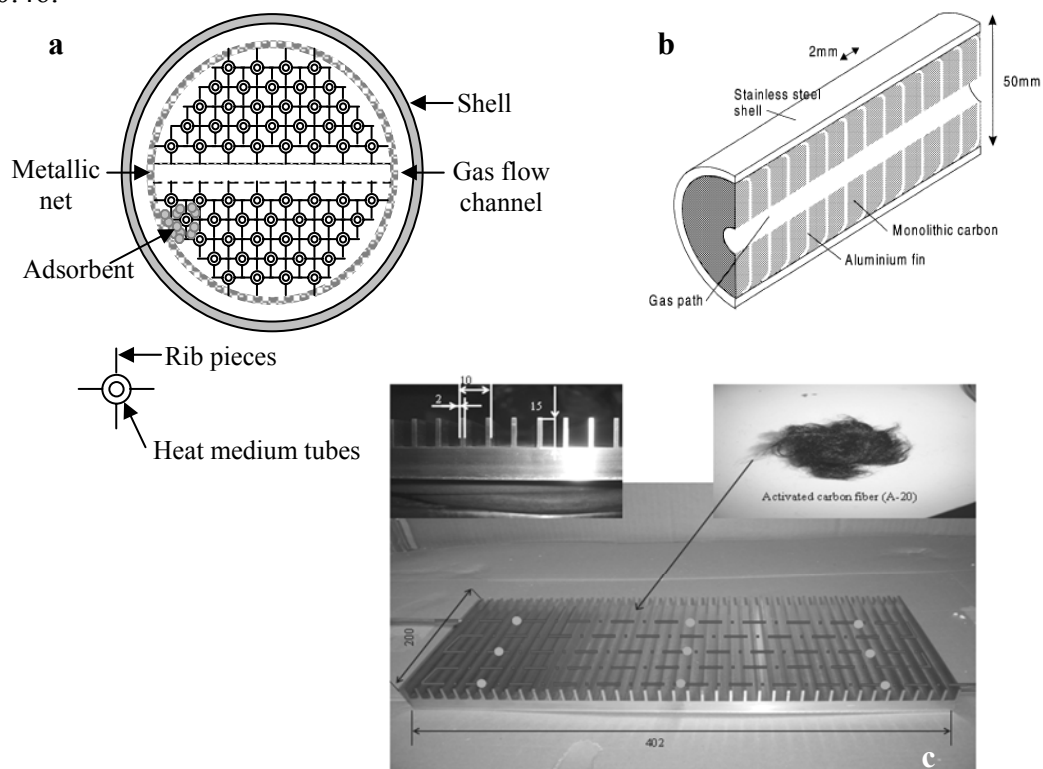


Figure 2.8. Photograph of unconsolidated type of adsorbent bed designs
(Source: Gui, et al. 2002, Critoph, et al. 2000, Saha, et al. 2006a)

Wang et al. (2006b) influenced thermal conductivity of activated carbon with CaCl₂ and cement is incorporated in mixture as binder as shown in Figure 2.9c. The thermal conductivity of granular activated carbon is 0.11 W m⁻¹ K⁻¹ and increased to 0.30 W m⁻¹ K⁻¹ by consolidation. Cacciola et al. (1992) prepared special shape zeolite 4A brick for increasing contact surface between adsorbent and adsorbent metal bed surface as shown in Figure 2.9d. They reported that bricks allow faster kinetic than pellets since good compromise between heat and mass transfer is achieved.

Table 2.3 illustrates the thermal and physical properties of unconsolidated and consolidated types of adsorbent in the literature. As is seen in the Table 2.3, concentration of binder in the consolidation of CaCl_2 – graphite is also important for improving thermal conductivity of adsorbent (Goetz and Marty 1992). Generally, consolidation of adsorbent improves the thermal conductivity properties of adsorbent. However, consolidation of adsorbent increases mass transfer resistance in the adsorbent particle.

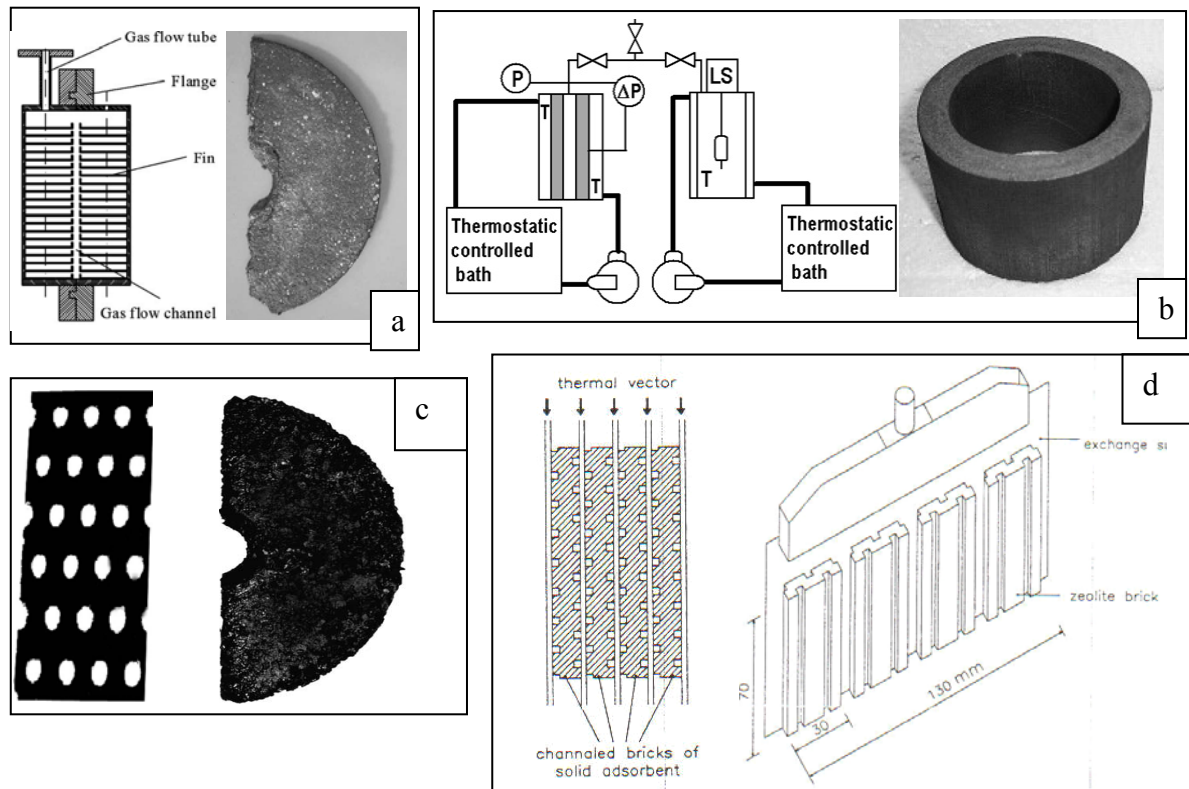


Figure 2.9. Photograph of a) structure of adsorber and CaCl_2 -expanded graphite composite b) simple design AHP and CaCl_2 -expanded graphite composite c) cross-section and top view of CaCl_2 -activated carbon composite d) zeolite 4A brick (Source: Wang, et al. 2006a, Oliveira and Wang 2007, Wang, et al. 2006b, Cacciola, et al. 1992)

Table 2.3. Types of adsorbent and physical properties

Ref.	Materials	Type	Atmosphere	λ_{eff} ($\text{W m}^{-1} \text{K}^{-1}$)	ρ (kg m^{-3})	C_p ($\text{kJ kg}^{-1} \text{K}^{-1}$)
Goetz and Marty 1992	Ca(NH ₃) ₂ Cl ₂ -graphite, 25% binder	Consolidated	NH ₃	0.3-0.4		
	Ca(NH ₃) ₆ Cl ₂ -graphite, 35% binder	Consolidated	NH ₃	0.4-0.7		
	Ca(NH ₃) ₂ Cl ₂ -graphite, 25% binder	Consolidated	NH ₃	0.35-0.4		
	Ca(NH ₃) ₆ Cl ₂ -graphite, 35% binder	Consolidated	NH ₃	0.65-0.8		
Guilleminot et al. 1993	AC 35 grain	unconsolidated		0.54		
	AC 35-CH ₃ OH	unconsolidated	CH ₃ OH	0.17-0.19		
	NaX, grain	unconsolidated		0.18		
	NaX – H ₂ O	unconsolidated	H ₂ O	0.09-0.12		
	4A	unconsolidated	Air	0.36		
	4A-Ni foam	Consolidated	Air	1.7		
	4A-Cu foam	Consolidated	Air/He	8.3/9.3		
	CaNi ₅ , LaNi ₅ , LaNi _{4.63} Al _{0.37} -20wt% Al	Consolidated	Air	5.1-6.7		
Wang et al. 2006a	80% CaCl ₂ – 20% Expanded Graphite	Consolidated	C ₂ H ₅ OH	6.5-10.5		
Wang et al. 2006b	80% CaCl ₂ – 20% Activated Carbon	Consolidated		0.3	600	0.93
Wang et al. 1999	Zeolite 13X		Air	0.056		
	Zeolite 13X - Polyanaline	consolidated	Air	0.235		
Eltom and Sayigh 1994	Activated Carbon	unconsolidated	Air	0.085		
	Activated Carbon- graphite powder	unconsolidated	Air	0.11		
	Activated Carbon- Cu powder	unconsolidated	Air	0.12		
Tanashev and Aristov 2000	Silica gel - CaCl ₂	consolidated	H ₂ O	0.44	1420	

CHAPTER 3

ADSORPTION

Adsorption is a process that occurs when a fluid (gas or liquid substance which is called as adsorptive) interacts with the surface of a solid (adsorbent). Two types of interactions occur between adsorbent surface and fluids which are physical adsorption (physisorption) and chemical adsorption (chemisorption). Physical Adsorption involves physical bonding (H-bonds, Van der Waals, dipole-dipole interactions etc...). Chemical adsorption takes place with chemical bonding (covalent bonds).

Chemical and physical adsorption can be distinguished by following properties.

- Physisorption generally occurs multilayer adsorption, chemisorption only takes place as monolayer adsorption
- Physisorption is a non-specific which means interactions (dispersion attractive and/or short range repulsion) between adsorbate and adsorbent does not specified. Contrarily, chemisorption is specific due to polar nature of the adsorbent or adsorptive.
- Physisorption occurs with polarization of adsorbate. In chemisorption, there is bond formation between adsorbate and surface of adsorbent.
- Physisorption is generally reversible process but chemisorption is irreversible process.
- Physisorption is always exothermic and evolved energy is not much larger than the energy of condensation of adsorptive. The energy of chemisorption is the same as the energy change in chemical reaction.
- At low temperature, in chemisorption the system can not be reach thermodynamic equilibrium but in physisorption the system attain equilibrium rapidly (Rouquerol et al. 1999, Ruthven 1984).

3.1- Types of Adsorption Isotherms

The amount of adsorbate depend on the equilibrium pressure (or concentration) and temperature. The adsorption isotherm is the variation of the amount of adsorbate

according to equilibrium pressure (or concentration) at constant temperature. The adsorption isotherms have a wide variety shapes according to properties of gas-solid systems. The international union of pure and applied chemistry (IUPAC) classified the adsorption isotherms as shown in Figure 3.1. The first five types of adsorption isotherms are defined by S. Brunauer, L.S. Deming, W.S. Deming and E. Teller at 1940. Type VI adsorption isotherm is proposed by Sing in 1982 (Yang 2003, Suzuki 1990).

Type I adsorption isotherms indicates that microporous structure of adsorbent and adsorbent-adsorbate interaction in micropores rather than adsorbate-adsorbate interaction. The limiting adsorption factor is micropore volume of adsorbent. Types II and IV defines that adsorption takes place on macropores of adsorbent or non-porous adsorbent. The adsorbate-adsorbate interaction is observed which is caused formation of multimolecular layer. The difference can be observed during desorption period due to hysteresis loop occurring capillary condensation of adsorbate in the mesopores. Types III and V adsorption isotherms indicates weak affinity between adsorbent and adsorbate. Types III and V isotherms do no exhibit knee shape on the curve like other isotherms (Types I, II, IV and VI) that indicative of weak adsorbent- adsorbate interactions. Type VI isotherm, indicative of nonporous adsorbent, occurs with layer by layer adsorption on a highly uniform surface. The sharpness of the steps depends on the system and the temperature (Rouquerol, et al. 1999, Webb and Orr 1997).

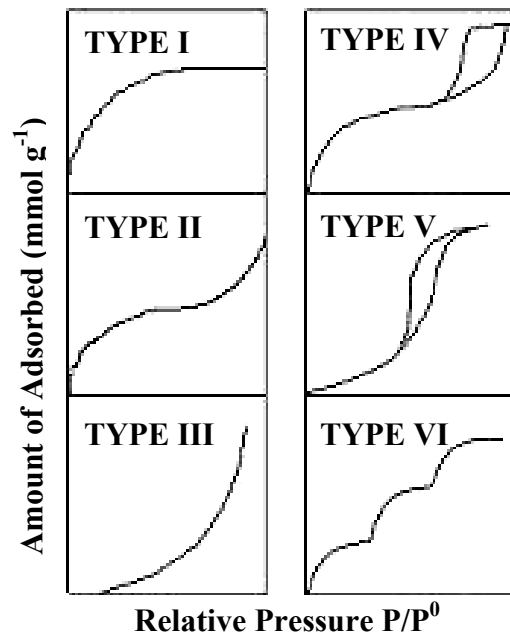


Figure 3.1. Types of adsorption isotherms
(Source: Gregg and Sing 1982)

3.2- Adsorbent (Porous and Non-Porous Adsorbent)

Adsorbent is a solid material which is capable to catch adsorptive. Adsorbents can be divided into two parts according to their structure porous and non-porous adsorbents. Structure of porous adsorbents is similar to sponge as shown in Figure 3.2. Porous structure increases surface area of adsorbents which related with adsorption. Adsorption capacity, adsorption rate, regeneration method, and life are the other major properties for adsorbents. The adsorption capacity of adsorbents can depend on surface area of adsorbent, size of adsorptive, polarity features of adsorbent and adsorptive, shape and size of pores etc. (Ülkü 1991). The pore geometry varies with different forms. In 1985, Sing classified pores with their effective width (Yang 2003, Suzuki 1990).

- Macropores (>50nm)
- Mesopores (2 – 50nm)
- Micropores (<2nm)

Activated carbon, silica gel, activated alumina and zeolites are examples of commercial adsorbents.

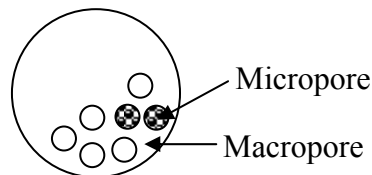


Figure 3.2. Bidisperse ideal spherical particle

3.2.1 Silica Gel

Silica gel is the abundant desiccant due to its large water adsorption capacity (~40% by weight) and low regeneration temperature (~150°C) compared with synthetic zeolites (~350°C). Pure silica (SiO_2) is amorphous and a non-polar material when it has hydroxyl functional groups (silanol group), the surface becomes very polar and hydrophilic as shown in Figure 3.3 (Yang 2003, Suzuki 1990).

In common types of silica gels, there are two different pore size distributions. According to its pore size distribution, silica gel exhibits two different type water vapor adsorption isotherms which are Type A and Type B as shown in Figure 3.4. The pore size distribution of Type A silica gels is 2.0-3.0 nm while that for Type B has larger

pore size about 7.0 nm. The internal surface areas are about $650 \text{ m}^2 \text{ g}^{-1}$ for Type A and $450 \text{ m}^2 \text{ g}^{-1}$ for Type B (Suzuki 1990).

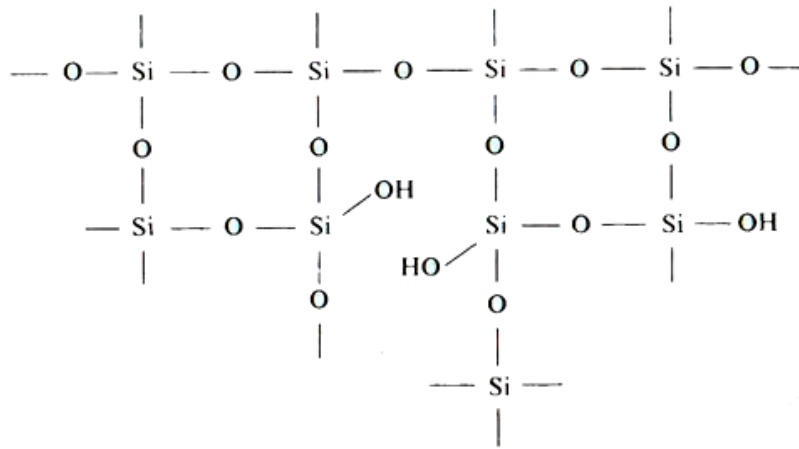


Figure 3.3. Hydroxyl group on surface of silica
(Source: Suzuki 1990)

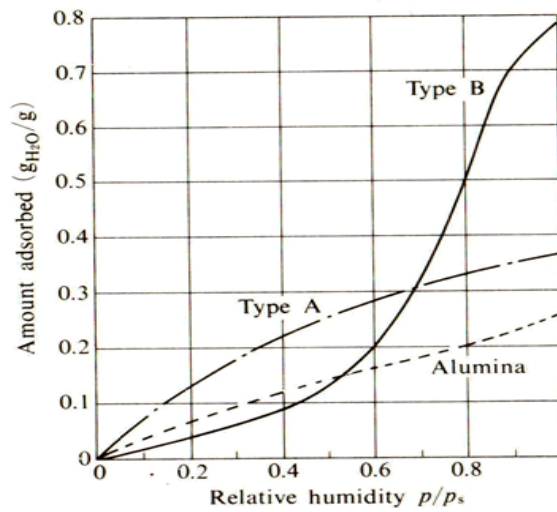


Figure 3.4. Adsorption isotherms of water vapor for Type A and Type B silica gels
(Source: Suzuki 1990)

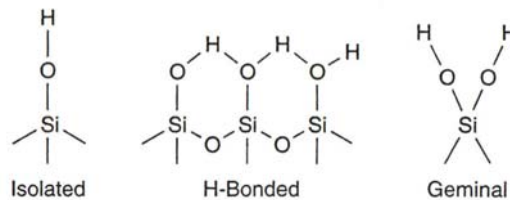


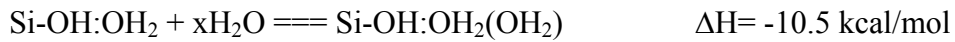
Figure 3.5. Three basic types of silanol groups

Adsorption of water or other organic compounds on silica gels is controlled by hydroxyl groups on surface of silica gels. There are three different hydroxyl groups on surface of silica gels as shown in Figure 3.5. The water vapor molecules are interacted hydroxyl (silanol) groups by hydrogen bonding. The interaction of water vapor with silanol groups and heat of adsorption is shown as follows in monolayer coverage and multilayer coverage (Yang 2003).

Monolayer adsorption



Multilayer adsorption



3.3 Mass Transfer around Adsorbents

Fluid can form a film (laminar boundary layer) that surround around the surface of an adsorbent as shown in Figure 3.6. If the fluid has more than one component, the external resistance occurs additional to the internal mass transfer resistances in the fluid phase. The mass transfer can occur only by the molecular diffusion through the laminar boundary layer. The thickness of boundary layer affects the external mass transfer resistance which depends on the hydrodynamic conditions of fluid. For the porous particles, even the external mass transfer resistance is essentially smaller than the internal mass transfer resistance; the external mass transfer resistance may have a significant effect.

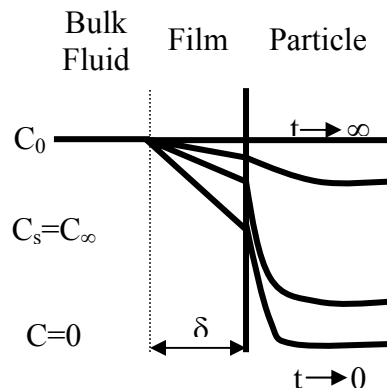


Figure 3.6. Schematic illustration of concentration profile due to external and internal mass transfer resistance

The mass transfer rate through the boundary layer can be expressed by the following equation.

$$\frac{dW}{dt} = k_f (C - C_\infty) \quad (3.1)$$

Where C is the adsorptive concentration in bulk phase and C_∞ is the adsorptive concentration at equilibrium with adsorbent phase concentration at the particle surface. The term k_f is the linearized mass transfer coefficient and depends on the hydrodynamic conditions, the physical properties of the fluid, the particle size of the adsorbent and the surface roughness of the adsorbent.

The film thickness generally can not be estimated and varies with the hydrodynamic conditions. The concentration gradient can be defined by a dimensionless number, which is the Sherwood number. Sherwood number is a function of Reynolds and Schmidt numbers. The relevant dimensionless numbers also characterize the hydrodynamics of boundary layer.

$$Sh = \frac{2k_f r_p}{D_m} = f(Re, Sc) \quad (3.2)$$

Where D_m is the molecular diffusivity of adsorptive at the boundary layer and r_p is the adsorbent particular radius.

Ranz and Marshall proposed correlation of convection heat and mass transfers for freely falling spherical particle.

$$\bar{Sh} = 2 + 0.6 Re^{1/2} Sc^{1/3} \quad (3.3)$$

$$\bar{Nu} = 2 + 0.6 Re^{1/2} Pr^{1/3} \quad (3.4)$$

In the limit of Re goes to zero, the equation 1.3 reduce to 2, which indicates the heat or mass transfer by conduction from a spherical surface to stationary, infinite medium around the surface (Incropera and De Witt 1996, Suzuki 1990).

The importance of external mass transfer resistance relative to the internal mass transfer resistance can be considered with the analysis of mass transfer Biot number. The mass transfer Biot number is a dimensionless parameter giving information about the concentration distribution inside the adsorbent. If mass transfer Biot number is smaller than 1, the concentration profile is homogeneous inside the particle that means the external mass transfer resistance is significant rather than internal mass transfer resistance. When mass transfer Biot number is equal to or higher than 1, there is concentration distribution inside the particle, which indicates that the internal mass

transfer resistance controls adsorption compared to the external mass transfer resistance. The mass transfer Biot number for spherical particle can be found by the following relation (Incropera and De Witt 1996, Ülkü 1992).

$$Bi_m = \frac{k_f r_p}{3\epsilon D_m} = \frac{Sh}{6} \frac{D_m}{D_p \tau} \quad (3.5)$$

Where $\frac{D_p}{D_m} = \frac{\epsilon}{\tau}$ the relation between effective diffusion coefficient (D_p) and diffusivity in bulk phase (D_m) equals to ratio among porosity (ϵ) and tortuosity (τ). The ratio between porosity (ϵ) and tortuosity (τ) is called as diffusibility, which depends on the structure or configuration of pore network. The tortuosity value of pore changes between 2 and 6.

The Lewis number (Equation 3.6) is a dimensionless number and defined as the ratio of mass diffusivity over thermal diffusivity. It is used to characterize the fluid flows in the presence of simultaneous heat and mass transfer by convection. The Lewis number can also be expressed in terms of the Schmidt number and the Prandtl number. The Schmidt number is a dimensionless number and described as the ratio of momentum diffusivity (viscosity) over mass diffusivity. It is used to characterize the fluid flows in the presence of simultaneous momentum and mass diffusion convection processes. The Prandtl Number which is a dimensionless number is the ratio of momentum diffusivity over thermal diffusivity.

$$Le = \frac{Sc}{Pr} = \frac{\alpha}{D} \quad (3.6)$$

3.4 Mass Transfer through the Porous Adsorbents (Diffusion)

The mass transfer of adsorbate flow through the porous adsorbent is approached as diffusion process since convective flow through the pores is negligible. Diffusion process is controlled by some mechanisms such as micropore diffusion, macropore diffusion and surface diffusion etc. Moreover, in physical adsorption, diffusion of adsorbate through the porous adsorbent may also be affected by heat generation. Additionally, polarity of adsorbent and adsorptive, molecular structure of adsorptive, pore structure of adsorbent and process conditions may control the mechanisms.

Macropore diffusion mechanisms can be described by such distinct mechanisms:

- Molecular diffusion
- Surface diffusion
- Knudsen diffusion
- Poiseuille flow

3.4.1 Molecular Diffusion

The pore diameter is larger than the mean free path and the collisions between diffusing molecules occur more frequently than collisions between molecules and pore walls. The molecular diffusivity can be shown as follows.

$$D_m = \frac{1}{3} \sqrt{\frac{8kT}{\pi M}} \frac{kT}{\sqrt{2}\pi\sigma^2 P} \quad (3.7)$$

Where the σ is collision diameter (A) and k refers to Boltzmann constant ($J K^{-1} molecule^{-1}$). The molecular diffusivity depends on pressure and temperature (Karger and Ruthven 1992).

3.4.2-Surface Diffusion

Surface diffusion occurs when there is significant adsorption on the pore wall. Physically adsorbed molecule are relatively mobile however, the mobility is substantially smaller than in the vapor phase. When adsorption equilibrium is favorable, the molecular density in the adsorbed layer may be relatively high. In the small pores, adsorbed layer blocks up entrance of the small pores. Therefore, diffusion of molecules depends on surface contributions. However, surface diffusion is insignificant at temperature which is relative to the normal boiling point of the sorbate and macropores (Karger and Ruthven 1992).

3.4.3-Knudsen Diffusion

In the micropores or at low pressure, the mean free path of gas (average distance between molecular collisions) is greater than pore diameter and collisions between a molecule and the pore walls occur more frequently than collisions between diffusing molecules. This flow is called as Knudsen diffusion or Knudsen flow. The Knudsen diffusivity can be found by employing force balance around straight cylindrical pore. Knudsen diffusivity changes only with temperature and it is independent from pressure

since the mechanism does not depend on intermolecular collisions as shown in Equation 3.8 (Karger and Ruthven 1992).

$$D_{kn} = \frac{2r kT}{M \sqrt{\frac{8kT}{\pi M}}} = r \sqrt{\frac{\pi kT}{2M}} = 97r \sqrt{\frac{T}{M}} \quad (3.8)$$

3.4.4 Poiseuille Flow

Poiseuille flow, laminar flow, occurs under the pressure gradient between the ends of a capillary. Poiseuille diffusivity can be expressed by following relation.

$$D_{poiseuille} = \frac{\Delta P r^2}{8\mu} \quad (3.9)$$

where P is the absolute pressure and μ is viscosity of adsorptive. Poiseuille flow is important only in large pores and at higher pressures. At 10atm and in 200Å pore diameter, Poiseuille flow can be effective (Karger and Ruthven 1992).

3.4.5 Effective Diffusivity for Microporous Single Particle

For lumped analysis for single spherical microporous particle, the effective diffusivity can be evaluated by using following assumptions and equations. The heat transfer inside the particle and between particle and surrounding are rapid and there are no temperature gradients. The mass transfer through the single particle is only occurred by diffusion. Mass transfer equation can be expressed as follows:

$$\frac{\partial W}{\partial t} = \frac{1}{r^2} \frac{\partial}{\partial r} \left(r^2 D_{eff} \frac{\partial W}{\partial r} \right) \quad (3.10)$$

The relevant initial and boundary conditions are:

$$t < 0 \quad C = C_0 \quad W = W_{init} \quad (3.10a)$$

$$t > 0 \quad C = C_\infty \quad W(r,t) = W_\infty \quad (3.10b)$$

$$\frac{\partial W}{\partial r} \Big|_{r=0} = 0 \quad \text{for all } t \quad (3.10c)$$

Analytical solution of Equation 3.10 can be defined by Equation 3.11. Equation 3.11 can be described into two periods which are short time region and long time region in Equations 3.11 and 3.12.

$$\frac{\bar{W}_t}{W_\infty} = 1 - \frac{6}{\pi^2} \sum_{n=1}^{\infty} \frac{1}{n^2} \exp\left[-\frac{n^2 \pi^2 D_{eff} t}{r_p^2}\right] \quad (3.11)$$

Equation 3.12 which is convenient for short times is valid if W_t/W_∞ is lower than 0.3.

$$\frac{\bar{W}_t}{W_\infty} = \frac{6}{\sqrt{\pi}} \sqrt{\frac{D_{eff} t}{r_p^2}} \quad (3.12)$$

Equation 3.13 can be employed if $W_t/W_\infty > 0.7$.

$$\frac{\bar{W}_t}{W_\infty} = 1 - \frac{6}{\pi^2} \exp\left[-\frac{\pi^2 D_{eff} t}{r_p^2}\right] \quad (3.13)$$

The slope of $\ln(1 - W_t/W_\infty)$ versus t gives micropore diffusivity constant at that temperature. The slope of curve equals to $-\pi^2 D_{eff}/r_p^2$ and intercept equals to $\ln(6/\pi^2)$ (Ruthven 1984).

Aristov et al. (2006) obtained sorption behavior of water vapor on Fuji RD silica gel by using CAHN 2000 thermo-balance. The Fuji RD silica gel has 820 m² g⁻¹ BET surface areas with 0.3-0.325, 0.355-0.425 and 0.8-1mm in particle size. Aristov et al. (2006) found out diffusivity of water vapor on Fuji RD silica gel at different temperature as shown in Table 3.1. Aristov et al. (2006) investigated the effect of adsorption temperature and grain size of particle on diffusivity of water vapor on silica gel. The apparent diffusivity D_{ap} which indicates the micropore diffusivity is calculated by using Arrhenius relation and the effective pore diffusivity D_e is measured experimentally from kinetic data. The apparent and effective diffusivities are slightly increased with increasing adsorption temperature and grain size of silica gel.

3.5- Heat of Adsorption

Heat which is called as heat of adsorption evolves during adsorption of gas or liquid molecules on solid surface. The heat of adsorption is a useful indication of the strength of the forces binding adsorbed molecules to the surface of the adsorbent. The heat of adsorption for a specific pair depends on process conditions (temperature and pressure) and surface coverage. There are three different definitions for heat of adsorption.

- Differential heat of adsorption
- Integral heat of adsorption

- Isosteric heat of adsorption

Table 3.1. Experimental kinetic parameter of water vapor adsorption on Fuji RD silica gel (Source: Aristov, et al. 2006)

T (°C)	A (s ^{-1/2})	D _{ap} (m ² s ⁻¹)	D _e (m ² s ⁻¹)
Grains 0.355-0.415 mm			
28.8	0.0845	1.8x10 ⁻¹¹	3.5x10 ⁻⁷
38.9	0.105	3.6x10 ⁻¹¹	3.7x10 ⁻⁷
49.0	0.114	4.1x10 ⁻¹¹	2.8x10 ⁻⁷
64.0	0.119	6.3x10 ⁻¹¹	2.4x10 ⁻⁷
Grains 0.8-1.0 mm			
28.9	0.0361	2.1x10 ⁻¹¹	3.9x10 ⁻⁷
35.0		2.1x10 ⁻¹¹	
38.8	0.046	3.8x10 ⁻¹¹	4.0x10 ⁻⁷
49.1	0.062	6.7x10 ⁻¹¹	4.5x10 ⁻⁷
50.0		6.4x10 ⁻¹¹	
63.9	0.082	1.2x10 ⁻¹⁰	4.7x10 ⁻⁷

3.5.1- Differential Heat of Adsorption

In physical adsorption, heat of adsorption depends on to the internal energy change of adsorptive during change of state from adsorptive to adsorbate. The differential molar enthalpy of adsorption can be expressed by differential of enthalpy of adsorptive and adsorbate. The differential molar enthalpy of adsorption (differential heat of adsorption) becomes

$$\Delta_a h = -\frac{\partial Q}{\partial n_a} + V \frac{\partial P}{\partial n_a} \quad (3.14)$$

3.5.2- Integral Heat of Adsorption

The integral heat of adsorption is obtained by integrating the differential heat of adsorption against amount of adsorbate.

$$\Delta_a H = \int_0^{n_a} \Delta_a h dn_a \quad (3.15)$$

The above equation is valid at constant temperature.

3.5.3- Isotheric Heat of Adsorption

. The isotheric heat of adsorption can be calculated from adsorption isotherms that obtained at different temperatures by using Classius-Clapeyron relation.

Heat of adsorption also depends on surface energy of adsorbent. When adsorption sites are energetically homogeneous and when there is no interaction between adsorbates, the heat of adsorption is independent of amount of adsorbate.

When the adsorbed surface have heterogeneous energy levels and when interaction between adsorbate can not be ignored. The heat of adsorption varies with the surface coverage. Moreover, heat of adsorption decreases with increasing surface coverage.

$$dG_{\text{adsorbate}}=V_s dP_{\text{sat}}-S_s dT \quad (3.16)$$

$$dG_{\text{adsorptive}}=V_g dP_{\text{sat}}-S_g dT \quad (3.17)$$

At constant T, P, amount of adsorbate, Gibbs energy of adsorbate equals to Gibbs energy of adsorptive $dG_{\text{adsorbate}}=dG_{\text{adsorptive}}$

$$\frac{dP^{\text{sat}}}{dT} = \frac{S_s - S_g}{V_s - V_g} = \frac{\Delta S}{\Delta V} = \frac{\Delta H}{T\Delta V} \quad (3.18)$$

$$\Delta H = T\Delta S \quad \text{Latent heat of phase transition} \quad (3.19)$$

$$\Delta V = \frac{RT}{P^{\text{sat}}} \quad \text{Ideal gas relation} \quad (3.20)$$

And finally after integration of above equation Classius-Clapeyron equation can be obtained.

$$\frac{d \ln P^{\text{sat}}}{d(1/T)} = -\frac{\Delta H}{R} \quad (3.21)$$

Wang et al. (2004) investigated isotherm of silica gel water pair. They used Type A silica gel having BET surface area $716 \text{ m}^2 \text{ g}^{-1}$ and 0.8-5nm pore size. Figure 3.7 illustrates the isotherms of Type A silica gel water pair. The isotherms are obtained by using constant-volume-variable-pressure (CVVP) and variable pressure TGA. The maximum water uptake is observed at 303K for A type silica gel. The increasing adsorption temperature reduces water uptake amount of A type silica gel. Wang et al. (2004) calculated heat of adsorption from the isotherms of water-silica gel pair by using Equation 3.10 as 2510 kJ kg^{-1} .

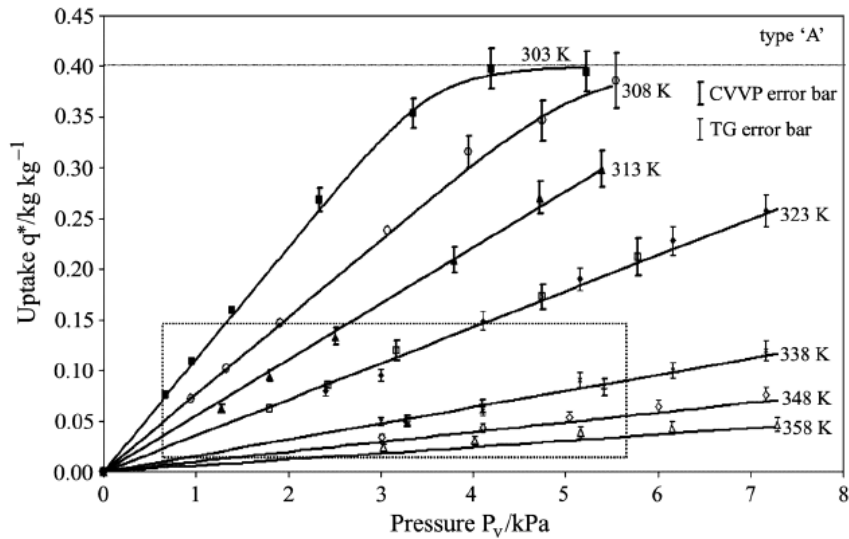


Figure 3.7. Isotherm data for type A silica gel water pair
(Source: Wang, et al. 2004)

3.6- Calorimetric Techniques for Measuring Differential Heat of Adsorption

3.6.1- Tian-Calvet Type Microcalorimeter

The differential heat of adsorption can be measured directly by calorimetric techniques. One of common isothermal calorimetry techniques is applied by Tian at 1923 and improved by Calvet at 1958. It is called as Tian and Calvet type microcalorimeter as shown in Figure 3.8. The Tian and Calvet type microcalorimeter composed of three components:

- Heat sink
- Sample bed
- Thermopile

The sample cell is placed into a sample bed. The cell is surrounded by a thermopile that made of more than 1000 thermocouples and connected in series. Thermopile has two functions. First, it transfers the released heat during adsorption from sample cell to heat sink block. Second, it generates signal during transferring heat. Signal acquired as mW versus time by software. The integral of curve gives differential heat of adsorption.

Handy et al. (1993) used Tian-calvet heat flux microcalorimeter for measuring differential heat of CO adsorption on Pt/SiO₂ catalyst. Spiewak and Dumesic (1996) measured differential heat of CO, N₂ and H₂ adsorption on Pt/SiO₂ and Ni powder with microcalorimeter technique. They emphasized that microcalorimetry provide information about direct measurement of heat of adsorption, reaction on solid, acid sites of zeolite and probe sites on supported metal catalysts with in-situ analytic techniques.

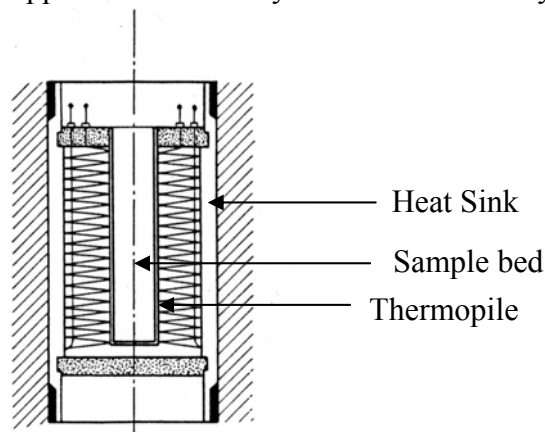


Figure 3.8. Schematically illustration of Tian-Calvet type calorimeter

3.6.2- Survey of Measurement of Heat of Adsorption

Figure 3.9 illustrates the differential heat of CO adsorption versus surface coverage of catalyst at 298K. The graph is good example for describing behavior of differential heat of adsorption against surface coverage. O'Neil et al. (1985) is obtained the differential heat of adsorption of CO on high surface area solid by using Tian-Calvet type calorimeters. The experiments are made twice and the curve of heat of adsorption versus fractional coverage is very repeatable at 298K. The heat of adsorption of CO on high surface area solid (300m² g⁻¹) reduces with increasing fractional surface coverage. The curve consists of three regions which are initial region at around 75 kcal gmole⁻¹ and decline region which extends to 1.5% and region of very low heat of adsorption.

Moise et al. (2001) investigated water vapor adsorption on Ba-exchanged synthetic zeolite X and Y by microcalorimeter at 298 and 423K. Figure 3.10 shows the obtained results. Heat of adsorption of barium exchanged zeolite Y is higher than that of Ba-exchanged zeolite X for both temperatures. This situation is explained by cation diameter. The diameter of Ba⁺² (0.270nm) cation is larger than Na⁺ (0.194nm). The large Ba cation lies out of the plane of the zeolitic oxygen framework and then more water molecules diffuse the zeolitic framework. The increasing adsorption temperature

(423K) decreases the heat of adsorption due to reducing adsorbate-adsorbent interactions as shown in Figure 3.9.

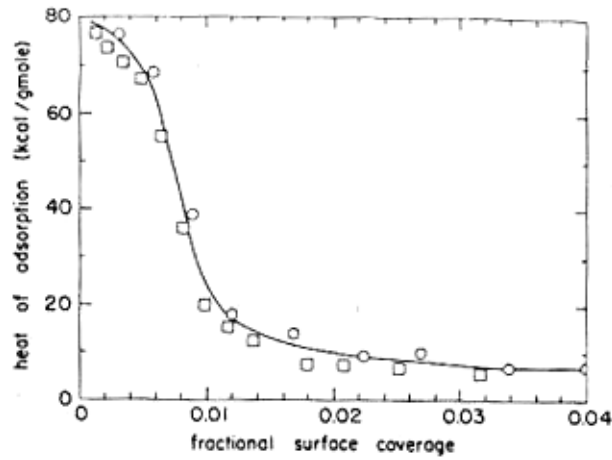


Figure 3.9. Differential heat of CO adsorption at 298K
(Source: O'Neil, et al. 1985)

Janchen et al. (2005) investigated differential heat of adsorption of water vapor on zeolite, AlPO_4 and CaCl_2 . Figure 3.11 compares the differential heat of water vapor adsorption on zeolite and CaCl_2 at 313K. The different behavior of heat curves of zeolite and CaCl_2 indicates the different water vapor adsorption behavior of zeolite and CaCl_2 materials.

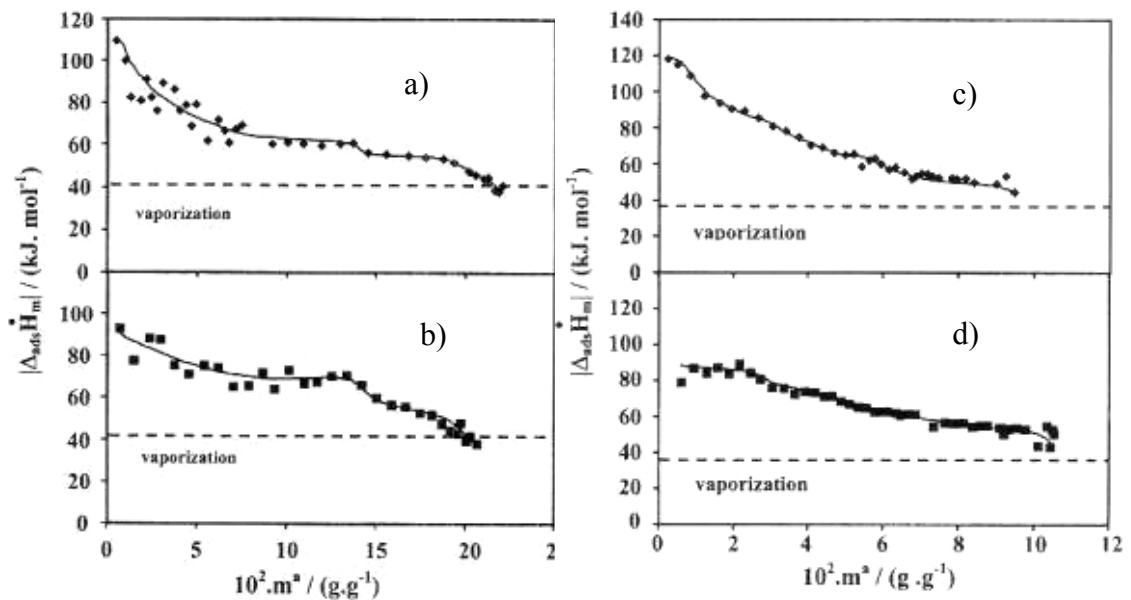


Figure 3.10. Heat of water vapor adsorption on a) BaY at 298K, b) BaX at 298K, c) BaY at 423K and d) BaX at 423K (Source: Moise, et al. 2001)

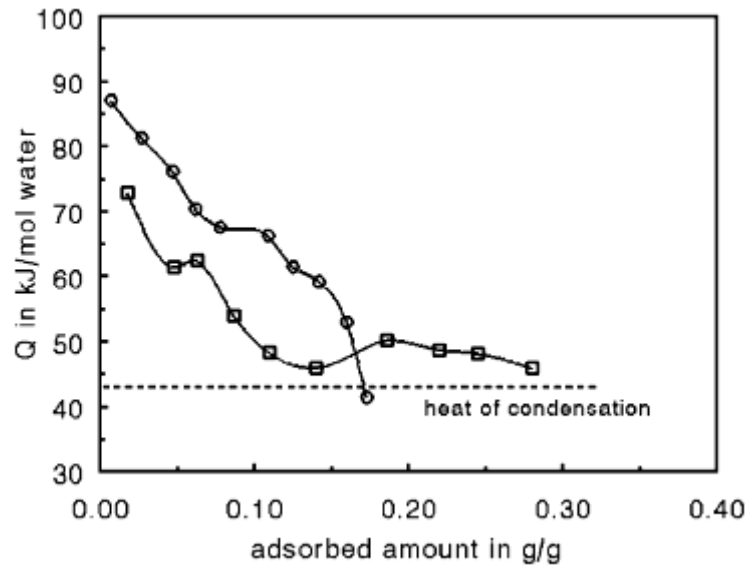


Figure 3.11. Differential heat of adsorption of water vapor on zeolite (□) and CaCl₂ (○) at 313K (Source: Janchen, et al. 2005)

CHAPTER 4

EXPERIMENTAL STUDIES

The physical properties of silica gel, which was used as the adsorbent in two of the different intermittent adsorption heat pumps, were given in this chapter. Two different adsorption heat pump systems were designed and constructed. The heat transfer area in the adsorbent bed of first AHP was 0.74 m^2 which provided by using 6 fins. The adsorbent bed of second AHP contains 12 main fins and four small fins attached to the each main fin. Therefore, the heat transfer area for the second AHP was increased from 0.74 m^2 to 4.1 m^2 . The construction of designed adsorption heat pumps and experimental procedure were also explained in this chapter. In order to enhance the thermal diffusivity of adsorbent bed, metal additives were used. The thermal diffusivities of mixtures of silica gel-metal additives were used for the enhancement of heat transfer rate in the annular adsorbent bed. The investigation on these mixtures by a thermal diffusivity apparatus was also described in this chapter. As mentioned before, the isosteric heat of adsorption of water - silica gel pair is important for the analysis of COP of designed systems at different operational conditions. In order to find isosteric heat of adsorption of water-silica gel pair, the Tian-Calvet type microcalorimeter was used. The experimental setup and procedure of microcalorimetry were explained in detail.

4.1 Materials

The silica gel (supplied from Merck Co.) was used as adsorbent in the adsorption heat pump system. The equivalent diameter of adsorbent granules varies between 3 - 5 mm. The water adsorption capacity of silica gel is given as 25%. BET surface area and average pore diameter of silica gel were determined as $626 \text{ m}^2 \text{ g}^{-1}$ and 2.0-2.5 nm respectively by ASAP2010 micromeritics.

The stainless steel (St-St), copper (Cu), aluminum (Al) and brass (40% Zinc, 60% Copper) pieces shown in Figure 4.1 were supplied from local raw material depot.

A special attention was paid for the selection of metal piece additives. It is assumed that the shapes of selected metal pieces do not cause mass transfer resistance through the adsorbent bed. All metal pieces were washed with alcohol and were sieved for separation into two fractions which are 1 – 2.8mm and 2.8 – 4.75mm. The shape of brass piece is different than the shapes of Al, Cu and St-St metal pieces and it is like tiny hand fan as shown in Figure 4.1d. The length of brass pieces is between 10 and 13mm.



Figure 4.1. A photograph of used metal pieces a) Copper b) Aluminum c) Stainless steel d) Brass

4.2 Experimental Setups and Procedures

4.2.1 Adsorption Heat Pump-1

The designed single bed adsorption heat pump was mainly composed of an annular adsorbent bed, an evaporator and a condenser. The main components of adsorption heat pump and the location of thermocouples and pressure transducers are shown schematically in Figure 4.2. The front view of heat pump and top view of inside bed are illustrated in Figure 4.3(a) and (b); respectively. The mass and thermal properties of materials used in the adsorbent bed are presented in Table C.1. The amount of silica gel supplied from Merck Co. in the adsorbent bed was 37.5 kg. The volume of water in the evaporator was 10 liter. The total mass of metal body of adsorbent bed was 55 kg. The annulus adsorbent bed was heated by electrical resistance which was surrounded around outer surface of the adsorbent bed. The power of

electrical resistance was controlled by a PID temperature controller during the isosteric heating and isobaric desorption periods. The annular adsorbent bed was cooled by a fan throughout the isosteric cooling and isobaric adsorption processes.

All parts of the system were made of stainless steel. Six fins were symmetrically welded onto the adsorber inner surface to increase heat transfer area and accelerate heating and cooling of the adsorbent bed. The annulus adsorbent bed was constructed from a stainless steel with 5 mm thickness and 335 mm diameter. The height of annular adsorbent bed was 725 mm. In the middle of the adsorbent bed, a free space with 60 mm diameter in vertical direction was provided to accelerate adsorbate transfer, thus mass transfer of adsorbate occurs in radial direction. The free space and silica gel particles were separated from each other by using stainless steel mesh.

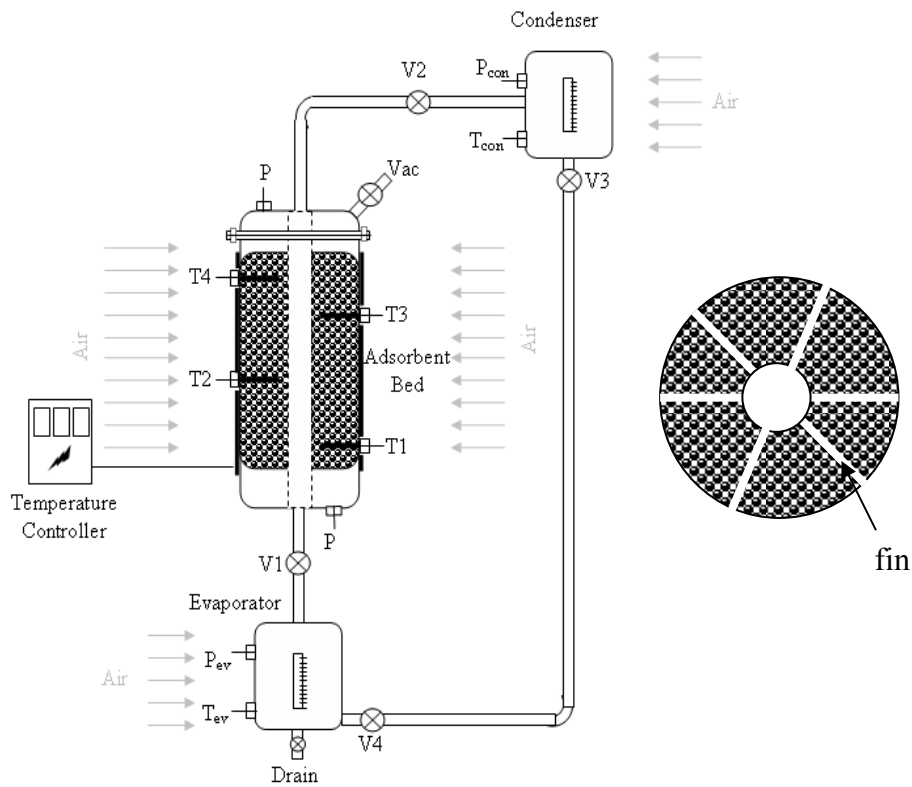


Figure 4.2. Schematic view of the designed intermittent adsorption heat pump

The temperature and pressure were measured by the sensors and transferred to the computer by using a data logger card and software. The raw data and procedure of data processing were explained in Appendix B. Four thermocouples were mounted at different radial and axial positions in the adsorbent bed to measure the variations of temperature in the bed as shown in Figure 4.4. The thermocouples were located at 0, 60,

180 and 240 degrees in θ direction and the distance between thermocouples in axial direction is 140 mm.

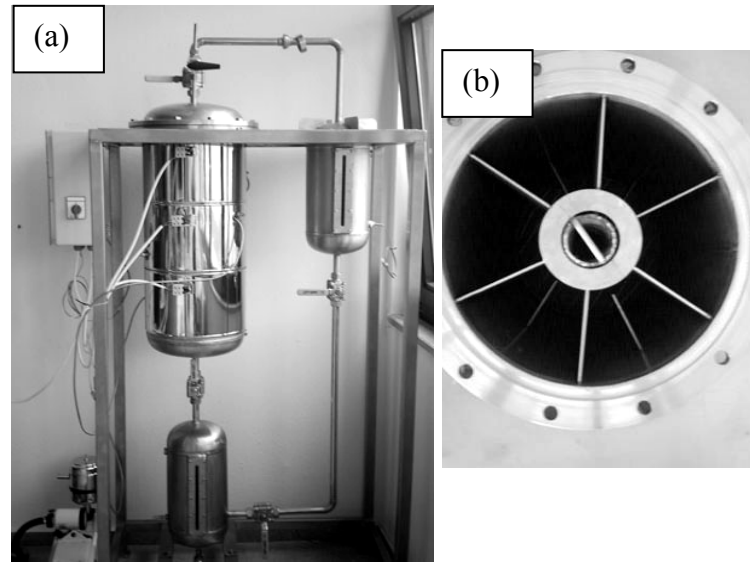


Figure 4.3. Photographs of the intermittent adsorption heat pump a) front view, b) top view of adsorbent bed

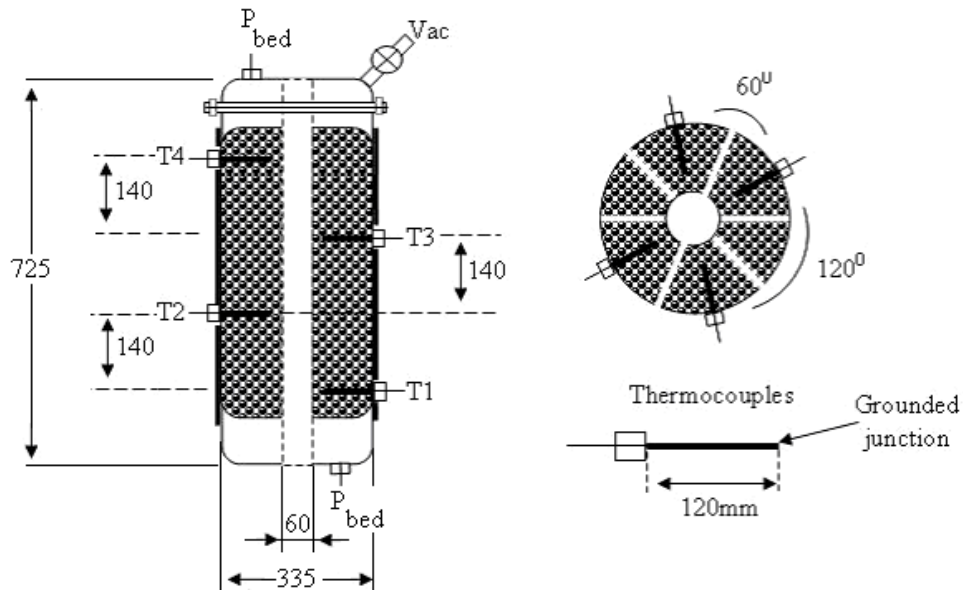


Figure 4.4. Location of thermocouples and pressure sensors in the AHP-1

The junction thermocouples were grounded which means that the junction is welded to the stainless steel sheath with 120 mm length (Figure 4.4). In other words, temperature is not measured only from tip of thermocouples and also affected by stainless steel sheath. In the adsorbent bed, adsorbent particles contact with thermocouples throughout the surface of stainless steel sheath of thermocouples. Hence, the thermocouples measure the average bed temperature in the radial direction. All

thermocouples were calibrated by using Fluke 714 temperature calibrator which has 0.025% accuracy. The surface temperature of the adsorbent bed is measured by a thermocouple which is in contact only with the adsorbent bed surface and insulated from the surrounding. The pressure transducers which have $\pm 0.25\%$ accuracy were located at the evaporator, condenser and adsorbent bed. The vacuum tight valves were located between the evaporator, condenser and adsorber to complete intermittent cycle. The valve between evaporator and condenser can play the same role of expansion valve if it is carefully opened and closed. The level of adsorbate was viewed and measured from the sight glasses mounted in the casing of evaporator and condenser.

4.2.2 Experimental Procedure for AHP-1

The evaporator was filled with 10L of deionized water. After filling the annulus adsorbent bed with 37.5 kg silica gel and before starting the first cycle, it was evacuated while being heated for removing moisture of silica gel. The drying process of silica gel was continued for 48 hours. The removal of moisture and other gases from adsorbent is important for utilization of maximum water adsorption capacity of adsorbent. During the drying process, valves (V2 and V3) were closed. The locations of valves are illustrated in Figure 4.2.

In order to start the cycle, the valve between evaporator and adsorbent bed was slightly opened and evaporated water was adsorbed by silica gel. The temperature of adsorbent bed increased during the adsorption process; however it was cooled to T_a temperature by a fan. The cycle was started from point “a” which is shown in Figure 2.2. After a complete adsorption process, the valve (V1) was closed and adsorbent bed was heated for the isosteric heating process. When the pressure of the adsorbent bed was reached to the desired condenser pressure, the valve (V2) was opened for the isobaric desorption process while the heating of adsorbent bed was continued. Once isobaric desorption was completed, the isosteric cooling process was started with closing valve (V2) and adsorbent bed was cooled by fan. After reducing the adsorbent bed pressure to the evaporator pressure, the isobaric adsorption process was performed by opening the valve (V1). During the adsorption process, cooling of adsorbent bed was continued. The isobaric adsorption process was continued until the level of water inside the evaporator becomes fixed. Hence, the cycle of intermittent adsorption heat pump was completed. The same procedure was repeated for next cycles.

The control of isosteric heating and cooling periods was performed according to the pressure of bed. The valve between the adsorbent bed and condenser was opened when the adsorbent bed pressure reached to the condenser pressure. Similarly, the valve between evaporator and bed was opened when the bed pressure fell to the evaporator pressure. The control of isobaric adsorption and desorption periods was performed according to the rate of adsorbed or desorbed water which are viewed from the sight glass. All valves were opened and closed manually.

4.2.3 Adsorption Heat Pump-2

In order to improve the heat and mass transfer in the annular adsorbent bed, the second adsorption heat pump was designed and constructed. Moreover, in the second adsorption heat pump, the evaporator and condenser were heated and cooled by using water which circulates in the heat exchanger inside the evaporator and condenser. The inlet water temperature of the heat exchanger was maintained constant by a constant temperature water bath. Thus, the heating/cooling capacity of condenser/evaporator and power of condenser/evaporator can be evaluated by measuring inlet and outlet temperature of heat exchanger fluid during the circulating between constant temperature bath and unit. The constructed single bed adsorption heat pump was composed of an annulus adsorbent bed, an evaporator and a condenser as shown in Figure 4.5. This system also operates with silica gel - water pair. The annulus adsorbent bed was heated with electrical resistances which are controlled by a PID temperature controller during isosteric heating and desorption periods. It was cooled by three axial fans during isosteric cooling and adsorption processes.

The main difference between the first AHP and the second AHP is in the design of the adsorbent bed. Twelve fins were welded onto the inner adsorber surface to accelerate heating and cooling of adsorbent. Fins were located vertically in radial directions and four small fins were welded onto both sides of each radial fin. The heat transfer area of annular adsorbent bed of AHP-1 is 0.74 m^2 and it was increased to 4.08 m^2 by using the fins in AHP-2. Moreover, the mass transfer rate in the adsorbent bed was increased by leaving more free spaces between fin blocks and additionally in the middle of the adsorbent bed.

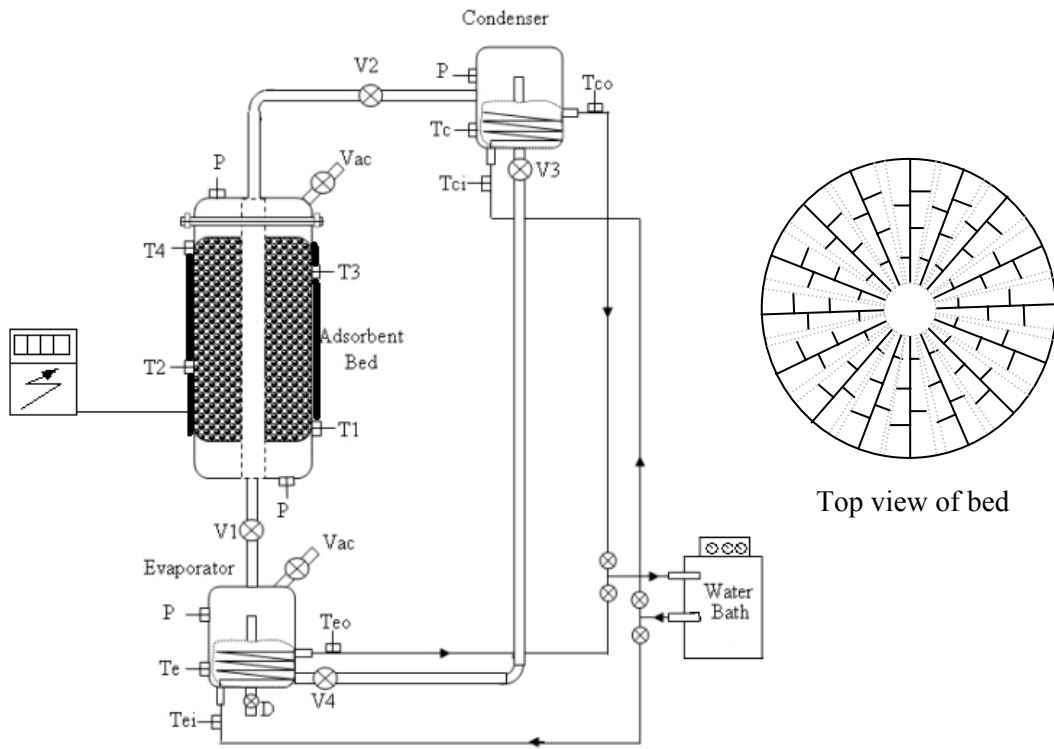


Figure 4.5. Schematic view of AHP-2

The thermocouples were located as similar way as in AHP-1 as shown in Figure 4.6. The types and properties of thermocouples and pressure transducers were same with the ones used in AHP-1. The photograph of the adsorption heat pump and top view of the adsorbent bed are shown in Figure 4.7.

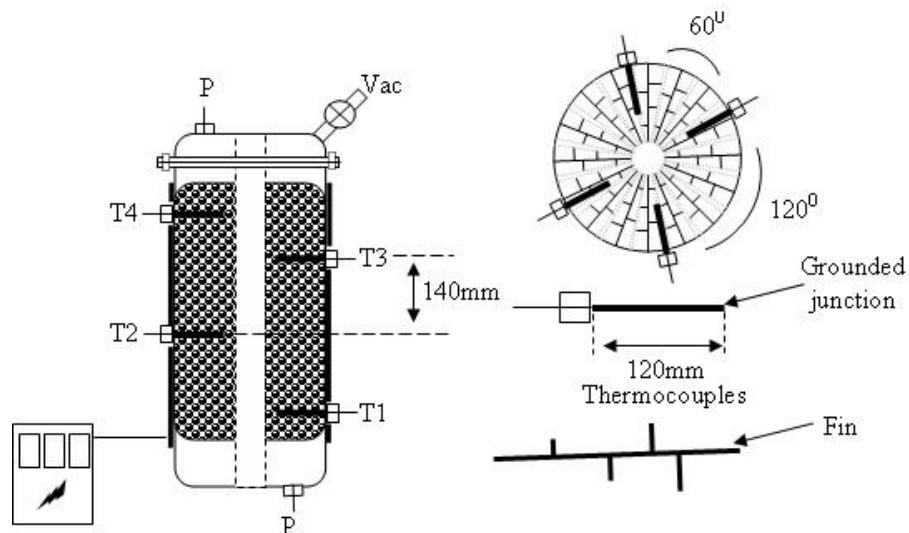


Figure 4.6. Schematic view of designed bed, top view of bed, fins configuration and thermocouple inside the bed of AHP-2

4.2.4 Experimental Procedure for AHP-2

The same silica gel was used as adsorbent in the second AHP and the amount of silica gel in the adsorbent bed was 40 kg. The evaporator was filled with 15L of deionized water. After filling the adsorbent bed with silica gel, the adsorbent bed was evacuated while being heated for removing all moisture of silica-gel as similar procedure of AHP-1. The drying process of silica-gel was continued for 48 hours. The removal of moisture and other gases from adsorbent are important for using the maximum adsorption capacity of adsorbent. After drying process, valves (V2 and V3) were closed.

The procedure of opening and closing the valves for passing between the processes of the cycle is similar with the AHP-1. Additionally, temperature of evaporator/condenser was adjusted by using constant temperature water bath before starting the isobaric adsorption/ desorption process. The same procedure was repeated for the next cycles.

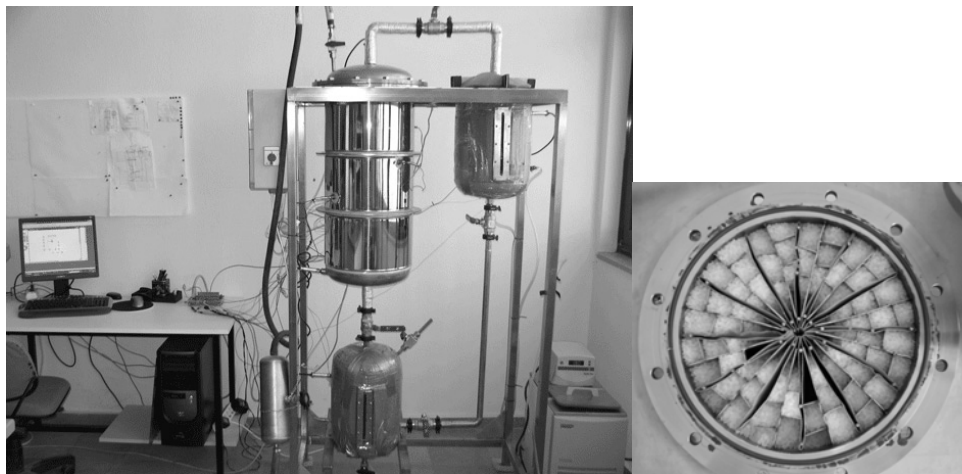


Figure 4.7. Photograph of the intermittent adsorption heat pump and top view of adsorbent bed of AHP-2

4.2.5 Microcalorimetry

The heat of adsorption of adsorbent was measured with Tian-Calvet type microcalorimetry. The Tian-Calvet type microcalorimetry system configuration was modified as shown in Figure 4.8. The old configuration had many connections and pipes in large diameter as shown in Figure 4.8a. The volume of old configuration was 2 L and this volume was too large to study low water vapor dose which is important for measuring heat of adsorption accurately. The microcalorimetry configuration was

improved by using vacuum tight valves and pipes in small diameter as shown in Figure 4.8b. Hence, the operation volume was reduced after modification to 0.14L. The more water vapor dose can be sent off with reducing operational volume. For preventing water condensation on stainless steel tubes, stainless steel tubes were covered with electrical resistance. During experiment, stainless steel tubes were heated by this electrical resistance. The temperature of stainless steel tubes was kept constant at 45°C. The system pressure was measured with MKS 121 Baratron pressure transducer from 0 to 100 mbar with accuracy 0.05% at reading and 0.01 resolutions.

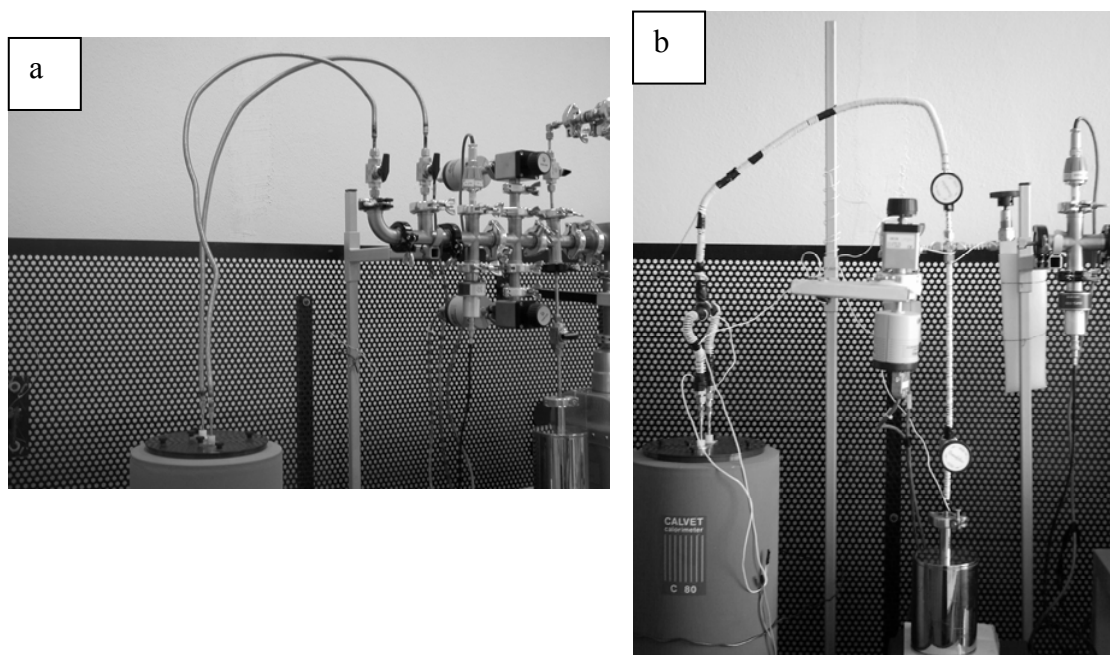


Figure 4.8. Configuration of microcalorimetry a) before modification b) after modification

The leak problem of system was also overcome after modification of the configuration of microcalorimetry. In the old configuration, system pressure increases from 1×10^{-7} mbar to 1mbar for 3h. After modification, system pressure increases from 1×10^{-7} mbar to 1mbar for 48h. At operating pressure (30mbar), the pressure system remains constant for 3 weeks which provides enough time for completing one experiment.

4.2.5.1 Operation Principle of Microcalorimetry

The calorimeter consists of thermopile, heat sink block and sample bed. The thermopile section includes up to 1000 thermocouple junctions which are wired in

series. The thermopiles generate a voltage proportional to the temperature difference between sample cell and heat sink block as shown in Figure 4.9. Briefly, the thermopiles have two functions which are transferring the heat and generating voltage.

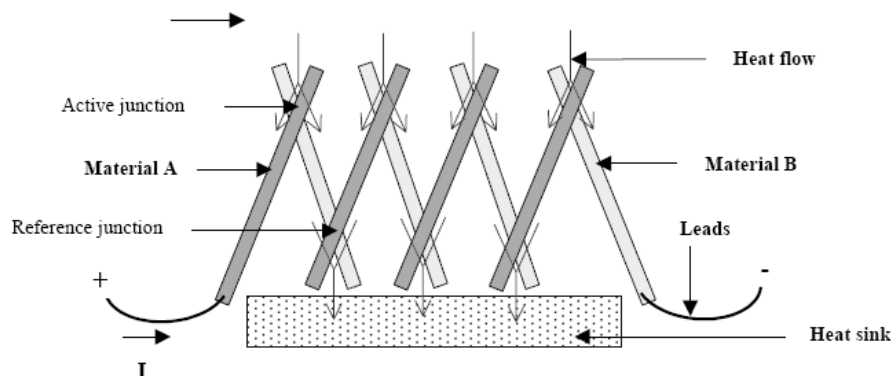


Figure 4.9. Illustration of thermopile

The generated voltage is acquired and plotted versus time (Figure 4.10) for calculating formation of heat according to Equation 4.1.

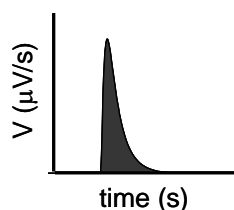


Figure 4.10. Generated voltage versus time

$$\Delta H_a = \int_{t_0}^{t_1} \frac{dH_a}{dt} = \frac{\lambda}{C_1} \int_{t_0}^{t_1} V_t dt \quad (4.1)$$

Where Q is the differential heat of adsorption and k is thermal conductivity. V is voltage generated by the thermopile and C_1 (μVK^{-1}) is Seebeck coefficient that depends on thermocouple junctions.

4.2.6 Experimental Procedure for Microcalorimetry

The following steps were performed to determine heat of adsorption at a specified temperature. The data was acquired to computer and processed by software. These steps

should be repeated for different temperatures to obtain heat of adsorption, kinetics and adsorption isotherms.

- 500mg adsorbent (silica gel) was put into sample vacuum cell.
- Sample vacuum cell was connected to the system and pressure test was employed for the detection of leakage
- For degassing of the silica gel, sample cell was heated to 120°C inside the system for 1°C/min under vacuum at 10^{-7} mbar.
- This process proceeds for one day.
- Stainless steel tubes were heated by electrical resistance to 45°C
- Microcalorimeter was adjusted to provide operating temperatures (30, 35, 40, 60, 75, 90, 100, 110 and 120°C).
- After the system reaches to equilibrium, one dose of water vapor, which has a partial pressure of 30mbar, was injected to the system.

4.2.7 Measurement of Thermal Diffusivity

The thermal diffusivity of adsorbent bed can be enhanced by mixing silica gel with the metal pieces, having high thermal diffusivity properties. For the selection of appropriate type, size and loading of metal additives, thermal diffusivity of apparatus was made as shown in Figure 4.11. The thermal diffusivity of pure silica gels, pure metal pieces (copper, stainless steel, aluminum and brass) and silica gel-metal pieces mixture were measured. The metal pieces were mixed with silica gel at different weight percentages which are 5, 10 and 15%. The apparatus was composed of long glass cylinder (130mm) with outer diameter 45mm and inner diameter 43mm. Inner temperature of apparatus was measured at the center with thermocouple which has 120mm length and can measure average temperature longitudinal of apparatus. The apparatus was filled with 200g sample and heated up to 40°C by using electrical resistance tape. When the temperature of apparatus was reached the equilibrium, the apparatus was suddenly immersed into static water bath which has constant temperature of 5°C as shown in Figure 4.12. The temperature of the apparatus and water bath were measured against time.

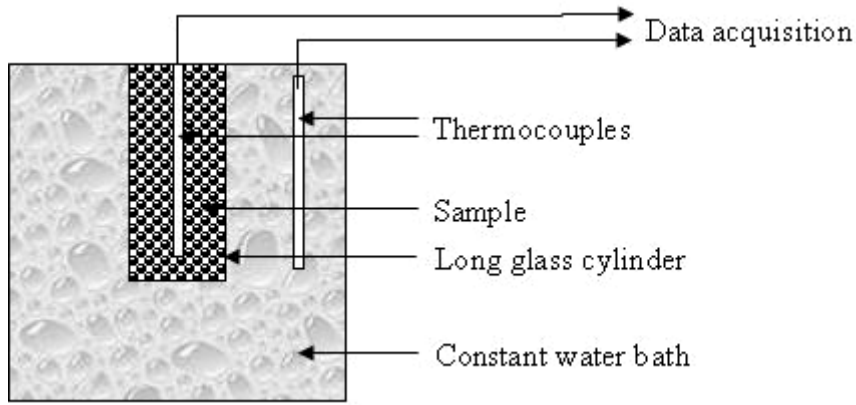


Figure 4.11. Schematically illustration of test apparatus



Figure 4.12. Photograph of test apparatus and water bath during experiment

4.2.7.1 Determination of Bed Thermal Diffusivity

For evaluation of the thermal diffusivity of the adsorbent bed, the solution of dimensionless form of transient heat conduction equation for a cylinder was obtained. The test apparatus can be assumed as a long cylinder in which conduction heat transfer is a function of time and radius.

$$\frac{\partial \theta}{\partial \tau} = \frac{1}{r^*} \frac{\partial}{\partial r^*} \left(r^* \frac{\partial \theta}{\partial r^*} \right) \quad (4.2)$$

where θ is the dimensionless temperature and it is defined as $\theta = (T - T_\infty) / (T_{init} - T_\infty)$. The independent parameters τ and r^* represent the

dimensionless radius ($r^* = r/R$) and time ($\tau = \alpha t/R^2$). The boundary conditions of the problem can be written as;

$$\text{at } r^* = 0 \quad \partial\theta / \partial r^* = 0 \quad (4.3a)$$

$$\text{at } r^* = 1 \quad \theta = 1 \quad (4.3b)$$

$$\text{and for } \tau = 0 \quad \theta = 0 \quad (4.3c)$$

After obtaining the solution of heat conduction equation (Equation 4.2), the variation of temperature of centerline ($r^*=0$) with dimensionless time was drawn. The results of the experiment (i.e. centerline temperature versus time) were transformed to the dimensionless form and compared with the obtained theoretical solution. A trial and error approach was used to determine the mixture thermal diffusivity. The multiplication of calculated thermal diffusivity with the effective thermal capacitance of the mixture yields the thermal conductivity of the mixture. Figure 4.13 shows a representative diagram in which the variations of the experimental and theoretical dimensionless temperatures with dimensionless time were presented. As can be seen from the Figure 4.13, a good agreement is observed between the experimental and theoretical values indicating the accuracy of the employed method.

In the literature, there are many experimental equations for evaluating the effective thermal diffusivity of solids mixture. Maxwell equation can be defined comprehensively complex non-spherical inclusions. Maxwell equation (Equation 4.4) was used also for evaluating the thermal conductivity of simple unconsolidated granular beds as complex non-spherical inclusions in a continuous solid phase.

$$\frac{\lambda_{eff}}{\lambda_0} = \frac{(1-\phi) + \beta\phi(\lambda_1/\lambda_0)}{(1-\phi) + \beta\phi} \quad (4.4)$$

where λ_1 is the thermal conductivity of particle embedded in a bulk solid phase with thermal conductivity λ_0 . The symbol ϕ represents the volume fraction of embedded solids (metal pieces).

$$\beta = \frac{1}{3} \sum_{j=1}^3 \left[1 + \left(\frac{\lambda_1}{\lambda_0} - 1 \right) g_j \right]^{-1} \quad (4.5)$$

where g_j is shape factor.

The shape factor for aluminum, copper and stainless steel were assumed as $g_1=g_2=g_3=1/3$. For the brass piece, $g_1=g_2=1/8$ and $g_3=3/4$ were used (Bird, et al. 2002).

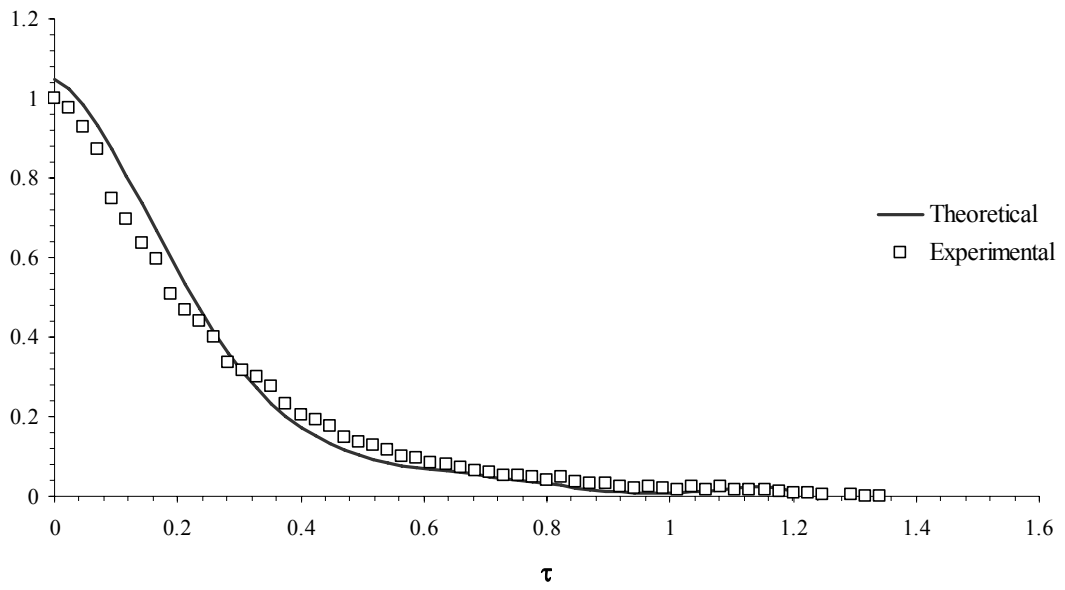


Figure 4.13. Change of temperature of experimental and theoretical model in dimensionless form

CHAPTER 5

RESULTS OF EXPERIMENTAL STUDIES ON ADSORPTION HEAT PUMPS

The designed and manufactured adsorption heat pumps as well as the other employed experimental setups were explained in the Chapter 4. For two adsorption heat pumps, leakage problem was eliminated by using vacuum tight valves, connections and argon welding. First AHP was tested and results showed that the cycle period of first AHP was too long. In order to reduce this cycle period, the heat and mass transfers in the adsorbent bed of the second AHP were improved by increasing the heat and mass transfer areas. Although, the heat transfer area in the second AHP was increased by using fins, the desired cycle time was not achieved. The studies on enhancing the heat transfer rate in the adsorbent bed continued by mixing the silica gel particles with metal pieces. For the selection of appropriate metal additives, thermal diffusivities of pure silica gel, pure metal additives and silica gel – metal mixture at different mass ratios were investigated. The experiments on the second adsorption heat pump were repeated with the Aluminum - Silica gel loaded adsorbent bed. In this chapter, the experimental results of studies on two adsorption heat pumps and adsorbent with metal additives are presented.

5.1 Results of Adsorption Heat Pump-1

In the inner surface of adsorbent bed of AHP-1, six fins were located for acceleration of heat transfer rate in the bed. During construction of the system, avoiding from the extra junctions, complex design, we have used proper design and manufacturing methods. Hence, the leakage problem which is the main difficulty in the adsorption heat pumps was overcome and the repetition of cycles under the same pressure levels was provided. The influence of regeneration temperature on the performance criteria of AHP-1 was investigated. For this purpose, two regeneration

temperatures were selected which were 90 and 110°C. The represented cycles for two regeneration temperatures were obtained after the AHP-1 operated in stability at adjusted conditions as shown in Table 5.1.

Figure 5.1 illustrates the measured temperature and pressure of the adsorbent bed in $\ln P$ vs. $(-1/T)$ diagram for two cycles¹. The average of four temperatures which were sensed by probes located in the adsorbent bed was used in the graph.

Table 5.1. The operation conditions for two cycles

Parameters	Cycle 1	Cycle 2
T_a (°C)	25	19
T_b (°C)	77	71
T_c (°C)	102	93
T_d (°C)	52	52
T_{ev} (°C)	10	11
T_{cond} (°C)	62	64
P_{ev} (kPa)	1.4	1.4
P_{cond} (kPa)	21.0	23.0

All processes of an AHP cycle can be seen from Figure 5.1. The adsorbent bed pressure remains approximately constant during the adsorption and desorption processes. During the isosteric heating process, concentrations of adsorbate in the adsorbent bed were 0.064 and 0.048 kg_w kg_s⁻¹, and these values decreased to 0.0101 kg_w kg_s⁻¹ and 0.0053 kg_w kg_s⁻¹ in isosteric cooling process for cycle 1 and 2, respectively. The maximum capacity of water adsorption for the used silica gel was approximately 25%, however, for the achieved cycles the adsorbed water was below the expected capacity. The poor heat and mass transfer in the adsorbent bed in radial direction may be the main reason of this difference.

Figure 5.2 illustrates the variation of the adsorber surface temperature and adsorbent average temperature throughout the cycle. The transient behaviors of cycle 1 and 2 were similar to each other. During the heating process, the surface temperature of the adsorber was higher than the adsorbent; however in the cooling process the adsorbent was warmer than the adsorber surface. In the isosteric heating (a-b) and isobaric desorption (b-c) processes, differences between the temperatures of the adsorber surface and adsorbent were observed due to poor heat transfer in the adsorbent bed. As is seen, at the end of the desorption process the adsorbent temperature and the surface temperature became close to each other and the adsorbent temperature reached to desorption

¹ All obtained cycles from AHP-1 were given in Figure C1 in Appendix C.

temperature. The temperatures of the adsorber surface and the adsorbent were close to each other in the isosteric cooling (c-d) and the isobaric adsorption (d-a) since the adsorbent bed was slowly cooled. The periods of isosteric heating and cooling were not too long and most of the cycle time was consumed for the processes of isobaric adsorption (d-a) and isobaric desorption (b-c) due to poor heat transfer in the bed.

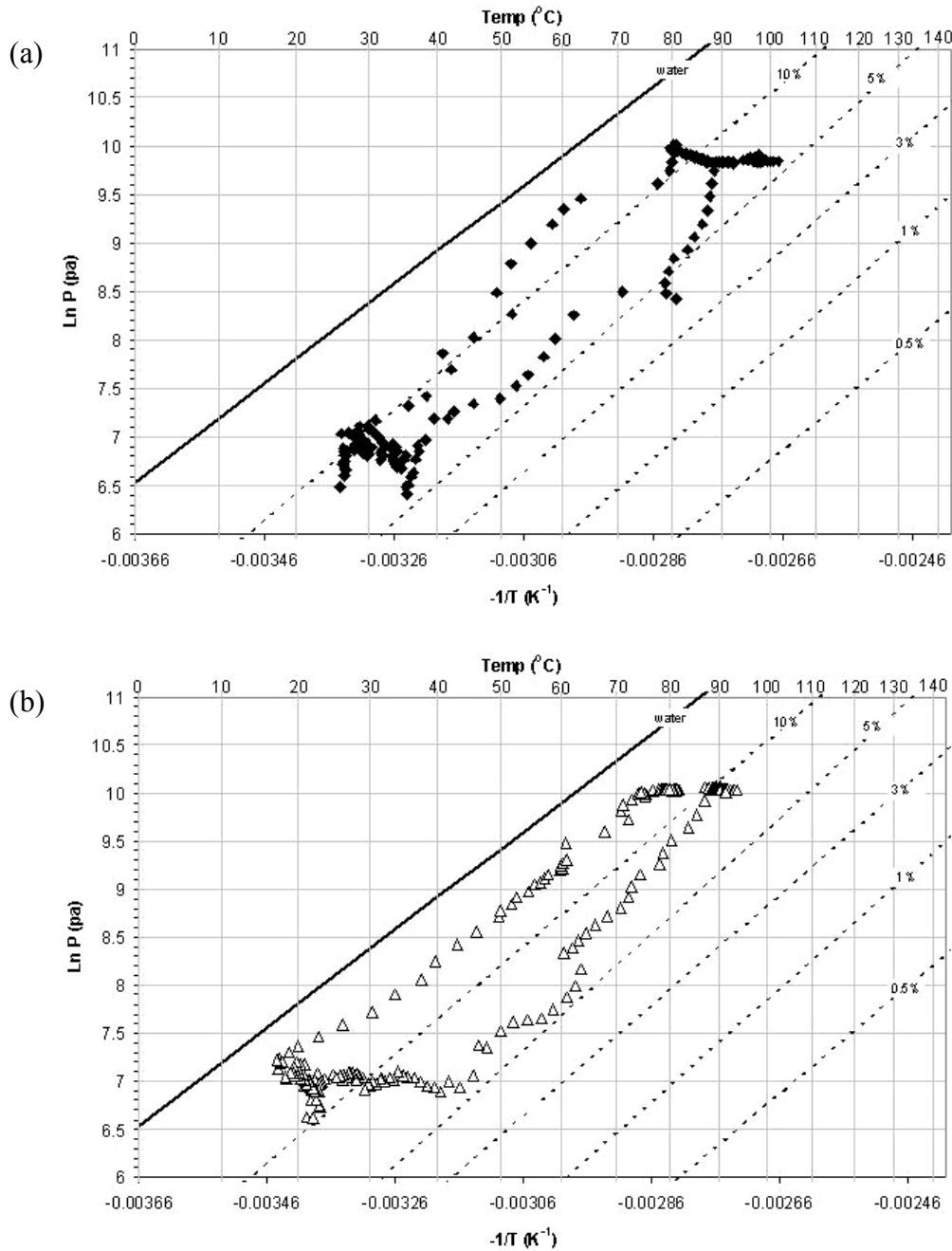


Figure 5.1. The variations of pressure with temperature in the adsorbent bed a) cycle 1 b) cycle 2¹

¹ Isosteric diagrams were explained in detail in Chapter 6.

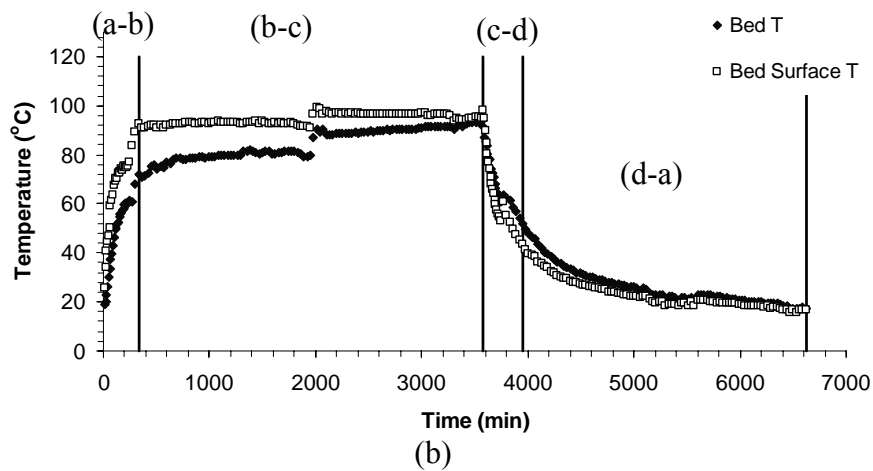
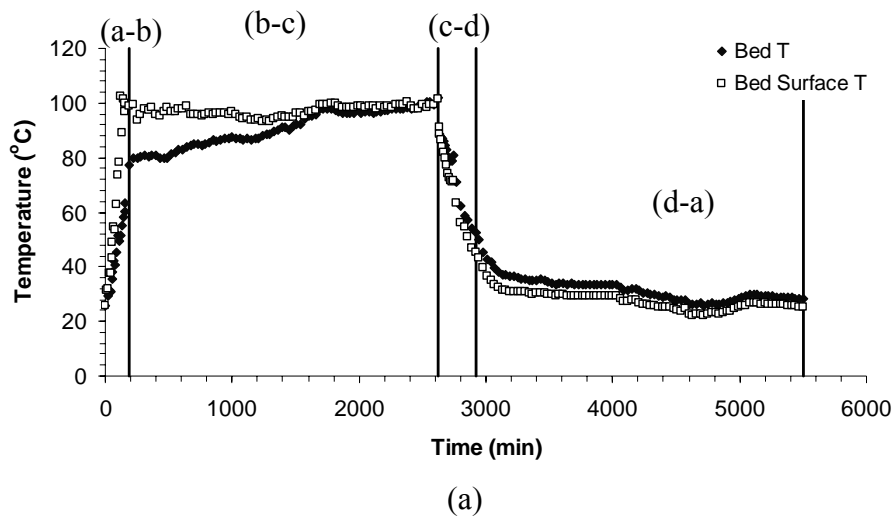


Figure 5.2. The variations of adsorbent bed and adsorber surface temperatures during cycle a) cycle 1 b) cycle 2

The variations of the adsorbent bed temperature and pressure throughout the cycle are shown in Figure 5.3. Both pressure and temperature in the adsorbent bed have rapidly changed during the isosteric heating and cooling while they did not significantly vary during the adsorption and desorption processes. The duration of isobaric desorption process in cycle 2 was longer than cycle 1 since the surface temperature of cycle 1 was higher. The increase of the desorption temperature reduced the period of desorption process.

The temperature and pressure of the evaporator during adsorption process are shown in Figure 5.4 (a) and (b) for cycle 1 and 2. The evaporator was at ambient temperature before the opening valve (V1). With opening the valve and starting the adsorption process, a portion of extracted heat of the evaporated water was spent to

decrease the temperature of the evaporator to the operation conditions which were 10°C and 11°C for cycle 1 and 2, respectively. After attaining to the desired evaporator temperature, the complete heat of evaporation was spent for the cooling of environment. The pressure of evaporator approximately remained constant during the isobaric adsorption process for both cycle 1 and 2.

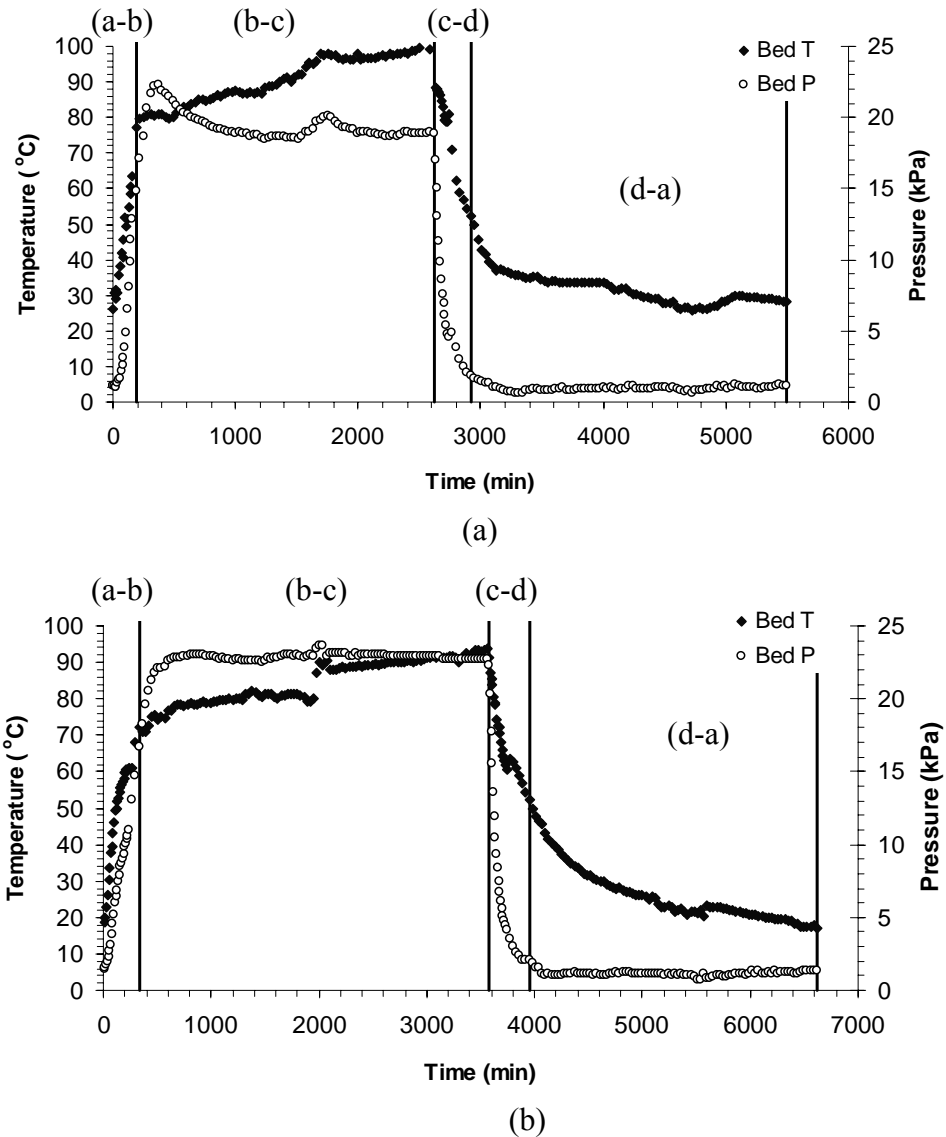
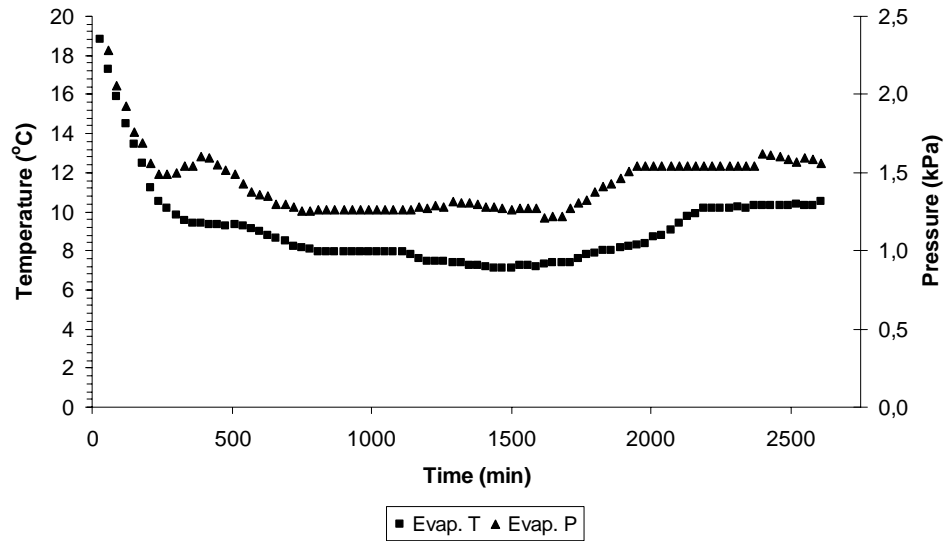


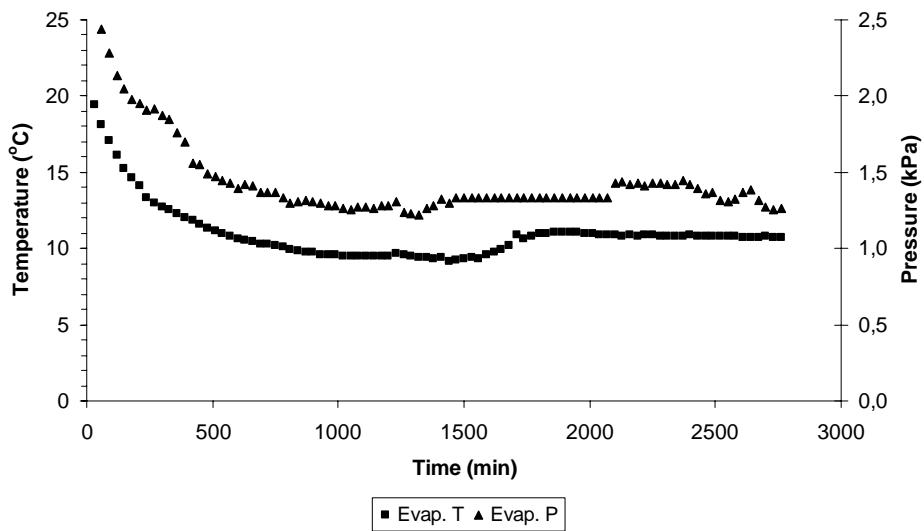
Figure 5.3. The variations of adsorbent bed temperature and pressure during the cycle a) cycle 1 b) cycle 2

The change in the amount of adsorbed water against time is shown in Figure 5.5. The amount of adsorbed water, which is the evaporated water from evaporator, increased with time during the adsorption process. The total amount of adsorbate for cycle 1, which is 2L, was greater than cycle 2 (1.6L) due to the higher regeneration temperature of cycle

1. The adsorption process was interrupted before the saturation of silica gel as shown in Figure 5.5. The amount of the adsorbed water can be increased with increasing adsorption period process; however the increase of adsorption period increases the cycle period and consequently the specific heating/cooling power decreases.



(a)



(b)

Figure 5.4. The changes of evaporator temperature and pressure during the adsorption process a) cycle 1 b) cycle 2

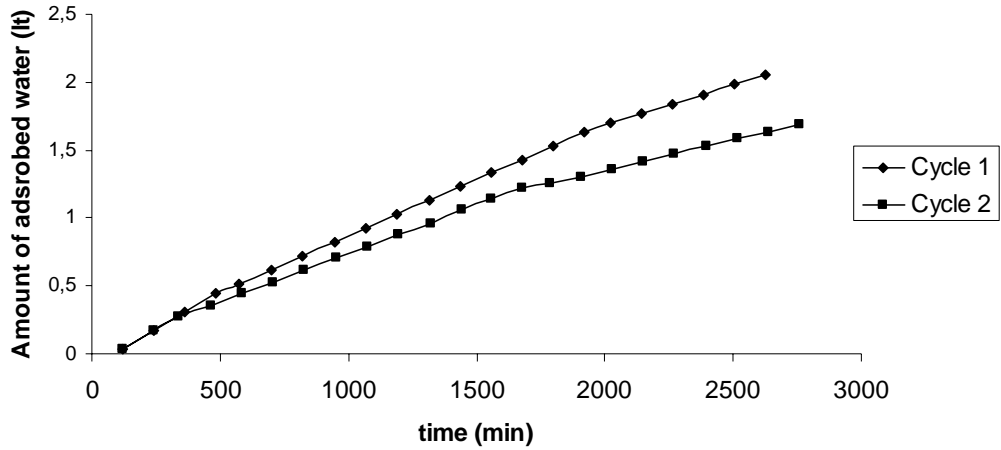


Figure 5.5. The amount of adsorbed water during the adsorption process for two cycles

The transferred amounts of heat from the evaporator, condenser and adsorbent bed were calculated by using Equations 2.3 to 2.8 and represented in Table 5.2. The heat extracted from environment (Q_{ev}) for cycle 1 was higher than that for cycle 2 due to higher amount of adsorbed water. The maximum heat transfer, between the AHP and heat reservoirs occurred during the isobaric adsorption and desorption processes for both cycles. According to the first law, the summation of transferred heat between the cycle and surroundings should be zero. The summation of presented values in Table 5.2 for cycles 1 and 2 are $\sum Q=12 \text{ kJ kg}_s^{-1}$ and $\sum Q=8 \text{ kJ kg}_s^{-1}$, respectively. The heat losses and experimental errors during reading of evaporated and condensed water amounts were the reasons of these differences. However, when we have compared these differences to the transferred heat ($Q_{a-b} + Q_{b-c}$), it was observed that the ratios were in an acceptable range of 4% for both cycles.

The coefficient of performance, the second law efficiency and specific heating/cooling power values were calculated and presented in Table 5.3. The COP values for cooling were found as 0.44 and 0.41 for cycles 1 and 2. For the same cycles, the COP values for heating were determined as 1.42 and 1.39. The Carnot performance values for cooling, which were the maximum performances, were 1.12 and 1.08 for the first and second cycles respectively.

The total entropy generations of the cycles were calculated by Equation 2.12 and given in Table 5.3. The total entropy generation for cycle 1 and 2 were 3.74 kJ K^{-1} and 3.56 kJ K^{-1} . The expected COP values for the cooling process were determined by the Equation 2.22 with the experimental temperatures were found as 0.57 and 0.50 for

cycles 1 and 2. These values are 51% and 46% lower than the Carnot COP values. These differences were due to the irreversibilities formed during the cycle. Although, the definitions of both COP_{exp} and COP_{ref} are the same, there is a difference between their values, as seen in Table 5.3, because the expected COP does not contain heat losses or experimental errors in reading of the evaporated and condensed water. The second law efficiencies (η_{II}) were found as 0.51 and 0.46 for cycle 1 and 2 respectively due to the Equation 2.23.

Table 5.2. The amounts of heat transfer between cycle and heat reservoirs for two cycles

Heat transfer in		
processes (kJ kg_s⁻¹)	Cycle 1	Cycle 2
Q_{a-b}	95	92
Q_{b-c}	181	146
Q_{c-d}	-80	-65
Q_{d-a}	-185	-165
Q_{ev}	123	97
Q_{cond}	-128	-101

Table 5.3. Performance indicators for two cycles

Parameters	Cycle 1	Cycle 2
COP_{ref}	0.44	0.41
COP_h	1.42	1.39
SCP (W kg_s⁻¹)	0.37	0.25
SHP (W kg_s⁻¹)	1.17	0.83
COP_{exp}	0.57	0.50
COP_C	1.12	1.08
η_{II}	0.51	0.46
ΔS (kJ K⁻¹)	3.74	3.56

As it was mentioned before, the SCP and SHP values are important parameters for the commercialization of AHP. By using Equations 2.24 and 2.25, the SCP and SHP values were found as 0.37 W kg⁻¹ and 1.17 W kg⁻¹ for cycle 1, 0.25 W kg⁻¹ and 0.83 W kg⁻¹ for cycle 2. The SCP and SHP values of cycle 2 were smaller than cycle 1, since desorption period was longer and the amount of the circulated water was smaller. As it was mentioned before, high SCP or SHP promotes the applicability of an AHP. For the

present design, increase in adsorption and desorption periods increase the cycle periods, hence this considerably reduces SHP and SCP values. The solution for the increase of SCP or SHP is improvement of heat and mass transfer inside the adsorbent bed.

5.2 Results of Adsorption Heat Pump-2

The experiments were performed with the described intermittent adsorption heat pump having special adsorbent bed design for the increasing heat and mass transfer rate. The two regeneration temperatures (90 and 110°C) were studied for investigating the performance criteria of AHP-2 at low temperature resources. The influence of heating rate on the expansion of adsorbent bed pressure during isobaric desorption process and condenser cooling surface area was also researched.

Table 5.4 illustrates the operation conditions of two representative cycles which are presented in Figure 5.6¹. These cycles are the two samples among many cycles which were performed in series.

Table 5.4. The operation conditions for two cycles

Parameters	Regeneration Temperature (°C)		Heating rate (°C/min)		Condenser cooling surface area (m ²)	
	Cycle 1	Cycle 2	Cycle 1	Cycle 2	Cycle 1	Cycle 2
	80	110	0.14	1	0.038	0.226
T_a (°C)	28	29	29	26	29	32
T_b (°C)	54	56	56	55	56	55
T_c (°C)	80	110	110	111	110	114
T_d (°C)	51	57	57	58	57	68
T_{ev} (°C)	12	16	16	13	16	17
T_{cond} (°C)	30	31	31	25	31	26
P_{ev} (kPa)	2.6	3.7	3.7	2.9	3.7	4.1
P_{cond} (kPa)	7.6	10.3	10.3	12.9	10.3	12.7

Figure 5.6 illustrates the measured temperature and pressure of the adsorbent bed and corresponding ideal cycles in ln P vs. (-1/T) diagram for two representative cycles. The average of four temperatures (with a standard deviation of 3°C) which were sensed by probes located in the adsorbent bed was plotted in the graph. The experimental and theoretical cycles were different from each other. The deviations were observed for isobaric processes. In the experimental cycles, the pressures of adsorbent

¹ All obtained cycles from AHP-2 were given in Figure C2 in Appendix C.

bed were not constant for the adsorption and desorption processes. The circulated amount of the water in the cycle of 80°C regeneration temperature was less than the cycle of $T_d=110^\circ\text{C}$.

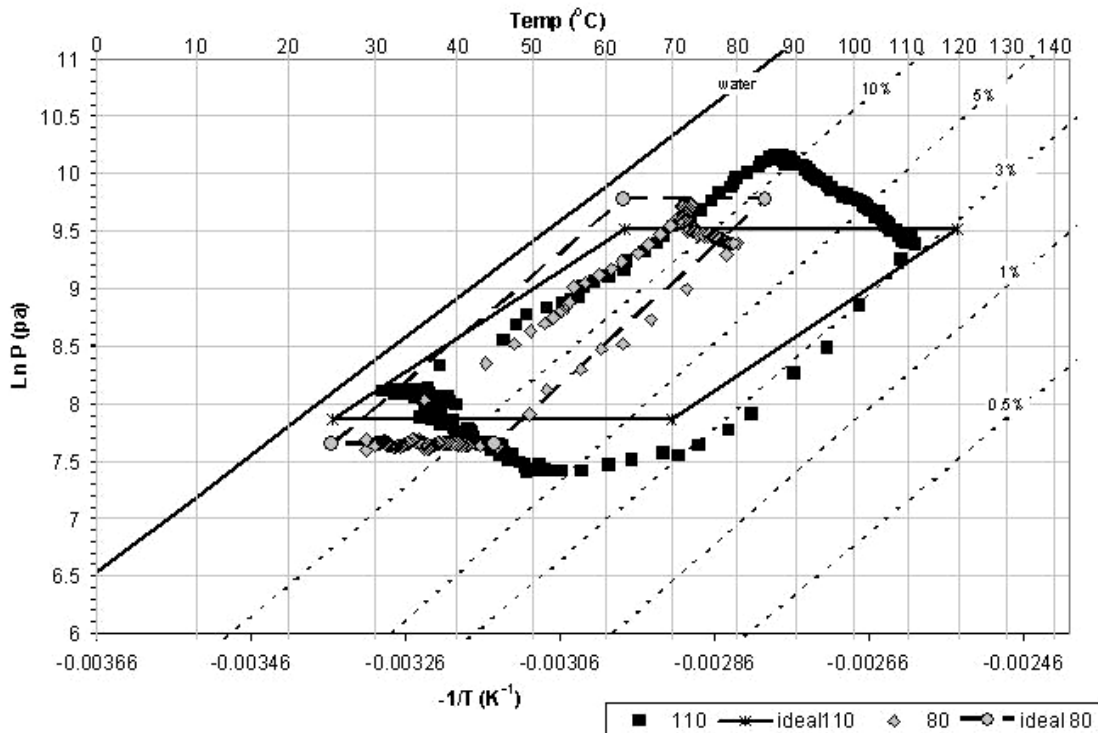


Figure 5.6. Experimental and theoretical cycles of intermittent AHP for 80°C and 110°C¹

Figure 5.7 depicts the variation of adsorbent bed pressure and temperature through the cycles with different regeneration temperatures. For both of the cycles, the adsorbent bed pressure, which theoretically should be constant, considerably varied during the isobaric desorption. It rapidly increased and then decayed to the desired condensation pressure. The main reason for this change of pressure was the insufficient cooling surface area of the condenser. The desorption rate of adsorbate from the adsorbent was higher than the condensation rate in the condenser. Since the wall of adsorbent bed was maintained at the desorption temperature, the pressure of adsorptive in the adsorbent bed has risen. The evaporator was designed properly; hence the pressure of adsorbent bed during adsorption process was almost constant for both of the regeneration temperatures. The period of desorption process for 110°C regeneration temperature was longer than that of 80°C. The amount of adsorbate which should be

¹ Isotheric diagrams were explained in detail in Chapter 6.

desorbed was greater and a longer period was required for attaining to 110°C in the adsorbent bed.

Figure 5.8 shows the variations of temperature and pressure of evaporator for both of the regeneration temperatures. The evaporator temperature of both cycles has almost remained constant. For both cycles, the evaporator was not at the evaporation temperature at the beginning of isobaric adsorption process; therefore a temperature drop occurred in the evaporator. At the beginning of adsorption process for cycle with 110°C regeneration temperature, a rapid adsorption was observed due to high adsorption capacity and consequently a steep pressure drop formed.

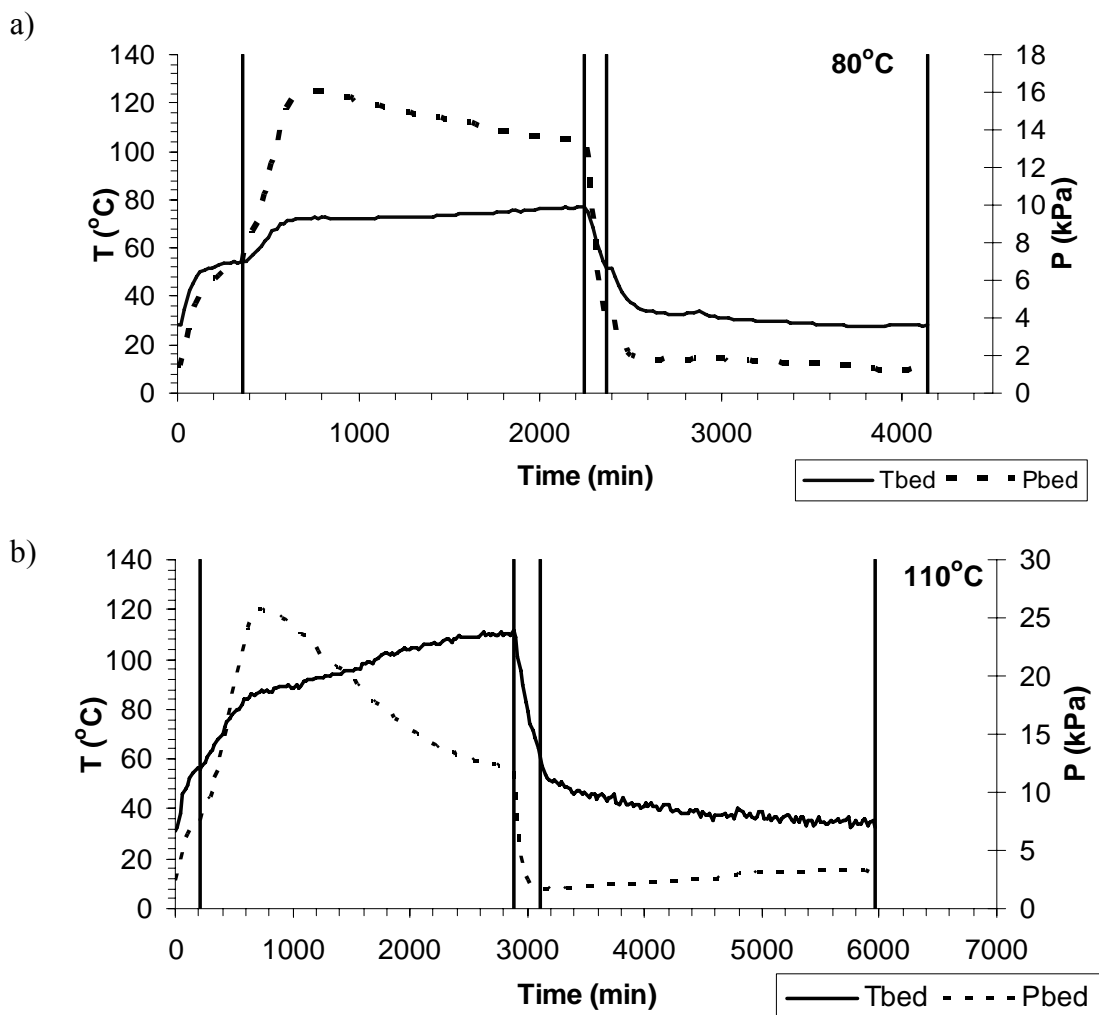


Figure 5.7. Change of pressure and temperature of adsorbent bed with time a) 80°C and b) 110°C¹

¹ Variation of bed temperatures which are measured with four thermocouples at different location of the bed according to time is shown in Figure C4 in Appendix C.

The variations of inlet and outlet temperatures of water which was supplied to heat the evaporator are illustrated in Figure 5.9 for both cycles. The water flow rate was 384.6 ml/min in the heat exchanger. As is seen, at the beginning of adsorption, the inlet and outlet temperature of water in the heat exchanger was same however; after a short period the temperature difference appeared. The average temperature difference between inlet and outlet ($\bar{T}_{inlet} - \bar{T}_{outlet}$) was 2°C for both of the 80°C and 110°C regeneration temperatures. The temperature difference between the inlet and outlet water decreased due to the diminishing of adsorption capacity as well as evaporation rate for both cycles.

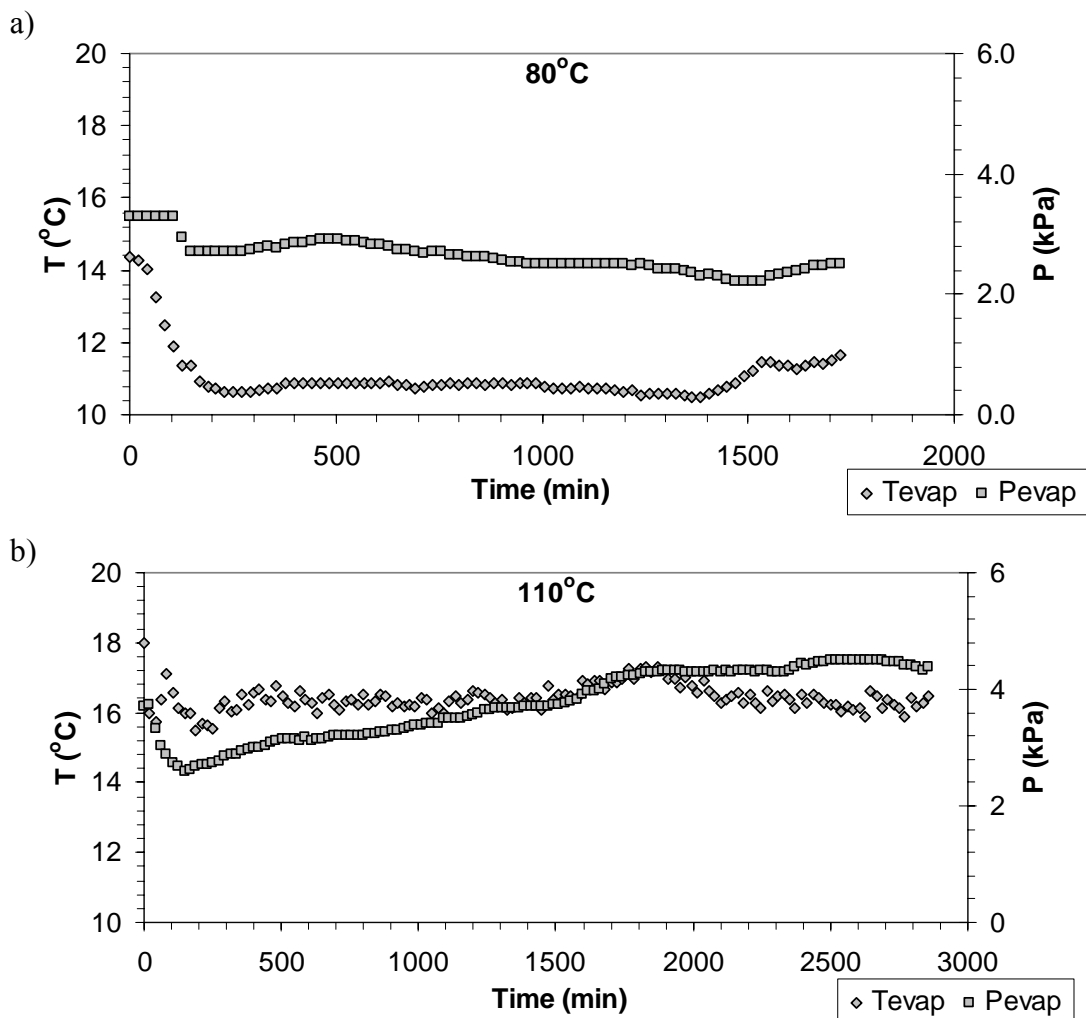


Figure 5.8. Pressure and temperature variations in the evaporator during isobaric adsorption a) 80°C and b) 110°C

Figure 5.10 illustrates the variation in the transferred heat from heat exchanger fluid to adsorptive during the adsorption process for 80°C and 110°C regeneration

temperatures. The total amount of transferred heat was found as 139 kJ kg_s^{-1} and 207 kJ kg_s^{-1} for the cycles with 80°C and 110°C regeneration temperatures, respectively. The difference between the transferred heat calculated from the inlet and outlet temperatures of heat exchanger fluid and heat transferred from evaporated adsorptive (Equation 2.7) may come from heat losses and measuring errors during observation of adsorptive level from sight glasses. For both cycles, the power of evaporator was not constant during the adsorption process. It was close to zero at the beginning of adsorption process and then rapidly increased. After attaining to a maximum value, it has decreased. It would approach to zero, if the process was continued. The slope of evaporator power for cycle with 110°C regeneration temperature was higher than the cycle with 80°C due to the greater adsorption capacity of adsorbent bed. The variation of evaporator power during the adsorption process may be considered as a disadvantage for this kind of heat pumps since a constant cooling power is needed for the most of industrial applications.

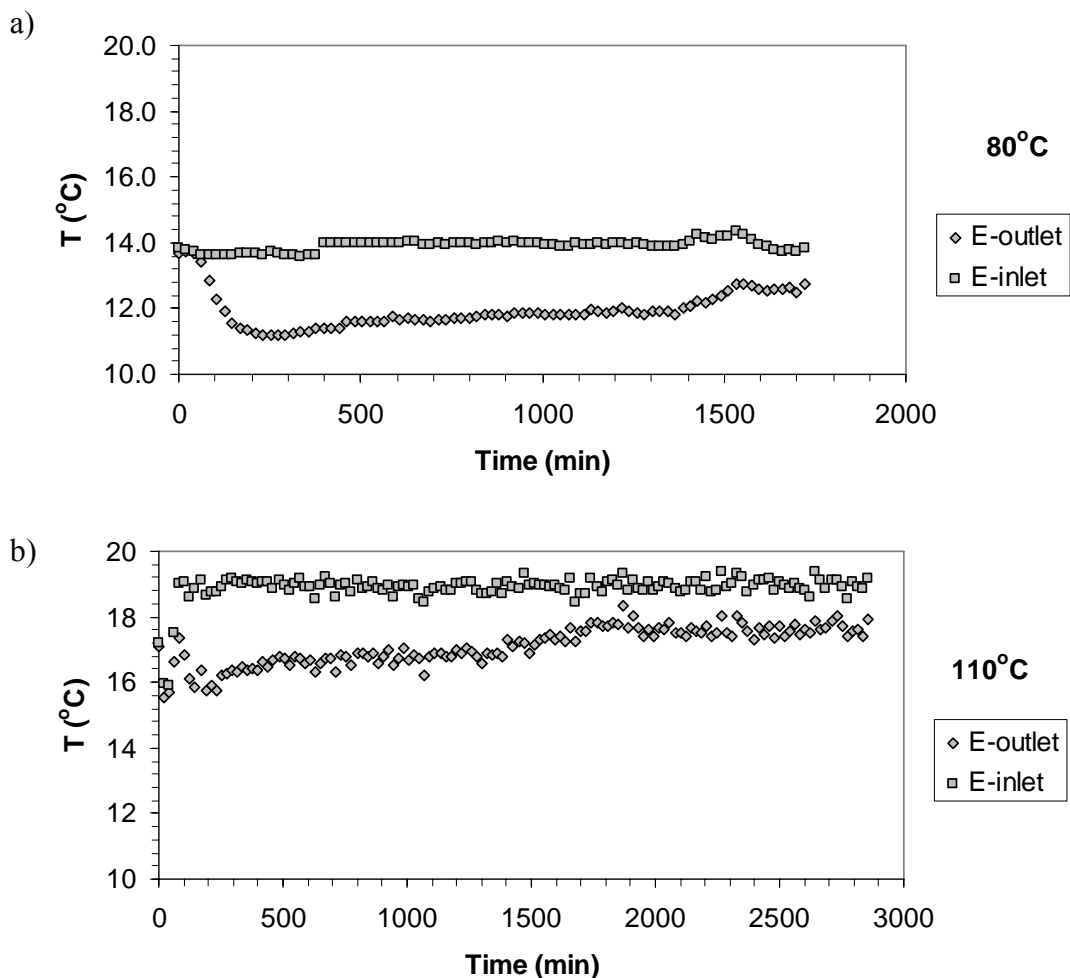


Figure 5.9. The variation of inlet and outlet temperatures of heat exchanger fluid in evaporator during isobaric adsorption process a) 80°C and b) 110°C

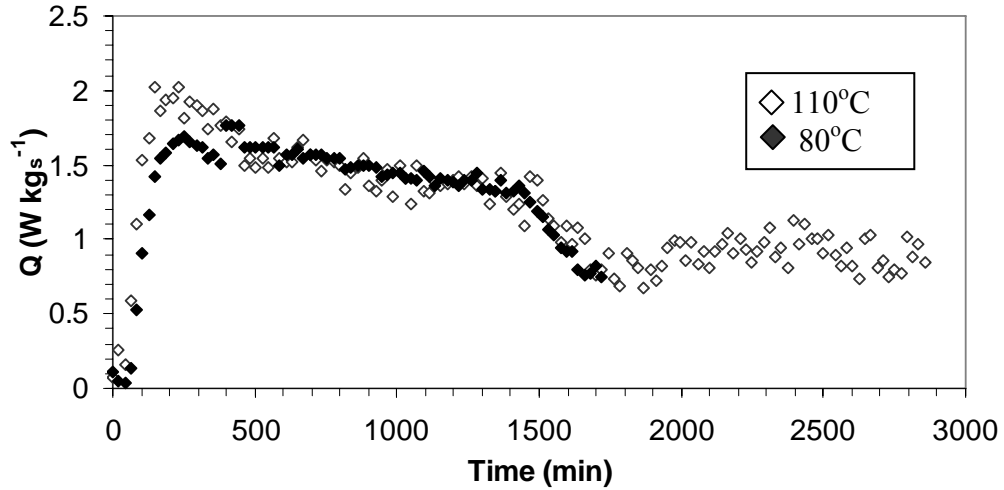


Figure 5.10. The variation of heat transfer from heat exchanger fluid to adsorptive during isobaric adsorption process

The amount of adsorptive evaporated in the evaporator during adsorption process for two different regeneration temperatures was shown in Figure 5.11. The amount of evaporated adsorptive for 110°C was considerably higher than 80°C. The amounts of adsorptive were 3.40L and 2L, for 110°C and 80°C, respectively. Figure 5.11 was plotted and followed during the experiment and the isobaric adsorption was stopped when the amount of adsorbed water tended to a constant value.

Figure 5.12 shows the amount of condensed water during the desorption process for 110°C and 80°C regeneration temperatures. For both cycles, the amount of adsorptive evaporated during the adsorption process was almost desorbed. The period of desorption process for higher regeneration temperature was longer since the amount of water, which should be desorbed, was higher.

The amounts of heat transferred from the evaporator, condenser and adsorbent bed were calculated by using Equations 2.3 through 2.6 are given in Table 5.4. The physical and thermodynamical properties of the materials used in AHP are given in Table C1 in Appendix C. The amounts of heat transfer between the AHP and heat reservoirs during four of the processes are represented in Table 5.5. The specific heat of all materials and isosteric heat of adsorption were assumed as constant.

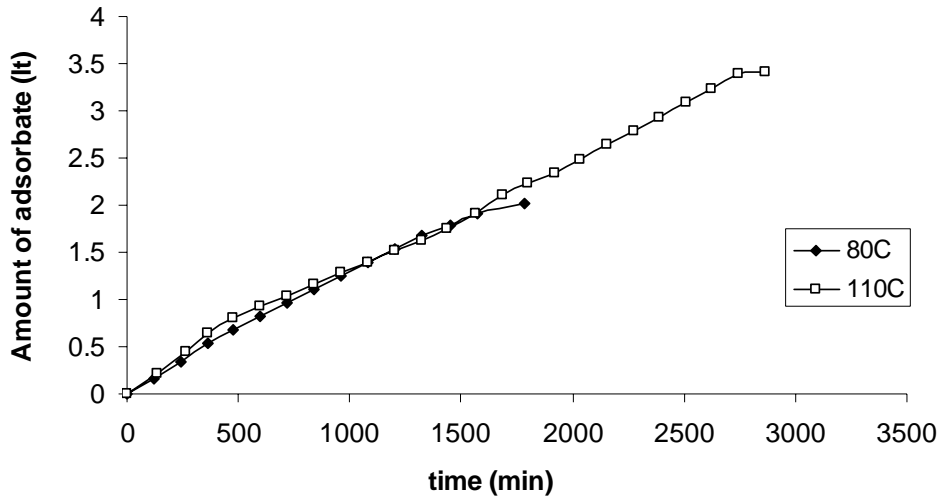


Figure 5.11. Change of amount of evaporated adsorptive with time

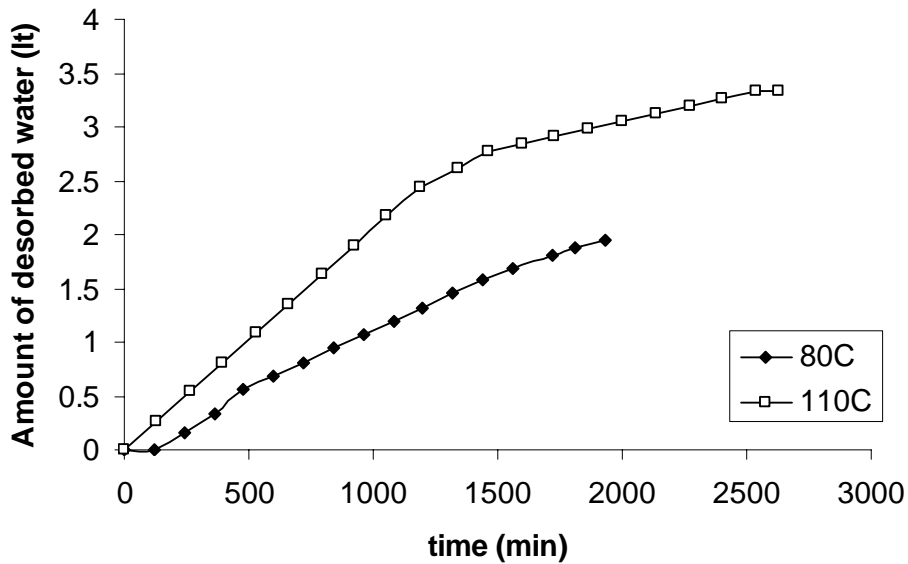


Figure 5.12. Change of amount of desorbed water with time during isobaric desorption

The heat transferred through the heat exchanger in the evaporator (Q_{ev}) is higher for the cycle 110°C than for the cycle 80°C due to higher amount of adsorbed water. The amount of heat given from regeneration heat source was essentially higher for cycle 110°C as expected. According to the first law, the summation of transferred heat between the adsorption heat pump and surroundings should be zero. The summation of presented values in Table 5.5 for cycles 110°C and 80°C are $\sum Q=14 \text{ kJ kg}_s^{-1}$ and $\sum Q=5 \text{ kJ kg}_s^{-1}$, respectively. The possible experimental errors in reading of the amount of evaporated and condensed water and heat losses may be the two reasons of these residuals. However, when we compare these differences to the transferred heat ($Q_{a-b} + Q_{b-c}$), it is observed that

the ratios were in an acceptable range as 2% and 4% for 80°C and 110°C cycles, respectively.

Table 5.5. The amounts of heat transfer between adsorption heat pump and heat reservoirs for two cycles

Heat transfer in processes (kJ kg ⁻¹)	Regeneration Temperature (°C)		Heating rate (°C/min)		Condenser cooling surface area (m ²)	
	80	110	0.14	1	0.038	0.226
Q _{a-b}	54	60	60	67	54	60
Q _{b-c}	170	328	328	395	170	328
Q _{c-d}	-49	-103	-103	-99	-49	-103
Q _{d-a}	-170	-271	-271	-344	-170	-271
Q _{ev}	118	203	203	265	118	203
Q _{cond}	-115	-198	-198	-257	-115	-198

The coefficient of performance and specific heating/cooling power values were calculated for the cycles and presented in Table 5.6. The COP values for cooling were found as 0.53 and 0.52 and the COP for heating were determined as 1.49 and 1.47 for the cycles with 80°C and 110°C desorption temperature. The results show that the COP values of two cycles were almost the same although the amounts of adsorbate were different from each other. The total entropy generations of the cycles were calculated by Equation 2.19 and given in Table 5.6. The total entropy generation for cycles with 80°C and 110°C desorption temperature were 2.16 kJ K⁻¹ and 7.12 kJ K⁻¹, respectively. The total entropy generation of cycle 110°C was higher than that of cycle 80°C since the irreversibilities in the system may have been increased due to high amount of transferred heat. The COP_{exp} values for the cooling process which can be determined by Equation 2.22 were found as 1.07 and 1.49 for cycles of 80°C and 110°C, respectively. These values were 52% and 64% lower than the COP_C values. These differences are due to the irreversibilities formed during the cycle. The difference between COP_{exp} and COP_{ref} indicates that there are heat losses and/or experimental errors in reading of the evaporated and condensed water. The second law efficiencies were found as 0.48 and 0.36 for cycle 80°C and 110°C, respectively calculated with the Equation 2.23.

The significant differences between the performances of two cycles were observed on the SCP and SHP values of the system. The SCP and SHP values were found as 0.47 W kg⁻¹ and 1.34 W kg⁻¹ for 80°C, 0.57 W kg⁻¹ and 1.60 W kg⁻¹ for 110°C

regeneration temperatures. Although the period of cycle with 80°C regeneration temperature was shorter, the amount of circulated adsorptive was smaller than that of 110°C. Therefore, the SCP and SHP values of lower regeneration temperature were smaller.

Table 5.6. Performance indicators for two cycles

Parameters	Regeneration Temperature (°C)		Heating rate (°C/min)		Condenser cooling surface area (m ²)	
	80	110	0.14	1	0.038	0.226
COP_{ref}	0.53	0.52	0.52	0.57	0.52	0.53
COP_h	1.49	1.47	1.47	1.52	1.47	1.48
SCP (W kg_s⁻¹)	0.47	0.57	0.57	0.80	0.57	0.64
SHP (W kg_s⁻¹)	1.34	1.60	1.60	2.12	1.60	1.76
COP_{exp}	1.07	1.49	1.49	1.95	1.49	2.27
COP_C	2.22	4.15	4.15	5.28	4.15	7.15
η_{II}	0.48	0.36	0.36	0.37	0.36	0.32
ΔS (kJ K⁻¹)	2.16	7.12	7.12	8.62	7.12	7.27

5.2.1 Effect of Heating Rate in Regeneration

In Figure 5.6, comparing the expected ideal cycles with experimental cycles, the isobaric desorption process of cycles were significantly different in the isobaric desorption process of the ideal cycle. In the isobaric desorption process of experimental cycles, pressure increased rapidly at the beginning of the process. The increasing adsorbent bed pressure may be caused from rapid increasing of adsorbent bed temperature during desorption process. The increment of pressure may be reduced by adjusting the heating rate in regeneration. For this purpose, the adsorbent bed surface temperature was increased with 0.14°C min⁻¹ and 1°C min⁻¹ during the isobaric desorption process as shown in Figure 5.13. The regeneration temperatures were 120°C for both cycles. The effect of heating rate of surface temperature on the performance of the system was also investigated and results are shown in Table 5.5 and 5.6. For high (1°C min⁻¹) heating rate, the adsorbent bed pressure rapidly increased to 30kPa and then reduced to 13kPa. The isobaric desorption process has taken 2457 minutes for high heating rate. For low (0.14°C min⁻¹) heating rate, the pressure of adsorbent bed raised

slowly to 26kPa and then decreased to 12kPa. The isobaric desorption process of $0.14^{\circ}\text{C min}^{-1}$ heating rate continued for 2667 minutes. The COP of $1^{\circ}\text{C min}^{-1}$ heating rate was higher than that of $0.14^{\circ}\text{C min}^{-1}$ heating rate, since the amount of adsorbed water vapor for $1^{\circ}\text{C min}^{-1}$ heating rate was 4.4L and 3.2L for $0.14^{\circ}\text{C min}^{-1}$ heating rate. The SCP and SHP values of $1^{\circ}\text{C min}^{-1}$ heating rate was also higher than that of $0.14^{\circ}\text{C min}^{-1}$ heating rate due lower desorption process time that affects the total cycle time. When comparing total entropy generations, for $1^{\circ}\text{C min}^{-1}$ heating rate the total entropy generation was higher than that for $0.14^{\circ}\text{C min}^{-1}$ heating rate, since irreversibilities of system was increased with rapid heating rate. The second law efficiencies indicated that, two cycles have the same efficiency although heating rates of cycles were different. Consequently, the scope should be operating the system for obtaining a cycle as similar as the ideal. The rapid increment of the pressure may cause other problems in long period such as leakage problem, shifting operation conditions etc.

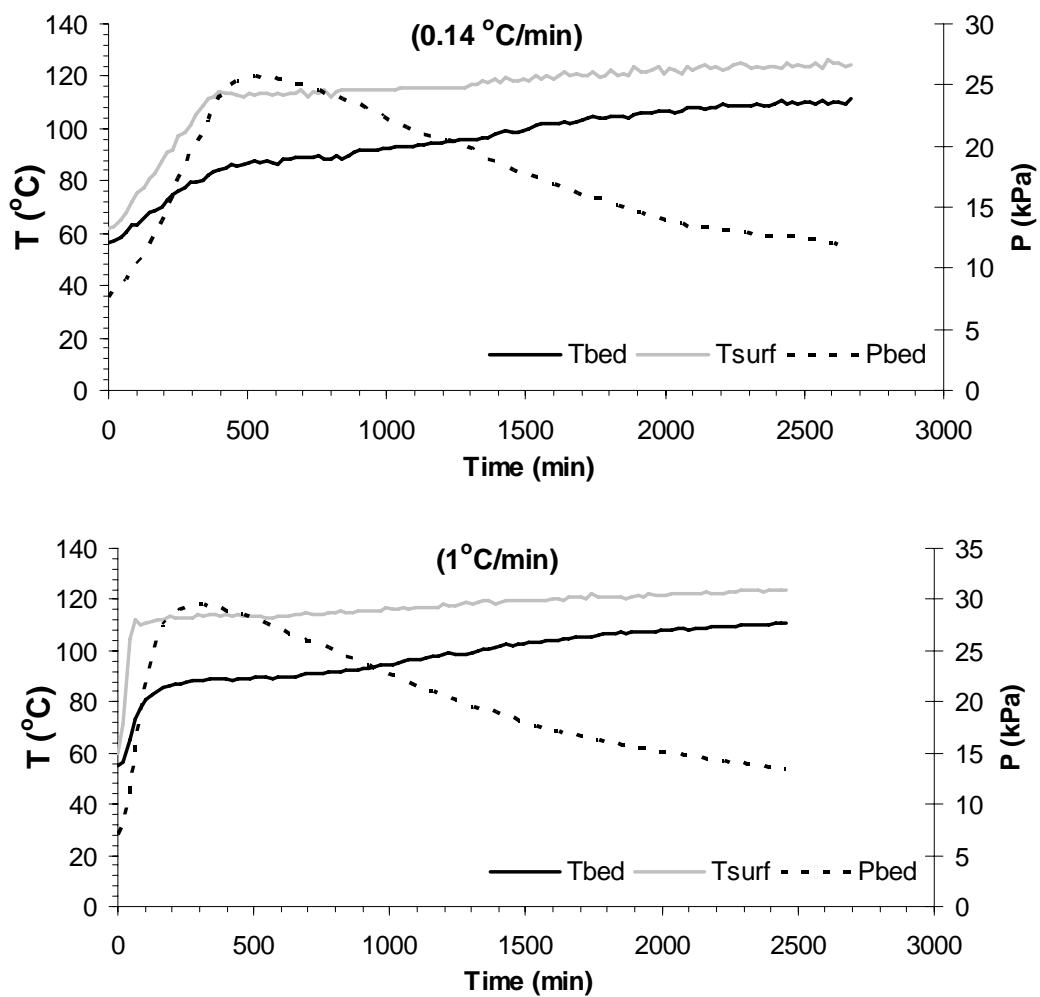


Figure 5.13. Effect of heating rate on cycle during isobaric desorption process

5.2.2 Effect of Condenser Design

Figure 5.14 illustrates the effect of condenser cooling surface area on cycle during the isobaric desorption process. The rapid increment of pressure during desorption process may be caused by inefficient condensing capacity of condenser. The increasing pressure in adsorbent bed indicates desorption of adsorbate from adsorbent. This adsorbate should be condensed in the condenser for preventing pressure fluctuation in the adsorbent bed. In Figure 5.6, the desorbed adsorbate was not condensed immediately in the condenser since the adsorbent bed pressure increased rapidly. The desorption process of cycles were obtained of 0.14°C/min heating rate and 120°C adsorbent bed surface temperature. The effect of cooling surface area of condenser on the performance of system was also investigated and results are showed in Table 5.5 and 5.6. In Figure 5.14, two different cooling surface areas were represented as 0.038m² and 0.226m². The adsorbent pressure rose to 26kPa for 0.038m² cooling surface area of condenser. The adsorbent pressure of cycle (0.226m² cooling surface area of condenser) increased to 20kPa and remained constant during the desorption process period. The amount of desorbed water from adsorbent was condensed rapidly in condenser which has 0.226m² cooling surface area thus; adsorbent bed pressure did not increase that much for the condenser having lower cooling surface area. The amount of heat transferred between the processes and performance indicators for both cycles are very close each other as shown in Table 5.5 and 5.6. The desorption process period for cycle of 0.226m² cooling surface area was 300 minutes shorter than that of cycle of 0.038m² cooling surface area due to the higher condensation capacity. The shorter desorption period affects the total cycle period thus, the SCP and SHP values of cycle having 0.226m² cooling surface area were slightly higher than that of cycle having 0.038m² cooling surface area.

The results indicate that the proper condenser design should be performed since the proper condenser design may increase the condensation of desorbed water during the isobaric desorption process which is one of the reasons to obtain a long period of cycle. In the design and construction of the condenser, throttling effect should be taken into account, since connection of adsorbent bed and condenser with pipes having small diameter may cause throttling effect.

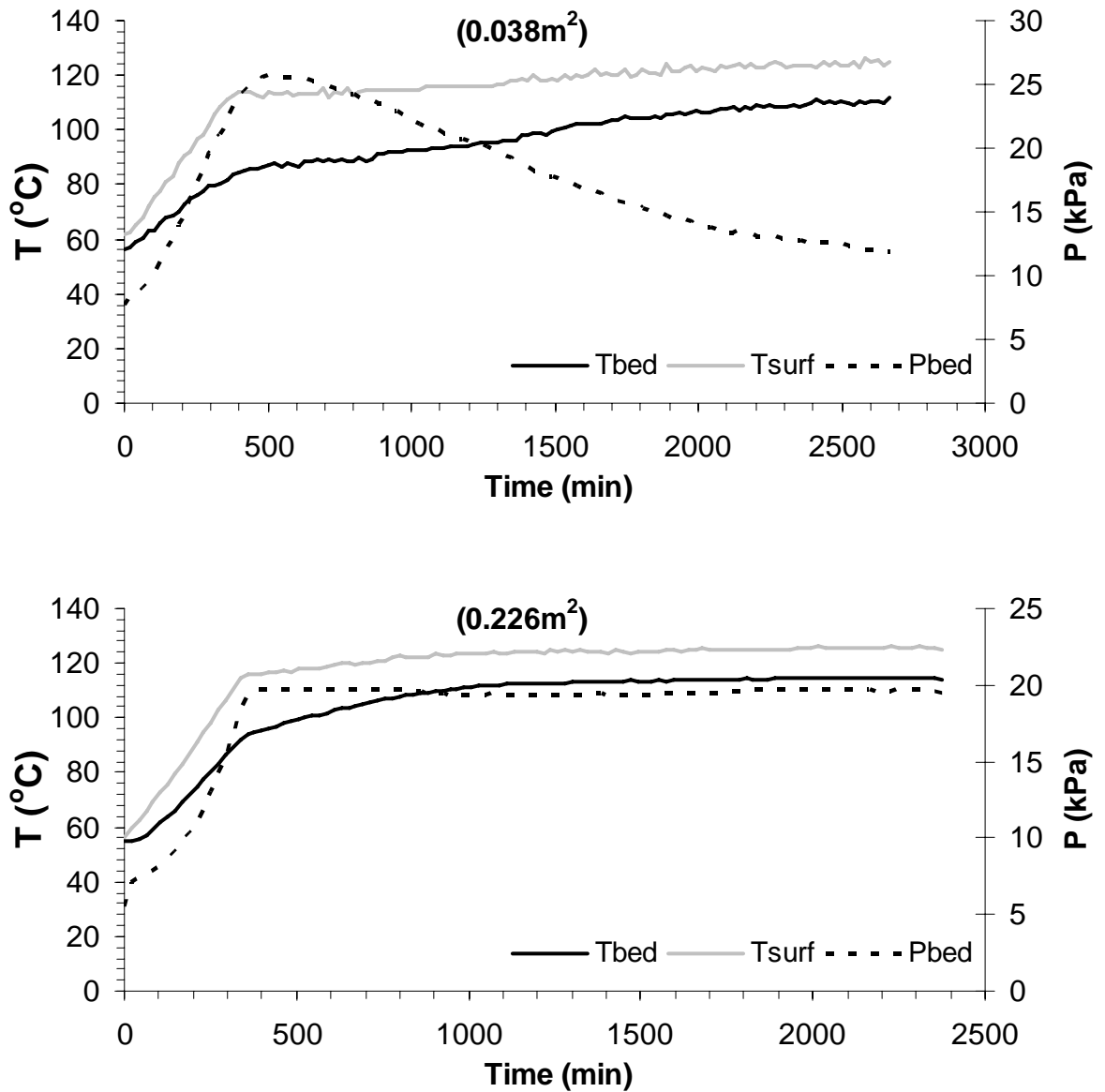


Figure 5.14. Effect of cooling surface area of condenser on cycle

5.3 Heat Transfer Enhancement with Metal Additives

For reducing the cycle period, the heat transfer rate in the adsorbent bed should be improved. The simple and cheapest way was to mix the silica gel with highly thermal conductive additives such as metal additives. However, it should be considered that the mass transfer resistance in the adsorbent bed should not be increased with the addition of metal additives. Therefore, for the selection of appropriate metal type and size, the following experiments were done and results were represented by graphically and in tables. The results were compared with the theoretical model which was proposed by

Maxwell. Figure 5.15 shows the variation of center temperature with time for four of the metal pieces and two different piece sizes as 1.0 – 2.8mm and 2.8 – 4.75mm. For all of the metal pieces, the initial temperature was 40°C and it declined with the time and then reached to 5°C which was the bath temperature. The decreasing rate of the temperature has shown variability with the material and the size of pieces. Table D2 in Appendix D presents the thermal properties of four used materials. Aluminum had the minimum heat storage capacity of $2.4 \times 10^6 \text{ J m}^{-3} \text{ K}^{-1}$, whereas the heat storage capacity values of brass, copper and stainless steel were $3.2 \times 10^6 \text{ J m}^{-3} \text{ K}^{-1}$, $3.4 \times 10^6 \text{ J m}^{-3} \text{ K}^{-1}$ and $3.8 \times 10^6 \text{ J m}^{-3} \text{ K}^{-1}$, respectively. The highest heat transfer rate was expected in the bed containing the aluminum pieces and the lowest heat transfer rate in the bed may be found for the stainless steel pieces. Figure 5.15 validates the expectation and the lowest and highest decreasing rates of the center temperature were observed for the stainless steel with 2.8 – 4.75mm and the aluminum with 1.0 – 2.8mm, respectively. The cooling rate of bed with stainless steel piece of 1.0 – 2.8mm was also slow but not as much as that of stainless steel with 2.8 – 4.75mm, indicating the effect of metal size. The heat transfer rate through the bed has enhanced with the decreasing size of metal pieces due to the increasing contact area between the particles. The curves of the bed containing copper and brass pieces were between the curves of aluminum and stainless steel pieces as is seen in Figure 5.15. The temperature variation of aluminum and copper with 2.8 – 4.75mm overlaps which can be originated from their different shapes.

Table 5.7 shows the calculated thermal diffusivity of the bed with metal pieces whose center temperatures are presented in Figure 5.15. The maximum thermal diffusivity was observed for the aluminum pieces with 1.0 – 2.8mm and this highest thermal diffusivity value was followed by the copper with 1.0 – 2.8mm, aluminum with 2.8 – 4.75mm, brass, St-St with 1.0 – 2.8mm and St-St with 2.8 – 4.75mm. The thermal diffusivity of the bed containing Al with 1.0 – 2.8mm was 26 times greater than that of adsorbent bed with 100wt% silica gel granules. Deviation values which are shown in Tables 5.7 and 5.8 indicate the fitting grade between theoretical and experimental data. The standard deviation was calculated based on the difference between theoretical and experimental values. The highest thermal conductivity was observed for aluminum with 1.0 – 2.8mm and it decreased for the other materials as expected. The thermal conductivity of the bed having 15wt% aluminum with 1.0 – 2.8mm was approximately 2.5 times greater than that of bed having solely silica gel granules.

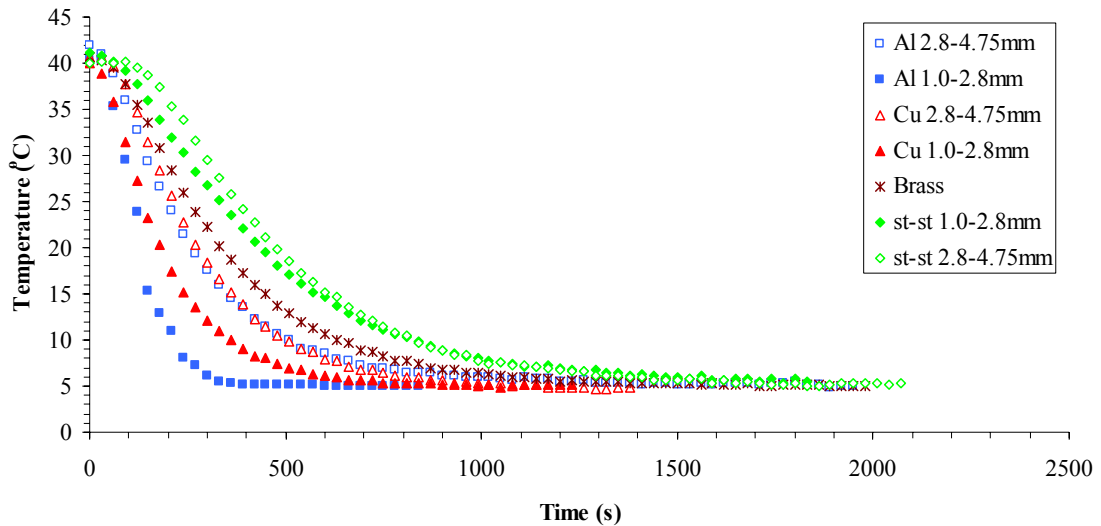


Figure 5.15. Variations of temperature of metal pieces according to dimensions

Figures from 5.16 to 5.19 illustrate the variation of the adsorbent bed center temperature with time for four different cases in which the metal pieces (1.0 – 2.8mm) were mixed with the silica gel at different weight ratios which were 0%, 10wt%, 15wt% and 100wt%. For all cases, the lowest heat transfer rate belongs to the bed with pure silica gel while the beds with 100 wt% metal pieces have the highest rate of heat transfer. The increase of percentage of metal pieces improves the heat transfer through the bed.

Table 5.7. The thermal diffusivity and thermal conductivity of the metal pieces

Samples	Thermal Diffusivity ($\text{m}^2 \text{s}^{-1}$)	Thermal conductivity ($\text{Wm}^{-1} \text{K}^{-1}$)	Deviation
Silica gel	2.1×10^{-7}	0.159	0.027
Al 1.0-2.8mm	1.7×10^{-6}	4.150	0.042
Al 2.8-4.75mm	8.2×10^{-7}	2.000	0.023
Cu 1.0-2.8mm	9.3×10^{-7}	3.200	0.016
Cu 2.8-4.75mm	7.6×10^{-7}	2.610	0.013
Brass	4.1×10^{-7}	1.970	0.019
St-St 1.0-2.8mm	4.7×10^{-7}	1.770	0.024
St-St 2.8-4.75mm	4.2×10^{-7}	1.580	0.019

Table 5.8. Thermal properties of mixtures of silica gel – metal (1.0-2.8mm) and improvements

Samples	Thermal Diffusivity ($\text{m}^2 \text{s}^{-1}$)	Thermal conductivity ($\text{Wm}^{-1} \text{K}^{-1}$)	Deviation	Improvement of Diffusivity (%)	Improvement of Conductivity (%)
5%Al-Si	3.0×10^{-7}	0.252	0.040	42.9	58.5
10%Al-Si	3.8×10^{-7}	0.351	0.037	81.0	120.8
15%Al-Si	4.0×10^{-7}	0.403	0.036	90.5	153.5
5%Cu-Si	2.3×10^{-7}	0.205	0.045	9.5	28.9
10%Cu-Si	2.6×10^{-7}	0.266	0.039	23.8	67.3
15%Cu-Si	2.8×10^{-7}	0.324	0.029	33.3	103.8
5%Brass-Si	2.6×10^{-7}	0.229	0.044	23.8	44.0
10%Brass-Si	2.8×10^{-7}	0.281	0.032	33.3	76.7
15%Brass-Si	3.1×10^{-7}	0.349	0.040	47.6	119.5
5%St-St-Si	2.2×10^{-7}	0.199	0.027	4.8	25.2
10%St-St-Si	2.4×10^{-7}	0.254	0.024	14.3	59.7
15%St-St-Si	2.6×10^{-7}	0.314	0.023	23.8	97.5

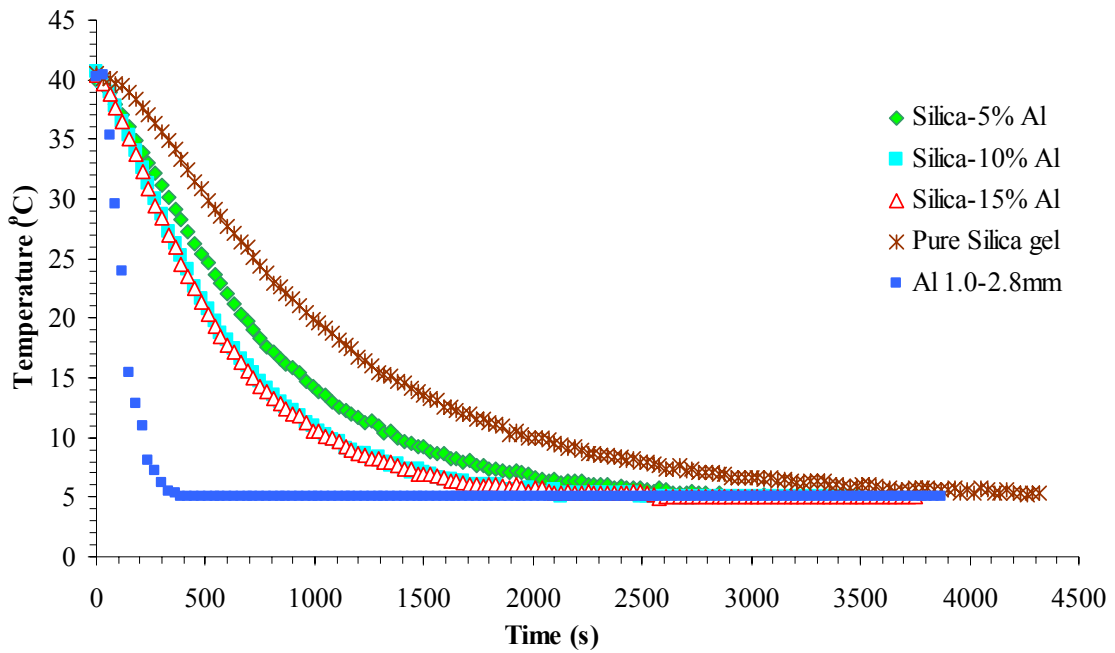


Figure 5.16. Variations of temperature of Si-Al mixture, silica gel and aluminum

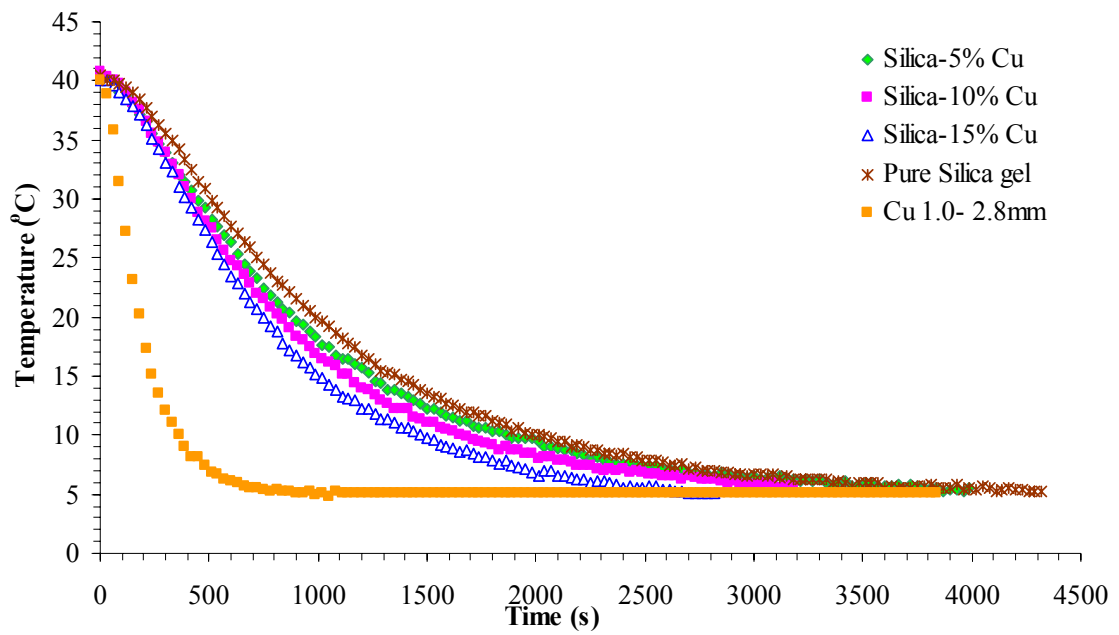


Figure 5.17. Variations of temperature of Si-Cu mixture, silica gel and copper

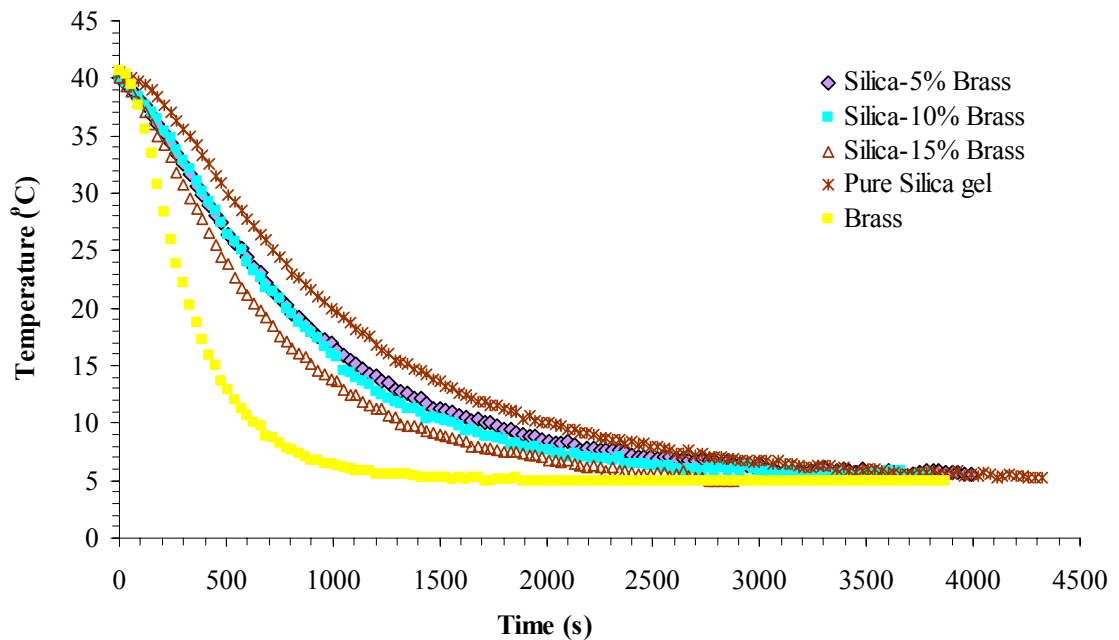


Figure 5.18. Variations of temperature of Si-Brass mixture, silica gel and brass

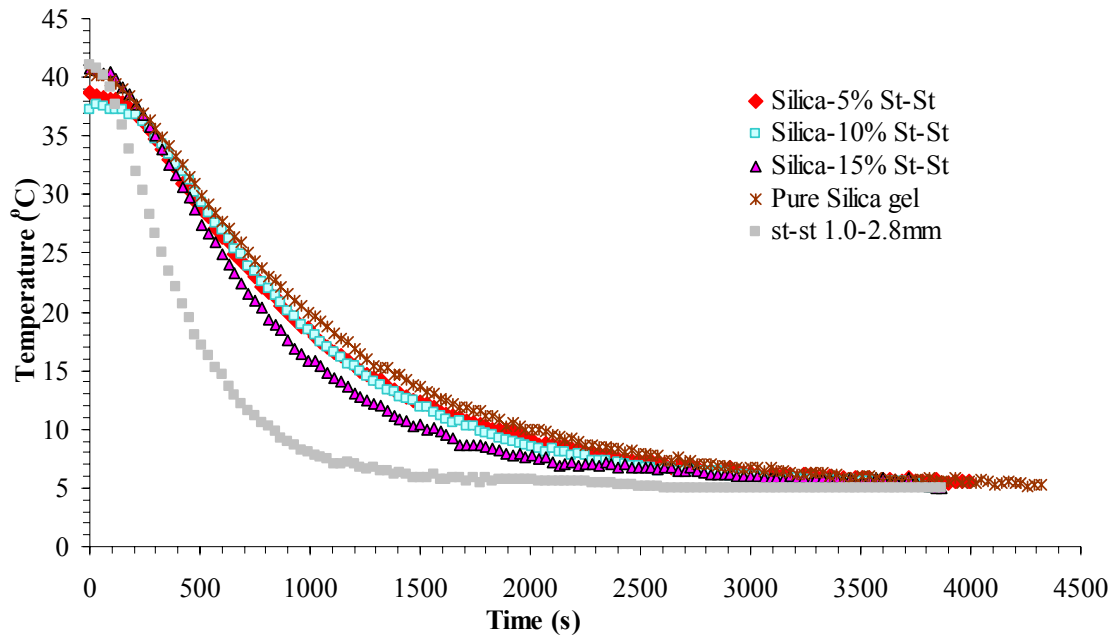


Figure 5.19. Variations of temperature of Si-St-St mixture, silica gel and stainless steel

The temperature variation of silica gel – metal piece mixtures versus time is illustrated in Figure 5.20. The mixing ratio was kept at 15wt% for all of the mixtures. The bed with aluminum additive has reached to the equilibrium faster than the other mixtures. As mentioned before, the thermal diffusivity of aluminum was higher than the other experimented metals; hence the decreasing rate of the center temperature for aluminum mixture is expected to be higher. The interesting point of Figure 5.20 is that the silica gel-brass mixture bed has cooled faster than the silica gel-copper bed, though; the rate of heat transfer in the bed filled completely with the brass was less than that of bed with copper. The special shape of brass piece may have improved its cooling rate.

Table 5.8 illustrates the calculated thermal diffusivity and thermal conductivity of the silica gel – metal piece mixtures with size of 1.0 – 2.8mm. The enhanced percentage of thermal diffusivity and thermal conductivity of the silica gel bed by adding metal additives are also calculated and revealed in the same table. The maximum enhancement of the thermal diffusivity of 90.5% was observed for 15wt% of Al additive. For the same weight percentage, brass, copper and stainless steel additives follow the aluminum additive with 47.6%, 33.3% and 23.8% enhancement rates. The effective thermal conductivity of the silica gel bed minimally was improved for 25.2% by adding 5wt% of stainless steel pieces with 2.8 – 4.75mm size and the maximum improvement was observed as 153.5% by adding 15wt% aluminum pieces with 1.0 – 2.8mm size.

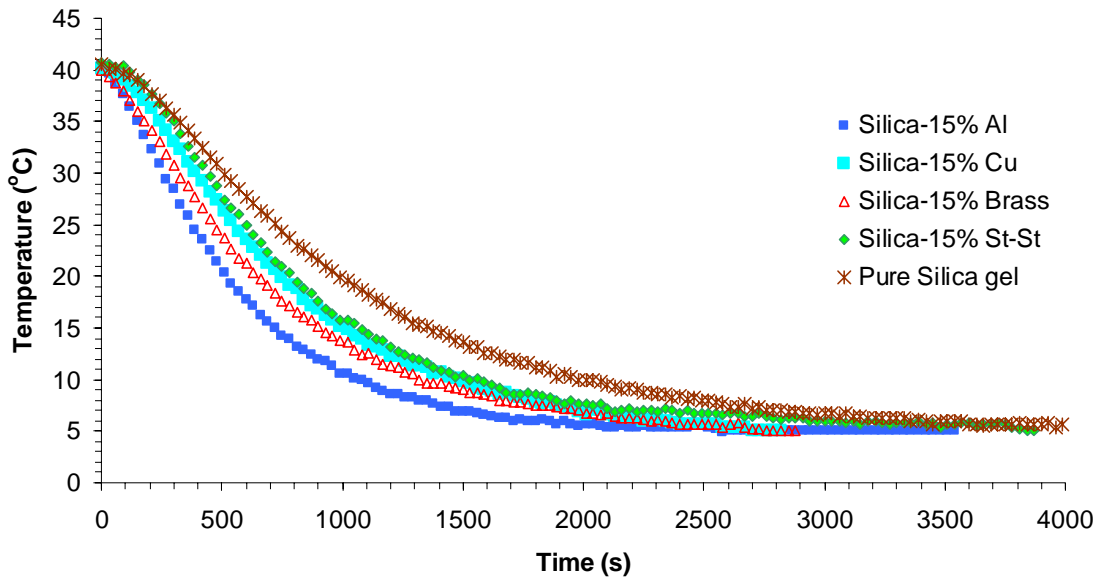


Figure 5.20. Comparison of temperature profile of silica gel-metal pieces mixture and pure silica gel

In the literature, only one study on this area was found. Eltom and Sayigh (1994) have researched the effect of copper and graphite powder (without any treatment) addition on thermal conductivities of charcoal and they found that those metal additives improve the thermal conductivity of charcoal between 2 and 25%. The aluminum additive improves the thermal features of the silica gel bed more than the other metal additives due to high thermal conductivity and low thermal energy storage capacity. Hence, the silica gel – aluminum mixture may be a good choice for the heat transfer enhancement in a granular adsorbent bed. Moreover, enhancement of heat transfer rate in the granular bed decreased the cycle period of AHP and increased SCP of adsorption heat pump. Because the low SCP and long cycle period were the main obstacles on application of adsorption heat pump.

In the literature, there are many relations for predicting effective thermal diffusivity of heterogeneous solids mixture, but the comprehensive relation has not defined yet for complex non-spherical inclusions (Tavman 1998, Bird, et al. 2002). A comparison between the obtained values shows that Maxwell equation may be an appropriate relation for this kind of adsorbent beds. Table 5.9 illustrates the effective thermal conductivity obtained based on the experimental results and Maxwell relation (Equation 4.4). A term called as shape factor, g , is seen in the Equation 4.5. The shape of copper, aluminum and stainless steel were assumed as spherical, and shape of brass was assumed as complex non-spherical inclusion. The thermal conductivity values

evaluated by using the Maxwell relation were close to the values based on the experimental results. The error values which were evaluated by the differentiation of experimental and theoretical values were in an acceptable range.

Table 5.9. Effective thermal conductivity of silica gel – metal (1.0-2.8mm) mixtures

Sample	Effective Thermal Conductivity ($\text{Wm}^{-1}\text{K}^{-1}$)	Error (%)
5%Al-Si	0.238	5.6
10%Al-Si	0.329	6.4
15%Al-Si	0.429	-6.5
5%Cu-Si	0.197	3.7
10%Cu-Si	0.232	12.9
15%Cu-Si	0.265	18.1
5%Brass-Si	0.220	4.0
10%Brass-Si	0.265	5.8
15%Brass-Si	0.314	10.2
5%St-St-Si	0.211	-6.3
10%St-St-Si	0.255	-0.4
15%St-St-Si	0.298	5.0

Although the increase of metal additive in the adsorbent bed enhances heat transfer rate through the bed, it reduces the loading of silica gel granules in the bed. The decrease in the adsorbent amount reduces theoretical amount of adsorbed water. Figure 5.21 shows the changes in amount of adsorbate and the thermal diffusivity of silica gel – Al mixture with the aluminum loading. The amount of adsorbate has decreased with the increasing aluminum amount in the mixture due to the reducing amount of silica gel in the mixture. However, the effective thermal diffusivity of mixture has increased with further Al loading. The optimum weight percentage for the mixture of aluminum pieces with 1-2.8 mm size and silica gel granules with 3-5mm size should be determined by considering both thermal diffusivity and amount of adsorbate.

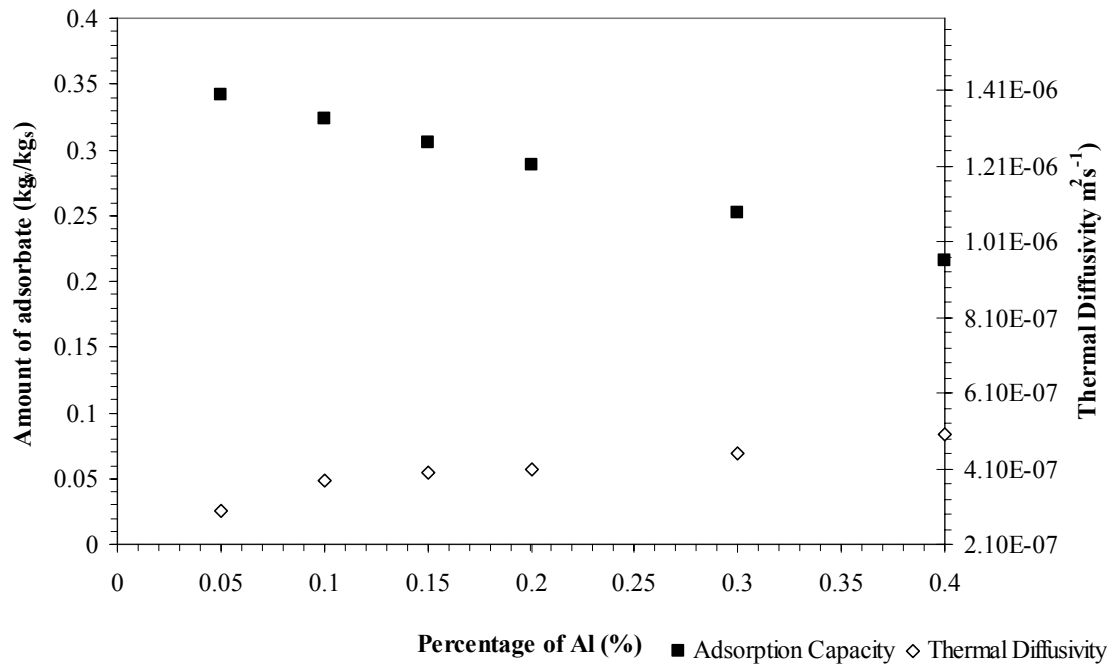


Figure 5.21. Amount of adsorbate and thermal diffusivity of silica gel – Al mixture with respect to aluminum concentration in mixture

5.4 Additive Loaded AHP-2

The SCP and SHP values of AHP-2 were still low, although the enhancement in the heat transfer area of adsorbent bed was supplied by twelve main fins and four little fins on the each main fin. After measuring the thermal diffusivities of metal additives, the aluminum was selected as the best additive for improving the heat transfer rate of adsorbent bed of AHP-2. The heat transfer rate of the adsorbent bed of AHP-2 was enhanced by homogeneously mixing the 10wt% of aluminum metal pieces of 1- 2.8mm size with the silica gel granules. Table 5.10 illustrates the operational condition of Al-loaded AHP-2 which was kept similar with the operation conditions of AHP-2 without Al metal piece additives. Figure 5.22 reveals experimental results of pressure versus temperature behavior of Al-loaded second AHP and ideal (expected according to operational conditions) cycle on the Classius-Clapeyron diagram. Isobaric and isosteric processes of Al-loaded second AHP cycle can be easily seen. The experimental cycle is very close to ideal cycle.

Figure 5.23 shows the variation of adsorbent bed pressure and temperature through the cycles with and without Al pieces additive. For both cycles, the adsorbent bed pressures during isobaric desorption process rapidly increased and remained constant. The adsorbent bed pressure reached 25kPa for AHP-2 without metal additives

and 15kPa for metal loaded setup. The adsorbent bed pressure for metal loaded setup did not increase as much as the setup without metal additives. The enhancement of heat transfer rate by addition of aluminum pieces in the adsorbent bed provides homogeneous adsorbent bed temperature. Hence, desorption of water from the adsorbent may be regular and also condensation of this desorbed water may occur regularly. The enhancement of the heat transfer rate in adsorbent bed reduced the duration of cycle processes. Thus, whole processes (isobaric and isosteric) operated significantly in shorter periods than processes of setup without metal additives.

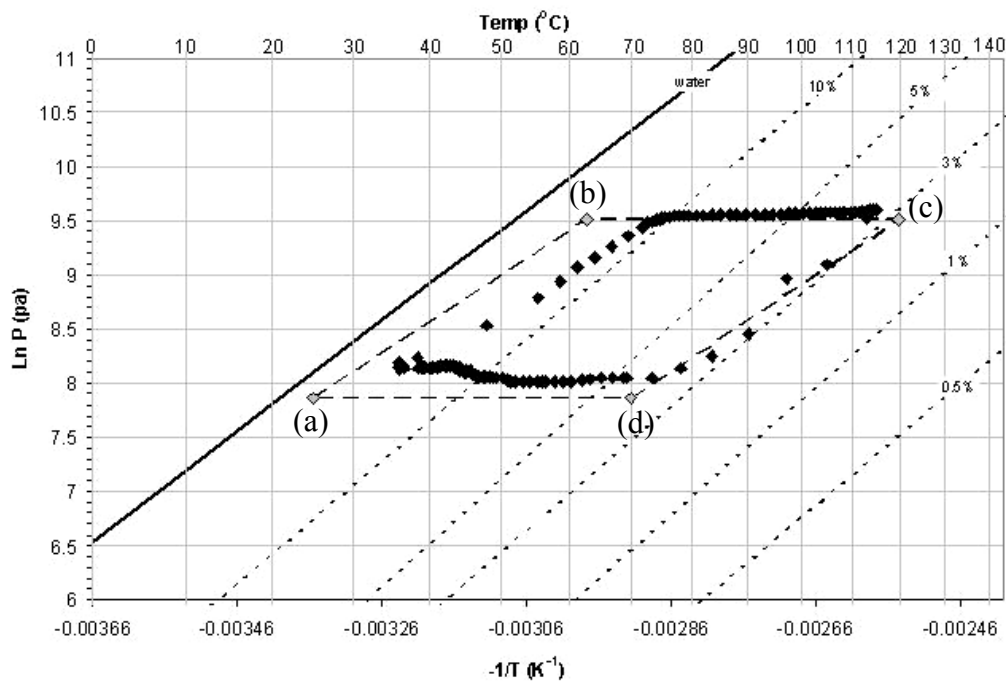


Figure 5.22. Temperature and pressure profile of Al-loaded second setup (dots) and ideal cycle (dashed line)¹²

Figure 5.24 depicts the variation of inlet and outlet temperatures of heat exchanger fluid in evaporator during the isobaric adsorption process for AHP-2 without metal additives and metal loaded. At the beginning of isobaric adsorption, the inlet and outlet temperature of water in the heat exchanger was same for both cases. However; after a short period the temperature difference can be observed. The temperature between the inlet and outlet water were close to each other due to the filling of adsorption capacity for both cycles. Considering the temperature differences, the

¹ Isosteric diagrams were explained in detail in Chapter 6.

² All obtained cycles from Al loaded AHP-2 were illustrated in Figure C3 in Appendix C.

isobaric adsorption process was stopped with closing the valve 2 and isosteric heating process was started by opening the jacket type heater.

Table 5.10. The operation conditions for two cycles

Parameters	Second setup	Second setup
	without Al-pieces	with Al-pieces
T_a (°C)	30	26
T_b (°C)	76	71
T_c (°C)	110	116
T_d (°C)	69	71
T_{ev} (°C)	17	19
T_{cond} (°C)	26	31
P_{ev} (kPa)	5	4.8
P_{cond} (kPa)	25	8

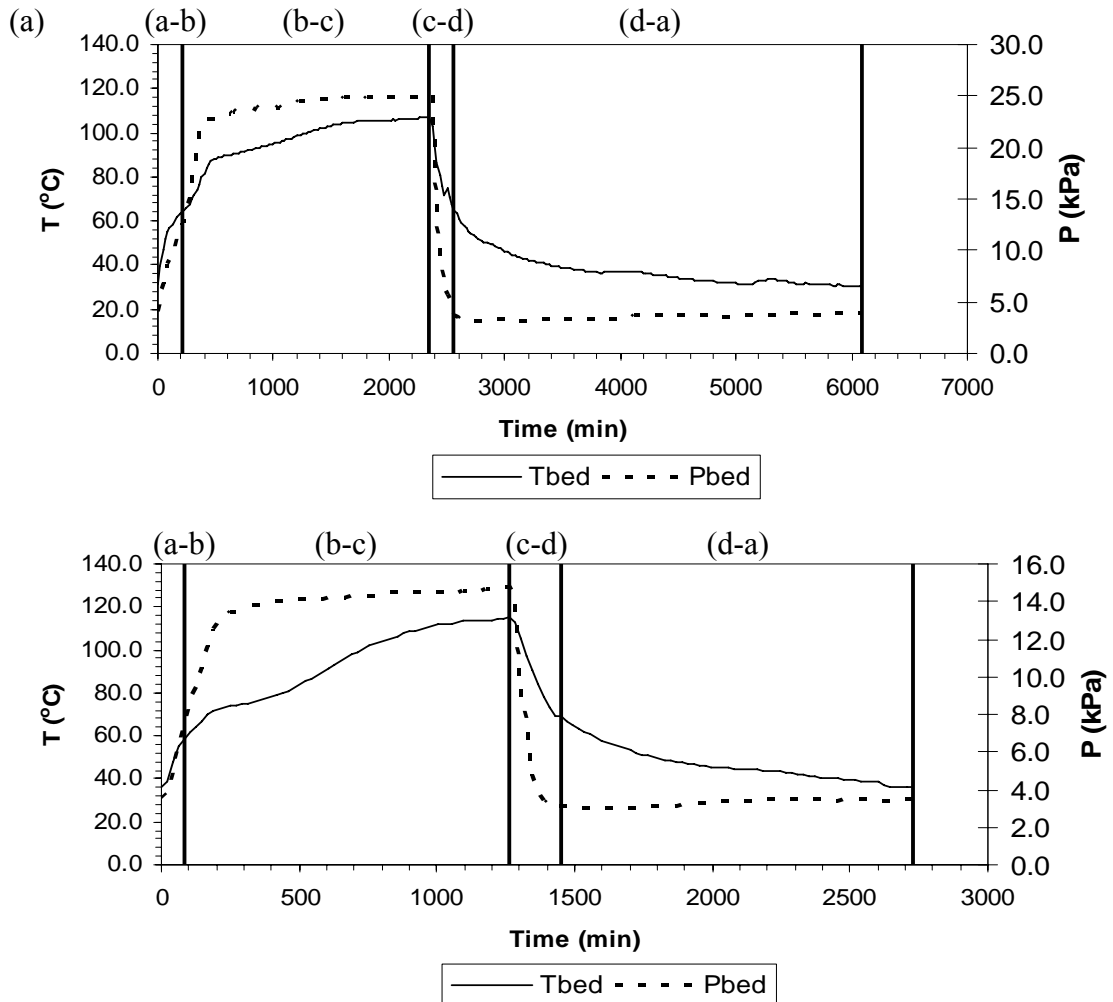


Figure 5.23. Change of temperature and pressure of adsorbent bed during the cycle (a) without and (b) with metal additives

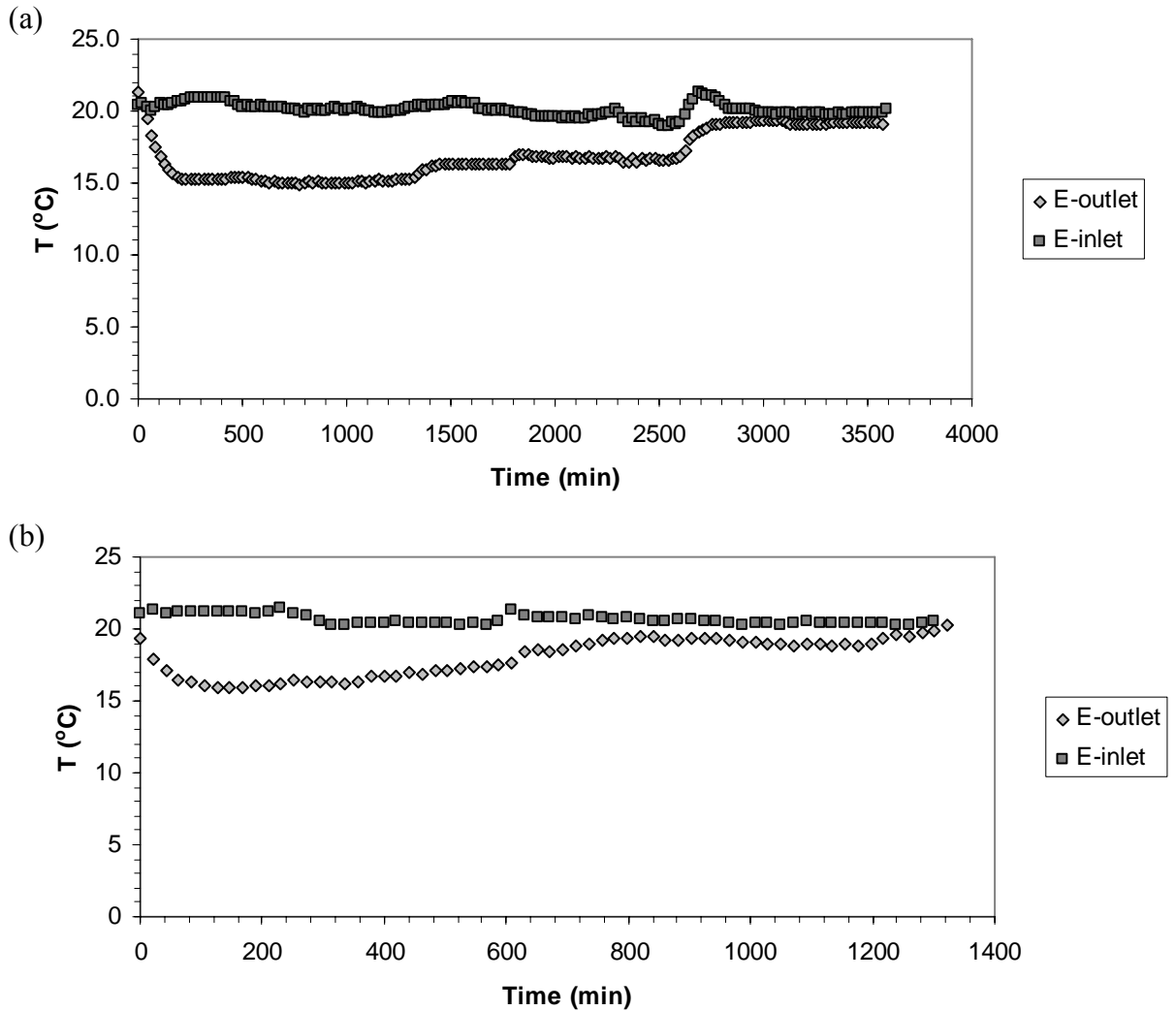


Figure 5.24. The variation of inlet and outlet temperatures of heat exchanger fluid in evaporator during isobaric adsorption process, (a) setup without metal additives and (b) metal loaded setup

The variation in the amount of evaporated adsorptive from evaporator during adsorption process for both cycles were shown in Figure 5.25. The amount of evaporated water from evaporator reached to their maximum values in both cases. The amounts of evaporated water were 2.6L and 3L for metal loaded AHP-2 and AHP-2 without metal additives respectively. The amounts of evaporated water from evaporator were very close to each other compared to the period of adsorption processes and amount of silica gel of adsorbent bed. The addition of Al pieces in the adsorbent bed reduced the amount of silica gel in the adsorbent bed. The evaporation rate of water for metal loaded setup was faster than setup without metal additives since the heat of adsorption, which evolves during adsorption of water on silica gel, removes from

adsorbent bed rapidly due to enhanced heat transfer rate of adsorbent bed with Al pieces.

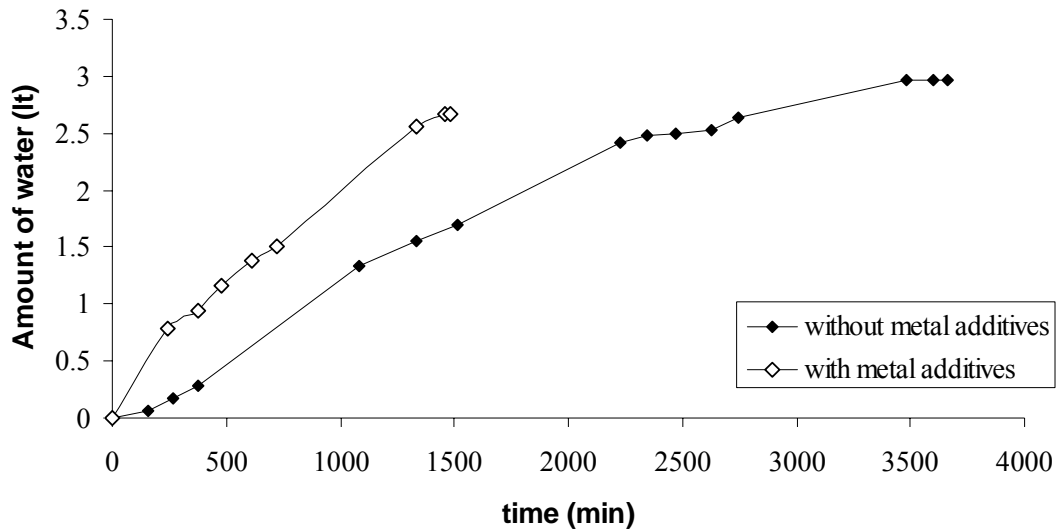


Figure 5.25. The amount of evaporated adsorptive during adsorption process for both cycles

The variations of heat transfers from heat exchanger fluid to adsorptive in the evaporator are shown in Figure 5.26 for both cases. The transferred heat for Al-loaded AHP-2 was faster than that for AHP-2 without metal additives since generated heat was removed rapidly in the adsorbent bed of Al-loaded AHP-2. The initial slope of evaporator power for Al loaded setup was higher than the setup without metal additives due to the higher adsorption rate. The maximum transferred heats for Al-loaded AHP-2 and AHP-2 without metal additives were 4.5 W kg_s^{-1} and 3.8 W kg_s^{-1} , respectively. After attaining to a maximum value, the transferred heats of cycles decreased. They approached to zero due to the disappearing adsorption rate.

The amounts of heat transferred from the evaporator, condenser and adsorbent bed were determined by using Equations 2.3 to 2.6 considering the operation conditions given in Table 5.10. The physical and thermodynamical properties of material used in AHP are illustrated in Table C1. Table 5.11 shows the amounts of heat transfer between AHP and heat reservoirs during four processes for both cases. As mentioned before, the total amount of transferred heat between adsorption heat pump and environment should be zero. The differences were 3.5% of the amount of transferred heat ($Q_{a-b} + Q_{b-c}$) for both cycles. These differences are very small and may come from heat losses and measuring error during observation of water level of condenser/evaporator.

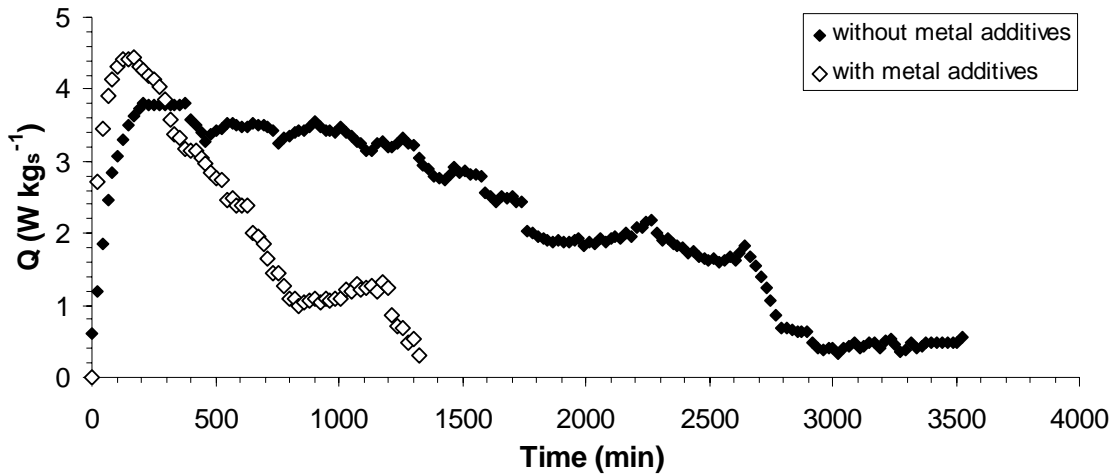


Figure 5.26. Variations of transferred heat from heat exchanger fluid to adsorptive during adsorption process for with and without metal loaded setup

Table 5.11. The amounts of heat transfer between adsorption heat pump and heat reservoirs for two cycles

Heats (kJ kg ⁻¹)	Second setup with Al- pieces	Second setup without Al- pieces
Q_{a-b}	115	100
Q_{b-c}	287	234
Q_{c-d}	-102	-76
Q_{d-a}	-287	-247
Q_{ev}	171	161
Q_{cond}	-166	-155
Residual Q	13	12

Table 5.12 shows the performance indicators for AHP-2 without metal additives and with metal additives. The heating and cooling coefficient of performances of setup without metal additives were higher than that of metal loaded AHP-2 since the addition of metal decreased the amount of silica gel in the adsorbent bed as well as it reduced the amount of evaporated water and gained heat from environment. However, specific cooling and the heating power of metal loaded setup were 2.5 times higher than the values of AHP-2 without metal additives since the metal addition into the bed decreased the cycle period. Short cycle period may cause to increase irreversibilities in the system and entropy generation in the system.

Table 5.12. Performance indicators for two cycles

Parameters	Second setup with Al-pieces	Second setup without Al-pieces
COP_{ref}	0.43	0.48
COP_h	1.38	1.43
SCP (W kg_s⁻¹)	1.03	0.44
SHP (W kg_s⁻¹)	3.34	1.31
COP_{exp}	1.54	2.16
COP_C	5.63	6.66
η_{II}	0.27	0.32
ΔS (kJ K⁻¹)	7.25	6.15

The mixing of 10wt% of Al with silica gel in the adsorber may increase heat transfer rate in the adsorbent bed, hence the cycle period is reduced significantly. Moreover, the reduction of amount of silica gel in the adsorber did not influence significantly the amount of evaporated water from the evaporator.

CHAPTER 6

RESULTS OF MICROCALORIMETRIC STUDY

For the selection of an appropriate adsorbent – adsorbate pair, properties of adsorbent – adsorbate pair should be well known. Therefore, adsorption capacity, isosteric heat of adsorption, water diffusivity inside silica gel particle and isothermal behavior should be described. These properties of adsorbent – adsorbate pair were utilized in considering the performance criteria of designed adsorption heat pump at desired operational conditions. Microcalorimetric study was performed for providing these valuable data. The microcalorimetric study was performed by using Tian-Calvet type microcalorimeter which was described in Chapter 4. The results of microcalorimetric study were given in this chapter.

6.1 Water Vapor Isotherms

The microcalorimeter setup is a volumetric system that means the amount of adsorptive in the system can be determined by using ideal gas relation if the system pressure is measured accurately. At low pressure, water vapor behaves as ideal gas. Therefore, the amount of adsorbed water on silica gel can be calculated by using ideal gas relationship. The calculation procedure for microcalorimetry study was given in Appendix E. Figure 6.1 illustrates the adsorption isotherm of water vapor on silica gel at 30, 35, 40, 60, 75, 90, 100, 110, and 120°C. As can be seen in the figure, water vapor adsorption reached equilibrium which can be interpreted as monolayer adsorption is finished. The amount of adsorbate decreased with the increasing adsorption temperature. Silica gel adsorbed 0.6, 0.98, 1.1, 1.4, 2, 3.5, 11, 13 and 15 %wt water vapor at 120, 110, 100, 90, 75, 60, 40, 35 and 30°C, respectively.

6.2 Differential Heat of Adsorption

Figure 6.2 illustrates representative heat flow peaks for water vapor adsorption on silica gel at 35°C. Water vapor pressure doses were changed 1-30 mbar and heat was

measured by Tian-Calvet type C80 microcalorimetry for each dose against time. Differential heat of adsorption for water vapor – silica gel pair can be calculated by integrating the area under the peak for each dose by using SETSOFT software.

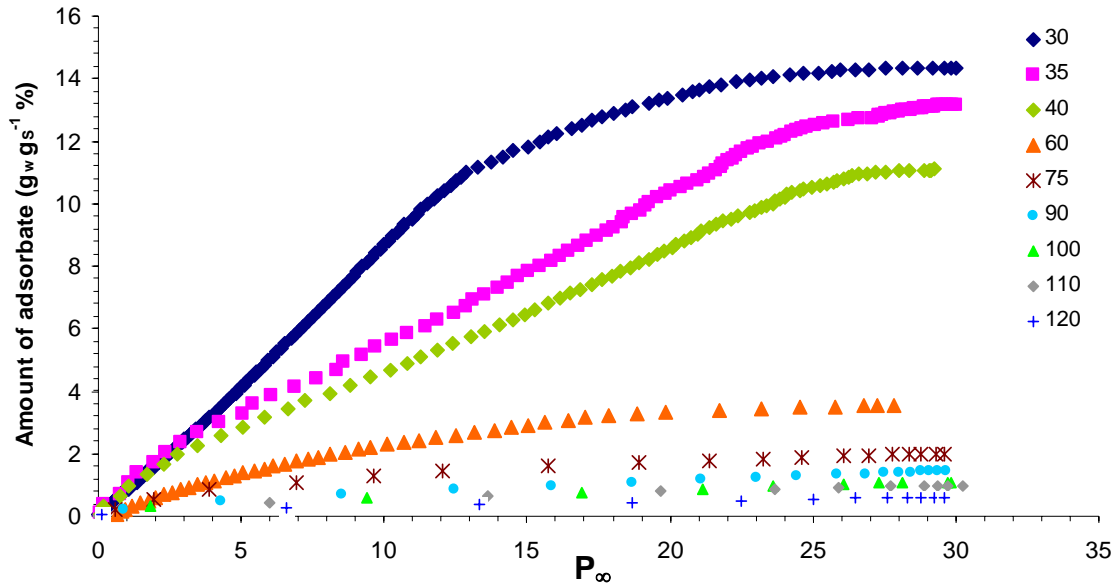


Figure 6.1. Isotherms of water vapor adsorption on silica gel¹

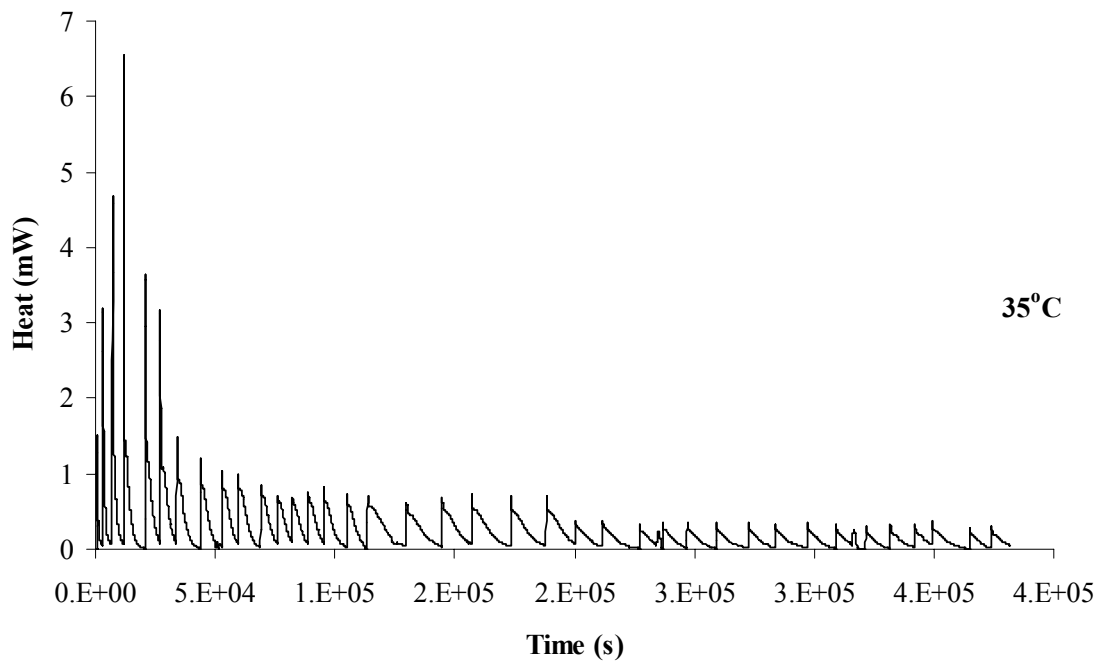


Figure 6.2. Heat flow versus time curve of water vapor – silica gel pair at 35°C

¹ The raw data and calculation procedure were shown in Table E1 in Appendix E.

Figure 6.3 depicts the differential heat of adsorption of water vapor – silica gel pair against amount of coverage at 35, 40 and 60°C. There are three regions that should be taken into account as shown as lines in Figure 6.3. First region is at lower coverage, maximum differential heat of adsorption was observed that caused by tightly bound water vapor to silica gel. The second is at higher coverage, differential heat of adsorption can be seen as a plateau which extends between 2% to 10% of coverage and the third section is sharply declining of heat of adsorption after 11% amount of water molecule coverage. The zero coverage differential heat of adsorption is 140kJ/mol at 35°C. The increasing adsorption temperature decreased the heat of adsorption due to reducing adsorbate-adsorbent interactions as shown in Figure 6.3.

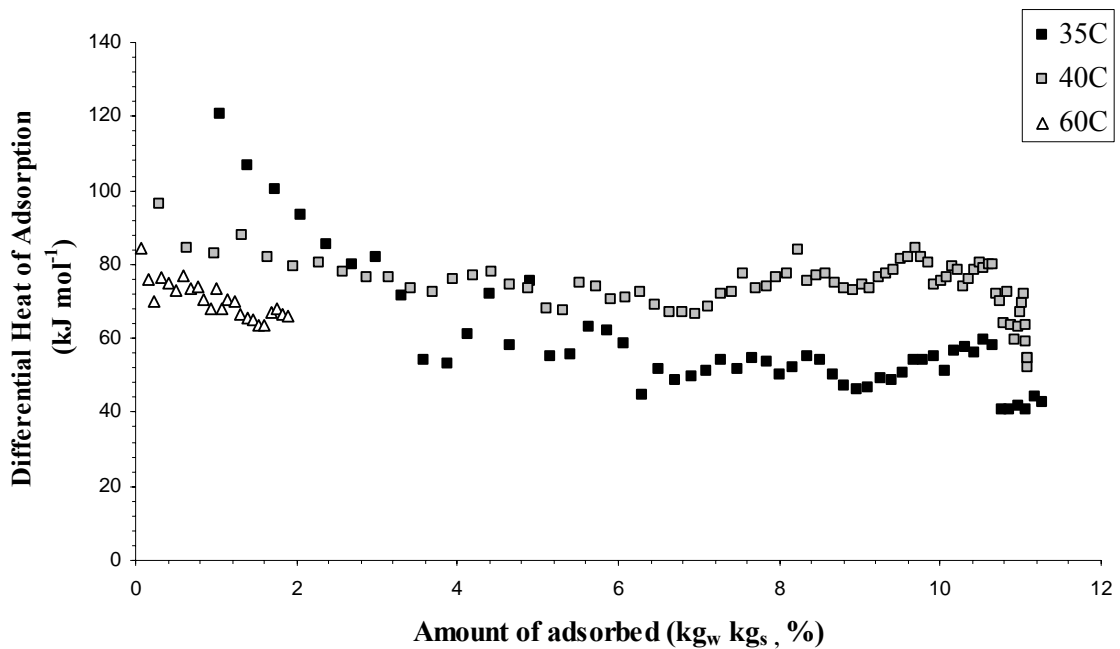


Figure 6.3. Heat of adsorption versus water vapor loading curve at 35, 40, and 60°C

6.3 Isothermic Heat of Adsorption

The isothermic heat of adsorption can be calculated by using Clausius-Clapeyron relation which is shown in Equation 6.1 from isotherms of water vapor adsorption on silica gel.

$$\ln P = \frac{-\Delta H_{st}}{RT} \quad (6.1)$$

The change of pressure according to the temperature at constant amount of adsorbate can be determined as shown in Figure 6.4. In order to calculate the temperature and the pressure at constant amount of adsorbate from water vapor isotherms, isotherms were modeled by using Langmuir relationship as shown in Equation 6.2.

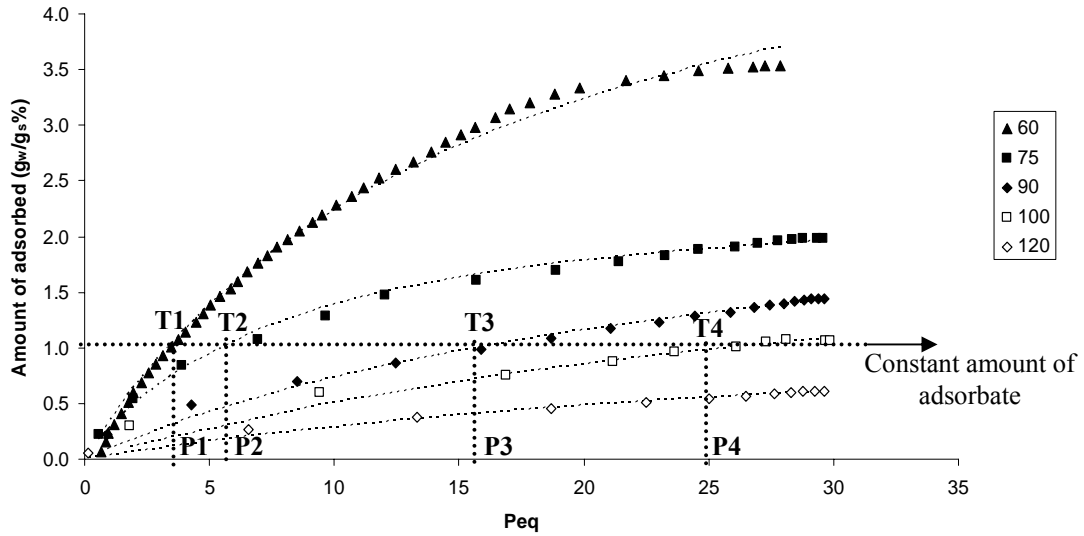


Figure 6.4. Calculation of isosteric heat of adsorption

$$W_{langmuir} = \frac{C_{\infty} W_m b}{b C_{\infty} + 1} \quad (6.2)$$

Where, C_{∞} can be calculated with the ideal gas relation at equilibrium pressure. The “b” is Langmuir constant and W_m is monolayer coverage. The monolayer coverage and Langmuir constant can be found by plotting C_{∞}/W versus C_{∞} graph as shown in Figure 6.5. The inverse slope gives monolayer coverage. The multiplication of the intercept with monolayer coverage gives inverse Langmuir constant. The Langmuir models are shown by dotted lines in Figure 6.4. As is seen in Figure 6.5, Langmuir model of water vapor isotherms well fitted the experimental results.

The Classius – Clapeyron diagram can be plotted as $-1/T$ versus $\ln P$ by using temperature and pressure which were provided from isotherms at constant amount of adsorbate as shown in Figure 6.6. The Classius – Clapeyron diagram was drawn only until the 10% ($\text{kg}_w \text{ kg}_s^{-1}$) amount of adsorbate since the maximum amount of adsorbate can be obtained as 13% ($\text{kg}_w \text{ kg}_s^{-1}$) due to low water vapor pressure dose. The slope $\ln P$ versus $-1/T$ curves gives the $\Delta H_{st}/R$. The obtained equations of $\ln P$ versus $-1/T$ for

constant amount of adsorbate are shown in Equation 6.3. Figure 6.7a shows the variations of the intercept of equations versus amount of adsorbate and Figure 6.7b illustrates the changes of the slope of equations versus amount of adsorbate. The experimental data was shown with dots and fitted polynomial equation was illustrated straight line in Figure 6.7. The slope and intercept of $\ln P$ versus $-1/T$ for constant amount of adsorbate were modeled by fitting polynomial equation for numerical study in Equations 6.4 and 6.5. The isosteric heat of adsorption and the temperature versus pressure behavior at constant amount of adsorbate data are important for adsorption heat pump systems. The operation conditions (temperatures and pressures of processes of AHP) can be defined by using Classius –Clapeyron diagram. Moreover, the coefficient of performance of AHP at that operation conditions can be easily evaluated.

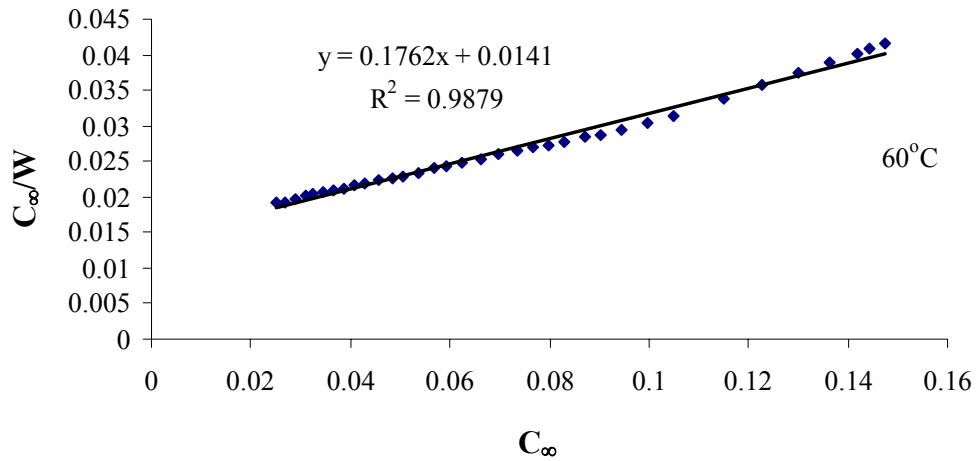


Figure 6.5. Representative graph of Langmuir model

$$\ln P = B\left(-\frac{1}{T}\right) + A \quad \text{for general equation} \quad (6.3)$$

$$\ln P = 5576.6\left(-\frac{1}{T}\right) + 21.692 \quad \text{for 0.5\%} \quad (6.3a)$$

$$\ln P = 5899.8\left(-\frac{1}{T}\right) + 23.642 \quad \text{for 1\%} \quad (6.3b)$$

$$\ln P = 5754.4\left(-\frac{1}{T}\right) + 24.234 \quad \text{for 3\%} \quad (6.3c)$$

$$\ln P = 4709.9\left(-\frac{1}{T}\right) + 21.984 \quad \text{for 5\%} \quad (6.3d)$$

$$\ln P = 5633.3\left(-\frac{1}{T}\right) + 25.927 \quad \text{for 10\%} \quad (6.3e)$$

$$\ln P = 6768.6 \left(-\frac{1}{T} \right) + 30.081 \quad \text{for 13\%} \quad (6.3f)$$

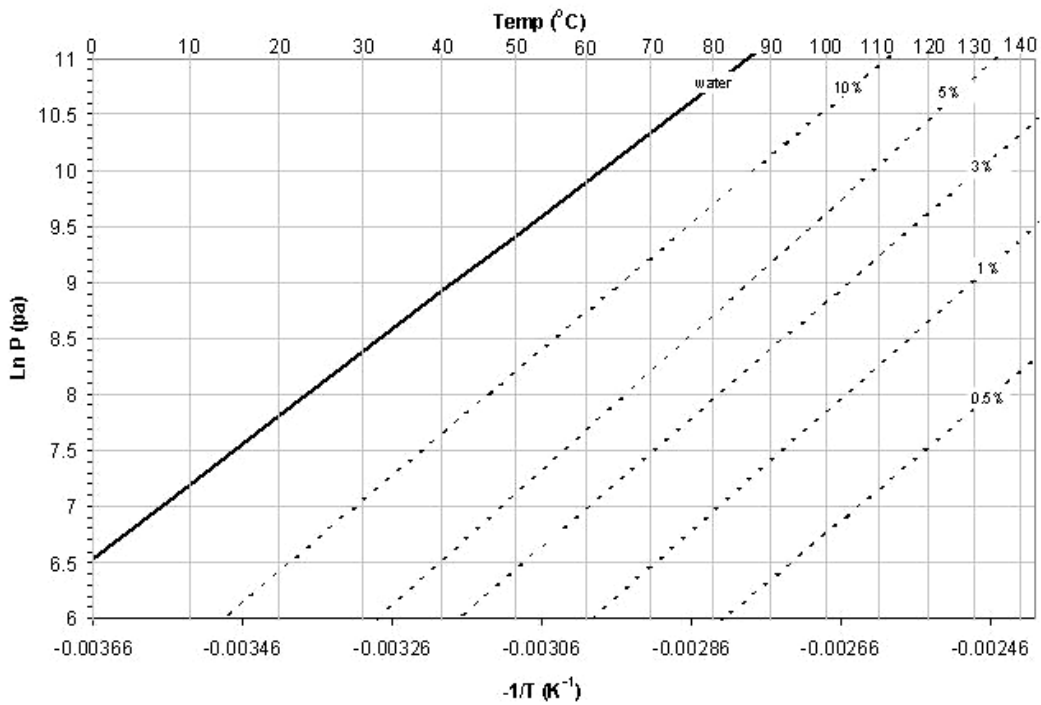


Figure 6.6. Classius – Clapeyron diagram of water vapor on silica gel

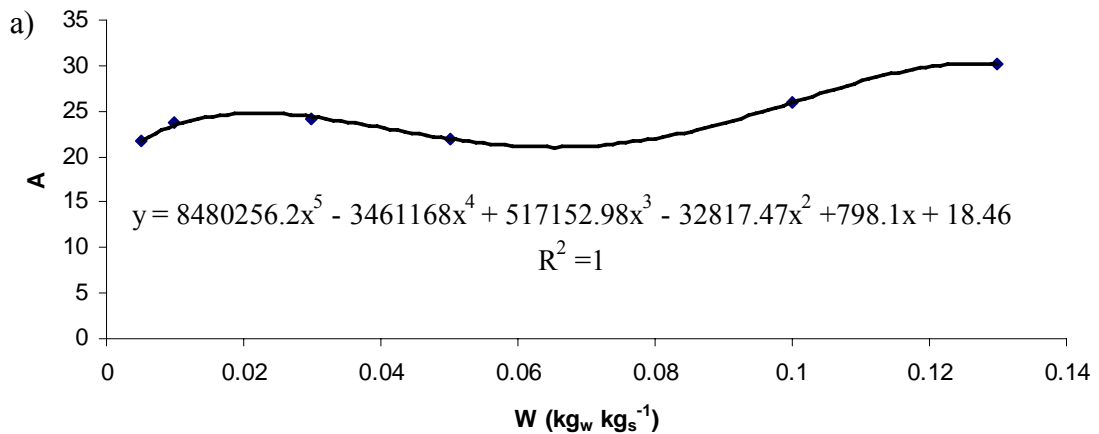


Figure 6.7. The variations of intercept and slope of $\ln P$ versus $-1/T$ with constant amount of adsorbate (a) intercept (b) slope

(cont. on next page)

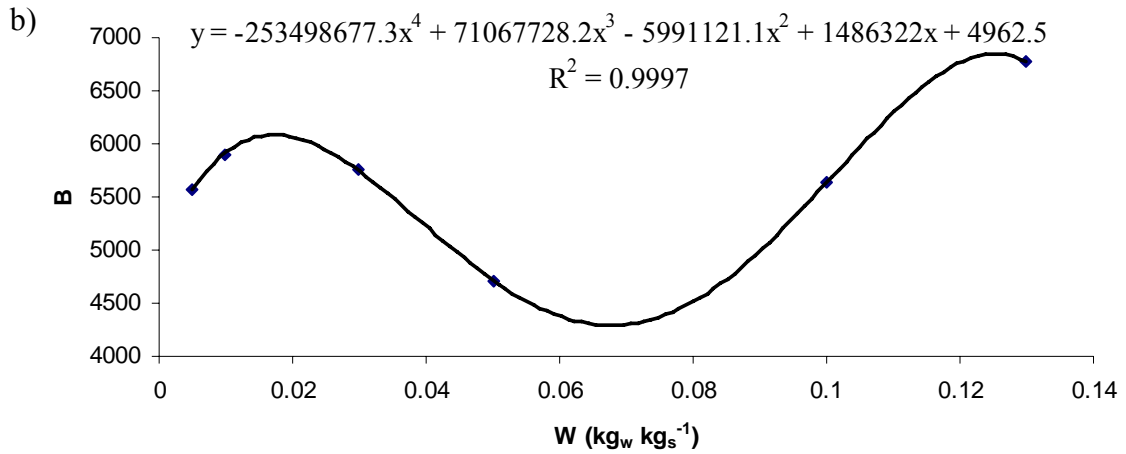


Figure 6.7. (cont.) The variations of intercept and slope of $\ln P$ versus $-1/T$ with constant amount of adsorbate (a) intercept (b) slope

$$A = 8480256.2W^5 - 3461168W^4 + 517152.98W^3 - 32817.47W^2 + 798.1W + 18.46 \quad (6.4)$$

$$B = -253498677.3W^4 + 71067728.2W^3 - 5991121.1W^2 + 1486322W + 4962.5 \quad (6.5)$$

6.4 Water Vapor Diffusivity

Figure 6.8 shows the kinetics of water vapor adsorption on silica gel. The total adsorption time reduced with decreasing amount of adsorbate. The diffusivity of water vapor through the silica gel particles was calculated by using these kinetics data. Diffusion of water vapor through the silica gel can be calculated by using Equation 3.12 and 3.13 which are valid for short and long range periods and isothermal conditions. Equation 3.12 can be employed if $W_t/W_\infty < 0.3$. The effective diffusivity for the short range period can be found from the slope of W_t/W_∞ versus $t^{1/2}$ plot. Equation 3.13 can be employed if $W_t/W_\infty > 0.7$. The slope of $\ln(1 - W_t/W_\infty)$ versus t curve gives the effective diffusivity constant at that temperature for the long range period. In Figures E1 and E2 in Appendix E, linearity of $\ln(1 - W_t/W_\infty)$ versus t and W_t/W_∞ versus $t^{1/2}$ plots can be seen for all operating temperature. The obtained effective diffusivities of water-silica gel pair were estimated for both short and long range periods and shown in Table 6.1. The radius of particle was taken as 1.6mm. At low temperatures, the effective diffusivities for short range periods were lower than that for long range periods due to long path from the surface of particle to inner side of particle. At high adsorption temperature, the effective diffusivities for both short and long range periods are very

close to each other since the total amount of adsorbate at these temperatures are very low.

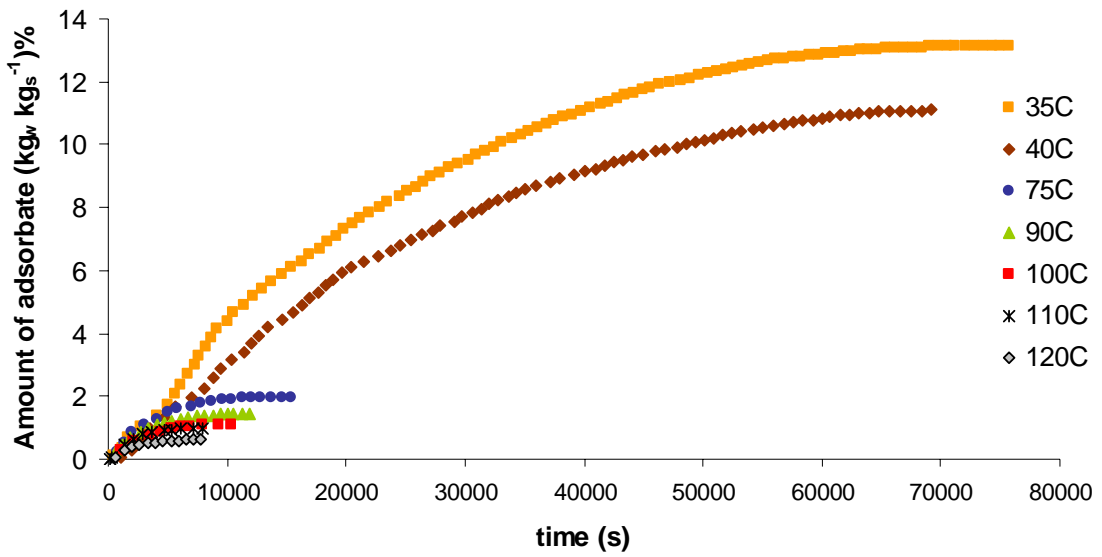


Figure 6.8. Kinetics of water adsorption on silica gel

Table 6.1. Water vapor diffusivities against temperature

Temperature (°C)	Short range	Long range
	D_{eff} ($\text{m}^2 \text{s}^{-1}$)	D_{eff} ($\text{m}^2 \text{s}^{-1}$)
30	3.92E-13	2.52E-11
35	4.21E-12	2.32E-11
40	4.76E-12	2.83E-11
60	2.88E-12	7.03E-11
75	7.21E-11	1.26E-10
90	8.19E-11	1.43E-10
100	1.04E-10	2.35E-10
110	9.29E-11	2.53E-10
120	2.28E-10	2.80E-10

Figure 6.9 shows the variations of water vapor diffusivity on silica gel particle against adsorption temperatures for short and long range periods. The water vapor diffusivity increased exponentially with the increasing adsorption temperature for both short and long range periods. The effective diffusivity formulas can be found by fitting experimental data to Arrhenius equation. The effective diffusivity can be described with Arrhenius form as shown in Equation 6.6. The D_0 indicates the reference diffusivity and E (J mol^{-1}) is activation energy. The gas constant indicates with R ($\text{J mol}^{-1} \text{K}^{-1}$). The plot of $\text{Ln}(D_{\text{eff}})$ versus $1/T$ gives linear expression. The slope of this curve gives activation

energy and intercept gives reference diffusivity as shown in Figure E3 in Appendix E. The effective diffusivities of water on silica gel in Arrhenius form for short and long range periods are shown in Equations 6.7 and 6.8 with 0.842 and 0.9678 regressions, respectively.

Aristov et al. (2006) found out diffusivity of water vapor on Fuji RD silica gel at different temperatures as shown in Table 3.1. The diffusivity values found by Aristov et al. (2006) are between 1.8×10^{-11} and $6.3 \times 10^{-11} \text{ m}^2 \text{ s}^{-1}$ for the temperatures at 30-65°C. These values are quite similar to our experimental (Table 6.1) data although the silica gel particle sizes are significantly different.

$$D_{eff} = D_0 e^{\left(\frac{-E}{RT}\right)} \quad (6.6)$$

$$D_{eff} = 1.28 \times 10^{-2} e^{\left(\frac{-57758}{RT}\right)} \quad (6.7)$$

$$D_{eff} = 2.48 \times 10^{-6} e^{\left(\frac{-29066}{RT}\right)} \quad (6.8)$$

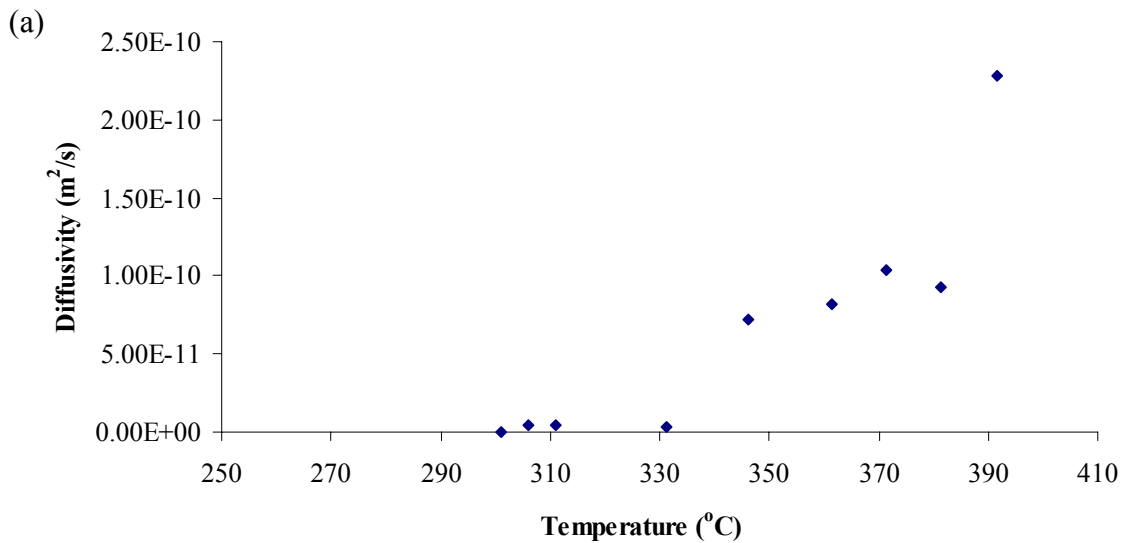


Figure 6.9. Variations of water vapor diffusivity on silica gel with temperatures a) short range period and b) long range period

(cont. on next page)

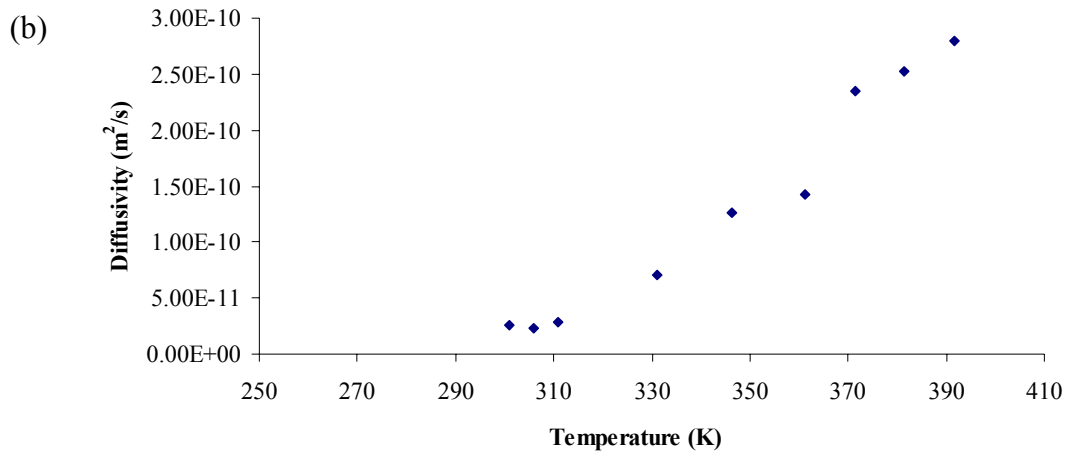


Figure 6.9. (cont.) Variations of water vapor diffusivity on silica gel with temperatures a) short range period and b) long range period

As mentioned above, the effective diffusivities of water vapor through silica gel particle were found for short and long range periods of kinetics of water adsorption by using Equations 3.12 and 3.13. The effective diffusivities of water vapor through silica gel particle were also modeled as function of temperature by using Arrhenius relations for both short and long range periods as shown in Equations 6.7 and 6.8. The amount of adsorbate through a silica gel particle can be calculated by using Equation 3.11 which is analytical solution of Equation 3.10. Figure 6.10 shows the experimental amount of adsorbate for low and high temperatures and theoretical amount of adsorbate calculated by using Equation 3.10 and modeled diffusivities for short and long range periods. At low temperature, theoretical amount of adsorbate calculated by using short range diffusivity value closes to experimental values until the $W_t/W_\infty < 0.4$. For long range diffusivities, theoretical amount of adsorbate modeled to experimental values after the $W_t/W_\infty > 0.8$. At high temperatures, theoretical amount of adsorbate determined by using both short and long range diffusivities behaves very close to experimental values for all W_t/W_∞ values. As mentioned before the Equation 3.11 is valid for spherical particle under isothermal conditions. The tested silica gel particles are not uniform spheres therefore solution of Equation 3.11 may be affected by the particle shape. For this case, Karger and Ruthven (1992) interpreted that this approximation is clearly excellent in the short range region of the uptake curve, but it becomes less satisfactory in the long range period. Moreover, the heat transfer resistance inside the particle significantly affects the long range periods of the uptake curve; the short range periods remains close to the

ideal isothermal curve. Consequently, the short range vapor diffusivity through the silica gel should be used for further study.

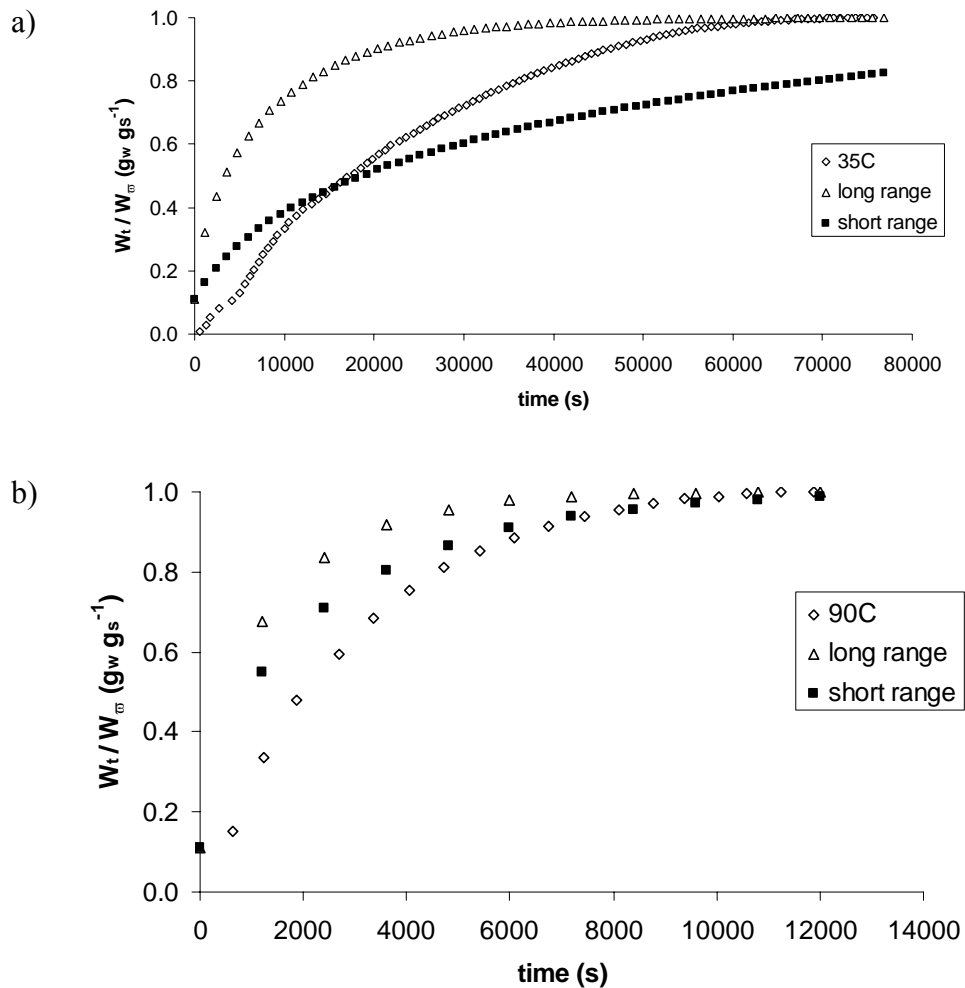


Figure 6.10. Experimental and theoretical amount of adsorbate fractions a) 35°C and b) 90°C

6.5 Diffusion in Porous Silica Gel

In the previous section, the water vapor diffusion inside the silica gel particle was found regardless of the external film resistance. As mentioned in Chapter 3, the importance of intraparticle mass transfer resistance to the external film resistance can be analyzed by mass Biot number (Equation 3.5). For the mass Biot number, the Sherwood number (Equation 3.3) can be assumed as 2.0 since can be assumed as stagnant fluid. Therefore, Reynolds number of external fluid film can be neglected. The diffusion of water molecules for the external stagnant fluid film can be calculated by using Equation 3.7. The effective diffusivity of water molecules through the silica gel particle is determined by using Equation 6.7 which is valid for short range water vapor diffusivity.

The mass Biot numbers were evaluated under the mentioned assumptions and shown in Table 6.2. The values of collision diameter (σ) and collision integral (Ω) of water molecule, used in Equation 3.7, are illustrated in Table D3 in Appendix D.

Table 6.2. Biot mass number for silica gel – water pair at different temperatures

Temperature (K)	Pressure (kPa)	Dm (m ² s ⁻¹)	D _{eff} (m ² s ⁻¹)	Bi _m
T _a =307	2	7.1x10 ⁻⁴	1.9x10 ⁻¹²	4.2x10 ⁷
T _b =359	20	9.7x10 ⁻⁵	5.1x10 ⁻¹¹	2.1x10 ⁵
T _c =398	20	1.2x10 ⁻⁴	3.4x10 ⁻¹⁰	3.9x10 ⁴
T _d =338	2	8.6x10 ⁻⁴	1.5x10 ⁻¹¹	6.4x10 ⁶

Table 6.2 indicates that the external film resistance is not dominant resistance for mass transfer. Therefore, the intraparticle mass transfer resistance is important relative to the external mass transfer resistance. Thus, mass transfer around the adsorbent particle may be defined by using Equation 3.11. The effective diffusivity in Equation 3.11 depends on temperature and properties of adsorbent such as diameter of pore, diameter of crystals, pore structure, surface area etc.

As mentioned before, the Lewis number is relevant with the characterization of fluid flows in the presence of simultaneous heat and mass transfer by convection. The estimated Lewis numbers with different temperature for cycle processes are shown in Table 6.3. Mass diffusivity in the porous adsorbent bed is described by using Equation 7.4. The thermal diffusivity of adsorbent bed is assumed as constant for all temperature since the thermophysical properties of silica gel does not varies significantly at operational conditions. As it seen in Table 6.3, the Lewis numbers for all temperatures are very close to zero that indicates the thermal resistance in the adsorbent bed is dominant compared to the mass transfer resistance in the bed.

Table 6.3. Lewis number for silica gel – water pair at different temperatures

Temperature (K)	D _{bed} (m ² s ⁻¹)	α (m ² s ⁻¹)	Le
T _a =307	2.4x10 ⁻⁴	2.1x10 ⁻⁷	8.8x10 ⁻⁴
T _b =359	3.2x10 ⁻⁵		6.6x10 ⁻³
T _c =398	4.0x10 ⁻⁵		5.3x10 ⁻³
T _d =338	2.9x10 ⁻⁴		7.2x10 ⁻⁴

CHAPTER 7

SIMULATION OF HEAT AND MASS TRANSPORT IN ADSORBENT BED

In the previous chapters, the designed and constructed adsorption heat pump setups and the obtained experimental results were explained. The results showed that heat and mass transfer in the adsorbent bed is the main difficulty in the improvement of performance criteria of the adsorption heat pump. Simulation of heat and mass transfer in the adsorbent bed provide significant information about the design of adsorbent bed. In this chapter, the mechanism of the heat and mass transfer in the adsorbent bed is explained. The governing equations which are conservation of mass, conservation of energy for the adsorbent bed and mass transfer equation for the adsorbent particle with appropriate initial and boundary conditions are presented. The solution method is briefly explained and the results of three cases were given. In the first case, the distributions of temperature, adsorptive density, adsorbate concentration and pressure along the radius of the adsorbent bed were obtained only during the adsorption process for a completely dried adsorbent bed. In the second case, the results for a complete cycle of the adsorption heat pump were obtained and the results were discussed. In third case, the cycle of adsorption heat pump was simulated by using the silica gel – water data which were obtained in microcalorimetric study. The obtained results were discussed and compared with the experimental data.

7.1 Mechanism of Heat and Mass Transfer in Adsorbent Bed

Theoretical studies have shown that the performance of adsorption heat pump is highly influenced from the heat and mass transfer in the adsorbent bed. Liu and Leong (2005) numerically investigated the influence adsorption, regeneration, condensing and evaporating temperatures on the performance of an adsorption heat pump operating with zeolite 13X-water pair. They found that these factors significantly affect the performance and they optimized operating conditions for their system (Liu and Leong

2005). Chahbani et al. (2004) discussed the influence of heat and mass transfer limitations on the system efficiency. They reported that low heat and mass transfer rate through the adsorbent bed significantly reduces coefficient of performance and specific cooling power values as expected (Chahbani, et al. 2004).

The adsorptive flow in the adsorbent bed involves the adsorptive transfer through the porous bed (inter-particle flow) and transfer of adsorptive in the porous adsorbent particle (intra-particle). Different mass transfer mechanisms as pressure difference, molecular diffusion, Knudsen diffusion, and surface diffusion cause the adsorptive flow in the bed. In order to determine temperature, adsorptive and adsorbate concentration profiles in the adsorbent bed, heat and mass transfer equations have to be solved for the adsorber. The set of governing equations for the problem are coupled and should be solved simultaneously. The COP, SHP and SCP values with acceptable accuracy for a cycle can be estimated. Table F1 in Appendix F shows a list of theoretical studies performed on simulation of heat and mass transfer in an adsorbent bed. The list presents the governing equations, their employed assumptions and solution method for the described system and adsorbent – adsorbate pairs. As it was mentioned before, solution of the governing equations for the adsorbent bed of adsorption heat pump is difficult and many assumptions have been done as seen from Table B1. In most of the performed studies, the diffusivity value in the adsorbent particle is determined by theoretical model. Similarly, in the most of studies, the mass transfer inside particle (i.e. intra-particle mass transfer) is modeled by using linear driving force (LDF) model. Some researchers such as Sun and Besant (2005), Tatlier et al. (1999), and Restuccia (2002) studied cylindrical adsorbent beds.

The governing equations of heat and mass transfer in an adsorbent bed of an adsorption heat pump can be listed as follows:

- Continuity equation in the adsorbent bed.
- Momentum transfer equation through the adsorbent bed.
- Heat transfer equation through the adsorbent bed.
- Mass transfer equation in the adsorbent particle

The continuity equation refers to the conservation of adsorptive in the adsorbent bed which means that for any arbitrary control volume in the bed, adsorptive transfer rate to the control volume is equal to the adsorptive transfer rate leaves the control

volume plus the rate of adsorptive dissipated or generated during adsorption or desorption process, respectively.

Mass transfer equation through the bed mathematically represents the motion of adsorptive through the adsorbent bed. Generally, for adsorption heat pump problems, Darcy's relation is used to describe the transfer of the adsorptive in the voids between the adsorbent particles. The effects of other forces such as inertia forces, viscous forces on motion of the adsorptive are neglected.

As can be seen from most of the performed studies (Appendix F, Table F1), the temperature of adsorptive in the voids was assumed to be equal to the temperature of solid adsorbent. The heat transfer resistance in the adsorbent particle was assumed as negligible. Therefore, the heat transfer equation was written only to simulate the heat transfer in an adsorbent bed.

Mass transfer equation in the adsorbent describes intra-particle mass transfer mathematically. In practical applications, the size of particles in the adsorbent bed is generally small, therefore they can be assumed as isothermal for an instant. In other words, the temperature of an adsorbent particle is only the function of time. Hence, LDF method can be employed to represent adsorptive transfer in the adsorbent particle.

7.2 Fluid Flow in Porous Bed

The transfer of adsorptive through the adsorbent bed can be represented by Darcy relation. Darcy found that the volumetric flow rate is directly proportional to the pressure difference and inversely proportional to the radius of the porous bed as shown in the following equation (Bird, et al. 2002).

$$u = \frac{Q_w}{A} = \frac{K_{app} \Delta P}{\mu R} \quad (7.1)$$

where the Q_w ($m^3 s^{-1}$) is volumetric flow rate and A (m^2) is the cross-sectional area of the bed. K_{app} refers to apparent permeability of porous bed. The viscosity of fluid is shown by μ (Nsm^{-2}), and R represents porous bed radius in meter.

The porous bed consists of many twisted and interconnected voids of varying cross-sectional area and shape. The fluid follows path between these twisted and interconnected voids. The relationship between the flow rate through the porous bed and driving pressure depend on the structure of the voids.

The fluid flow path in porous bed can be idealized as a bundle of tangled tubes which is called as tube bundle model as shown in Figure 7.1. The apparent permeability of porous bed depends on inherent permeability of porous (K) which can be described by Blake-Kozeny equation and the diffusion mechanism which are Knudsen diffusion, molecular diffusion and surface diffusion. The apparent permeability relation is shown in Equation 7.2 (Leong and Liu 2004).

$$K_{app} = K + \frac{\varepsilon\mu}{P} D_{bed} \quad (7.2)$$



Figure 7.1. a) Porous packed bed having cylindrical shape b) tube bundle model
(Source: Bird, et al. 2002)

Blake and Kozeny described the pressure drop for a fluid flow on idealized tube bundle model which is valid for small superficial velocity, porosity of bed less than 0.5 and laminar flow regime. According to Blake-Kozeny relationship, the inherent permeability (K) of a porous bed can be obtained as follows (Bird, et al. 2002);

$$K = \frac{4r_p^2 \varepsilon^3}{150(1 - \varepsilon)^2} \quad (7.3)$$

In addition to the inherent permeability, flow of the adsorptive in porous bed is influenced by Knudsen, molecular and surface diffusion flows. The surface flow diffusion can be assumed as insignificant in large macroporous bed. Therefore, the diffusion of adsorptive through porous bed can be prescribed by following relations;

$$\frac{1}{D_{bed}} = \tau \left(\frac{1}{D_m} + \frac{1}{D_{kn}} \right) \quad (7.4)$$

The symbol “ τ ” is the tortuosity factor and it is the correction factor between diffusion path length and idealized cylindrical channel length. The reported experimental macropore tortuosity factor varies widely from 1.7 to 6. The tortuosity factor is typically 3 for straight cylindrical pores (Ruthven 1984).

7.3 The Considered Annular Adsorbent Bed

Figure 7.2 shows the schematic view of the analyzed the annular adsorbent bed filled with the adsorbent granules. In this study, the adsorbent granules are silica gel grains and adsorptive is water vapor. The adsorbent bed has a cylindrical annular shape. The adsorptive can easily flow in the center annulus and enter to the portion filled with granules with a uniform velocity. The adsorptive flows from $R=R_i$ surface towards the outer surface, $R=R_o$. The upper and bottom surfaces of the adsorbent bed are insulated and the heat and mass transfer is assumed only in radial direction. The thermal resistance of the metal casing is neglected. The inner and outer radiuses of the cylindrical annulus are $R_i = 0.06$ m and $R_o = 0.19$ m, respectively. The equivalent radius of the adsorbent (i.e. silica gel) granules is $r_c = 0.0016$ m.

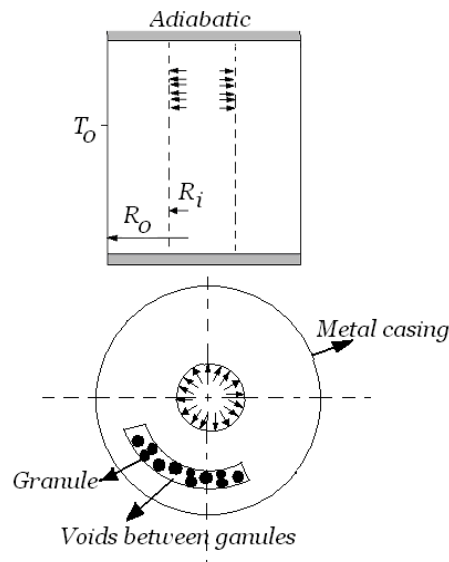


Figure 7.2. A schematic view of the adsorbent bed

7.3.1 Governing Equations

The mechanisms of heat and mass transfer in a granular adsorbent bed are coupled and complex, hence some assumptions have to be made to pose the governing equations. The employed assumptions in this study are;

- 1) The adsorbent bed consists of uniform size adsorbent granules, thus the bed porosity is assumed constant for each cases;
- 2) The adsorptive and adsorbent granules are in thermodynamic equilibrium.
- 3) The adsorptive behaves as an ideal gas
- 4) The effect of thermal resistance within the adsorbent granule is neglected.

- 5) The temperature of an adsorbent granule equals to its surrounded adsorptive.
- 6) The thermal properties of the adsorbent, adsorbate and adsorptive are constant.
- 7) The heat transfer rate at inner surface, $R = R_i$, is negligible.

Under the above assumptions, the governing equation for the problem can be written as:

$$\left((\rho C_p)_{eff} + \rho_s C_{pw} W \right) \frac{\partial T}{\partial t} = \lambda_{eq} \frac{1}{R} \frac{\partial}{\partial R} \left(R \frac{\partial T}{\partial R} \right) - \frac{1}{R} \frac{\partial}{\partial R} (\rho_w C_{pw} R u T) + \rho_s \Delta H_{st} \frac{\partial W}{\partial t} \quad (7.5)$$

$$\frac{\partial \rho_w}{\partial t} + \left(\frac{1}{\varepsilon} \right) \rho_s \frac{\partial W}{\partial t} + \frac{1}{\varepsilon R} \frac{\partial}{\partial R} (R \rho_w u) = 0 \quad (7.6)$$

$$\frac{\partial W}{\partial t} = \frac{15 D_{eff}}{r_p^2} (W_\infty - W) \quad (7.7)$$

The equations 7.5 and 7.6 are the heat and mass transfer equations for the adsorbent bed. As is seen, the heat and mass are transferred in the radial direction of the bed and the effect of adsorption within the granule is contributed by $\partial W / \partial t$. The Equation 7.7 is the mass balance equation for the adsorbent particle. The distribution of adsorptive pressure in the bed can be found from the distribution of adsorptive density by using the ideal gas relation. By the application of ideal gas relation to the Darcy law, the Equation 7.1 describes the velocity field. The apparent permeability of the adsorbent bed, K_{app} , can be calculated by the Equation 7.2 (Leong and Liu 2004):

The diffusion flow in bed (Equation 7.4) depends on two diffusion mechanisms of the adsorptive in the adsorbent bed as Knudsen and molecular diffusions and it can be predicted by the following relations (Bird, et al. 2002).

$$D_{Kn} = 97 r_p \sqrt{T/M} \quad (7.8)$$

$$D_m = 0.02628 \frac{\sqrt{T^3/M}}{P \sigma^2 \Omega} \quad (7.9)$$

All physical and thermal properties of the silica gel and water vapor are given in Table D3 in Appendix D (Bird, et al. 2002, Cussler 1997). The symbol W_∞ in Equation 7.7 shows the equilibrium concentration of the adsorbate and it can be determined by the following model;

$$W_\infty = W_0 \left(\frac{P_{sat}}{P} \right)^{1/n} \quad (7.10)$$

where n represents linear driving for relationship constant given in Table D3 in Appendix D. The effective diffusivity of the adsorbent varies with granule temperature and can be calculated by using Arrhenius equation as shown in the following equation (Ben Amar, et al. 1996):

$$D_{eff} = D_o e^{-E/RT} \quad (7.11)$$

The effective thermal conductivity and effective thermal capacitance of the bed $(\rho C_p)_{eff}$ are determined as follows (Chua, et al. 2004):

$$\lambda_{eff} = \lambda_s^{(1-\varepsilon)} \lambda_w^\varepsilon \quad (7.12)$$

$$(\rho C_p)_{eff} = \varepsilon(\rho C_p)_w + (\rho C_p)_s \quad (7.13)$$

7.3.2 Initial and Boundary Conditions for Case 1

The initial and boundary conditions for the unknown dependent variables which are temperature, adsorptive density, adsorbate concentration, pressure and adsorptive velocity are presented in Table 7.1.

Table 7.1. Initial and boundary conditions for the problem

Dependent parameter	Boundary conditions at $R=R_i$	Boundary conditions at $R=R_o$	Initial condition at $t=0$
Temperature (K)	$\partial T / \partial R = 0$	$T = 300$	$T = 300$
Adsorptive pressure (kPa)	$P = P_{ev} = 1.917$	$\partial P / \partial R = 0$	$P = f(T, \rho)$
Adsorptive density (kg m^{-3})	$\rho_w = f(P, T)$	$\rho_w = f(P, T)$	$\rho_w \approx 0$
Amount of adsorbate ($\text{kg}_w \text{ kg}_s^{-1}$)	$W = f(P, T)$	$W = f(P, T)$	$W = 0$
Adsorptive velocity (m s^{-1})	$U = f(\rho_w, K_{app})$	$\partial U / \partial R = 0$	$U = 0$

7.3.3 Initial and Boundary Conditions for Case 2

The initial and boundary conditions for the unknown dependent variables of the case 2 are presented in Table 7.2 for a complete cycle. A cycle involves four processes as isobaric adsorption, isosteric heating, isobaric cooling and isosteric cooling. The initial and boundary conditions for each process are presented separately.

Table 7.2. Initial and boundary conditions for the problem

Processes	Dependent parameter	Boundary conditions at $R=R_i$	Boundary conditions at $R=R_o$	Initial condition at $t=0$
Isobaric adsorption process (start-up)	Temperature (K)	$\partial T / \partial R = 0$	$T = 300$	$T = 300$ *
	Adsorptive pressure (kPa)	$P = P_{ev} = 1.9$	$\partial P / \partial R = 0$	$P = f(T, \rho)$ *
	Adsorptive density (kg m^{-3})	$\rho_w = f(P, T)$	$\rho_w = f(P, T)$	$\rho_w \approx 0$ *
	Amount of adsorbate ($\text{kg}_w \text{kg}_s^{-1}$)	$W = f(P, T)$	$W = f(P, T)$	$W = 0$ *
	Adsorptive velocity (m s^{-1})	$U = f(\rho_w, K_{app})$	$\partial U / \partial R = 0$	$U = 0$ *
Isosteric heating process	Temperature (K)	$\partial T / \partial R = 0$	$T=403$	Last values of isobaric adsorption process
	Adsorptive pressure (kPa)	$\partial P / \partial R = 0$	$\partial P / \partial R = 0$	
	Adsorptive density (kg m^{-3})	$\rho_w = f(P, T)$	$\rho_w = f(P, T)$	
	Amount of adsorbate ($\text{kg}_w \text{kg}_s^{-1}$)	$W = f(P, T)$	$W = f(P, T)$	
	Adsorptive velocity (m s^{-1})	$\partial U / \partial R = 0$	$\partial U / \partial R = 0$	
Isobaric desorption process	Temperature (K)	$\partial T / \partial R = 0$	$T=403$	Last values of isosteric heating process
	Adsorptive pressure (kPa)	$P = P_{con} = 20$	$\partial P / \partial R = 0$	
	Adsorptive density (kg m^{-3})	$\rho_w = f(P, T)$	$\rho_w = f(P, T)$	
	Amount of adsorbate ($\text{kg}_w \text{kg}_s^{-1}$)	$W = f(P, T)$	$W = f(P, T)$	
	Adsorptive velocity (m s^{-1})	$U = f(\rho_w, K_{app})$	$\partial U / \partial R = 0$	
Isosteric cooling process	Temperature (K)	$\partial T / \partial R = 0$	$T=300$	Last values of isobaric desorption process
	Adsorptive pressure (kPa)	$\partial P / \partial R = 0$	$\partial P / \partial R = 0$	
	Adsorptive density (kg m^{-3})	$\rho_w = f(P, T)$	$\rho_w = f(P, T)$	
	Amount of adsorbate ($\text{kg}_w \text{kg}_s^{-1}$)	$W = f(P, T)$	$W = f(P, T)$	
	Adsorptive velocity (m s^{-1})	$\partial U / \partial R = 0$	$\partial U / \partial R = 0$	

* The given values are for start-up and for next cycles the last values of the isosteric cooling are used.

The cycle is started from the isobaric adsorption and it continues to the next processes. The last values of each process are the initial condition of the next process as can be seen from the Table 7.2. As is seen the outer surface of the adsorbent bed is

maintained at 300 K during isobaric adsorption process and it rises to 340 K during the isosteric heating and finally it increases to 403K for isobaric desorption process. The pressure of the adsorptive at inlet for adsorption and desorption processes are 1.9kPa and 20 kPa respectively.

7.3.4 Details of Solution Procedure

The set of the governing equations are highly nonlinear and coupled. Furthermore, the granule diffusivity and adsorbent bed apparent permeability values are function of dependent variables. The governing equations with the written boundary and initial conditions are solved by Finite Difference Method (FDM). Brief information about the finite difference method is given in Appendix G. In finite difference method, the space and time are discretized to pieces and then the linearized governing equations are written for each node in the computational domain. The set of algebraic equations are solved by inverse matrix method or iterative methods.

The algorithm of solution procedure is illustrated in Figure G3 in Appendix G. The finite difference forms of the convection and diffusion terms are written based on the central difference scheme and implicit method is applied. Firstly, the average adsorbate concentration within adsorbent granule is calculated by using granule mass balance equation (Equation 7.7). The energy equation (Equation 7.5) is solved to find temperature in the adsorbent bed. Based on the obtained adsorbate concentration and temperature fields, the mass transfer equation for the adsorbent bed (Equation 7.6) is solved to determine the distribution of the adsorptive density. The pressure field and velocity distribution in the bed are determined by using the new values of adsorptive density. An inner iteration is performed before increasing a time step. The inner iteration is continued until the defined convergence criterion is satisfied. The following criterion is used to terminate the inner iteration;

$$\left| \frac{(\varphi^{n+1} - \varphi^n)}{\varphi^n \cdot \Delta t} \right|_{max} < 10^{-4} \quad (7.23)$$

where n is a step of inner iteration and φ represents values of the temperature and adsorptive density. The criterion for the outer iteration which provides the termination of program is $\bar{W} < 0.34$ for case 1. The grid distribution is uniform and numbers of grids are 14 for case 1 and 10 grids for case 2. The computer code is written by

FORTTRAN computer language. The following formula is used to determine the average value of a dependent variable (T, P, ρ_w, W) in the bed.

$$\bar{\varphi}(t) = \frac{\int_{R_i}^{R_o} 2R\varphi(rR,t)dR}{(R_o^2 - R_i^2)} \quad (7.24)$$

7.4 Results and Discussions of Case 1

As it was mentioned before, in the study of case 1 heat and mass transfer in an annular adsorbent bed for adsorption process is simulated. The distributions of the bed temperature, adsorbate concentration, adsorptive density and pressure for 0.1 and 0.3 porosities during the adsorption process are illustrated in Figure 7.3. The temperature distribution in the bed can be seen from Figure 7.3a. The initial bed temperature was 300 K. The outer surface temperature of annular bed is assumed to be constant at 300 K. The temperature of the both adsorbent beds increases with time due to the increase in heat of adsorption. After half an hour, the differences between the behaviors of 0.1 and 0.3 porosity cases can be seen in Figure 7.3a. The temperature of the inner shell of annulus ($R = R_i$) for $\varepsilon=0.1$ rapidly rises to $T = 384$ K. The generated heat is not transferred rapidly from the inner surface to the outer surface of annular adsorbent bed due to the low thermal conductivity of the bed. For $\varepsilon=0.3$, the increment in the temperature of inner annulus is more than the increment in the bed temperature with $\varepsilon=0.1$ because of the heat transfer resistance. The thermal conductivity of the bed with $\varepsilon=0.3$ is lower than that of the bed with $\varepsilon=0.1$ due to the poor contact between particles. The adsorbent temperature at the inner shell of annulus reaches to 388 K after 30 min for the 0.3 porosity. Due to the decreasing rate of adsorption, the temperature of the bed decreases with time and at $R = R_i$ the temperature of the bed with $\varepsilon=0.1$ drops to $T = 350$ K after 24 hours. This value for the bed with $\varepsilon=0.3$ is $T = 360$ K. The adsorption rate and consequently the generation of heat in the bed decrease with time and finally the bed temperature drops to 300 K which is the outer surface temperature.

The adsorbate concentration profiles in the bed during the adsorption process are shown in Figure 7.3b. The initial value of adsorbate concentration is zero and it reaches to $0.34 \text{ kg}_w \text{ kg}_s^{-1}$ (or 34%) when the computer program is terminated. As is seen, the adsorbate concentration in the bed increases with time. For the bed with $\varepsilon=0.1$ at $t = 1/2$ hour, the adsorbate concentration in the inner shell of annulus, where the

adsorptive enters, is slightly higher than the adsorbate concentration in the outer shell of annulus. However; the same trend is not observed for the bed with $\epsilon=0.3$. For the adsorbent bed with $\epsilon=0.3$ at $t = 1/2$ hour, the adsorbate concentration in the outer region is higher than the concentration in the inner shell of annulus bed. The increase in the porosity reduces the mass transfer resistance; hence the adsorptive reaches to the outer region of the bed faster. As mentioned in Chapter 6, the adsorption capacity of silica gel increases with the decreasing bed temperature. The numerical results predicted that the adsorption rate is high at the outer shell of annulus (at $R = R_o$) which has lower temperature than the inner shell of annulus. After 24 hours, the adsorbate concentration in the outer surface reaches to its maximum value while a small change of the concentration is seen in the inner shell of annulus. This trend of variation of adsorbate concentration clearly shows that the thermal resistance in the bed controls the heat and mass transfer through the bed. The temperature of the inner shell of annulus decreases with time and the adsorbate concentration increases as a result. Although at the beginning of adsorption periods, the adsorbate concentration in the bed with $\epsilon=0.3$ is higher than the adsorbate concentration of the bed with $\epsilon=0.1$, after 24 hours it becomes less than the concentration of $\epsilon=0.1$ bed due to the high bed temperature. It is known that adsorbate concentration decreases with the increasing bed temperature.

The variation of the adsorptive density through the bed during the adsorption process is shown in Figure 7.3c. Initially, there is no adsorptive in the bed. For $\epsilon=0.1$, a steep density gradient is seen after the first 30 min since adsorptive transfer between the granules is slow due to the low porosity. In the case of $\epsilon=0.3$ porosity, the distribution of adsorptive density in radial direction is completely different. There is no adsorptive density gradient in most of the regions of the bed, except the gradients in the region close to the outer shell due to the temperature difference. The adsorptive density in the outer portion of the bed is higher due to lower temperature in this region. The adsorptive density profiles of two cases approach to each other because of the slow rate of adsorption in the $\epsilon=0.3$ bed.

The variations of adsorptive pressure for both cases are shown in Figure 7.3d. The low porosity in the bed with $\epsilon=0.1$ causes a steep pressure gradient in the radial direction at the beginning of the process as seen from the pressure profile for $t = 1/2$ hour. The gradient of pressure in the radial direction decreases with the increasing time. The trend of the pressure distribution in the bed with $\epsilon=0.3$ is different. The gradients of pressure for both $t = 1/2$ hour and $t = 2$ hours are considerably smaller than the gradients

in the bed with $\varepsilon=0.1$ due to the larger voids between the granules. It should be mentioned that in Figure 7.3d the pressure distribution in the radial direction for $\varepsilon=0.3$ may seem uniform due to the scale of the Y axis chosen to plot the pressure distributions for the both beds in the same graphic. There is no doubt that, a pressure gradient and consequently an adsorptive flow in the radial direction must exist until the final equilibrium condition.

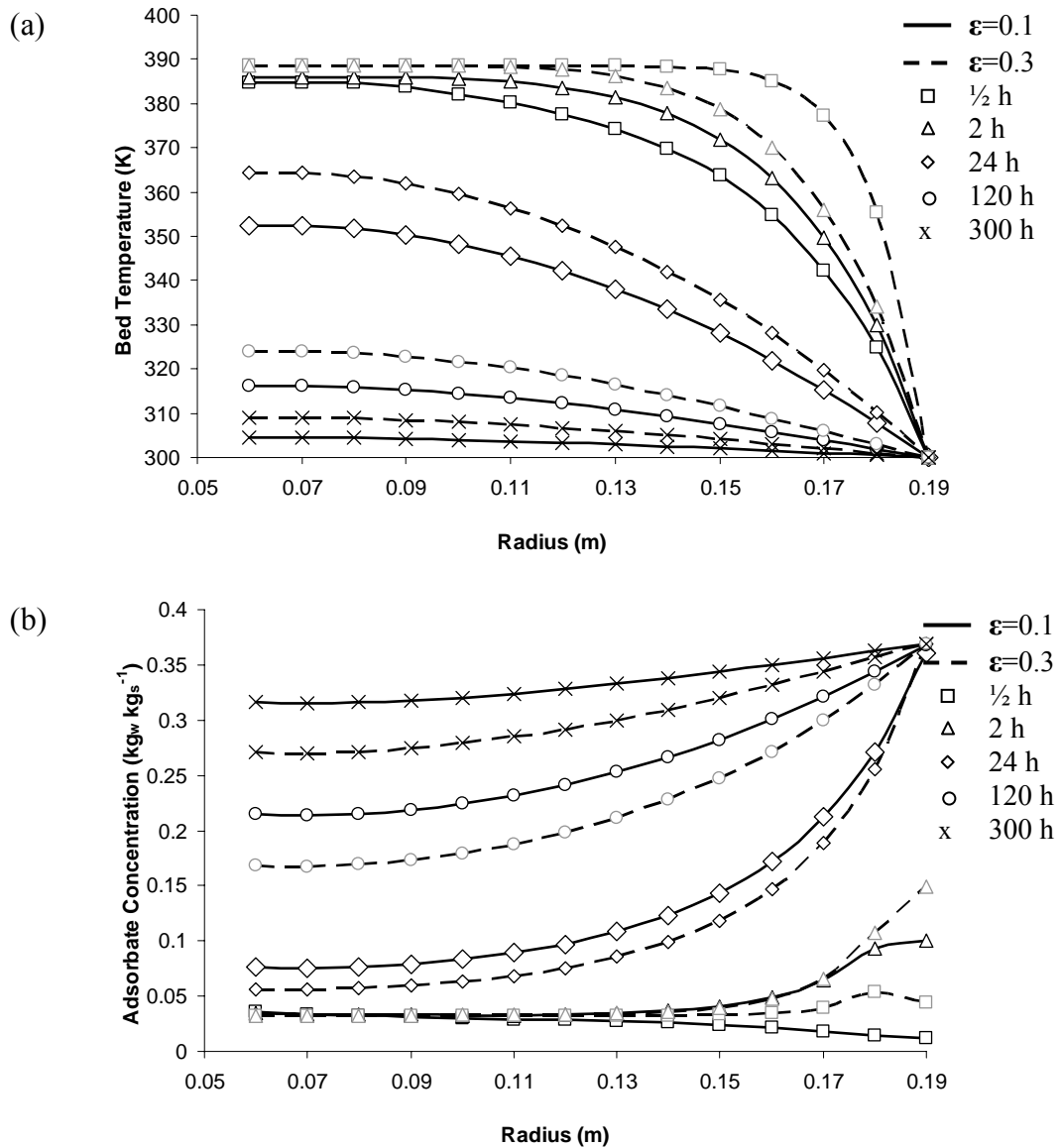


Figure 7.3. Variations of temperature, adsorbate concentration, adsorptive density and pressure in radial direction of adsorbent bed with time, (a) temperature, (b) adsorbate concentration, (c) adsorptive density, (d) pressure

(cont. on next page)

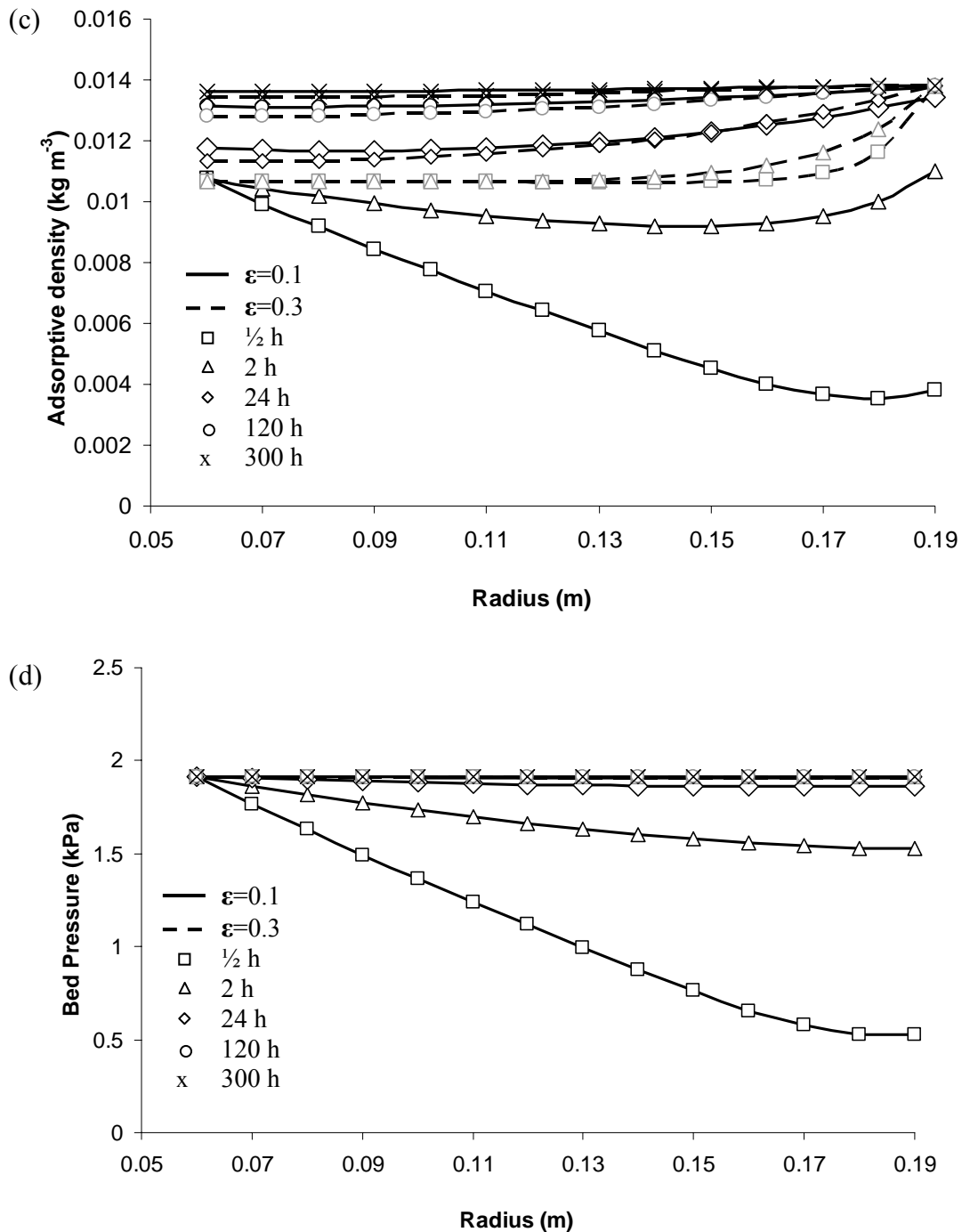


Figure 7.3. (cont.) Variations of temperature, adsorbate concentration, adsorptive density and pressure in radial direction of adsorbent bed with time, (a) temperature, (b) adsorbate concentration, (c) adsorptive density, (d) pressure

The averages of the bed temperature, adsorbate concentration, adsorptive density and pressure during the adsorption process are shown in Figure 7.4. The averages of these dependent variables are calculated by using Equation 7.24. The change of average temperature during the adsorption process is presented in Figure 7.4a. For the early

starting period, the variation of average temperature is also shown as a small graph in Figure 7.4a. After starting of the adsorption process, the temperature of the bed rapidly increases due to the generated heat in the bed. For 0.1 porosity, the average bed temperature increases rapidly from 300 K to 370 K almost at the beginning of the adsorption process. The increase of the porosity from 0.1 to 0.2 causes the rise of the maximum average temperature and it becomes as 378 K in the bed. The average temperature increases with the increasing porosity value since the generated heat can not be transferred through the outer shell of annulus due to the poor thermal conductivity. The increase of porosity from $\varepsilon=0.2$ to $\varepsilon=0.3$ has a smaller effect on the maximum average temperature. After the maximum temperature has been reached, the average temperature slowly declines with time and reaches to the outer surface temperature for three of the adsorbent beds.

The variations of the average adsorbate concentration with time for the three beds are shown in Figure 7.4b. The increase of porosity extends the period of adsorption process. As it was mentioned before, the mass transfer through a granule decreases with the increase of temperature. The increase of porosity reduces the bed thermal conductivity and extends the required time for transferring the generated heat from the bed to the environment. The periods of adsorption process in order to reach to the average adsorbate concentration of $W=0.34 \text{ kg}_w \text{ kg}_s^{-1}$ are 304, 376 and 465 hours for 0.1, 0.2 and 0.3 porosities, respectively.

The variations of the average adsorptive density and pressure are shown in Figures 7.4c and 7.4d, respectively. After beginning of the adsorption process, the averages of both dependent variables approach to the steady state rapidly. These graphics indicate that, the thermal resistance controls the heat and mass transfer in the bed for the studied granular adsorbent, since both adsorptive density and pressure values rapidly reach to almost final equilibrium condition.

In brief, the distributions of temperature and adsorbate concentration are influenced from the bed porosity and the adsorption period increases with the increase of the porosity value. The porosity considerably affects the pressure and adsorptive density distributions at the beginning of the process and after a relatively short time, the averages of these variables approach to the final equilibrium state.

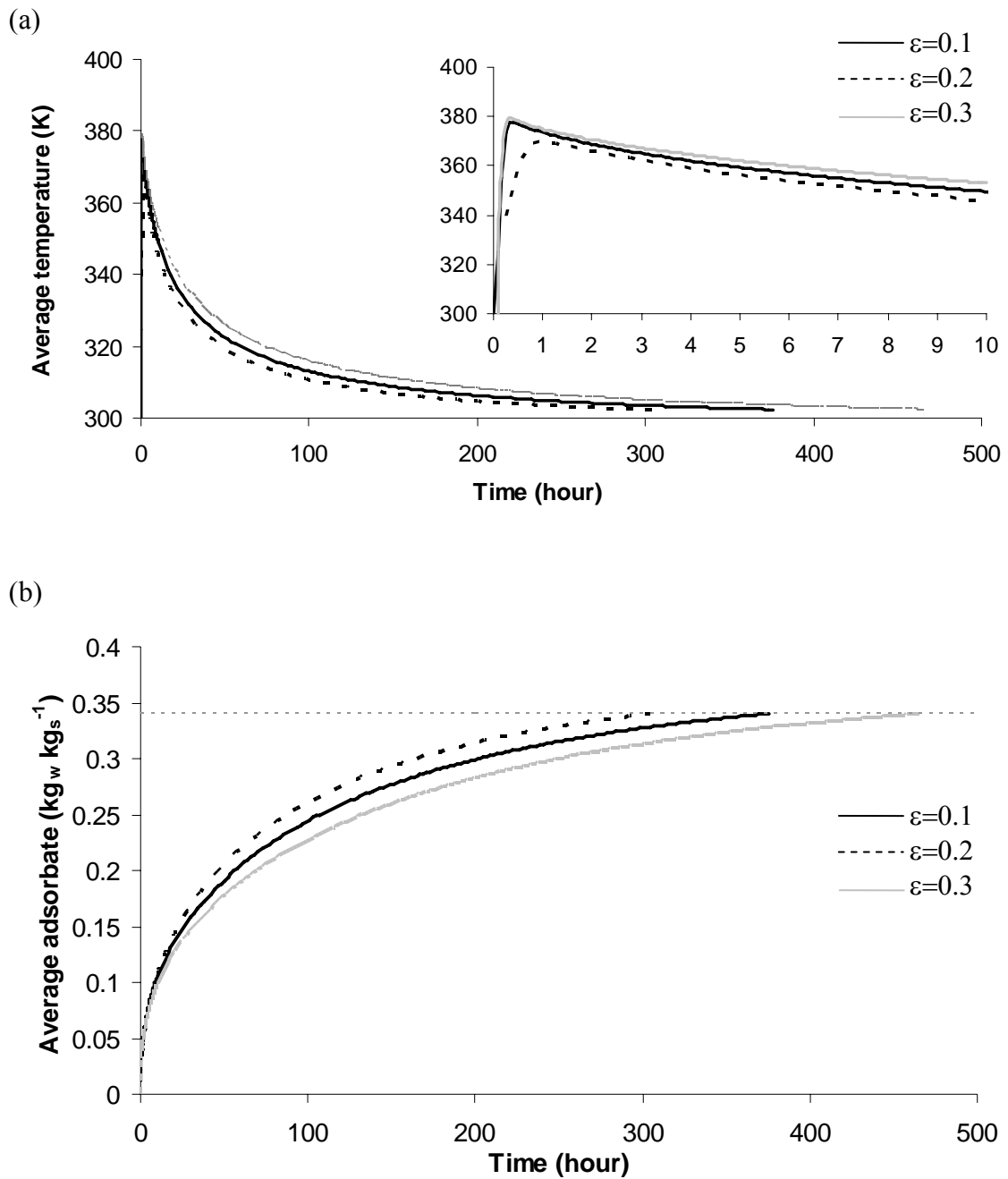


Figure 7.4. The comparisons of averages of temperature, adsorbate concentration, adsorptive density and pressure during the adsorption process for three different adsorbent beds, (a) average temperature, (b) average adsorbate concentration, (c) average adsorptive density, (d) average pressure

(cont. on next page)

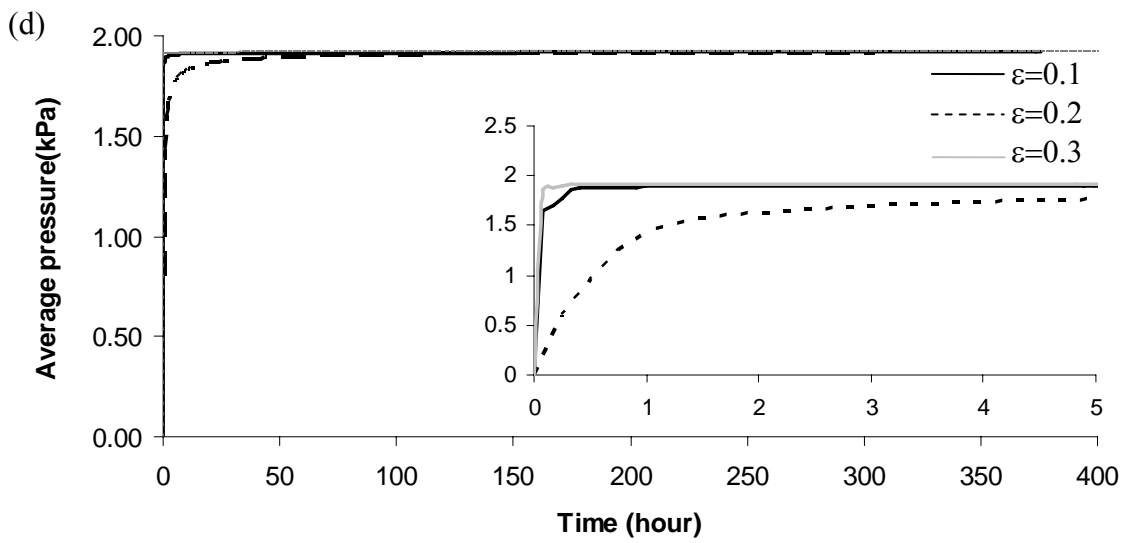
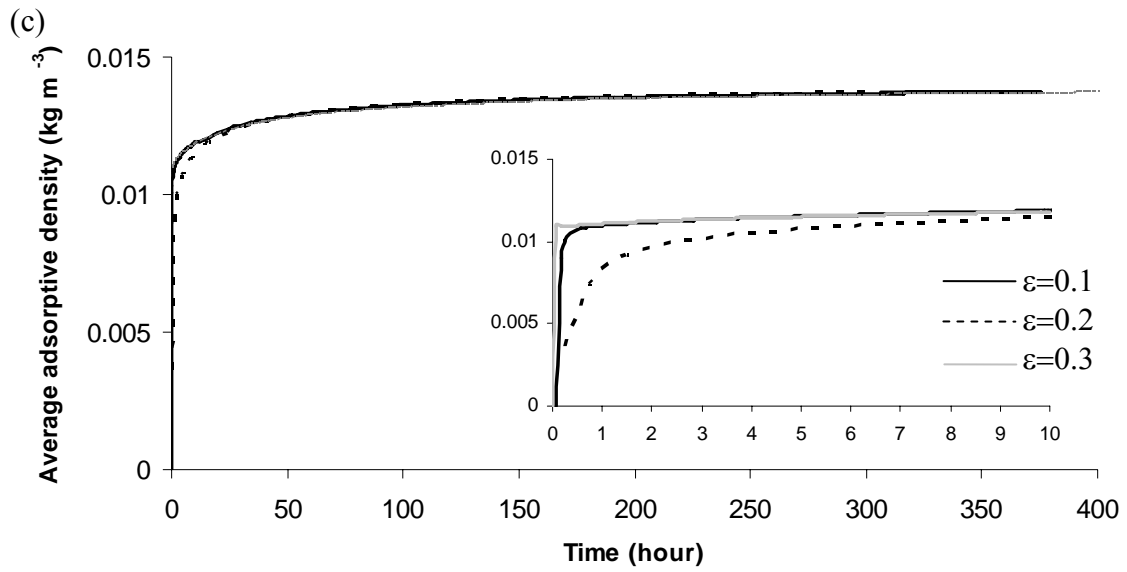


Figure 7.4. (cont.) The comparisons of averages of temperature, adsorbate concentration, adsorptive density and pressure during the adsorption process for three different adsorbent beds, (a) average temperature, (b) average adsorbate concentration, (c) average adsorptive density, (d) average pressure

7.5 Results and Discussions of Case 2

The heat and mass transfer in the annular adsorbent bed for all cycle processes is studied in case 2. Figure 7.5 illustrates the obtained cycle based on the average pressure and temperature in the adsorbent bed. The dashed line shows the ideal cycle according to the boundary conditions defined in Table 7.2 and continuous lines shows the obtained cycle. The first cycle is called as start up cycle in this study. This cycle is different than the cycles 2 and 3. The difference appears particularly in the isobaric adsorption process. The other processes of the cycle 1 (isosteric heating, cooling and isobaric desorption) are same with the cycle 2 and cycle 3. The reason of the difference between cycle 1 and cycles 2 and 3 comes from the initial conditions. The heat of adsorption increased the adsorbent bed temperature when the adsorption process is started in the completely dried bed. As mentioned in Chapter 6, the heat of adsorption at low coverage is greater. Thus, the high heat of adsorption increases the adsorbent bed temperature to 473K for the isobaric adsorption process in start-up cycle.

The initial conditions of the cycle 2 are obtained from the results of the cycle 1 and the procedure is continued for the cycle 3. The cycles 2 and 3 are same as can be seen from the Figure 7.5. Hence, the cycle 3 is the permanent cycle and the further cycles have the same behavior of the cycle 3. In this chapter, all discussions are performed for cycle 3.

The adsorption process is completely isobaric, the adsorptive pressure does not change and it is constant as 1.9 kPa for cycles 2 and 3. The adsorbate concentration in the adsorbent bed increases from 11.5 % $\text{kg}_w \text{kg}_s^{-1}$ to 30% $\text{kg}_w \text{kg}_s^{-1}$. During the isosteric heating, the adsorbate concentration is constant and the adsorbent pressure increases from the evaporator to the condenser pressure.

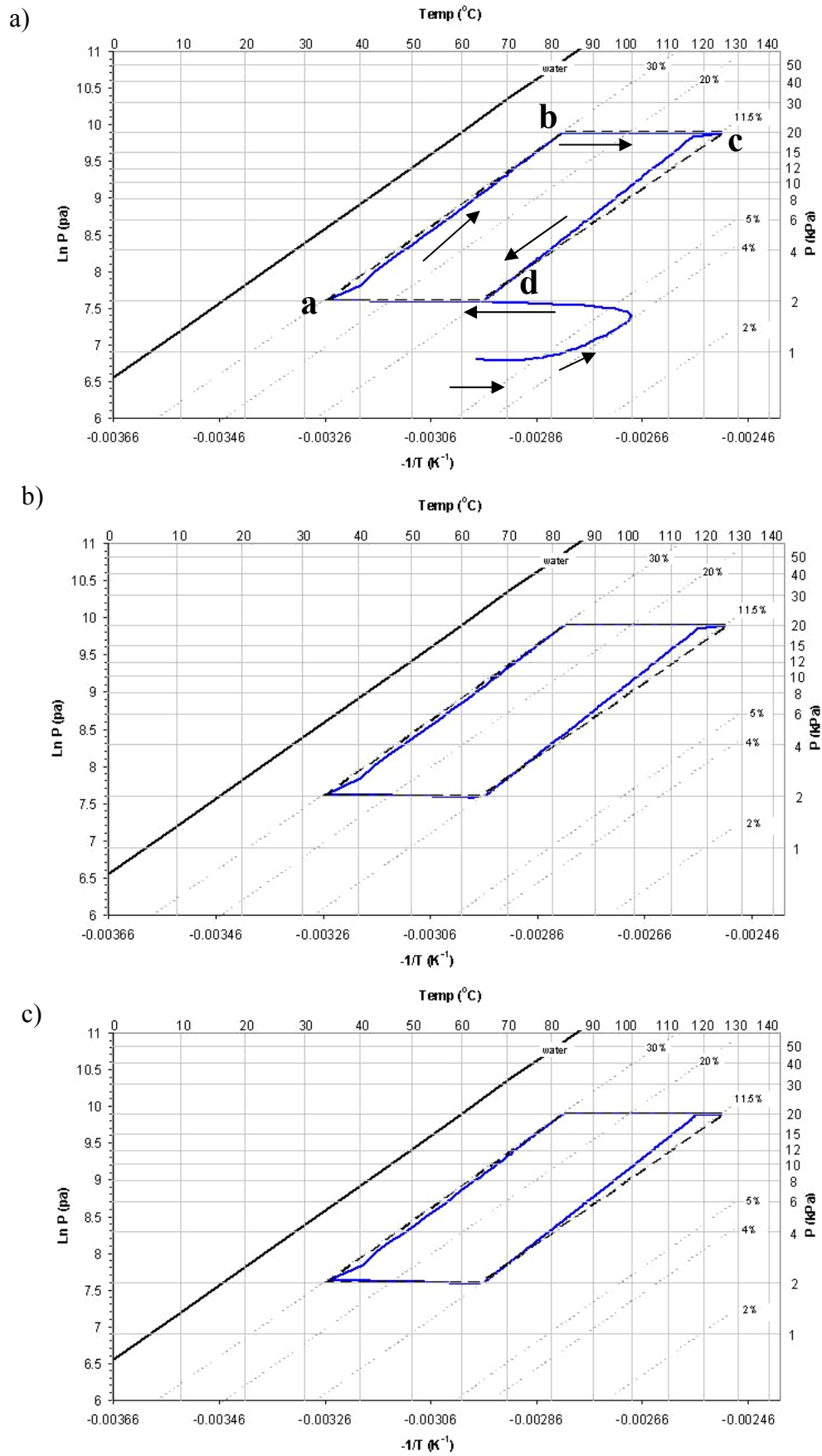


Figure 7.5. $\ln P$ vs $-1/T$ diagram of simulated a) startup cycle b) cycle 2 and c) cycle3

The isobaric desorption process almost fits the ideal cycle as shown in Figure 7.5c. A small deviation during the isosteric cooling is observed, but cooling of the adsorbent bed and decreasing of pressure from condenser to the evaporator pressure is almost isosteric. The reason for these small deviations during the isosteric cooling may be the sudden change of temperature from 403 K to 300 K. The small deviation may be eliminated by using great number of grids and reducing numerical errors.

The temperature distribution in the radial direction of the bed for four processes of the cycle is shown in Figure 7.6. The temperature distribution in the bed during adsorption process is shown in Figure 7.6a. The outer surface of the adsorbent bed is 300 K and the adsorbent temperature is higher in the inner region. The temperature of the adsorbent bed decreases with time except the inner region because of the low thermal conductivity of the adsorbent bed. Just after 6 hours, the temperature of the inner surface of annulus ($R = R_i$) starts to decrease as shown in Figure 7.6a. The generation of heat during the adsorption process is another reason of slow cooling of the adsorbent bed. After 80 hours, the average temperature of the bed decreases to approximately 307 K.

The surface of the adsorbent bed is maintained at the 403 K during isosteric heating process as seen from Figure 7.6b. A steep temperature gradient is observed in the region close to the outer surface of annulus. The bed temperature starts to rise and the temperature in most of the regions of the adsorbent bed are uniform. After 50 minutes, the bed temperature reaches to 360K.

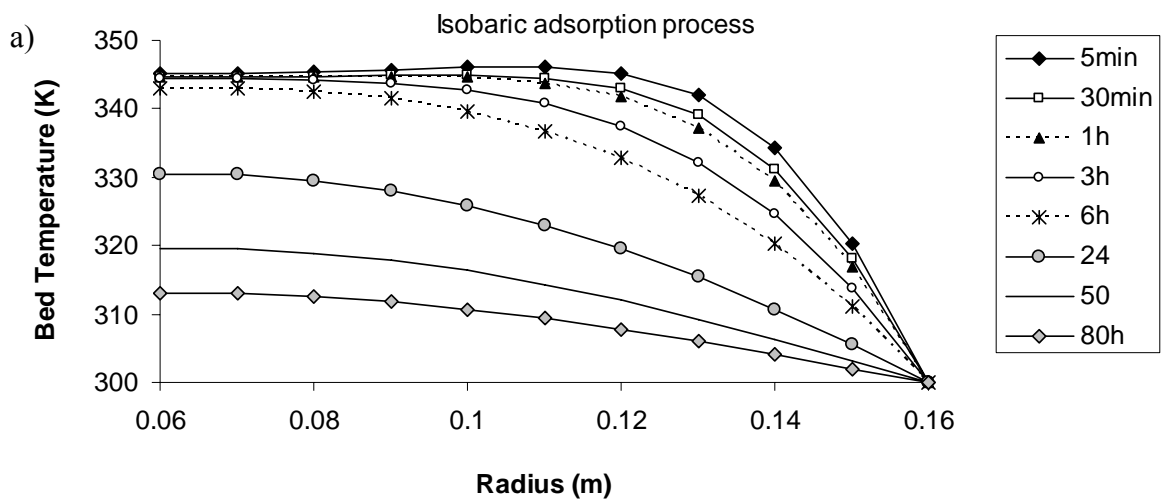


Figure 7.6. The distribution of bed temperature in the adsorbent bed a) isobaric adsorption process, b) isosteric heating process, c) isobaric desorption process, d) isosteric cooling process

(cont. on next page)

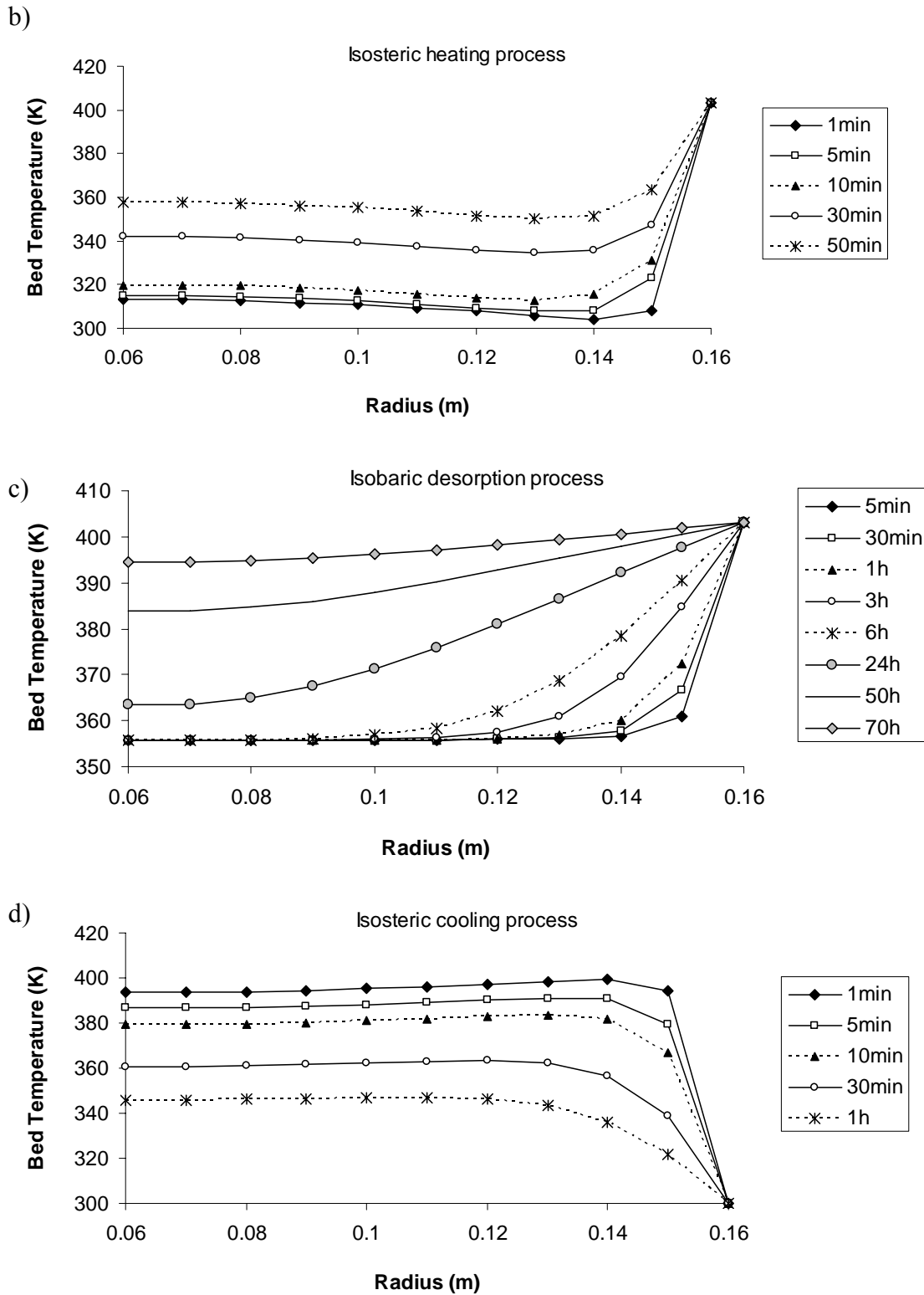


Figure 7.6. (cont.) The distribution of bed temperature in the adsorbent bed a) isobaric adsorption process, b) isosteric heating process, c) isobaric desorption process, d) isosteric cooling process

In isobaric desorption process shown in Figure 7.6c, the outer surface of adsorbent bed is still at 403 K. The temperature of outer region of annulus increases rapidly however; the temperature of the inner region of the annulus increases slowly

because of the poor thermal conductivity of adsorbent bed. A portion of heat which is transferred from the outer surface of the annulus to the adsorbent bed is also used to desorb adsorbate from the adsorbent particle. The adsorbent bed can reach to the point c, shown in Figure 7.5, after the 70 hours. The temperature distribution for the isosteric cooling process is shown in Figure 7.6d. Similar to the isosteric heating, the temperature distribution in most of the regions of the adsorbent bed is uniform during the isosteric cooling and the process is finished rapidly. After 1 hour, the temperature of the adsorbent bed drops to T_d temperature.

The variation of adsorbate concentration in the granules along the radius of the bed is shown in Figure 7.7 for four processes of the cycle. The change of the adsorbate concentration in the adsorbent bed during the adsorption process is shown in Figure 7.7a. The adsorbate concentration is high in the region near to the outer surface of annulus which has lower temperature. The temperature strongly affects the mass transfer in the adsorbent granule although the effective diffusivity of the granule increases with the increasing temperature in the adsorbent bed as shown in Figure 6.5 in Chapter 6. The presence of high temperature reduces the concentration of the water vapor adsorption in the adsorbent as shown in Figure 6.1. Hence, the adsorbate concentration in the outer region is higher than that of inner region of the annulus adsorbent bed. The adsorbate concentration at the inner region of the annulus increases when the temperature of the adsorbent in that region decreases. The average concentration of the adsorbate has reached to $30\% \text{ kg}_w \text{ kg}_s^{-1}$ after 80 hours. Figure 7.7a also shows that the thermal resistance in the adsorbent bed controls the heat and mass transport in the adsorbent bed.

In Figure 7.7b, which refers to the isosteric heating, the adsorbate concentration fluctuates in the adsorbent bed due to the change of temperature in the bed. The average of the adsorbate concentration remains constant during the isosteric heating process. The fluctuations of the adsorbate concentration in the adsorbent bed disappear after 50 minutes.

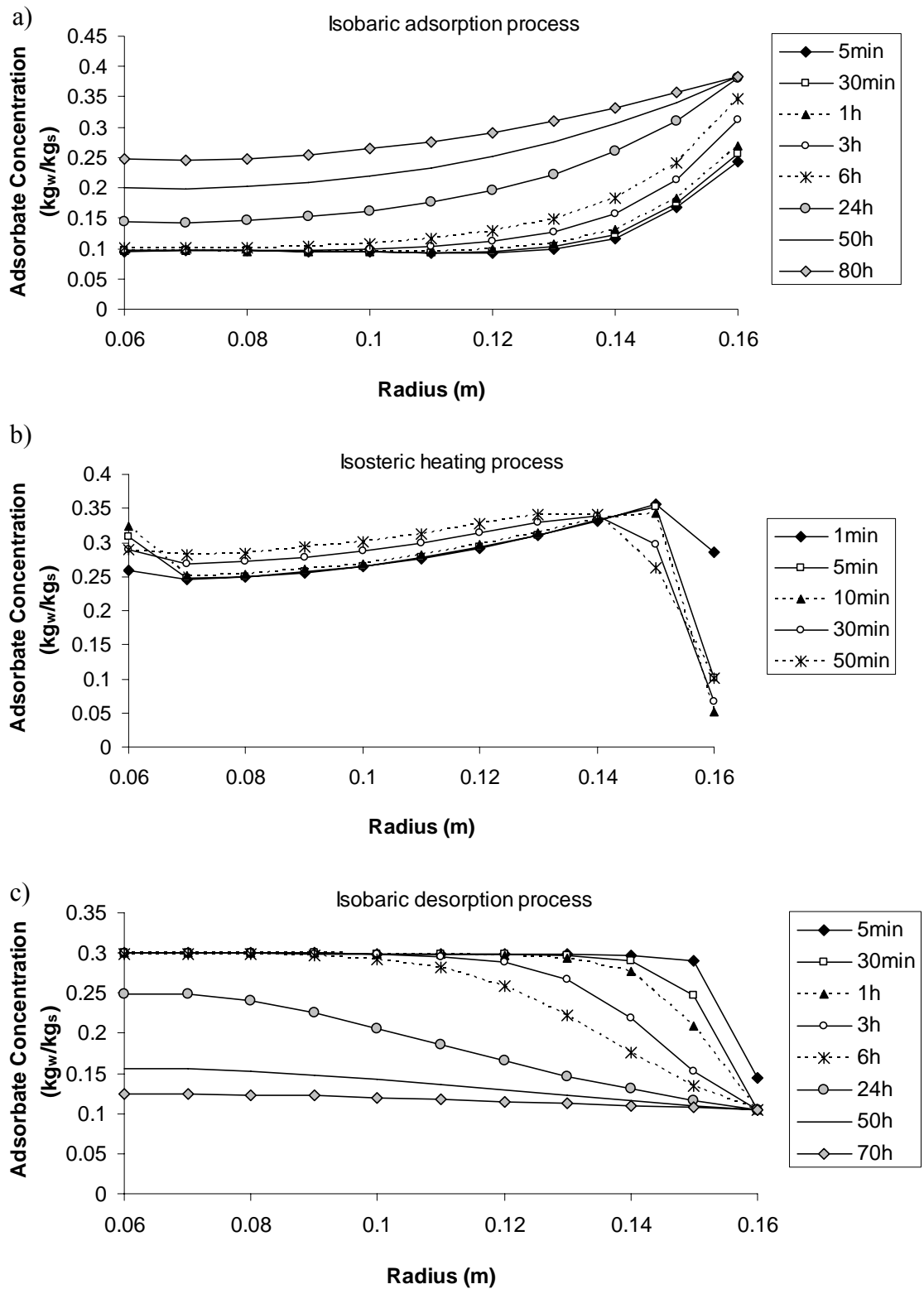


Figure 7.7. The variation of adsorbate concentration in the adsorbent bed for a) isobaric adsorption process b) isosteric heating process c) isobaric desorption process d) isosteric cooling process

(cont. on next page)

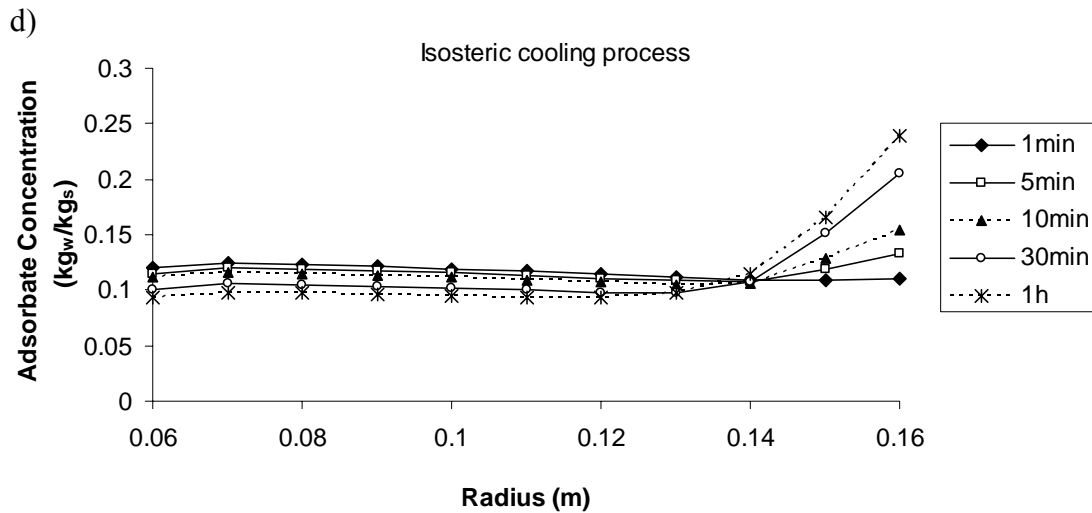


Figure 7.7. (cont.) The variation of adsorbate concentration in the adsorbent bed for a) isobaric adsorption process b) isosteric heating process c) isobaric desorption process d) isosteric cooling process

The distribution of the adsorbate concentration in the isobaric desorption process is shown in Figure 7.7c. The adsorbate concentration at inner region of the adsorbent bed remains constant during the first 6 hours. The poor heat transfer rate prevents rapid transfer of heat through the inner region of the adsorbent bed and, furthermore a portion of transferred heat to the adsorbent bed is consumed to desorb water from the adsorbent particle (heat of desorption). Therefore, the adsorbate concentration decreases from 0.3 to 0.115 kg_w kg_s⁻¹ just after a long period as 70 hours.

Figure 7.7d illustrates the distribution of adsorbate concentration in the adsorbent bed during the isosteric cooling in which the adsorbate concentration is low. The small adsorbate concentration fluctuations are observed because of the temperature variations in the bed. However, the average of adsorbate concentration remains constant as expected since the isosteric heating/cooling is defined as the change of pressure against temperature at constant adsorbate concentration.

The variation of adsorptive pressure in the bed during adsorption process is shown in Figure 7.8 for processes of cycle 3. In early stages of adsorption process, the increase in the amount of adsorbate decreased the bed pressure at outer region as shown in Figure 7.8a. After 1 hour, the steep gradient of pressure in the adsorbent bed disappears and the adsorptive pressure in the whole region of the adsorbent bed becomes close to the evaporator pressure. During the isosteric heating and cooling (Figure 7.8b and d), a uniform pressure distribution is observed in the bed since the adsorbate concentration is constant during these processes and there is no adsorptive

inlet and outlet to/from the adsorbent bed. The uniform bed pressure gradually increases or decreases with increasing or decreasing bed temperature during the isosteric heating or cooling processes. The pressure distribution in the adsorbent bed during isosteric heating and cooling (Figures 7.8a and c) indicates that mass transfer resistance in the adsorbent bed is not so high when compared to the thermal resistance since the pressure is almost constant.

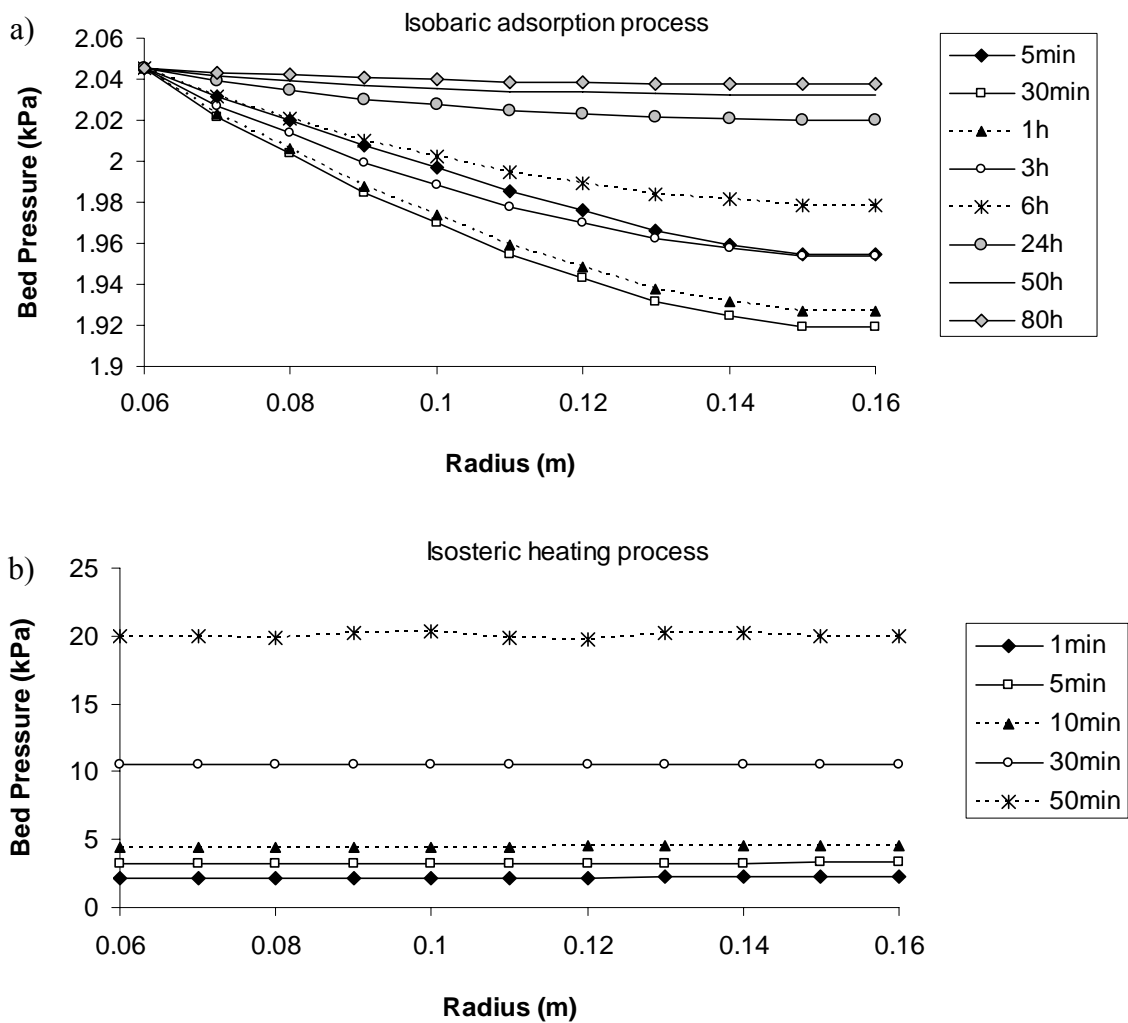


Figure 7.8. Pressure variation in the adsorbent bed a) isobaric adsorption process b) isosteric heating process c) isobaric desorption process d) isosteric cooling process

(cont. on next page)

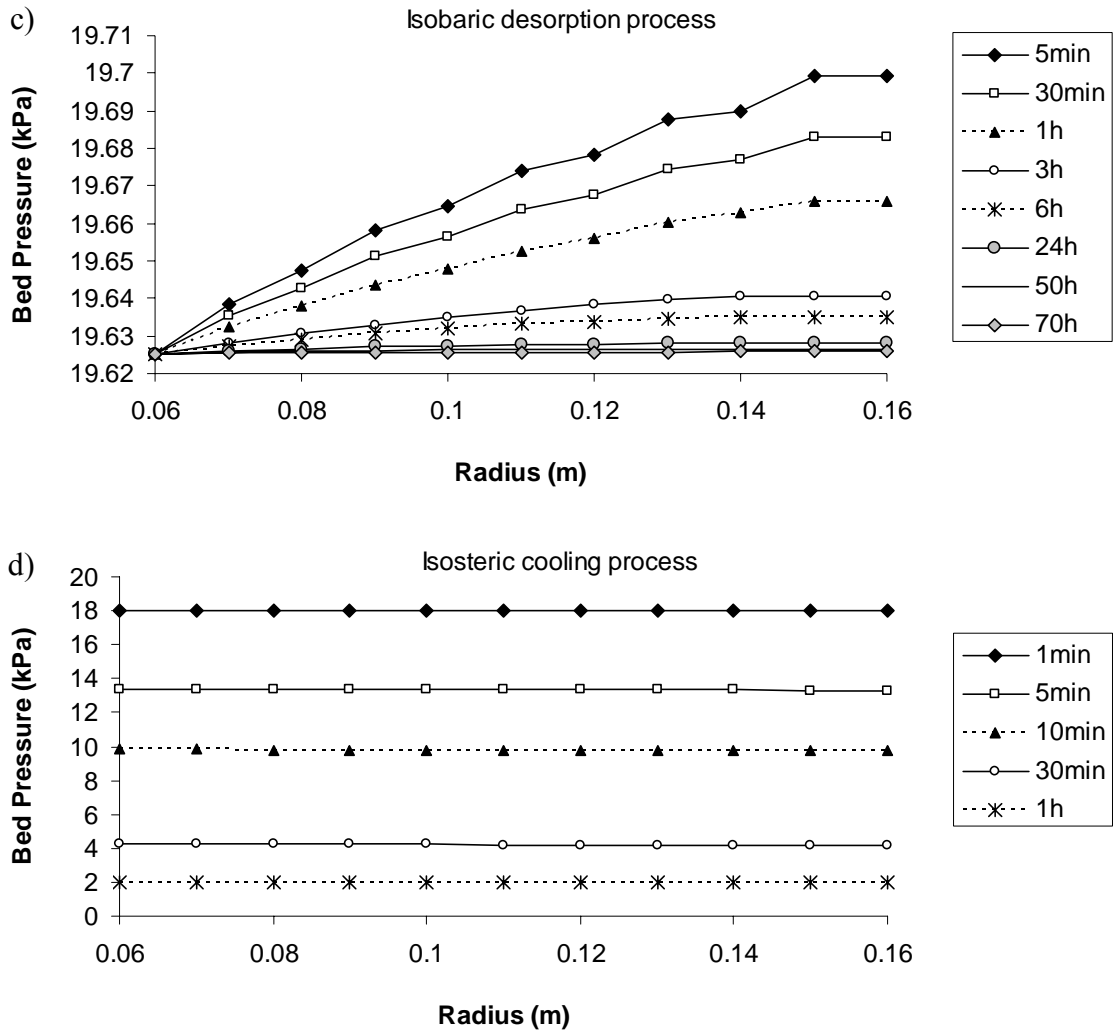


Figure 7.8. (cont.) Pressure variation in the adsorbent bed a) isobaric adsorption process b) isosteric heating process c) isobaric desorption process d) isosteric cooling process

Figure 7.8c illustrates the pressure distribution in the adsorber during the isobaric desorption process. The bed pressure in the outer region of the annular adsorber is higher compared to the inner region and this causes the flow of adsorptive from the outer region to the inner region. After 6 hours, the pressure gradient in the adsorbent bed is decreased considerably. Although the process is isobaric, a small pressure difference exists along the radius of the adsorbent bed which causes the flow of adsorptive from adsorbent bed to the condenser.

Figure 7.9 shows the variations of the average temperature of the adsorber for processes of cycle. The dashed line shows adsorber outer surface temperature and continuous lines show the average temperature of adsorber. The isosteric heating and cooling processes are too short, around 1 hour; hence they can be seen as a vertical line

in the graph. The outer surface temperature of adsorber is 300 K during isosteric cooling and adsorption process and it is maintained at 403 K during the isosteric heating and isobaric desorption. The average temperature of the bed is approximately 340 K at the beginning of the adsorption process and it gradually drops to 307 K. The average bed temperature drops to the temperature of point “a” after 80 hours. The bed temperature increases to 356 K during the isosteric heating process and then increases to 400 K during isobaric desorption process. As is seen in Figure 7.9, most of the cycle period is consumed during the isobaric adsorption and desorption processes. The low thermal conductivity in the annular adsorbent bed is the main reason for this long adsorption and desorption periods.

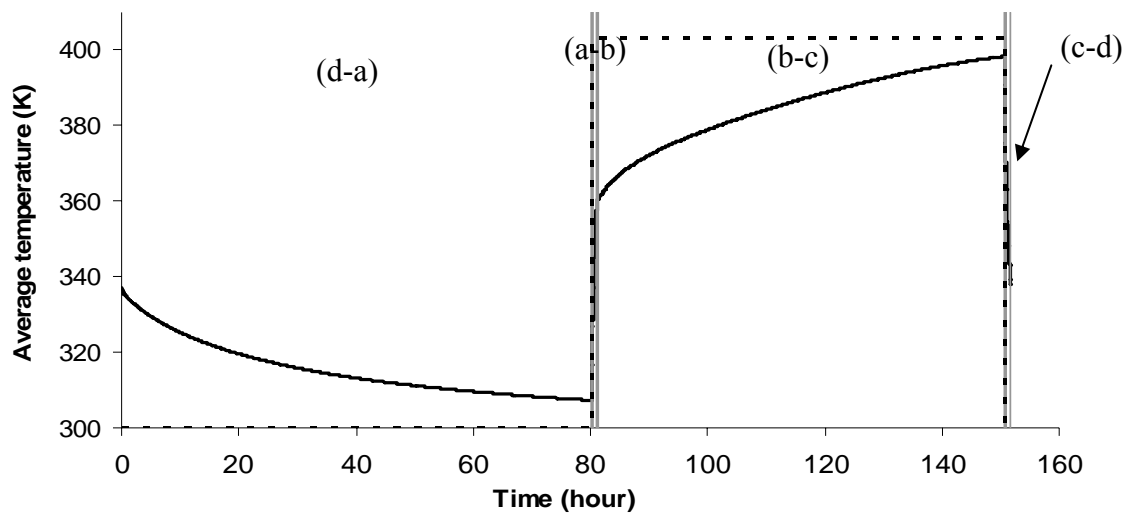


Figure 7.9. The variation of the adsorbent bed average temperature for a cycle

The average adsorbate concentration in the adsorbent bed for a complete cycle is illustrated in Figure 7.10. The average adsorbate concentration increases from $0.115 \text{ kg}_w \text{ kg}_s^{-1}$ to $0.30 \text{ kg}_w \text{ kg}_s^{-1}$ during the isobaric adsorption process and it remains constant during the isosteric heating process. In the isobaric desorption process, the water is removed from the adsorbent by heating the adsorbent bed and the average adsorbate concentration is reduced to 0.115. The adsorbent bed is cooled during the isosteric cooling process for reducing the bed pressure to the evaporator pressure while the adsorbate concentration remains constant.

Figure 7.11 depicts the average bed pressure against time for the four processes of the cycle. The average bed pressure remains constant for the isobaric adsorption and desorption processes as expected. The bed pressure gradually increases to 20 kPa during

isosteric heating process and decreases to 1.9 kPa during the isosteric cooling process. As it was mentioned before, the periods of isosteric heating and cooling are too short and the changes of adsorbent pressure during these processes are too steep.

The simulation of heat and mass transfer is successfully performed for an annular adsorbent bed. The obtained results showed that most of the cycle period is consumed for isobaric adsorption and desorption. The thermal resistance is the main parameter that causes slow heat transfer in the bed and also affects the mass transfer.

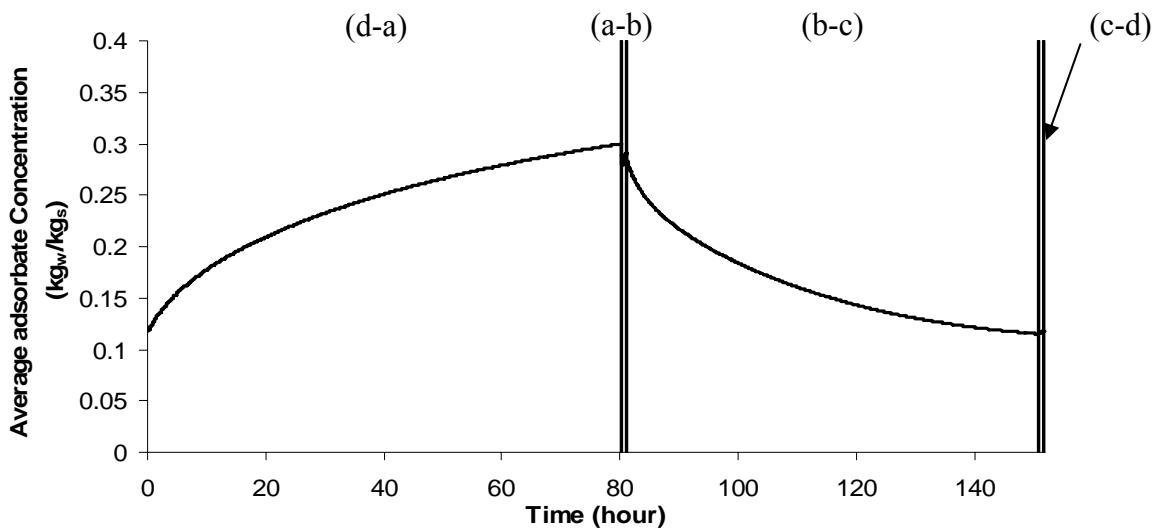


Figure 7.10. The change of average adsorbate concentration during a cycle

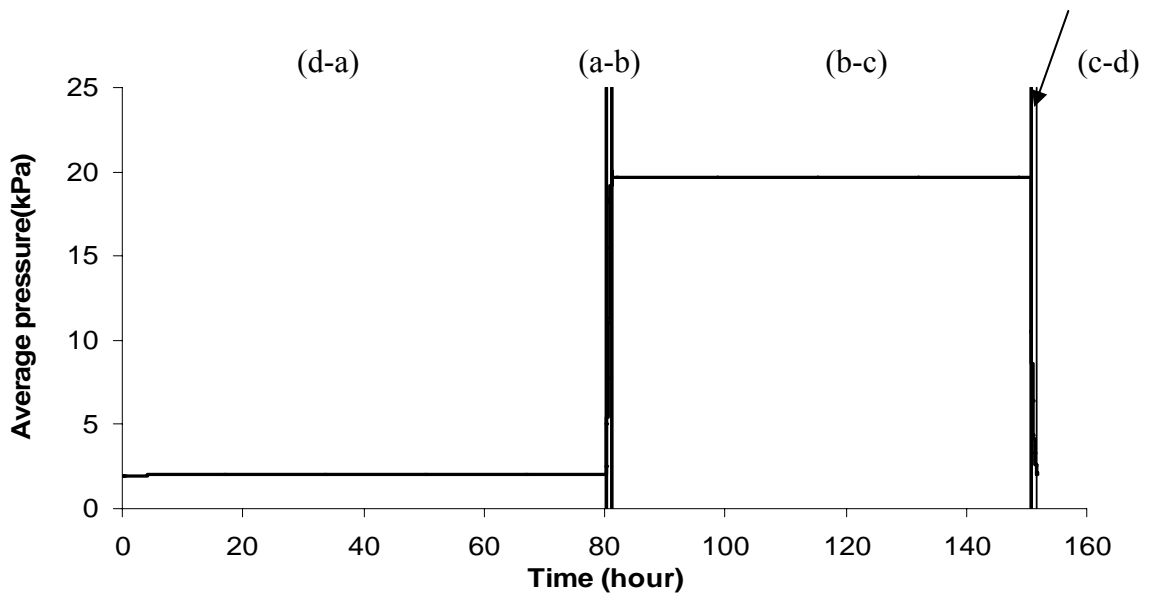


Figure 7.11. The variation of average bed pressure during a cycle

7.5.1 Comparison of Experimental and Numerical Cycles

The adsorption heat pump cycle was numerically simulated for the considered adsorbent bed. The dimensions and configuration of the considered adsorbent bed were very similar with the first designed adsorption heat pump. Figure 7.12 illustrates the variation of average bed temperature during the cycle processes for experimental and numerical cycles. The cycle processes of AHP-1 are represented with dotted line while the cycle processes of the considered adsorbent bed are presented with straight line. The period of the experimental cycle was 6600 minutes whereas the period of the numerical cycle was 9100 minutes. The general behaviors of the experimental and the numerical cycles are very similar but the periods of cycle processes are significantly different. The reason is that the heat transfer in the adsorbent bed of AHP-1 was enhanced by six fins whereas the considered adsorbent bed does not contain any fin.

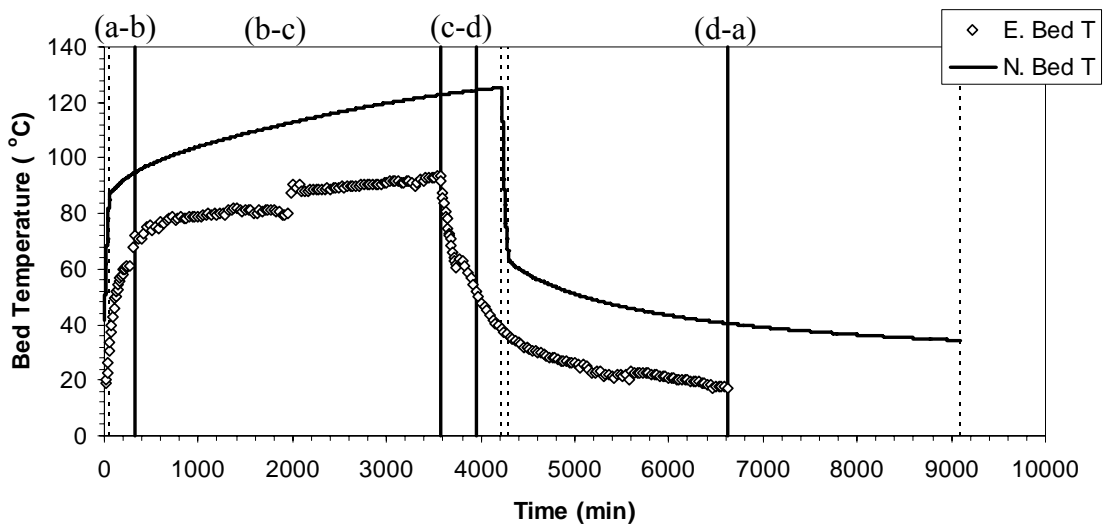


Figure 7.12. The variations of average bed temperature for experimental and numerical cycles

Figure 7.13 shows the variations of average bed pressure during cycle processes for the experimental and the numerical cycles. The average bed pressures are constant for the experimental and the numerical cycles during isobaric adsorption and desorption processes. The periods of isobaric and desorption processes of AHP-1 are significantly shorter than that of the considered adsorbent bed. However, the periods of isosteric cooling and heating processes of AHP-1 are longer than that of the considered adsorbent bed. In the experimental study, the adsorbent bed was heated gradually during the

isosteric heating processes thus, the period of isosteric heating process of AHP-1 was observed longer than that of the numerical cycle. The surface temperature of adsorbent bed for AHP-1 was not kept at 300 K as similar as numerical simulated cycle. Therefore, the cooling period of adsorbent bed of AHP-1 is longer than the cooling period of the considered adsorbent bed.

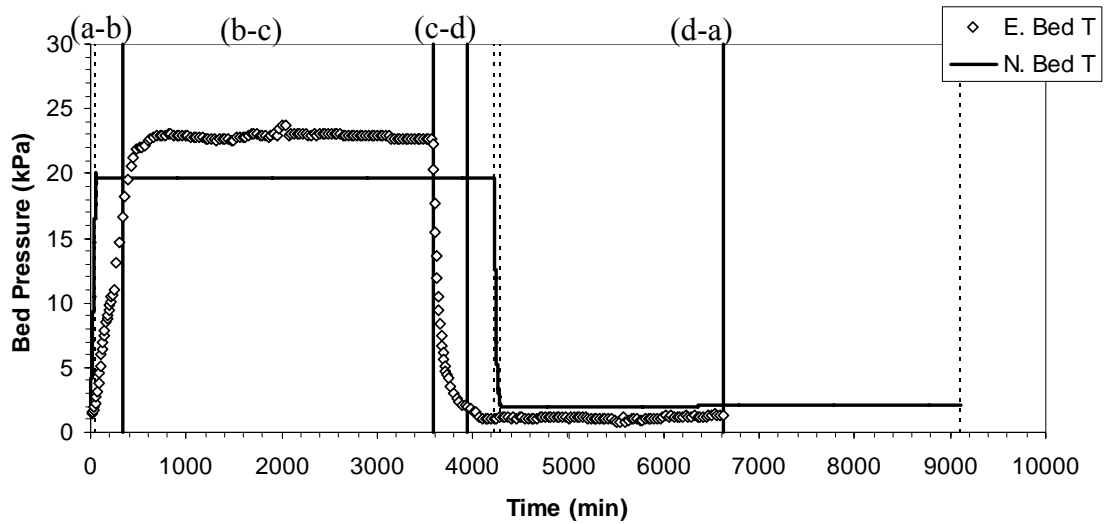


Figure 7.13. The variations of average bed pressure for experimental and numerical cycles

Table 7.3 illustrates the amount of heat transferred during the processes of experimental and numerical cycles. The heats are evaluated by using the Equations from 2.3 to 2.6. The summations of transferred heats for experimental and numerical cycle are 8 and 44 kJ kg^{-1} respectively. But these residues are only 2% of total transferred heat during the cycle processes.

Table 7.3. The amounts of heat transfer for cycle processes

Heats (kJ kg^{-1})	Experimental Cycle	Numerical Simulated Cycle
Q_{a-b}	92	112
Q_{b-c}	146	542
Q_{c-d}	-65	-82
Q_{d-a}	-165	-528
Q_{ev}	97	430
Q_{cond}	-101	-440
Residual Q	8	44

CHAPTER 8

CONCLUSIONS

Adsorption heat pumps (AHP) which have gained remarkable attention in recent years offer an alternative method for cooling and heating systems and for storing energy while considering environmental aspects which is one of the vital issues of novel technology. This study includes the working principle of adsorption heat pumps, a detailed literature survey, general information about adsorption phenomena, experimental results of two designed and constructed AHPs, the numerical analysis for modeling the systems and microcalorimetric research for obtaining isosteric heat of water vapor - silica gel pair. Based on the obtained numerical and experimental results, following remarks can be concluded from the study;

1- One of main problems in the application of adsorption heat pumps is leakage. This problem was overcome in the first and second designed and constructed adsorption heat pumps. Thus, the repetition of the cycle under the same pressure levels in spite of many connections such as valves, pressure transducers, and thermocouples were provided. The COP of cooling of the AHP-1 was found between 0.41 and 0.44. For the presented cycles, the SCP and SHP values were found as 0.25-0.37 and 0.83-1.17 W kg⁻¹ respectively. The period of the cycles was around 6600 minutes.

2- In order to increase COP, SCP and SHP values of the adsorption heat pump, the second intermittent adsorption heat pump was designed and manufactured. The heat transfer area of adsorbent bed of AHP-2 was increased from 0.74 m², which is heat transfer area of adsorbent of AHP-1, to 4.08 m² by using the fins. Additionally, heat exchangers were mounted in the evaporator and condenser to provide cold and hot water. The experiments were performed by the AHP-2 and two representative cycles were presented. The COP of presented cycles was achieved around 0.53 which is 22% higher than that of AHP-1. The SCP and SHP values were also found as 1.34 and 1.76 W kg⁻¹, respectively. These values are 200% and 170% greater than the SCP and SHP values of AHP-1. The improvement of heat transfer rate increased the SCP and SHP values of the system, since the period of cycle was reduced. The period of presented cycle was around 6000 minutes. However, the period of cycle of the second AHP-2 still

was long which may constitute an obstacle for commercial application. The results of the AHP-2 showed that the use of fins for enhancing heat transfer through the bed is not sufficient and hence another solution is required to accelerate the heat transfer. The use of fins decreased the ratio of mass of adsorbent over metal mass of bed, therefore the most of the energy is consumed to heat and cool the metal mass of bed.

3- In order to achieve higher SCP and SHP, the thermal conductivity of the adsorbent bed should be improved to possess a higher rate of heat transfer through the adsorbent bed of AHP-2. For the enhancement of thermal diffusivity of the silica gel bed, metal pieces were added to the adsorbent bed. The silica gel granules were mixed separately with four different metal pieces as aluminum, copper, brass and stainless steel (AISI-304). The experiments were performed for two size ranges of metal pieces as 1 – 2.8 mm and 2.8 – 4.75 mm. The obtained results showed that, the heat transfer rate in the bed containing aluminum additive of 1-2.8 mm size, is higher than other additives because of the higher thermal diffusivity. The thermal conductivity and thermal diffusivity of pure silica gel were enhanced by 153.5% and 90.5%, respectively with loading 15wt% aluminum additive. The increase of thermal diffusivity and conductivity of silica gel – Al can increase the performance criteria of adsorption heat pump.

For enhancing the heat transfer rate through the adsorbent bed without decreasing the COP of AHP-2, 10wt% of Al additive was mixed with silica gel adsorbent. The difference between the thermal diffusivity values of 10wt% and 15wt% Al loaded adsorbent bed was not significant. Moreover, the adsorption capacity for 10wt% Al-silica gel mixture is higher than that of the 15wt% Al-silica gel mixture due to the high amount of silica gel for 10wt% of Al addition. The addition of 10wt% of Al into silica gel in the adsorber increased the heat transfer rate and the cycle period was significantly reduced from 6000 min to 2800 min. However, the decrease of the COP of system compared to the AHP-2 without Al pieces was only 15%. The amount of silica gel in the adsorber was reduced from 40kg to 32kg. The SCP and SHP values of Al-loaded AHP-2 were found as 1.1 and 3.3 W kg⁻¹ and an increase around 250% for SCP and SHP values were observed.

4- The isotherms, kinetics and heat of adsorption of water vapor adsorption on silica gel were provided by using Tian-Calvet type microcalorimeter which is a volumetric system. The amount of adsorbate decreased with the increasing adsorption temperature. The silica gel adsorbed 0.6, 0.98, 1.1, 1.4, 2, 3.5, 11, 13 and 14 %wt water

vapor at 120, 110, 100, 90, 75, 60, 40, 35 and 30°C, respectively. Therefore the maximum water adsorption capacity of silica gel was found as 14% for 30°C adsorption temperature. The increasing adsorption temperature decreased the differential heat of adsorption due to the reducing adsorbate-adsorbent interactions as shown in Figure 6.3. The isosteric heats of adsorption were calculated by using Classius-Clapeyron equation from isotherms. The Classius – Clapeyron diagram of water-silica gel pair was also drawn by using obtained isotherms as shown in Figure 6.6. The obtained curves in the Classius – Clapeyron diagram were modeled (Equations 6.4 and 6.5) for using in numerical study. The diffusivities of water vapor inside the silica gel for short and long range periods were described by using kinetics data as a function of temperature (Equation 6.7 and 6.8) in Arrhenius form. For further study, the short range water vapor diffusivity can be used. The Biot mass numbers were estimated for the temperatures of cycle processes. The Biot numbers indicate that the intraparticle mass transfer resistance is dominant relative to the external mass transfer resistance around the adsorbent granule. For considering importance of heat or mass transfer inside adsorbent bed, the Lewis numbers were determined at four temperatures. The results indicate that the thermal resistance in the adsorbent bed is important relative to the mass transfer resistance in the bed.

5- The governing equation for heat and mass transfer in an annular adsorbent bed filled with the adsorbent granule were derived and these equations were numerically solved for two cases. In the first case, the temperature and concentration profiles of a dried adsorbent bed during the adsorption process were obtained. The obtained numerical results showed that the increase of porosity reduced the bed thermal conductivity and consequently heat transfer rate through the bed. Even for porosity of 0.1, heat transfer controls the period of adsorption process. At the beginning of adsorption and desorption process, a steep pressure gradient in the radial direction of the bed having low porosity occurs but the gradient decreases after a short period. In the second case; the numerical results for a complete cycle of adsorption heat pumps involve isobaric adsorption, isosteric heating, isobaric desorption and isosteric cooling were successfully obtained. The permanent cycle can be obtained after two cycles, in other words at least two cycles should be performed to reach the permanent cycle. The period of cycle takes 152h for the simulated annular adsorbent bed. The main reasons of the long period of cycle are the low thermal conductivity of adsorbent and poor contact between particles and between particle and metal of adsorbent bed. The results of the

second case also showed that heat transfer resistance controls the heat and mass transport through the bed rather than mass transfer resistance.

Gui et al. (2002) found experimental SHP of their system (Figure 2.8a) was about 400 W kg^{-1} and cycle period was 17min. Saha et al. (2006a) constructed plate fin adsorbent bed as shown in Figure 2.8c. The cycle period of this system was found as 125min. For commercial application of designed adsorption heat pump in cooling/heating purposes, further studies on adsorption heat pumps are required. The low SHP and SCP values can be accepted as the main obstacle on practical application of this kind of heat pump. However, the designed and constructed AHP-2, in which heat transfer rate was enhanced by loading aluminum pieces, was proper for heat recovery of waste gases or utilization of solar energy by using a parabolic solar collector despite of the low SCP and SHP values.

The heat and mass transfer in the adsorbent bed is the important phenomena which should be used to improve performance criteria of AHP. Therefore, simulation of heat and mass transfer in the bed may be an appropriate method to optimize a bed since the experimental studies are time-consuming and too expensive. The performance criteria of adsorption heat pump which are COP, SCP and SHP can be obtained by the simulation of heat and mass transfer in the adsorbent bed.

Based on the obtained experimental and numerical results, further studies should be performed on the following issues:

- The enhancement of heat transfer rate by using fins is limited. The use of metal additives in the adsorbent bed is an innovative approach to increase heat transfer in adsorbent bed. Further studies on enhancement of heat transfer rate assisted by metal additives should be performed for different types and shapes of metals.
- Further theoretical and numerical studies should be performed on the heat and mass transfer in two and three dimensional models through the adsorbent bed. The optimization of adsorbent bed can be provided by using solution of those models. Since many parameters affect COP, SHP and SCP values of an adsorption heat pump, the model should involve all of these significant parameters. The obtained numerical results should be supported and validated with the experimental studies.
- The selection of adsorbent-adsorbate pair is one of the important factors. The innovative adsorbent-adsorbate pairs should be investigated to be utilized in the adsorption heat pumps. The Classius – Clapeyron chart, heat of adsorption,

equations relevant to the thermal and mass diffusivities should also be investigated for the new types of adsorbent – adsorbate pairs.

REFERENCES

- Aittomaki, A. and M. Harkonen. 1986. Zeolite heat pump adsorption of methanol in synthetic zeolites 13X, 4A and 5A. *International Journal of Refrigeration* 9: 240-244.
- Al-Ansari A., Ettouney H. and El-Dessouky H., 2001. Water–Zeolite Adsorption Heat Pump Combined with Single Effect Evaporation Desalination Process. *Renewable Energy* 24: 91-111.
- Alberty, A.R. and J.R. Silbey, eds. 1997. *Physical chemistry*. 2nd Ed., New York: John Wiley and Sons.
- Alefeld G., Maier-Laxhuber P., Rothmeyer M., 1992. Zeolite heat pump and zeolite heat transformer for load management,). In *Proceeding of solid sorption refrigeration symposium* Paris. November, 855-860.
- Aristov, I.Y., Tokarev, M.M., Freni, A., Glaznev S.I. and G. Restuccia. 2006. Kinetics of water adsorption on silica Fuji Davison RD. *Microporous and Mesoporous Materials* 96: 65-71.
- Ben Amar, N., Sun, M.L. and F. Meunier. 1996. Numerical analysis of adsorptive temperature wave regenerative heat pump. *Applied Thermal Engineering*. 16: 405-418.
- Bird, B.R., Stewart, E.W. and N.E. Lightfoot. 2002. *Transport phenomena*. 2nd Ed., New York: John Wiley and Sons Inc.
- Bonaccorsi L. and Proverbio E., 2004. Synthesis of Thick Zeolite 4A Coatings on Stainless Steel. *Microporous and Mesoporous Materials* 74: 221-229.
- Bonaccorsi L., Freni A., Proverbio E., Restuccia G. and Russo F., 2006. Zeolite Coated Copper Foams for Heat Pumping Applications. *Microporous and Mesoporous Materials* 91: 7-14.
- Cacciola G., Cammarata G., Fichera A., and G. Restuccia, 1992. Advances on innovative heat exchangers in adsorption heat pumps. In *Proceeding of solid sorption refrigeration symposium* Paris. November, 18-20.
- Cerkvenik B., A. Poredos, and F. Ziegler, 2001. Influence of adsorption cycle limitations on the system performance. *International Journal of Refrigeration* 24: 475-485.

- Chahbani, H.M., Labidi, J. and J. Paris. 2002. Effect of mass transfer kinetics on the performance of adsorptive heat pump systems. *Applied Thermal Engineering* 22: 23-40.
- Chahbani, H.M., Labidi, J. and J. Paris. 2004. Modeling of adsorption heat pumps with heat regeneration. *Applied Thermal Engineering* 24: 431-447.
- Cho, S-H, Kim, J-N and Y-J You. 1992. Silica gel/water adsorption-cooling system. *In Proceeding of solid sorption refrigeration symposium* Paris November, 18-20.
- Choi C., and Jeong S., 2005. Experimental Study on the Development of Micro Adsorption Refrigerator. *International Sorption Heat Pump Conference* Denver, USA.
- Chua H.T., Ng K.C., Malek A., Kashiwagi T., Akisawa A. and Saha B.B., 2001. Multi-Bed regenerative adsorption chiller — improving the utilization of waste heat and reducing the chilled water outlet temperature fluctuation. *International Journal of Refrigeration* 24: 124-136.
- Chua, T.H., Ng, C.K., Wang, W., Yap, C. and L.X. Wang. 2004. Transient modeling of a two bed silica gel-water adsorption chiller. *International Journal of Heat Mass Transfer* 47: 659-669.
- Critoph R.E., and Y Zhong, 2004. Review of trends in solid sorption refrigeration and heat pumping technology. *Journal of Process Mechanical Engineering* 219: 285-300.
- Critoph R.E., 1998. Forced convection adsorption cycles. *Applied Thermal Engineering* 18: 799-807.
- Critoph R.E., Telto T. Z., Davies L.N.G., 2000. A Prototype of a Fast Cycle Adsorption Refrigerator Utilizing a Novel Carbon-Aluminium Laminate. *Journal of Process Mechanical Engineering* 214: 439-448.
- Cussler, E.L. 1997. *Diffusion mass transfer in fluid systems*. 2nd Ed. Cambridge: Cambridge University Press.
- Dawoud B., 2005. A Hybrid solar – assisted adsorption cooling unit for vaccine storage. *International Sorption Heat Pump Conference* Denver, USA.
- Dawoud, B., Vedder, U., Amer, H.E. and S. Dunne. 2007. Non-isothermal adsorption kinetics of water vapour into a consolidated zeolite layer. *International Journal of Heat and Mass Transfer* 50: 2190-2199.
- De Boer R., Smeding F.S., Grisel H.J.R., 2005. Development and testing of a sorbent filled heat exchanger for use in compact solid sorption cooling systems. *International Sorption Heat Pump Conference* Denver, USA.

- Dechang, W., Jingyi, W., Honggang, S. and W. Ruzhu. 2005. Experimental study on the dynamic characteristics of adsorption heat pumps driven by intermittent heat source at heating mode. *Applied Thermal Engineering* 25: 927–40.
- Demir, H., Mobedi, M. and S. Ülkü. 2008. A review on adsorption heat pump: problems and solutions. *Renewable and Sustainable Energy Reviews* 12: 2381-2403.
- Di, J., Wu, Y.J., Xia, Z.Z. and Z.R. Wang. 2007. Theoretical and experimental study on characteristics of a novel silica gel – water chiller under the conditions of variables heat source temperature. *International Journal of Refrigeration* 30: 515-526.
- Douss N. and F. Meunier, 1989. Experimental study of cascading adsorption cycles. *Chemical Engineering Science* 44: 225-235.
- Elgowainy A., S. Shelton, J. Hogan, 2005. Experimental Investigation of Activated Carbon-Ammonia Heat Pump System. *International Sorption Heat Pump Conference* Denver, USA.
- Eltom, M.M.O. and M.A.A. Sayigh. 1994. A simple method to enhance thermal conductivity of charcoal using some additives. *Renewable Energy* 4: 113-118.
- Gadalla, A.M. 2007. Simulation of intermittent thermal compression processes using adsorption technology. *Journal of the Franklin Institute* 344: 725-740.
- Goetz, V., Marty, A., 1992. A model for reversible solid/gas reactions submitted to temperature and pressure constraints; simulation of the rate of reaction in solid gas reactors used in chemical heat pump. *Chemical Engineering Science* 47: 4445–4454.
- Gregg, S.J. and K.S.W. Sing. 1982. *Adsorption surface area and porosity*. 2nd Ed. London: Academic Press.
- Groll M., 1992. Reaction beds for dry sorption machines. *In Proceeding of solid sorption refrigeration symposium* Paris. November, 18-20.
- Gross M.D. and B. Dawoud, 2005. Experimental Investigation of and Adsorptive Heat Storage, *International Sorption Heat Pump Conference*, Denver, USA.
- Gui, Y.B., R.Z., Wang, W., Wang, J.Y., Wu, and Y.X. Xu. 2002. Performance modeling and testing on a heat-regenerative adsorptive reversible heat pump. *Applied Thermal Engineering* 22: 309-320.
- Guilleminot J.J., Choisier A., Chalfen B.J., Nicolas S., and J.L. Reymonet, 1993. Heat transfer intensification in fixed bed adsorbers. *Heat recovery systems* 13: 297-300.
- Hamamoto Y, K.C. Amanul Alam, A. Akisawa, and T. Kashiwagi, 2005. Performance evaluation of a two-stage adsorption refrigeration cycle with different mass ratio. *International Journal of Refrigeration* 28: 344-352.
- Hamamoto Y., Akisawa A., Kashiwagi T., 2005. Study of a hybrid desiccant cooling system combined with a two – stage adsorption chiller. *International Sorption Heat*

Pump Conference Denver, USA.

- Hamamoto Y., Alam K.C.A., Saha B.B., Koyama S., Akisawa A. and Kashiwagi T., 2006. Study on adsorption refrigeration cycle utilizing activated carbon fibers. Part 1 adsorption characteristics. *International Journal of Refrigeration* 29: 305-314.
- Handy, E.B., Sharma, B.S., Spiewak, B.E. and J.A. Dumesic. 1993. A Tian-Calvet heat flux microcalorimeter for measurements of differential heats of adsorption. *Measurement Science and Technology* 4: 1350-1356.
- Hauer A., 2005. Evaluation of adsorbent materials for heat pump and thermal energy storage applications in open systems. *International Sorption Heat Pump Conference* Denver, USA.
- Hellmann, H-M. 2002. Carnot-COP for sorption heat pumps working between four temperature levels. *International Journal of Refrigeration* 25: 66-74.
- Henning H.M. and Wiemken E., 2003. Solar Assisted Air Conditioning of Buildings Overview on Technologies and State of The Art, Proceedings. *ISES Solar World Congress* Gothenburg, Sweden.
- Hsu, T.C., Cheng, P. and W.K. Wong. 1994. Modified Zehner-Schlunder models for stagnant thermal conductivity of porous media. *International Journal of Heat Mass Transfer* 37: 2751-2759.
- Incropera, P.F. and P.D. DeWitt. 1996. *Fundamentals of heat and mass transfer*. 4th Ed. New York: John Wiley and Sons.
- Janchen, J., Ackermann, D., Weiler, E., Stach, H. and W. Brösicke. 2005. Calorimetric investigation on zeolites, AlPO_4 's and CaCl_2 impregnated attapulgite for thermochemical storage of heat. *Thermochemica Acta* 434: 37-41.
- Karger, J. and M.D. Ruthven. 1992. *Diffusion in zeolites and other microporous solids*. New York: A Wiley-Interscience Pubs.
- Khan, I.Z.M., Alam, A.C.K., Saha, B.B., Akisawa, A. and T. Kashiwagi. 2007. Study on a re-heat two stage adsorption chiller – the influence of thermal capacitance ratio, overall thermal conductance ratio and adsorbent mass on system performance. *Applied Thermal Engineering* 27: 1677-1685.
- Khan, I.Z.M., Alam, A.C.K., Saha, B.B., Hamamoto, Y., Akisawa, A. and T. Kashiwagi. 2005. Parametric study of two stage adsorption chiller using re-heat– the effect of overall thermal conductance and adsorbent mass on system performance. *International Journal of Thermal Sciences* 45: 511-519.
- Kodama, A, Jin, W, Goto, M, Hirose, T. and M. Pons. 2000. Entropic analysis of adsorption open cycles for air conditioning. Part 2: interpretation of experimental data. *International Journal of Energy Research* 24: 263–278.

- Lafferty, M.J. 1998. *Foundation of vacuum science and technology*, New York: John Wiley & Sons Inc.
- Lambert, M.A. 2007. Design of solar powered adsorption heat pump with ice storage. *Applied and Thermal Engineering* 27: 1612–1628.
- Lemmini F. and Meunier F., 1990. Simulation of an adsorptive solar refrigerator operating in Morocco. *Journal of Islamic Academy of Sciences* 3: 273-279.
- Leong, C.K. and Y. Liu. 2004. Numerical modeling of combined heat and mass transfer in the adsorbent bed of a zeolite/water cooling system. *Applied Thermal Engineering* 24: 2359-2374.
- Leong, C.K. and Y. Liu. 2004. Numerical study of a combined heat and mass recovery adsorption cooling cycle. *International Journal of Heat and Mass Transfer* 47: 4761-4770.
- Liu, Y. and C.K. Leong. 2005. The effect of operating conditions on the performance of zeolite/water adsorption cooling systems. *Applied Thermal Engineering* 25: 1403-1418.
- Liu, Y. and C.K. Leong. 2006. Numerical study of a novel cascading adsorption cycle. *Applied Thermal Engineering* 29: 250-259.
- Marletta, L., Maggio, G., Freni, A., Ingrassiotta, M. and G. Restuccia. 2002. A non-uniform temperature non-uniform pressure dynamic model of heat and mass transfer in compact adsorbent beds. *International Journal of Heat and Mass Transfer* 45: 3321-3330.
- Metcalf, J.S. 2005. Simulation of the effect of generator heat transfer parameters on power density and efficiency in multiple-bed regenerative carbon – ammonia sorption heat pumps. *International Sorption Heat Pump Conference* Denver, USA.
- Meunier, F. 1985. Second law analysis of a solid adsorption heat pump operating on reversible cascade cycles: Application to the zeolite-water pair. *Journal of Heat Recovery Systems* 5: 133-141.
- Meunier, F. 2002. Adsorptive cooling: A clean technology. *Clean Products and Processes* 3: 8-20.
- Meunier, F., Kaushik, S.C., Neveu, P. and F.A. Poyelle. 1996. A comparative thermodynamic study of sorption systems: second law analysis. *International Journal of Refrigeration* 19: 414-421.
- Meunier, F., Neveu, P. and J. Castaing-Lasvignottes. 1998. Equivalent Carnot cycles for sorption refrigeration: Cycles de Carnot équivalents pour la production de froid par sorption. *International Journal of Refrigeration* 21: 472-489.

- Meunier, F., Poyelle, F. and M.D. LeVan. 1997. Second-law analysis of adsorptive refrigeration cycles: The role of thermal coupling entropy production. *Applied Thermal Engineering* 17: 43-55.
- Miltkau, T. and B. Dawoud. 2002. Dynamic modeling of the combined heat and mass transfer during the adsorption/desorption of water vapor into/from a zeolite layer of an adsorption heat pump. *International Journal of Thermal Sciences* 41: 753-762.
- Moise, J.C., Bellat, J.P. and A. Methiever. 2001. Adsorption of water vapor on X and Y zeolites exchanged with barium. *Microporous and Mesoporous Materials* 43: 91-101.
- Nunez T., Mittelbach W., Henning M.H., 2005. Development of a small capacity adsorption system for heating and cooling applications, *International Sorption Heat Pump Conference* Denver, USA.
- O'Neil, M., Lovrien, R. and J. Phillips. 1985. New microcalorimeter for the measurement of differential heats of adsorption of gases surface area solids. *Review of Scientific Instruments* 56: 2312-2318.
- Oertel K., Sprengel U., Mande S., Ghosh P., Kishore V.V.N., 1996. Development of an advanced solar-hybrid adsorption cooling system for decentralized storage of agricultural products in India, *DLR-TERI Joint project report*, The Commission of the European Communities.
- Okunev, N.B., Gromov, P.A., Heifets, I.L. and I.Y. Aristov. 2008. A new methodology of studying the dynamics of water sorption/desorption under real operating conditions of adsorption heat pumps: modeling of coupled heat and mass transfer in a single adsorbent grain. *International Journal of Heat and Mass Transfer* 51: 246-252.
- Oliveira, R.G. and R.Z. Wang. 2007. A consolidated calcium chloride-expanded graphite compound for use in sorption refrigeration systems. *Carbon* 45: 390-396.
- Pons M., Meunier F., Cacciola G., Critoph R.E., Groll M., Puigjaner L., Spinner B., Ziegler F., 1999. Thermodynamic based comparison of sorption systems for cooling and heat pumping. *International Journal of Refrigeration* 22: 5-17.
- Pons, M. and A. Kodama. 2000. Entropic analysis of adsorption open cycles for air conditioning. Part 1: first and second law analyses. *International Journal of Energy Research* 24: 251-262.
- Pons, M. and S. Szarzynski. 2000. Accounting for the real properties of the heat transfer fluid in heat-regenerative adsorption cycles for refrigeration. *International Journal of Refrigeration* 23: 284-291.
- Pons, M., Meunier, F., Cacciola, G., Critoph, R.E., Groll, M., Puigjaner, L., Spinner, B. and F. Ziegler. 1999. Thermodynamic based comparison of sorption systems for cooling and heat pumping. *International Journal of Refrigeration* 22: 5-17.

- Poyelle, F., Guillemot, J.J. and F. Meunier. 1999. Experimental tests and predictive model of an adsorptive air conditioning unit. *Industrial and Engineering Chemistry Research*.38: 298-309.
- Ramos M., Espinoza R.L. and Horn M.J., 2003. Evaluation of a zeolite-water solar adsorption refrigerator, *ISES Solar World Congress*, Göteborg, Sweden.
- Restuccia G., Vasta S., Freni A., Russo F., Aristov I .Y., 2005. An Advanced Solid Sorption Chiller Using SWS-1L: Performance Analysis and Hydrothermal Cycling Stability of the Sorbent Bed. *International Sorption Heat Pump Conference* Denver, USA.
- Restuccia, G., Freni, A. and G. Maggio. 2002. A zeolite-coated bed for air conditioning adsorption systems: parametric study of heat and mass transfer by dynamic simulation. *Applied Thermal Engineering* 22: 619-630.
- Riffat S.B., Williams M.D., and Corr S., 1997. Adsorption heat pump using HFC refrigerants. *International Journal of Energy Research* 21: 481-494.
- Rothmeyer M., Laxhuber M. P., Alefeld G., 1983. Design and performance of zeolite water heat pumps. *16th International Congress of Refrigeration* Paris.
- Rouquerol, F., Rouquerol, J. and K. Sing. 1999. *Adsorption by powders and porous solids*. London: Academic Press.
- Ruthven, M.D. 1984. *Principles of adsorption and adsorption processes*. New York: A Wiley-Interscience Pubs.
- Ruthven, M.D. 1997. *Fundamentals of diffusion in porous and microporous solids*, Eds: Fraissard J., Conner W.C., In *Physical Adsorption: Experiment, Theory and Applications*. *Kluwer Academic Pubs*. NATO ASI Series, v:491.
- Ruthven, M.D., Farooq, S. and S.K. Knaebel. 1994. *Pressure swing adsorption*. New York: A Wiley-Interscience Pubs.
- Saha B. B., Koyama S., El-Sharkawy I.I., Kuwahara K., Kariya K. and Ng K. C., 2006a. Experiments for Measuring Adsorption Characteristics of an Activated Carbon Fiber/Ethanol Pair Using a Plate-Fin Heat Exchanger. *HVAC&R Research* 12: 767-782.
- Saha B.B., Akisawa A., Kashiwagi T., 1997. Silica gel water advanced adsorption refrigeration cycle. *Energy* 22: 437-447.
- Saha B.B., S. Koyama, Ng. K. Choon, Y. Hamamoto, A. Akisawa, and T. Kashiwagi, 2006b. Study on a dual-mode, multi-stage, multi-bed regenerative adsorption chiller. *Renewable Energ.* 31: 2076-2090.
- Sakoda A. and Suzuki M., 1984. Fundamental study on solar powered adsorption

- cooling system. *Journal of Chemical Engineering of Japan* 17: 52-57.
- San, Y.J. 2006. Analysis of the performance of a multi-bed adsorption heat pump using a solid side resistance model. *Applied Thermal Engineering* 26: 2219-2227.
- San, Y.J. and M.W. Lin. 2008. Comparison among three adsorption pairs for using as the working substances in a multi-bed adsorption heat pump. *Applied Thermal Engineering* 28: 988-997.
- Schnabel L. And Henning M.H., 2005. Experimental and simulation study on the kinetics of water vapour adsorption on different kinds of adsorptive material matrices. *International Sorption Heat Pump Conference* Denver, USA.
- Sears, W.F. 1953. *An introduction to thermodynamics, the kinetic theory of gases, and statistical mechanics*. 2nd Ed. London: Addison-Wesley Pubs. Co.
- Spiewak, B.E. and J.A. Dumesic. 1996. Microcalorimetric measurements of differential heats of adsorption on reactive catalyst surfaces. *Thermochimica Acta* 290: 45-53.
- Spinner B., Sorin M., Stitou D., 2001. Internal energy flow analysis within a single effect sorption heat pump. *International Journal of Refrigeration* 24: 185-191.
- Srivastava N.C., and I.W. Eames, 1998. A review of adsorbents and adsorbates in solid-vapour adsorption heat pump systems. *Applied Thermal Engineering* 18: 707-714.
- Sumathy K., 2002. An energy efficient solar ice-maker, *8th International Symposium on Renewable Energy Education (ISREE8)* Aug. 4-8.
- Sun, J. and W.R. Besant. 2005. Heat and mass transfer during silica gel – moisture interactions. *International Journal of Heat and Mass Transfer* 48: 4953-4962.
- Suzuki M., 1990. *Adsorption engineering*, Amsterdam, Elsevier Science Publisher, Vol:25.
- Szarzynski S., Y. Feng, and M. Pons, 1997. Study of different internal vapour transports for adsorption cycles with heat regeneration. *International Journal of Refrigeration* 20: 390-401.
- Tahat M.A., 2001. Heat-pump/energy-store using silica gel and water as a working pair. *Applied Energy* 69: 19-27.
- Tanashev Yu.Yu. and Yu. I. Aristov, 2000. Thermal conductivity of a silica gel + calcium chloride system: the effect of adsorbed water. *Journal of Engineering Physics and Thermophysics* 73: 876-883.
- Tatlier, M. and E.A. Şenatalar. 1999. The effects of thermal and mass diffusivities on the performance of adsorption heat pumps employing zeolite synthesized on metal supports. *Microporous and Mesoporous Materials* 28: 195-203.

- Tatlier, M. and Erdem-Şenatalar, A., 2000c. Effects of metal mass on the performance of adsorption heat pumps utilizing zeolite 4A coatings synthesized on heat exchanger tubes. *International Journal of Refrigeration* 23: 260-268.
- Tatlier, M. and Erdem-Şenatalar, A., 2000a. Optimization of the cycle durations of adsorption heat pumps employing zeolite coatings synthesized on metal supports. *Microporous and Mesoporous Materials* 34: 23-30.
- Tatlier, M. and Erdem-Şenatalar, A., 2004. Polymeric heat exchangers to increase the COP values of adsorption heat pumps utilizing zeolite coatings. *Applied Thermal Engineering* 24: 69-78.
- Tatlier, M. and Erdem-Şenatalar, A., 2000b. The performance analysis of a solar adsorption heat pump utilizing zeolite coatings on metal supports. *Chemical Engineering Communications* 180: 169-185.
- Tatlier, M. and Erdem-Şenatalar, A., 2002. When do thin zeolite layers and a large void volume in the adsorber limit the performance of adsorption heat pumps? *Microporous and Mesoporous Materials* 54: 89-96.
- Tatlier, M., Ersolmaz, T.B. and E.A. Şenatalar. 1999. A novel approach to enhance heat and mass transfer in adsorption heat pumps using the zeolite – water pair. *Microporous and Mesoporous Materials* 27: 1-10.
- Tavman, I.H. 1998. Effective thermal conductivity of isotropic polymer composites. *International Communication Heat and Mass Transfer* 25: 723-732.
- Telto T.Z., 2005. Compact sorption generator prototype. *International Sorption Heat Pump Conference* Denver, USA.
- Thorpe N. R., Critoph E.R., Zhong Y., 2005. Sorption of ammonia on calcium chloride/alumina calcium chloride/active carbon composite materials *International Sorption Heat Pump Conference* Denver, USA.
- Ülkü, A.S. and M. Mobedi. 1989. Adsorption in energy storage. In Proceedings of the NATO Advanced Study Institute on Energy Storage Systems. *Series E. Applied Science* 167: 487-507.
- Ülkü, S. 1986. Adsorption heat pumps. *Journal of Heat Recovery System* 6: 277-84.
- Ülkü, S. 1987. *Solar adsorption heat pumps, Solar Energy Utilization: Fundamentals and Applications*, eds. Yüncü, H., Paykoç, E. and Y. Yener. The Netherlands: Martinus Nijhoff Publishers.
- Ülkü, S. 1991. Heat and mass transfer in adsorbent beds, Convective heat and mass transfer in porous media, Eds by Kakaç, S., Kilkış, B., Kulacki, A.F. and F. Arınc. NATO Series. London: *Kluwer Academic Pubs.* Vol. 196. pp: 695-724.

- Ülkü, S. 1992. Adsorption heat pumps (refrigerators). In *Proceeding of solid sorption refrigeration symposium* Paris. November, 18-20.
- Ülkü, S., Gürses, A.Ç. and M. Toksoy. 1987. *Enerji Tasarrufu ve Isı Pompaları*. In *Enerji Tasarrufu Semineri Bildiriler Kitabı*. İstanbul. pp: 27-38.
- Wang C.D., Wu Y.J., Wang Z.R., Xia Z.Z., 2005. Research on a novel adsorption chiller driven by low grade heat source. *International Sorption Heat Pump Conference* Denver, USA.
- Wang L., D. Zhu, Y. Tan, 1999. Heat transfer enhancement of the adsorber of an adsorption heat pump. *Adsorption* 5: 279-286.
- Wang S, and D.Zhu, 2002. A novel type of coupling cycle for adsorption heat pumps. *Applied Thermal Engineering* 22: 1083-1086.
- Wang S.G., R.Z. Wang, and X.R. Li, 2005. Research and development of consolidated adsorbent for adsorption systems. *Renewable Energy* 30: 1425-1441.
- Wang W.L., Wang Z.R., Lu S.Z., Xu X.Y., Wu Y.J., 2005. Split heat pipe type adsorption ice maker with compound adsorbent: A better choice for fishing boats. *International Sorption Heat Pump Conference* Denver, USA.
- Wang Z.R., Kong Q.X., Wu Y.J., Huangfu Y., Wu W.D., 2005. Performance research of a micro CCHP system with adsorption chiller. *International Sorption Heat Pump Conference* Denver, USA.
- Wang, K., Wu, J.Y., Wang, R.Z. and L.W. Wang. 2006a. Composite adsorbent of CaCl₂ and expanded graphite for adsorption ice maker on fishing boats. *International Journal of Refrigeration* 29: 199–210.
- Wang, L.W., Wang, R.Z., Lu, Z.S., Chen, C.J., Wang, K. and J.Y. Wu. 2006b. The performance of two adsorption ice making test units using activated carbon and a carbon composite as adsorbents. *Carbon* 44: 2671–2680.
- Wang, W. and R. Wang. 2005. Numerical simulation of intermittent operation and startup on adsorption refrigeration. *International Sorption Heat Pump Conference*. Denver, USA.
- Wang, X., Zimmermann, W., Ng, C.K., Chakraborty, A. and U.J. Keller. 2004. Investigation on the isotherm of silica gel-water systems TG and volumetric methods. *Journal of Thermal Analysis and Calorimetry* 76: 659-669.
- Webb, P.A. and C. Orr. 1997. *Analytical methods in fine particle technology*. Norcross: Micromeritics Instrument Cooperation.
- Wongsuwan W., S. Kumar, P. Neveu, and F. Meunier, 2001. A review of chemical heat pump technology and applications. *Applied Thermal Engineering* 2: 1489-1519.

- Wu J., D. Wang, X. Zhai, R. Wang, 2005. Research on Control Method of the Adsorption Chiller Driven by a Variable Heat Source-Solar Energy. *International Sorption Heat Pump Conference* Denver, USA.
- Wu J.Y., Wang R.Z. and Xu Y.X., 2002a. Influence of adsorption and desorption capacity on operating process for adsorption heat pump. *Applied Thermal Engineering* 22: 471-476.
- Wu, JY, Wang, R.Z and Y.X. Xu. 2002b. Dynamic analysis of heat recovery process for a continuous heat recovery adsorption heat pump. *Energy Conversion Management* 43: 2201–2211.
- Zegnani, A., Mhimid, A. and K. Slimi. 2007. Heat and mass transfer during desorption within a plane adsorber. *International Energy, Environment and Exergy Symposium* Evora.

APPENDICES

Table A1 in Appendix A illustrates the detailed list of the performed adsorption heat pump studies in the literature. A varies adsorbent-adsorbate pairs, operation conditions, regeneration heat source temperature were expressed for each study in this table. The COP values for the studies in which the cycle is theoretically or experimentally achieved were also shown.

Appendix B includes the raw data and procedure of data processing. Table B1 shows the raw data which was acquired from the thermocouples and pressure transducers and saved at every 1 minute. In Table B1, evaporator pressure (P_E), evaporator temperature (T_E), inlet temperature of heat exchanger fluid to evaporator (E_{Wi}), outlet temperature of heat exchanger fluid to evaporator (E_{Wo}), condenser pressure (P_C), condenser temperature (T_C), inlet temperature of heat exchanger fluid to condenser (C_{Wi}), outlet temperature of heat exchanger fluid to condenser (C_{Wo}), bottom bed pressure (P_B), top bed pressure (P_T), adsorbent bed outer surface temperature (T_{surf}), inside adsorbent bed temperatures at four different locations (T_1 , T_2 , T_3 and T_4) were tabulated. The whole raw data was given as the average of every 20 minutes to be able to reduce the number of data as shown in Table B2. The average of bed pressure (P_{bed}) and average of inside bed temperatures (T_{bed}) were also calculated and illustrated in Table B2. This data processing was made for all cycle processes. The variation of temperature of bed outer surface and average inside temperature of bed was plotted with the time for all cycle processes. The variation of average bed pressure and temperature were also plotted with the time including all cycle processes. The variation of evaporator pressure and temperature was drawn for isobaric adsorption process. The inlet and outlet temperatures of heat exchanger fluid to evaporator were drawn for observing the transferred heat during the isobaric adsorption process from heat exchanger fluids to evaporator. The similar analyses were made for the condenser unit.

In Appendix C, all of the cycles obtained from the intermittent adsorption heat pumps were presented. Figure C1 shows the cycle that was obtained from the first adsorption heat pump. Twelve cycles were obtained with AHP-1. Seven cycles can be presented in this figure since some data that belongs to the five cycles were missed due to computer damage. In Figure C2, seventeen cycles that belongs to the second AHP

were illustrated. The cycles from Figure C2 (h) to Figure C2 (l) were obtained with the low temperatures of regeneration heat source. As can be seen from the Figure C2, the cycles almost show the similar behaviors. Figure C3 shows all of the cycles of the Al-loaded AHP-2. Figure C4 illustrates the variation of four temperatures in the adsorbent bed. These four temperature values were measured by four thermocouples which were distributed in axial and radial directions of the adsorbent bed. This figure indicates that the adsorbent bed was heated homogeneously in isosteric heating and isobaric desorption processes and cooled during isosteric cooling and isobaric adsorption processes.

The properties of the materials, used in adsorption heat pump experiments were illustrated in Table D1 in Appendix D. Table D2 illustrates the thermal properties of the metal additives that were used for the acceleration of the heat transfer rate in the adsorbent bed. Thermodynamic properties of water and silica gels are revealed in Table D3. This data were used during solving of the governing equations for annulus adsorbent bed of AHP which operates silica gel-water pair.

In Appendix E, the raw data obtained from the microcalorimetric study and calculation procedure were illustrated. The linearity graphs of kinetics of water adsorption on silica gel for short and long range periods were also represented. Figure E3 shows the linearity of water vapor diffusivities for short and long ranges periods with temperatures for adopting them in Arrhenius form.

In Table F1, heat and mass transport in the porous adsorbent bed, considered systems, related assumptions and solution methods were illustrated. Generally, mass transfer equation in an adsorbent granule was solved by using lumped analysis. The mass transfer coefficient was assumed as constant into the adsorbent granule. Therefore, mass transfer equation in the adsorbent bed was solved by using Linear Driving Force model. The adsorbate diffusivity inside the particle was described by using the Arrhenius equation. Detailed information about assumptions, heat and mass conservation equations can be found in Table F1.

In Appendix G, driving procedure of the heat and mass transfer equations for considered annular adsorbent bed was given. Discretization of derived heat and mass transfer equations for annular adsorbent bed and solution procedure of these equations were also explained in this appendix. Information about finite difference method and implicit scheme was explained in detail.

APPENDIX A

LITERATURE SURVEY FOR ADSORPTION

HEAT PUMP

Table A1. Some researched system in literature

References	year	Adsorbent-adsorbate Pair	Condensation Temp. (°C)	Evaporation Temp. (°C)	Regeneration Temp. (°C)	COP	Remarks
Ülkü	1986	natural zeolite-water	53	27	123	0.34	Natural zeolite seems as alternative adsorbent for adsorption heat pump system.
Ülkü	1987	natural zeolite-water	52	25	200	0.4	Natural zeolite seems as alternative adsorbent for adsorption heat pump system.
Gui et al.	2002	carbon-methanol	36	9	110		The system is driven by waste heat exhausted from engine.
Poyelle et al.	1999	zeolite - water	40	4	230	0.74	The bed design enhanced mass and heat transfer rate.
Ülkü and Mobeidi	1989	Carbon-methanol zeolite-water carbon-ammonia					Common used adsorbent-adsorbate pairs are investigated.
Douss and Meunier	1989	Zeolite-water carbon-methanol	35	25	220 for zeolite bed, 100 for carbon bed	1.06	Heat required during regeneration of Carbon bed is provided from zeolite beds.
Szarzynski et al.	1997	zeolite - water	35	3	120 to 360	single 0.3-0.38 double 0.5-0.73	Effect of regeneration system temperature on COP of system.
Pons and Szarzynski	2000	zeolite-water	45	3	290		Influence of physical properties of heat transfer fluid on AHP system.
Hamamoto et al	2005	silica gel-water	30	14	55	0.25	Amount of adsorbent is allocated to adsorbent beds and effect of mass ratio is investigated.

(cont. on next page)

Table A1. (cont.) Some researched system in literature

References	Year	Adsorbent-adsorbate Pair	Condensation Temp. (°C)	Evaporation Temp. (°C)	Regeneration Temp. (°C)	COP	Remarks
Khan et al.	2005	silica gel-water	30	14	60	0.3-0.65	Effect of silica gel mass on COP is investigated.
Cerkvenik et al.	2001	Zeolite 13X-LiBr-Water	27-35	12-6	110	0.33	Zeolite-water adsorption system is combined LiBr-water absorption system for providing continuous system.
Restuccia et al.	2002	Zeolite-water	50	3	210		Optimum coating thickness is determined.
Hamamoto et al.	2006	AC-methanol	-5 to 35	-20 to +15	40-100	0.38	Mass transfer is enhanced by using activated carbon fiber.
Chua	2001		31	15	86	0.41	Compared two bed schemes with 4-bed scheme that improves the recovery efficiency by about 70%.
Tatlier and Şenatalar	2004	zeolite - water	20	2	150	0.3	Lighter adsorption heat pump system can be obtained with using polymeric heat exchanger tubes.
Meunier	1985	zeolite - water	40	0	350	0.94-1.008	Exergy analysis of four cascades cycled heat pump systems is performed.
Bonareccorsi et al	2006	zeolite - water	40	7	200	0.46	Open cell copper foam is applied on AHP for improving heat transfer properties.
Riffat et al	1997	AC-HFC refrigerant	-5	~60	150	0.43	System requires operating pressure about 8 bars for HFC as adsorbate
Bonareccorsi and Proverbio	2004	zeolite - water					Optimization of zeolite coating process on stainless steel tube.
Saha et al	2006a	Carbon fiber - ethanol	30		80		Adsorbent bed generally has heavy weight. Adsorbent must be designed lightweight to reduce sensible heat losses from body.
Wang et al.	2005	CaCl ₂ + A. carbon - ammonia		-20	135	0.36	Ice making system uses heat pipe principle to perform the heating and cooling process for adsorber.
Lambert	2007	carbon - ammonia	35	-15	160	1.20	A new configuration provides the higher contact area between adsorbent and heat exchanger.

(cont. on next page)

Table A1. (cont.) Some researched system in literature

References	Year	Adsorbent-adsorbate Pair	Condensation Temp. (°C)	Evaporation Temp. (°C)	Regeneration Temp. (°C)	COP	Remarks
Dechang et al.	2005	A. carbon - methanol					Dynamic simulation of AHP is studied
Tatlir and Şenatalar	2000	zeolite - water	20	2			Solar powered AHP is studied with zeolite coated adsorbent bed.
Wu et al.	2002	A. carbon - methanol	27	-10	100	0.5	Dynamic analysis of heat recovery process for AHP.
Tahat	2001	silica gel-water					Lab scale AHP system is constructed
Tatlir and Şenatalar	2000	zeolite - water	20	2	151		Effect of metal mass on the performance of AHP.
Oertel et al.	1996	silica gel - methanol	30	0	85	0.3	Solar-hybrid powered AHP system is designed and applied for decentralized cold storage of agricultural products.
Hening	2003	silica gel-water	35	10	80	0.6	AHP system is applied on air-conditioning of buildings.
Rothmeyer et al.	1983	zeolite - water			96	1.4	One of the first applications
Gross and Dawoud	2005	zeolite - water		10-40	150	0.43-1.04	New construction is designed and tested for zeolite- water AHP system.
Metcalf	2005	Carbon Ammonia	30-50	15	130-195	0.6-0.62	Computer simulation model of an isothermal carbon – ammonia AHP bed is developed in MATLAB software.
Nunez et al.	2005	Silica gel – water	35-45	10-20	80-95	0.5	Small capacity AHP is constructed and tested for heating and cooling applications.
Choi and Jeong	2005	Silica gel - water	40	25	100		Development of micro refrigeration system.
Dawoud	2005	Zeolite – Water SWS – water	55	-5	122	0.28	Hybrid adsorption cooling unit for vaccine storage utilizing solar energy as main power supply and a gas burner as an alternative power supply is developed and tested.
De Boer et al.	2005	Silica gel – water	20	15-20	95		Compact solid sorption heat pump is developed and tested.

(cont. on next page)

Table A1. (cont.) Some researched system in literature

References	Year	Adsorbent-adsorbate Pair	Condensation Temp. (°C)	Evaporation Temp. (°C)	Regeneration Temp. (°C)	COP	Remarks
Telto	2005	Carbon- Ammonia	20	9.5	150	0.3	Experimental test of compact sorption generator prototype.
Thorpe et al.	2005	CaCl ₂ +Al ₂ O ₃ – Ammonia CaCl ₂ +A. Carbon – Ammonia					Ammonia adsorption behavior on new adsorbent composite materials.
Hamamoto et al.	2005	Silica gel -water	30	14	55-65	0.117 0.143	Development of hybrid desiccant cooling system combined with 2 stage adsorption chiller.
Hauer	2005	Silica gel – water Zeolite - water					Comparison of adsorbents (zeolite & silica gel) due to their energy storage capacity.
Wang et al.	2005	Silica gel - water	30.5	15.1	55-67	0.32 – 0.4	Novel adsorption chiller is developed and tested.
Wang et al.	2005	Silica gel – water	30	15	60-92	0.4	Micro adsorption chiller is applied on natural gas & LPG power cogeneration system.
Elgowainy et al.	2005	A. carbon – ammonia				Cooling 0.36; Heating 1.1-1.15	2 ton solid sorption heat pump system is built and tested for cooling and heating performance evaluations.
Restuccia et al	2005	SWS – water	35	10	90	0.17-0.48	Advanced solid sorption chiller based on coated heat exchanger with SWS is tested and achieved a cycle time of 20-40 min.
Schanbel and Henning	2005				95		Experimental and numerical simulation of water vapor adsorption behavior on different adsorbents.
Wu et al.	2005	Silica gel – water				0.427- 0.434	Effects of variation of heat source on COP of AHP are investigated.

(cont. on next page)

Table A1. (cont.) Some researched system in literature

References	Year	Adsorbent-adsorbate Pair	Condensation Temp. (°C)	Evaporation Temp. (°C)	Regeneration Temp. (°C)	COP	Remarks
Al-Ansari et al	2001	zeolite - water	98	82	103		Waste heat of evaporation desalination process is used for cooling purposes by AHP.
Tatler and Şenatalar	2000	zeolite - water	20	2	135		Optimum coating thickness is determined
Tatler and Şenatalar	1999	zeolite - water	20	2	151		The effects of thermal and mass diffusivities on the performance of AHP are studied.
Tatler and Şenatalar	2002	zeolite - water					Optimum coating thickness is determined for zeolite type (13X and 4A).
Wu et al	2002	carbon-methanol		7	90		Influence of adsorption and desorption capacity on operating process for AHP is studied.
Sakoda and Suzuki	1984	silica gel-water	35	5	100		Solar energy driven adsorption heat pumps are studied.
Aittomaki and Harkönen	1986	zeolite - methanol	55	-5	155	1.34	Mini scale (lab) apparatus is constructed
Critoph	1998	carbon - water	42	0	250	0.95	Forced convection is used for improving mass transfer
Lemini and Meunier	1990	A. carbon - methanol				0.114	Adsorptive solar refrigeration system is simulated.
Ramos et al	2003	zeolite - water					Solar energy driven AHP is designed
Hening and Glaser	2002	silica gel - water				0.6	AHP system is applied on air-conditioning of buildings.
Sumathy	2002	A. carbon - methanol	35	-10	100	0.12	Solar powered AHP is used for ice-making.

APPENDIX B

REPRESENTATIVE RAW DATA OF INTERMITTENT AHP

Table B1. Raw data acquired from thermocouples and pressure transducers

Time (min)	P _E (kPa)	T _E (°C)	E _{WI} (°C)	E _{WO} (°C)	P _C (kPa)	T _C (°C)	C _{WI} (°C)	C _{WO} (°C)	P _B (kPa)	P _T (kPa)	T _{surf} (°C)	T ₁ (°C)	T ₂ (°C)	T ₃ (°C)	T ₄ (°C)
1	95.8	21.7	20.6	20.5	96.5	30.0	20.6	32.2	97.8	98.4	35.6	38.9	36.0	36.4	36.2
2	96.3	21.5	21.3	22.7	96.5	29.8	21.4	32.2	97.8	98.4	38.4	37.1	36.9	37.2	34.7
3	96.2	21.4	22.3	24.0	96.6	30.4	22.2	32.1	97.8	98.4	36.7	38.2	37.5	34.4	35.1
4	96.2	21.7	22.0	20.6	96.5	30.6	22.2	32.2	97.8	98.4	40.2	35.9	37.1	37.8	36.2
5	96.2	21.8	22.0	22.4	96.5	30.8	22.2	31.1	97.7	98.4	39.9	39.1	37.7	35.6	37.4
6	96.2	21.7	20.2	23.8	97.3	30.7	20.5	23.2	97.7	98.3	42.3	37.2	38.3	35.5	35.7
7	96.2	21.8	20.3	24.5	97.5	30.3	20.3	22.5	97.7	98.3	43.6	37.6	38.4	37.0	36.2
8	96.2	21.8	20.2	24.9	97.6	30.2	20.1	22.2	97.6	98.3	44.5	38.0	37.0	36.2	35.5
9	96.1	22.0	20.3	25.5	97.6	30.1	20.0	22.3	97.6	98.3	44.9	38.6	36.9	38.2	35.9
10	96.2	22.2	20.3	26.1	97.7	29.4	20.4	22.2	97.6	98.2	45.4	41.1	40.1	37.5	35.7
11	96.1	22.0	20.5	27.0	97.8	29.6	20.1	21.6	97.5	98.1	46.2	40.0	39.1	36.8	36.6
12	96.1	22.1	20.1	27.3	97.7	29.2	20.1	21.7	97.4	98.1	47.5	38.9	38.2	39.2	36.3
13	96.1	21.9	20.4	27.4	97.7	28.8	20.4	21.2	97.4	98.1	49.1	41.0	38.7	37.1	35.9
14	96.1	22.1	20.2	27.6	97.7	29.0	20.1	21.4	97.4	98.0	50.3	40.5	40.1	37.3	36.9
15	96.1	22.0	20.2	28.0	97.8	28.7	20.2	21.4	97.4	98.0	52.1	40.6	41.2	37.7	37.6
16	96.1	22.1	20.3	28.2	97.7	28.6	20.1	21.4	97.3	97.9	52.1	40.3	41.7	37.7	37.8
17	96.1	22.5	20.4	28.8	97.7	28.2	20.5	21.4	97.3	97.9	53.0	41.3	42.2	38.3	39.8
18	96.1	22.7	20.8	29.1	97.8	27.9	20.6	21.9	97.3	97.9	53.5	42.0	41.0	40.2	39.1
19	96.1	23.0	20.8	29.7	97.8	27.2	20.9	21.6	97.2	97.8	54.5	43.4	42.6	38.7	39.4
20	96.1	23.0	20.6	30.0	97.8	26.9	20.9	21.7	97.2	97.8	56.3	42.5	44.0	39.3	40.7
21	96.1	23.1	21.0	30.5	97.9	27.1	20.9	21.9	97.1	97.7	58.1	44.1	44.5	41.4	38.6
22	96.1	23.3	21.5	30.6	97.9	27.2	20.9	21.9	97.1	97.6	58.7	44.8	45.0	41.3	40.4
23	96.1	23.2	20.7	30.7	97.9	26.9	21.1	22.1	96.9	97.6	60.4	44.0	43.8	42.4	41.2
24	96.1	23.2	21.1	30.5	97.9	27.3	20.7	21.6	96.9	97.6	60.5	44.9	45.8	41.9	40.5
80	95.8	24.2	20.8	30.9	98.2	29.5	20.5	21.2	93.2	93.8	69.4	59.4	58.6	61.2	58.5

Table B2. Raw data acquired from thermocouples and pressure transducers

Time (min)	P _E (kPa)	T _E (°C)	E _{wi} (°C)	E _{wO} (°C)	P _C (kPa)	T _C (°C)	C _{wi} (°C)	C _{wO} (°C)	P _B (kPa)	P _T (kPa)	P _{bed} (kPa)	T _{surf} (°C)	T1 (°C)	T2 (°C)	T3 (°C)	T4 (°C)	T _{bed} (°C)
0	95.8	21.7	20.6	20.5	96.5	30.0	20.6	32.2	97.8	98.4	98.1	35.6	38.9	36	36.4	36.2	36.9
20	96.1	22.1	20.7	26.1	97.4	29.2	20.7	24.3	97.5	98.1	97.8	46.9	38.5	39.8	39.5	37.6	37.0
40	96.0	23.6	21.1	31.1	98.0	27.4	21.1	21.9	96.2	96.9	96.5	65.5	48.0	49.1	49.4	47.9	45.7
60	95.9	24.1	20.9	31.2	98.0	29.0	20.9	21.6	94.7	95.3	95.0	68.3	55.6	55.4	56.0	56.2	54.6
80	95.8	24.2	20.7	30.9	98.1	29.9	20.7	21.4	93.7	94.2	93.9	69.7	58.9	58.4	58.9	60.0	58.1

APPENDIX C

OBTAINED CYCLES FOR INTERMITTENT AHP

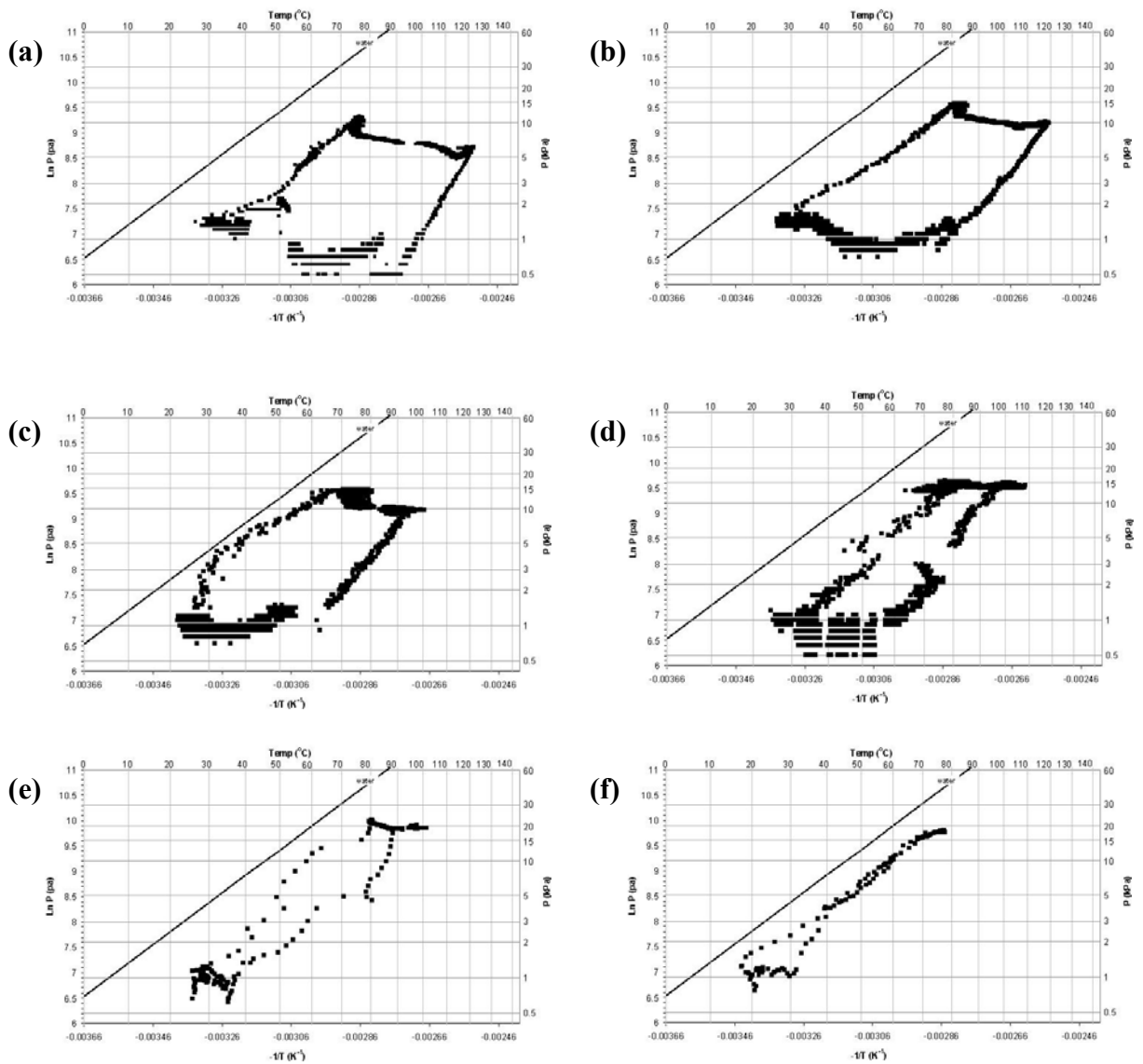


Figure C1. Cycles of first adsorption heat pump a) first cycle, b) second cycle, c) third cycle, d) 9th cycle, e) 10th cycle, f) 11th cycle, g) 12th cycle

(cont. on next page)

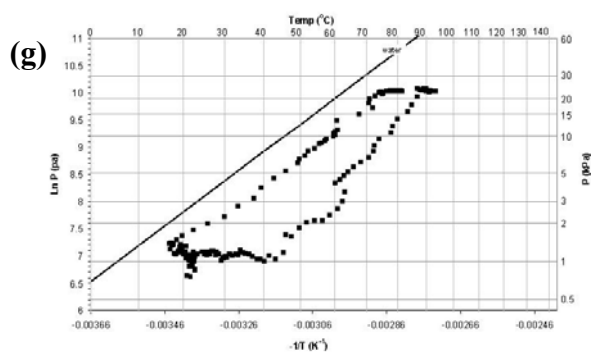


Figure C1.(cont.) Cycles of first adsorption heat pump a) first cycle, b) second cycle, c) third cycle, d) 9th cycle, e) 10th cycle, f) 11th cycle, g) 12th cycle

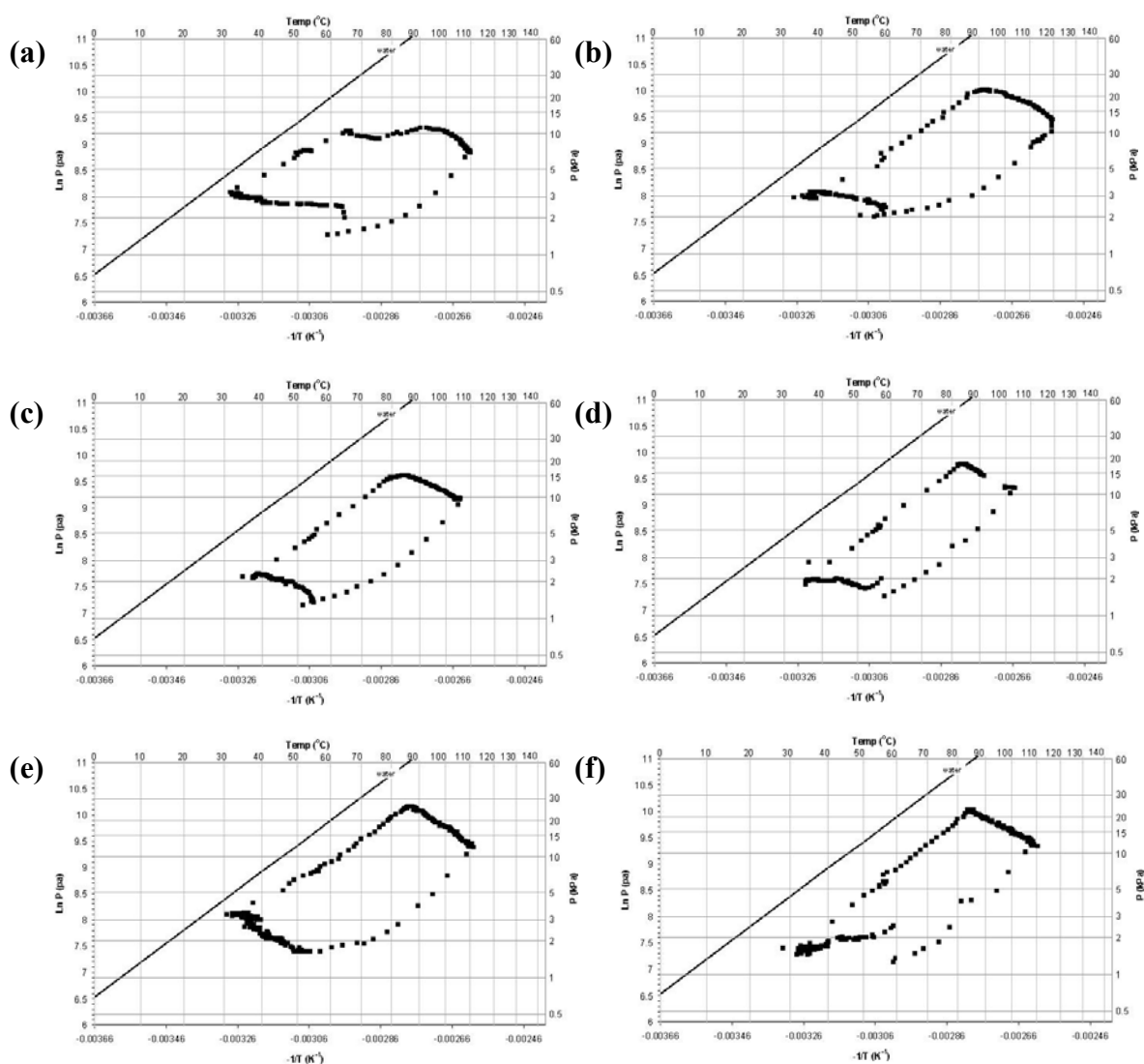


Figure C2. Cycles of second adsorption heat pump a) second cycle, b) third cycle, c) 4th cycle, d) 5th cycle, e) 6th cycle, f) 7th cycle, g) 8th cycle, h) 9th cycle, i) 10th cycle, j) 11th cycle, k) 12th cycle, l) 13th cycle, m) 14th cycle, n) 15th cycle, o) 16th cycle, p) 17th cycle

(cont. on next page)

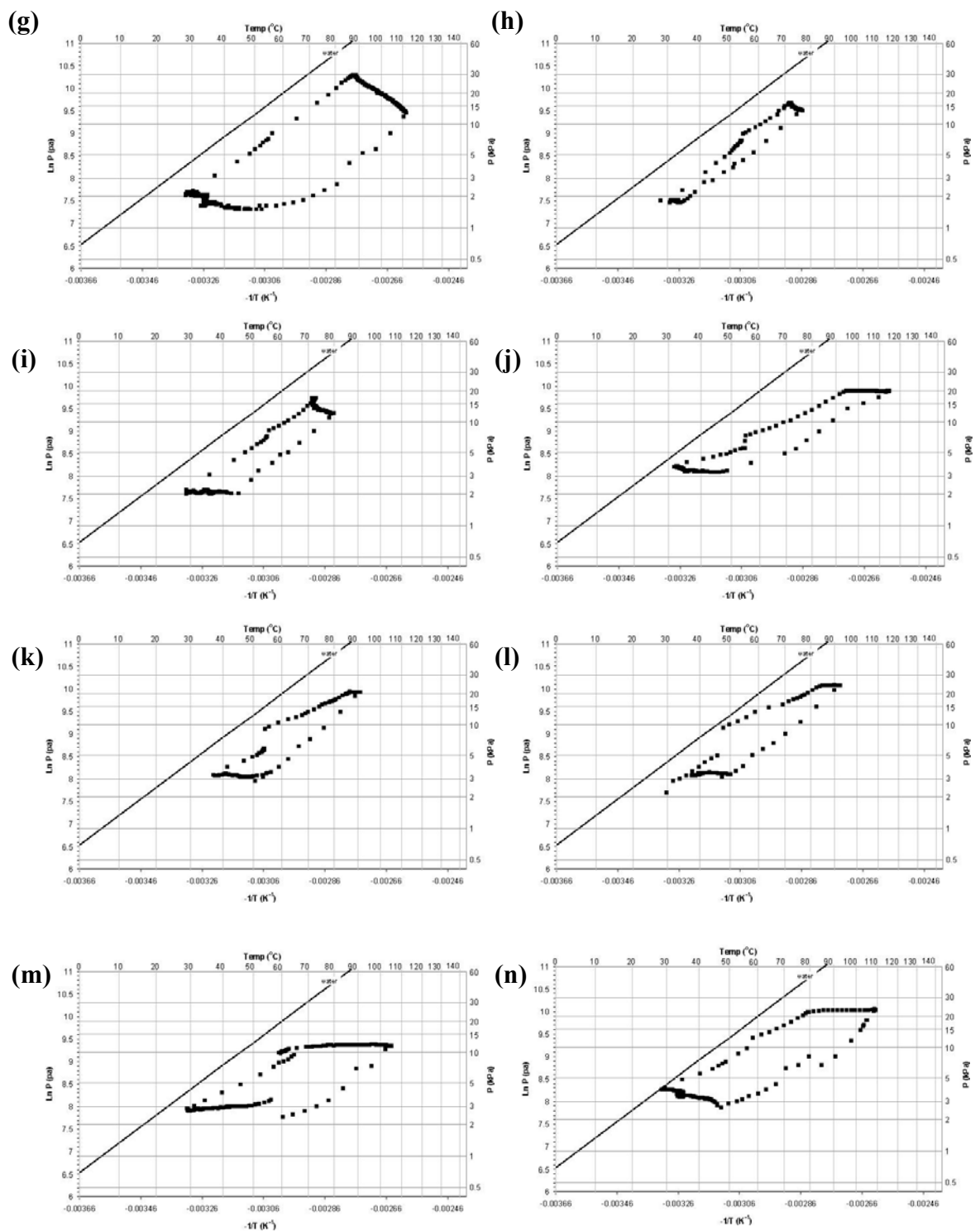


Figure C2. (cont.) Cycles of second adsorption heat pump a) second cycle, b) third cycle, c) 4th cycle, d) 5th cycle, e) 6th cycle, f) 7th cycle, g) 8th cycle, h) 9th cycle, i) 10th cycle, j) 11th cycle, k) 12th cycle, l) 13th cycle, m) 14th cycle, n) 15th cycle, o) 16th cycle, p) 17th cycle

(cont. on next page)

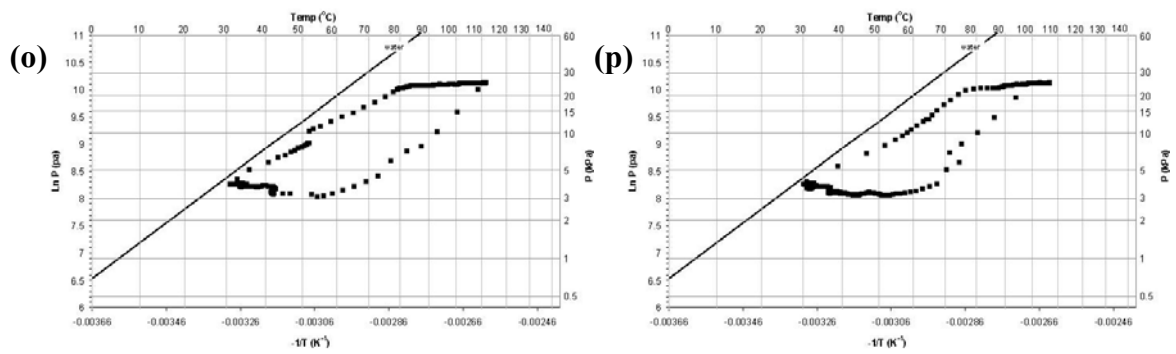


Figure C2. (cont.) Cycles of second adsorption heat pump a) second cycle, b) third cycle, c) 4th cycle, d) 5th cycle, e) 6th cycle, f) 7th cycle, g) 8th cycle, h) 9th cycle, i) 10th cycle, j) 11th cycle, k) 12th cycle, l) 13th cycle, m) 14th cycle, n) 15th cycle, o) 16th cycle, p) 17th cycle

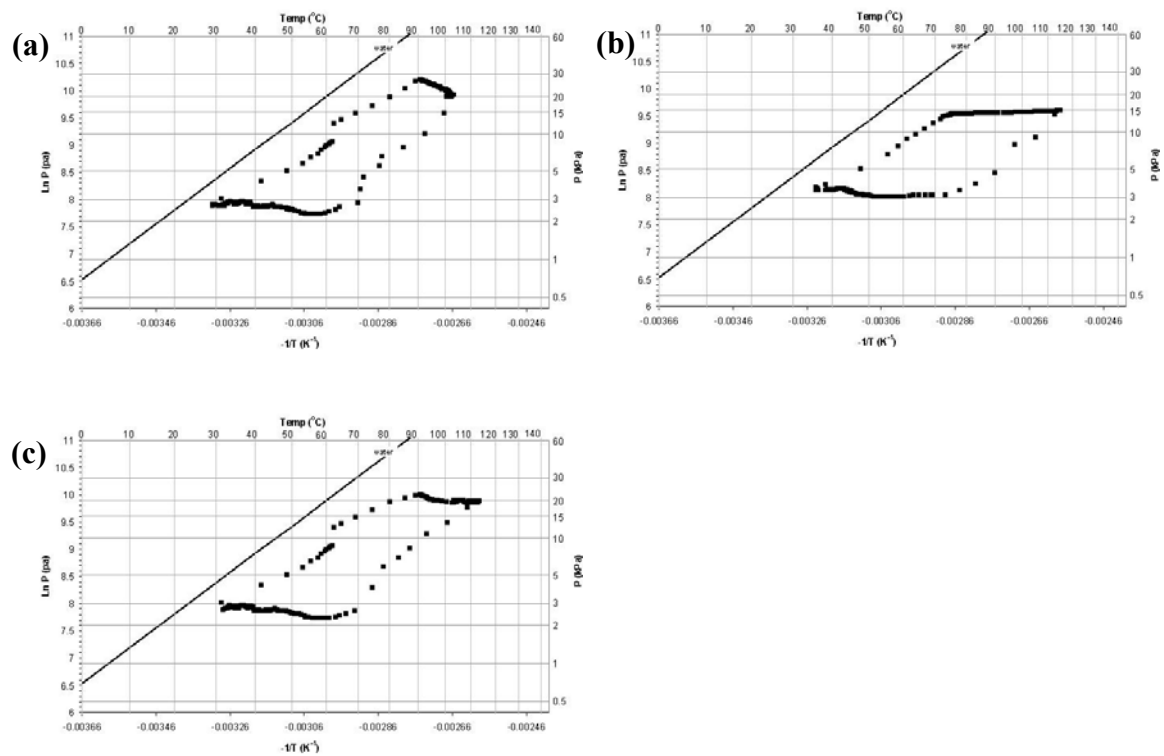


Figure C3. Cycles of Aluminum loaded AHP-2 a) first cycle, b) second cycle, c) third cycle

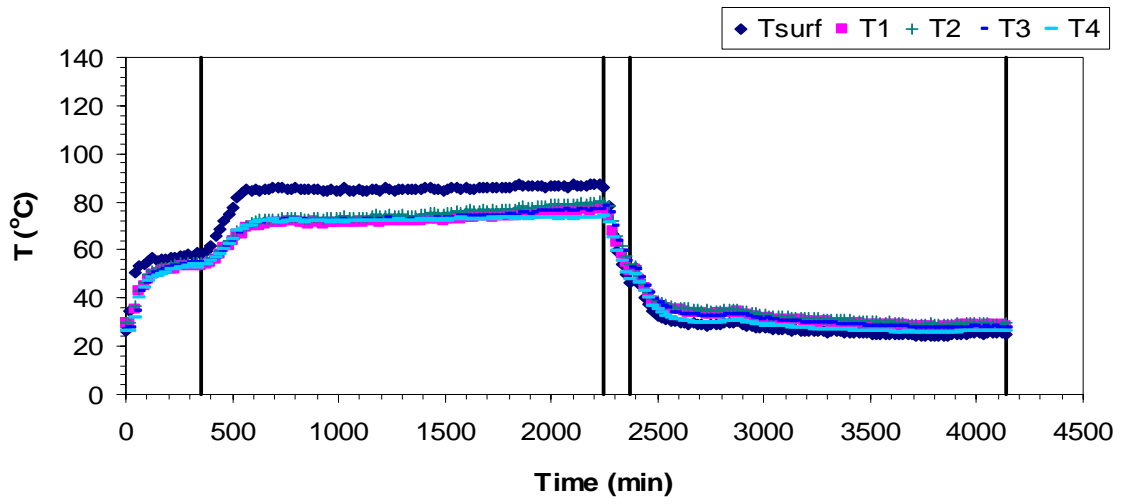


Figure C4. The variation of four temperatures in the adsorbent bed

APPENDIX D

PHYSICAL PROPERTIES OF MATERIALS

Table D1. The materials properties used in adsorption heat pump

Metal mass of adsorbent bed for AHP-1 (kg)	55
Metal mass of adsorbent bed for AHP-2 (kg)	84
Mass of Aluminum additives (kg)	3.6
Isothermic heat of adsorption (ΔH_a) (kJ kg ⁻¹ water)	2560
Specific heat of silica gel (kJ kg ⁻¹ K ⁻¹)	0.88
Specific heat of water (kJ kg ⁻¹ K ⁻¹)	4.217
Specific heat of stainless steel (AISI 316) (kJ kg ⁻¹ K ⁻¹)	0.468
Specific heat of Aluminum (kJ kg ⁻¹ K ⁻¹)	0.903
Latent heat of water in evaporator (kJ kg ⁻¹)	2500
Latent heat of water in condenser (kJ kg ⁻¹)	2376

Table D2. Thermal properties of metal pieces
(Source: Incropera and DeWitt 1996)

Material	Thermal Conductivity (W m ⁻¹ K ⁻¹)	Density (kg m ⁻³)	Specific Heat Capacity (J kg ⁻¹ K ⁻¹)	Thermal Diffusivity (m ² s ⁻¹)
Copper	401	8933	385	1.17×10^{-4}
Stainless Steel (AISI-304)	14.9	7900	477	3.95×10^{-6}
Aluminum	237	2702	903	9.71×10^{-5}
Brass (40%Zinc 60% Copper)	150	8500	380	4.6×10^{-5}

Table D3. Thermophysical properties of adsorbent granule and adsorbate considered in the present study (Source: Cussler 1997, Ben Amar, et al. 1996, Incropera and DeWitt 1996)

Parameter	Symbol	Value
Molecular weight of water, kg mol^{-1}	M	18
Density of adsorbent, kg m^{-3}	ρ_s	670
Specific heats of adsorbent, $\text{kJkg}^{-1} \text{K}^{-1}$	C_{p_s}	0.88
Specific heats of adsorptive at 303K, $\text{kJkg}^{-1} \text{K}^{-1}$	C_{p_w}	4.178
Specific heats of adsorptive at 330K, $\text{kJkg}^{-1} \text{K}^{-1}$	C_{p_w}	4.184
Specific heats of adsorptive at 373K, $\text{kJkg}^{-1} \text{K}^{-1}$	C_{p_w}	4.217
Specific heats of adsorptive at 360K, $\text{kJkg}^{-1} \text{K}^{-1}$	C_{p_w}	4.203
Specific heats of adsorptive at 303K, $\text{kJkg}^{-1} \text{K}^{-1}$	C_{p_v}	1.895
Specific heats of adsorptive at 330K, $\text{kJkg}^{-1} \text{K}^{-1}$	C_{p_v}	1.911
Specific heats of adsorptive at 373K, $\text{kJkg}^{-1} \text{K}^{-1}$	C_{p_v}	2.029
Specific heats of adsorptive at 360K, $\text{kJkg}^{-1} \text{K}^{-1}$	C_{p_v}	1.983
Thermal conductivity of adsorbent, $\text{kW m}^{-1} \text{K}^{-1}$	λ_s	0.198×10^{-3}
Thermal conductivity of adsorptive, $\text{kW m}^{-1} \text{K}^{-1}$	λ_w	1.96×10^{-5}
Heat of adsorption for water on silica gel, kJkg^{-1}	ΔH_s	2560
Limiting adsorption capacity of adsorbent $\text{kg}_w \text{kg}_s^{-1}$	W_0	0.552
Linear driving force relationship constant	n	1.6
Reference diffusivity, $\text{m}^2 \text{s}^{-1}$	D_0	2.54×10^{-4}
Diffusion activation energy, J mol^{-1}	E	4.2×10^4
Collision diameter for Lennard-Jones potential, A	σ	2.641
Collision integral at 307K	Ω	2.381
Collision integral at 359K	Ω	2.211
Collision integral at 398K	Ω	2.090
Collision integral at 338K	Ω	2.264
Boltzmann's constant ($\text{J K}^{-1} \text{molecule}^{-1}$)	k	1.38×10^{-23}
Tortuosity	τ	3
Viscosity of water vapor, kNsm^{-2} at 303K	μ	9.09×10^{-9}
Viscosity of water vapor, kNsm^{-2} at 330K	μ	10.29×10^{-9}
Viscosity of water vapor, kNsm^{-2} at 373K	μ	12.02×10^{-9}
Viscosity of water vapor, kNsm^{-2} at 360K	μ	11.49×10^{-9}
Viscosity of water vapor, kNsm^{-2} at 307K	μ	9.37×10^{-9}
Viscosity of water vapor, kNsm^{-2} at 398K	μ	12.98×10^{-9}
Viscosity of water vapor, kNsm^{-2} at 338K	μ	10.61×10^{-9}

APPENDIX E

RAW DATA OF MICROCALORIMETRY STUDY

Table E1. Raw data from microcalorimetry

ID	P_{dose} (mbar)	P_{∞} (mbar)	Gas adsorbed (mmol)	Molar coverage (mmol g_s^{-1})	Weight coverage ($g_w g_s^{-1}$)	Differential heat of adsorption ($J g_s^{-1}$)	Molar Differential heat of adsorption ($kJ mol^{-1}$)	Onset time (s)	Offset time (s)	Ads. Time (s)	Cumulative Adsorbed Time (s)	cumulative coverage ($kg_w kg_s^{-1}$)	$\ln(1-W_t/W_{\infty})$	W_t/W_{∞}
1	20	0.6	0.049776	0.125443	0.002258	7.1048	70.8	71161	71950	789.0	789	0.00225	-0.1	0.11
2	30	1.96	0.070639	0.178023	0.003204	18.1279	127.3	74470	75082	612.0	1401	0.00546	-0.3	0.27
3	30	3.89	0.064020	0.161341	0.002904	15.0408	116.5	77863	78484	621.0	2022	0.00836	-0.5	0.42
4	30	6.93	0.053032	0.133650	0.002406	12.1600	113.7	82863	83893	1030.0	3052	0.01077	-0.8	0.54
5	30	9.65	0.046678	0.117636	0.002117	9.9590	105.8	85833	86879	1046.0	4098	0.01289	-1.0	0.65
6	30	12.02	0.041330	0.104158	0.001875	9.1057	109.3	89219	90103	884.0	4982	0.01476	-1.4	0.74
7	30	15.72	0.028012	0.070595	0.001271	6.6006	116.9	92367	93215	848.0	5830	0.01603	-1.6	0.81
8	30	18.9	0.021155	0.053313	0.000960	5.3358	125.1	97000	98216	1216.0	7046	0.01699	-1.9	0.86
9	30	21.41	0.016098	0.040569	0.000730	4.0793	125.7	161316	162093	777.0	7823	0.01772	-2.2	0.89
10	30	23.28	0.013238	0.033363	0.000601	3.1825	119.2	164723	165563	840.0	8663	0.01832	-2.6	0.92
11	30	24.59	0.010855	0.027357	0.000492	2.1731	99.3	170564	171438	874.0	9537	0.01881	-2.9	0.95
12	30	26.07	0.006487	0.016348	0.000294	1.1140	85.2	174260	175087	827.0	10364	0.01911	-3.3	0.96
13	30	26.98	0.006116	0.015413	0.000277	0.8830	71.6	177411	178250	839.0	11203	0.01939	-3.7	0.98
14	30	27.76	0.004925	0.012411	0.000223	0.5968	60.1	179820	180644	824.0	12027	0.01961	-4.4	0.99
15	30	28.36	0.002754	0.006939	0.000125	0.4068	73.3	180755	181601	846.0	12873	0.01973	-5.0	0.99
16	30	28.76	0.002224	0.005605	0.000101	0.3007	67.1	181349	182170	821.0	13694	0.01983	-6.6	1.00
17	30	29.33	0.000265	0.000667	0.000012	0.0320	59.9	182300	183167	867.0	14561	0.01985	-7.1	1.00
18	30	29.6	0.000344	0.000867	0.000016	0.0426	61.4	183847	184702	855.0	15416	0.01986		1.00

Table E1 illustrates the raw data which obtained from microcalorimetry study. P_{dose} indicates the initial send water vapor dose. Equilibrium pressure (P_{∞}) was achieved after water vapor adsorption. Adsorbed water vapor on silica gel granules can be calculated by using ideal gas relation as shown in Equation E1.

$$\text{Adsorbed amount} = \frac{[P_{dose} V_{sys} - P_{\infty} (V_{sys} + V_{cell})]}{RT} \quad (E1)$$

Molar coverage was calculated by dividing molar adsorbed amount to weight of dried silica gel as shown in Equation E2.

$$\text{Molar Coverage} (mmol / g_s) = \frac{\text{Adsorbed amount} (mmol)}{\text{weight of dried silica - gel} (g_s)} \quad (E2)$$

Weight coverage (Equation (E2)) can be estimated by multiplying molar coverage with molar mass of water.

$$\text{Weight Cov.} (g_w / g_s) = \text{Molar Cov.} (mmol / g) \cdot \text{Molar mass of water} (g_w / mol) \quad (E3)$$

Differential heat of adsorption ($J g_s^{-1}$) was evaluated by SETSOFT software which is explained in Chapter 4. Molar differential heat of adsorption ($kJ mol^{-1}$) can be determined by multiplying differential heat of adsorption with molar coverage. Adsorbed time can be estimated by subtracting offset time from onset time which is obtained from SETSOFT software. Cumulative adsorbed time and weight coverage were calculated by addition of individual obtained data.

Water vapor adsorption on silica gel isotherms can be plotted cumulative weight coverage versus equilibrium pressure. Kinetics of water vapor adsorption was drawn by using cumulative weight coverage and cumulative adsorbed time data. Linearity of uptake curve for calculation of diffusivity in short range period can be checked by plotting $W_t W_{\infty}^{-1}$ versus square root of adsorbed time as shown in Figure E1. Linearity of water adsorption kinetics for calculation of diffusivity in long range period can be checked by plotting $\ln(1 - W_t / W_{\infty})$ versus adsorbed time as shown in Figure E2.

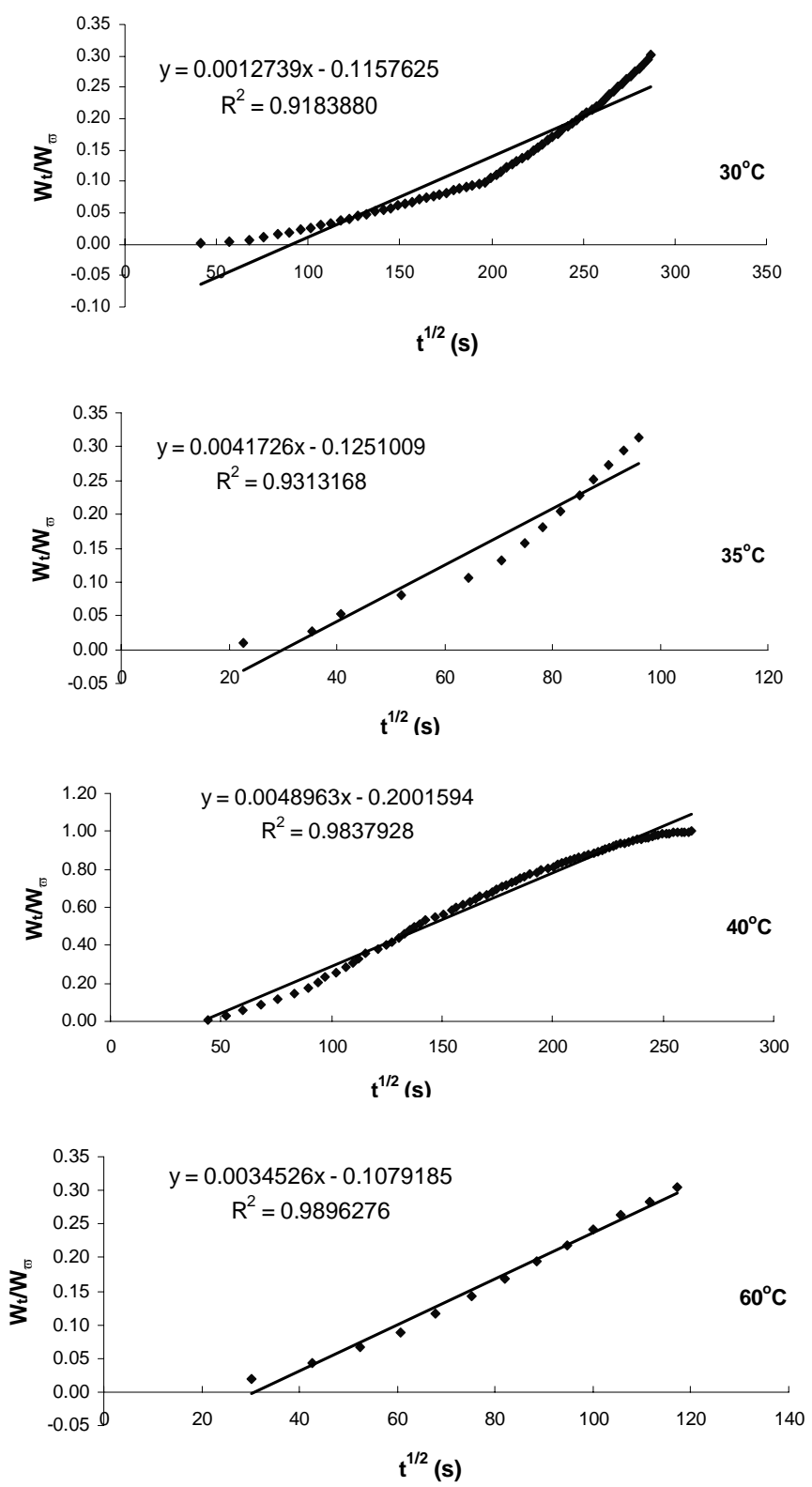


Figure E1. Linearity of uptake curve for calculation of diffusivity in short range period with different temperatures

(cont. on next page)

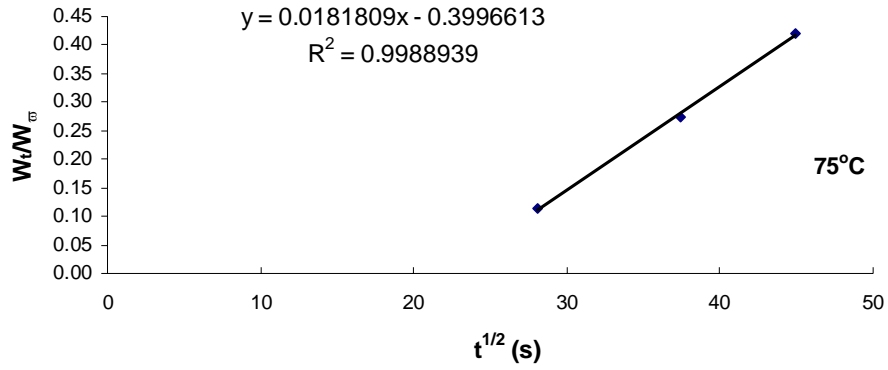


Figure E1. (cont.) Linearity of uptake curve for calculation of diffusivity in short range period with different temperatures

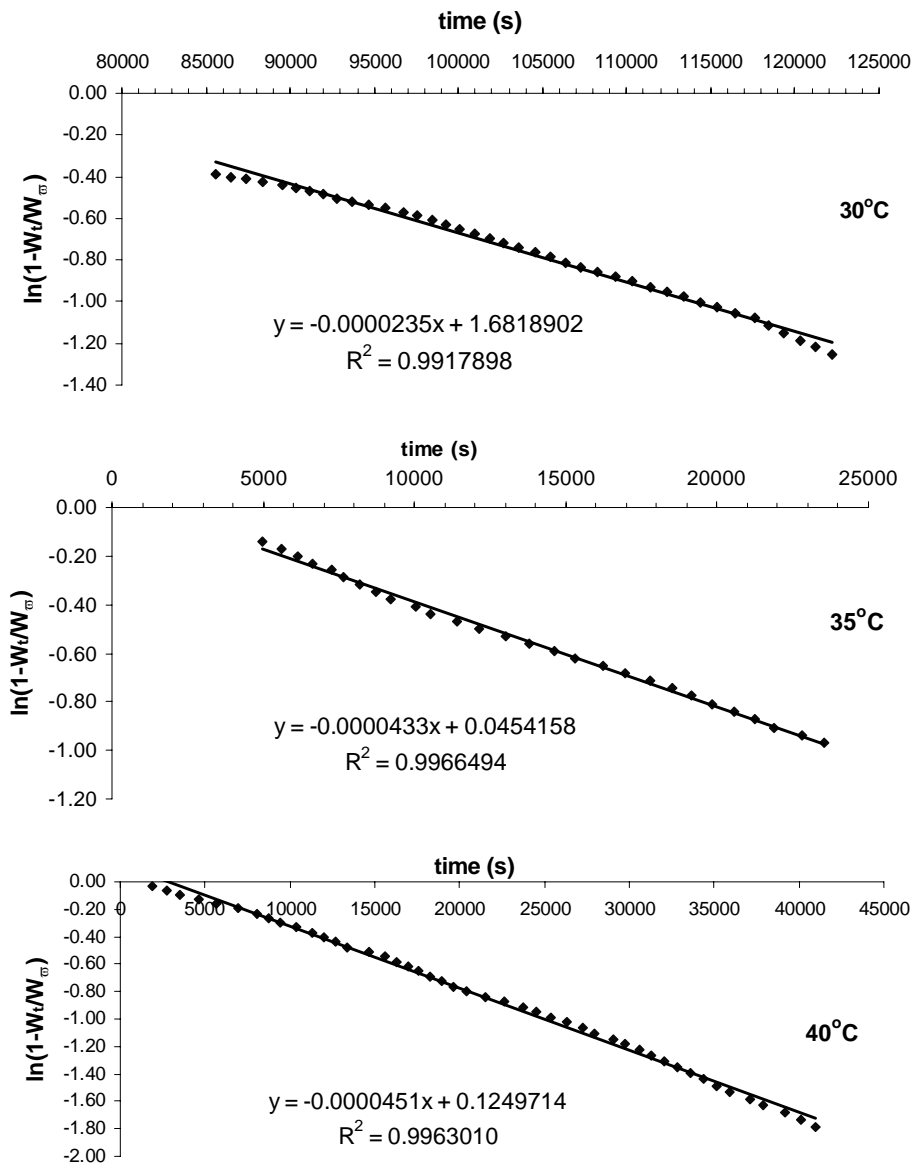


Figure E2. Linearity of uptake curve for calculation of diffusivity in long range period with different temperatures

(cont. on next page)

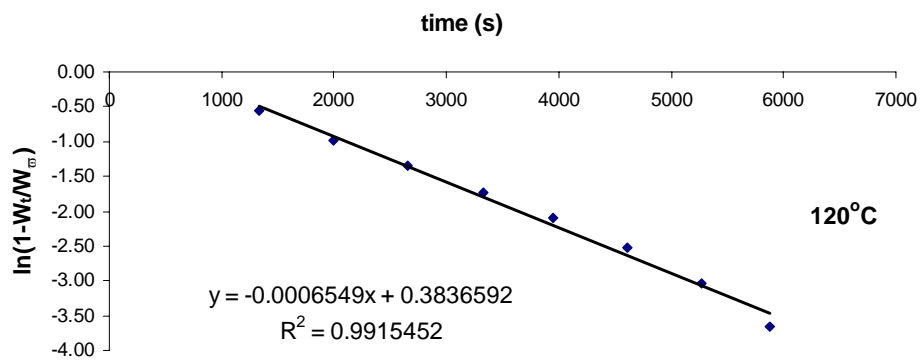
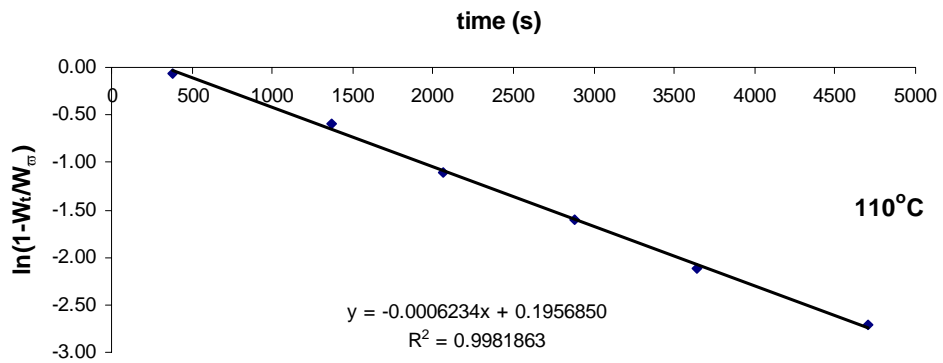
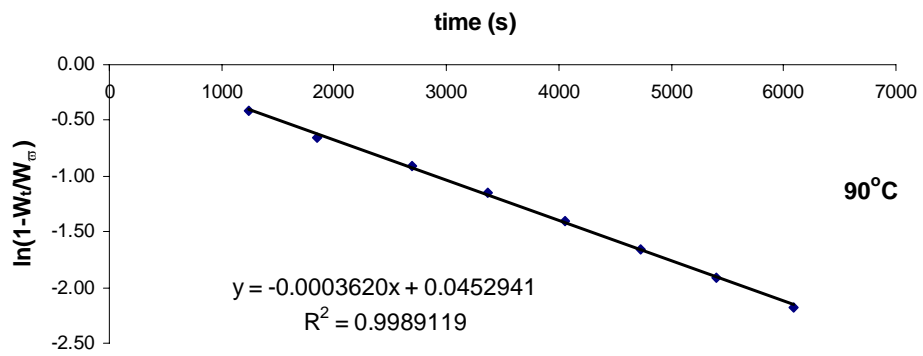
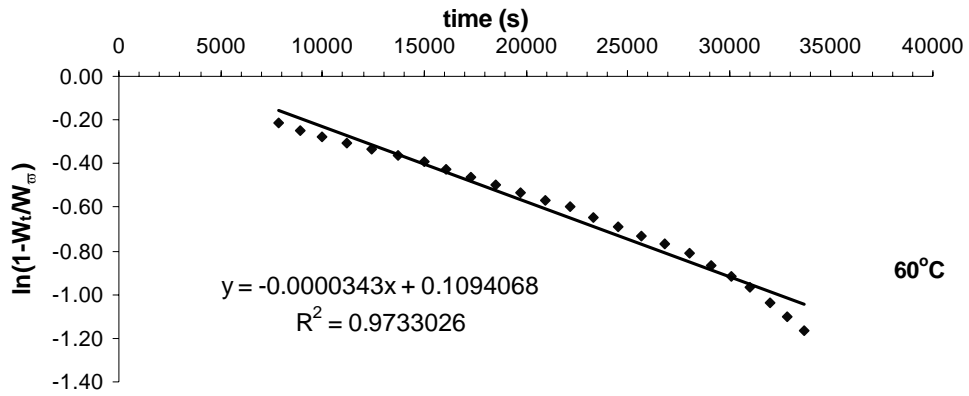


Figure E2. (cont.) Linearity of uptake curve for calculation of diffusivity in long range period with different temperatures

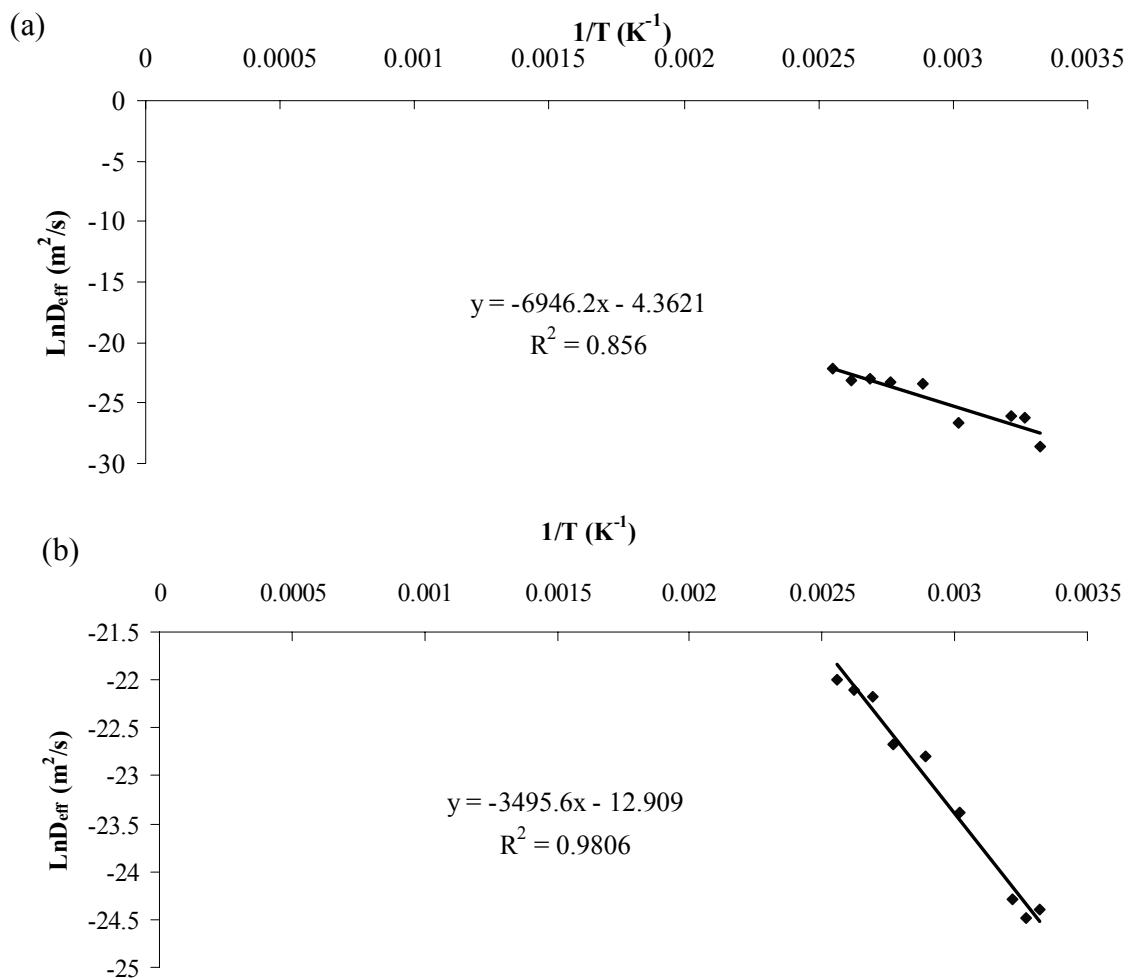


Figure E3. Fitting of experimental data to Arrhenius form (a) short range period and (b) long range period

APPENDIX F

LITERATURE SURVEY FOR NUMERICAL STUDY

Table F1. Governing equations for defining system in the literature

Ref.	Governing Equations	System	Assumption	Solution Method
Sun and Besant, 2005	<p>Vapor diffusion of internal particle</p> $\frac{\partial \rho_v}{\partial t} = \frac{D_i}{r^2} \cdot \frac{\partial}{\partial r} \left(r^2 \cdot \frac{\partial \rho_v}{\partial r} \right)$ <p>Momentum equation</p> $U_D = -\frac{K}{\mu} \cdot \frac{\partial P}{\partial x}$ <p>Energy equation</p> $\frac{\partial(\epsilon_\gamma \rho_\gamma c_{pm} T_\gamma)}{\partial t} + \frac{\partial(\rho_\gamma U_D c_{pm} T_\gamma)}{\partial x}$ $= \frac{\partial}{\partial x} \left(k_{\gamma,eff} \frac{\partial T_\gamma}{\partial x} \right) + h_{\sigma\gamma} S_\gamma (T_\sigma - T_\gamma)$ <p>Vapor mass diffusion equation inside bed</p> $\frac{\partial(\epsilon_\gamma \rho_a W_\gamma)}{\partial t} + \frac{\partial(\rho_a U_D W_\gamma)}{\partial x} = \frac{\partial}{\partial x} \left(\rho_a D_{v,eff} \frac{\partial W_\gamma}{\partial x} \right) - \dot{r}_v$	Silica gel-water pairs, forced convection humid air pass through the inside cylindrical packed bed	<ul style="list-style-type: none"> The transport processes within the silica gel bed are transient convection and diffusion of heat and water vapor Inside the particle, the gas phase is ideal gas, the dry air and water phase are in thermodynamic equilibrium state that is not necessarily equal to the gaseous phase equilibrium state at the same point in the bed There is no water mobility, solid dissolution and chemical reactions taking place in the silica gel bed Water vapor diffusion inside the silica gel particle is much slower than the rate of water vapor diffusion through air Porous medium properties of the particle bed are homogeneous and isotropic except for latent heat of adsorption term there is no particle movement in the bed initial condition of the silica gel particles is considered to be totally dry the local total gaseous pressure inside the pore space is assumed to the standard atmosphere pressure at any time 	Finite volume method is used

(cont. on next page)

Table F1. (cont.) Governing equations for defining system in the literature

Ref.	Governing Equations	System	Assumption	Solution Method
Miltkau and Dawoud 2002	<p>Energy equation</p> $\frac{\partial}{\partial t} (\rho_{zeo}(x) \cdot u(x, T)) = \frac{\partial}{\partial z} \left(\lambda \cdot \frac{\partial T}{\partial z} \right) - \frac{\partial}{\partial z} (m''_v \cdot h_v)$ <p>Mass equation</p> $\frac{\partial \rho}{\partial t} = - \frac{\partial m''_v}{\partial z}$ <p>Diffusivity</p> $D_{Kn} = \frac{4}{3} \cdot d_{MaP} \cdot \sqrt{\frac{M_g}{2 \cdot \pi \cdot R_m \cdot T}}$ $D_{geo} = \frac{\psi_{MaP} \cdot d_{MaP}}{\mu_{MaP}}$	Zeolite-water pairs Zeolite coated heat transfer tube reactor	<ul style="list-style-type: none"> All infinitesimally small zeolite sub-layers are considered to be phases in thermodynamic equilibrium The heat content of the vapor phase within the zeolite structure can be neglected as the density ratio between vapor and liquid phase is very small. The zeolite layer and the adsorbed water are considered to be incompressible 	Centered difference is applied by using gPROMS software finite
Okunev et al., 2007	<p>Energy balance</p> $\rho_s C_p(T, N, x) \frac{\partial T}{\partial t} - \rho_s \Delta H \frac{x}{\mu_{salt}} \frac{\partial N}{\partial t} = \lambda_p \Delta T$ <p>Mass balance</p> $\frac{\partial C_w}{\partial t} = D_c \Delta C_w - \frac{\rho_s x}{\mu_{salt} \varepsilon} \frac{\partial N}{\partial t} \quad D_{Kn} = \frac{4}{3} \cdot d_{MaP} \cdot \sqrt{\frac{M_g}{2 \cdot \pi \cdot R_m \cdot T}}$ <p>Diffusivity</p>	SWS-IL - water		Implicit difference method finite
Dawoud et al. 2007	<p>Energy equation</p> $\frac{\partial}{\partial t} (\rho_{zeo}(x) \cdot u(x, T)) = \frac{\partial}{\partial z} \left(\lambda \cdot \frac{\partial T}{\partial z} \right) - \frac{\partial}{\partial z} (m''_v \cdot h_v)$ <p>Mass equation</p> $\frac{\partial \rho}{\partial t} = - \frac{\partial m''_v}{\partial z}$ <p>Diffusivity</p> $D_0 = D_\infty \cdot \exp(-E_a / (R_m \cdot T))$	Zeolite-water pairs Zeolite coated heat transfer tube reactor	<ul style="list-style-type: none"> Heat and mass transfer problem is considered to be one dimensional The heat content of the vapor phase within the zeolite structure can be neglected as the density ratio between vapor and liquid phase is very small. The zeolite layer and the adsorbed water are considered to be incompressible 	Centered difference is applied by using gPROMS software finite

(cont. on next page)

Table F1. (cont.) Governing equations for defining system in the literature

Ref.	Governing Equations	System	Assumption	Solution Method
Chahbani et al. 2002 and 2004	<p>Energy balance</p> $(\rho_s C_{ps} + \bar{q} C_{pa}) \frac{\partial T_s}{\partial t} - \Delta H \frac{\partial \bar{q}}{\partial t} = \lambda_s \frac{\partial}{r} \frac{\partial}{\partial r} \left(r \frac{\partial T_s}{\partial r} \right)$ <p>Mass balance for particle</p> $\frac{\partial q}{\partial t} = \frac{1}{x^2} \frac{\partial}{\partial x} \left(x^2 D_s \frac{\partial q}{\partial x} \right)$ <p>LDF for particle</p> $\frac{\partial \bar{q}}{\partial t} = \frac{15 D_s}{r_p^2} (q^* - \bar{q})$	Carbon pair Two bed regenerated adsorption heat pump – ammonia heat	<ul style="list-style-type: none"> The pressure is uniform in the bed. The solid and gaseous phases are in thermal equilibrium. The gas behavior is ideal. The thermal resistance of the tube is negligible. The bed is composed of particles of uniform-size and the bed porosity is constant 	Finite method difference
Leong and Liu, 2004, 2005 and 2006	<p>Energy balance</p> $(\rho_s C_{ps} + \rho_s q C_{pa} + \varepsilon \rho_g C_{pg}) \frac{\partial T_s}{\partial t} + \frac{\partial (\rho_g C_{pg} u T_s)}{\partial z} + \frac{1}{r} \frac{\partial}{\partial r} (r \rho_g C_{pg} v T_s)$ $= \frac{\partial}{\partial z} \left(\lambda_{eq} \frac{\partial T_s}{\partial z} \right) + \frac{1}{r} \frac{\partial}{\partial r} \left(r \lambda_{eq} \frac{\partial T_s}{\partial r} \right) + \rho_s \Delta H \frac{\partial \bar{q}}{\partial t}$ <p>Mass balance</p> $\frac{\partial \left(\frac{\varepsilon M}{RT} P \right)}{\partial t} = \frac{\partial}{\partial z} \left(\frac{\rho_g K_{ap}}{\mu} \frac{\partial P}{\partial z} \right) + \frac{1}{r} \frac{\partial}{\partial r} \left(\frac{r \rho_g K_{ap}}{\mu} \frac{\partial P}{\partial r} \right) - \rho_s \frac{\partial \bar{q}}{\partial t}$ <p>Diffusivity</p> $D_{ek} = 1 / (1/D_m + 1/D_k) \quad D_m = 0.02628 \sqrt{T^3/M} / P \sigma^2 \Omega$ $D_k = \frac{200 r_p}{3} \left(\frac{8RT}{\pi M} \right)^{1/2} = 97 r_p \left(\frac{T}{M} \right)^{1/2}$	Zeolite 13X – water pair	<ul style="list-style-type: none"> The adsorbed phase is considered to be liquid, and the adsorbate gas is assumed to be an ideal gas. The adsorbent bed is composed of uniformly-sized particles and has isotropic properties. Except for the density of adsorbate vapor, the properties of the fluid, the metal tube and adsorbate vapor are constant. There are no heat losses in the adsorption cycle. The thermal resistance between the metal tube and the adsorbent bed is neglected 	Finite method volume

(cont. on next page)

Table F1. (cont.) Governing equations for defining system in the literature

Ref.	Governing Equations	System	Assumption	Solution Method
San 2006	<p>Mass balance</p> $\frac{\partial W}{\partial t} = \frac{1}{r^2} \frac{\partial}{\partial r} \left[r^2 D^* \frac{\partial W}{\partial r} \right]$ <p>Energy balance</p> $\frac{dT_i}{dt} = \left(\frac{1}{\tau_i} \right) (1 + R_{th}^*) (T_{eq} - T_i)$ <p>Diffusivity</p> $D = (D_0 / \tau_i) \exp(-0.45 \Delta H / \lambda K T_b)$	Activated carbon – methanol pair	<ul style="list-style-type: none"> • Methanol vapor is assumed as ideal gas. • In the adsorption/regeneration mode, the vapor pressure equals the saturation pressure at the evaporating/condensing temperature. • The cooling and heating fluid temperatures individually equal the condensing and evaporating temperatures. • The adsorbent temperature is uniform. • The vapor temperature is the same as the adsorbent temperature. • The mass of vaporized methanol is much smaller than that of activated carbon. Thus the vaporized methanol was neglected in the energy balance. • There is a constant overall heat transfer coefficient (U) between the activated carbon and insert and it is defined based on the surface area of the adsorbent 	Forward finite difference scheme
Chua et al., 2004	<p>Mass balance</p> $\int_V \left[\epsilon_t \frac{\partial \rho_v}{\partial t} + (1 - \epsilon_t) \rho_s \frac{\partial q}{\partial t} \right] dV = \dot{m}_{e/c,v}$ <p>Energy balance</p> $(1 - \epsilon_t) \left[\rho_s c_{ps} \frac{\partial T_s}{\partial t} + \rho_s q c_{p,g} \frac{\partial q}{\partial t} + \rho_s q c_{p,g} \frac{\partial T_s}{\partial t} \right] + \epsilon_t \frac{\partial (\rho_v u_v)}{\partial t} = \frac{\partial (k_s \frac{\partial T}{\partial r})}{r \partial r} + \frac{h_{fm,s}}{FS} (T_{fm,1} - T_s) - \frac{h_{fm,s}}{FS} (T_s - T_{fm,r})$ <p>Intraparticle mass balance</p> $\frac{\partial q}{\partial t} = 15 D_{so} \exp(-E_a / RT_s) / R_p^2 \cdot (q^* - q)$	Two bed silica gel – water adsorption chiller	<ul style="list-style-type: none"> • The adsorption bed is composed of uniform size particles and the bed porosity is a constant • The specific heat and the density of dry adsorbent are constant • The physical properties of metal tube and fin are constant 	Central difference scheme

(cont. on next page)

APPENDIX G

GOVERNING EQUATIONS

G.1 Conservation of Energy

Heat and mass transfer in the porous adsorbent bed are complex phenomenon and coupled thus, they should be solved simultaneously. Numerical simulation may provide important information for designing of adsorbent bed to estimate the capacity of adsorption for the given period. The following expression explains how the heat and mass transfer equation in the annular adsorbent bed was derived with respect to their assumptions. The conservation of energy in the adsorbent bed was obtained by following procedure. The control volume of adsorbent bed is shown in Figure G.1.

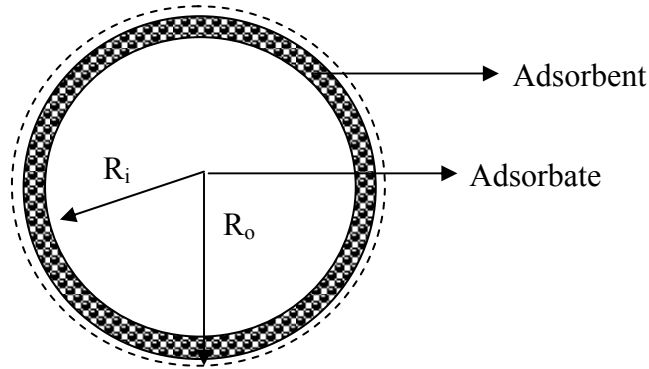


Figure G.1. Control volume of adsorbent bed

The overall energy conservation in control volume can be defined as following equation.

$$E_{in} - E_{out} + E_{generation} = E_{accumulation} \quad (G.1)$$

The inlet energy is described as follows:

$$q_{in}: q_{cond} + q_{conv}$$

The outlet energy in the control volume is

$$q_{out} = q_{in} + \frac{\partial q_{in}}{\partial R} dR \quad (G.2)$$

The accumulation term can be written as follows:

$$\left(\rho_s C p_s + \rho_w C p_w + \rho_s C p_w \bar{W} \right) \frac{\partial T}{\partial t} \quad (G3)$$

During water vapor adsorption/desorption on/from silica gel, the heat is generated or disappeared. The generated/disappeared energy can be written as

$$\rho_s \Delta H \frac{\partial \bar{W}}{\partial t} \quad (G4)$$

The inlet, outlet, accumulation and generation/consumption terms were put into the general energy equation (Equation G.1).

$$\begin{aligned} q_{in} - \left(q_{in} + \frac{\partial q_{in}}{\partial R} dR \right) + A \rho_s \Delta H \frac{\partial \bar{W}}{\partial t} &= A \left(\rho_s C p_s + \varepsilon \rho_w C p_w + \rho_s C p_w \bar{W} \right) \frac{\partial T}{\partial t} \\ - \frac{\partial}{\partial R} (q_{cond}) dR - \frac{\partial}{\partial R} (q_{conv}) dR + dV \rho_s \Delta H \frac{\partial \bar{W}}{\partial t} &= dV \left(\rho_s C p_s + \varepsilon \rho_w C p_w + \rho_s C p_w \bar{W} \right) \frac{\partial T}{\partial t} \end{aligned} \quad (G.5)$$

Conduction and convection terms can be defined as:

$$q_{cond} = -\lambda A \frac{\partial T}{\partial R} = -\lambda (2\pi R dz) \frac{\partial T}{\partial R} \quad (G6)$$

$$q_{conv} = \rho_w C p_w (2\pi R dz) u T \quad (G7)$$

Substitute the convection and conduction terms in Equation G.5.

$$\begin{aligned} \lambda 2\pi dz \frac{\partial}{\partial R} \left(R \frac{\partial T}{\partial R} \right) dR - 2\pi dz \frac{\partial}{\partial R} (\rho_w C p_w R u T) dR + (2\pi R dz) \rho_s \Delta H \frac{\partial \bar{W}}{\partial t} &= \\ (2\pi R dz) \left(\rho_s C p_s + \varepsilon \rho_w C p_w + \rho_s C p_w \bar{W} \right) \frac{\partial T}{\partial t} \end{aligned} \quad (G8)$$

Finally, conservation of energy equation becomes

$$\frac{\lambda}{R} \frac{\partial}{\partial R} \left(R \frac{\partial T}{\partial R} \right) - \frac{1}{R} \frac{\partial}{\partial R} (\rho_w C p_w R u T) + \rho_s \Delta H \frac{\partial \bar{W}}{\partial t} = \left(\rho_s C p_s + \varepsilon \rho_w C p_w + \rho_s C p_w \bar{W} \right) \frac{\partial T}{\partial t} \quad (G.9)$$

The units of conservation of energy equation can be checked as follows

$$\frac{W}{mK} \frac{1}{m} \frac{1}{m} \left(\frac{m}{m} \frac{K}{m} \right) - \frac{1}{m} \frac{1}{m} \left(\frac{kg}{m^3} \frac{J}{kgK} \frac{m}{s} K \right) + \frac{kg_s}{m^3} \frac{J}{kg_w} \frac{kg_w}{s} = \left(\frac{kg_s}{m^3} \frac{J}{kg_s K} + \frac{kg_w}{m^3} \frac{J}{kg_w K} + \frac{kg_s}{m^3} \frac{J}{kg_w K} \frac{kg_w}{kg_s} \right) \frac{K}{s}$$

G.2 Conservation of Mass

The equation for the conservation of mass in the adsorbent bed was derived by following procedure. The control volume of adsorbent bed is shown in Figure G.1. The general conservation of mass equation is written as

$$\dot{m}_{in} - \dot{m}_{out} - \dot{m}_{consumption} = \dot{m}_{accumulation} \quad (G.10)$$

The terms in general mass balance equation can be defined as follows:

$$\text{Inlet: } \dot{m}_{in} \quad (G.11)$$

$$\text{Outlet: } \dot{m}_{in} + \frac{\partial \dot{m}_{in}}{\partial R} dR \quad (G.12)$$

$$\text{Consumption: } \rho_s \frac{\partial W}{\partial t} \quad (G.13)$$

$$\text{Accumulation: } \frac{\partial \dot{m}}{\partial t} \quad (G.14)$$

The inlet, outlet, consumption and accumulation terms put into the Equation G.10.

$$\dot{m}_{in} - \left(\dot{m}_{in} + \frac{\partial \dot{m}_{in}}{\partial R} dR \right) - \rho_s \frac{\partial W}{\partial t} = \frac{\partial \dot{m}}{\partial t} \quad (G.15)$$

Where, \dot{m}_{in} equals to $\rho_w u$. The area and volume of control volume of adsorbent bed equal to $2\pi R dR$ and $2\pi R dR dz$ respectively. After substitution and rearrangement of Equation G.15, the final conservation of mass equation was obtained in following equation.

$$\frac{\partial \rho_w}{\partial t} + \frac{1}{\varepsilon} \frac{1}{R} \frac{\partial}{\partial R} (R \rho_w u) + \frac{1}{\varepsilon} \rho_s \frac{\partial \bar{W}}{\partial t} = 0 \quad (G.16)$$

The units of terms of conservation mass equation is showed as follows

$$\frac{kg_w}{m^3} \frac{1}{s} + \frac{1}{m} \frac{1}{m} \left(m \frac{kg_w}{m^3} \frac{m}{s} \right) + \frac{kg_s}{m^3} \frac{kg_w}{kg_s} \frac{1}{s} = 0$$

G.3 Numerical Solution of Governing Equations

Numerical solution generally is applied when analytical solution is not available for differential equations which have been used to model many physical problems consisting fluid/solid mechanics, chemical processes, biological event, material sciences, economics etc. An approximate solution of those problems can be found numerically. One of the numerical methods is finite difference method for finding approximate solution. The finite difference method discretizes the problem on a grid to find the approximate solution to the differential equation as shown in Figure G.2. Then, the governing equations are linearized for each grid and set-of algebraic equation is obtained. Then the equations are solved by different methods such as inverse matrix method and iterative method. For the coupled and non-linear problem, an outer iteration should be performed to obtain values of non-linear terms.

G.3.1 Discretization in Space

As it was mentioned before, the computational domain is divided to grids and governing equations are solved for each grid. Generally, central difference is used to linearize governing equation for internal nodes. The linearization of the boundary conditions depends on type of boundaries. The value of dependent variable may be defined at the boundary or derivative of the variable at the boundary may be known. If the derivative of the dependent variable at the boundary is known, backward or forward difference is used to linearize boundary condition. The definitions of central, backward and forward differences are given as follows:

$$\text{Central difference: } \frac{\partial^2 u}{\partial x^2} = \frac{u_{j+1} - 2u_j + u_{j-1}}{\Delta x^2} \quad (\text{G.17})$$

$$\text{Central difference: } \frac{\partial u}{\partial x} = \frac{u_{j+1} - u_{j-1}}{2\Delta x} \quad (\text{G.18})$$

$$\text{Forward difference: } \frac{\partial u}{\partial x} = \frac{u_{j+1} - u_j}{\Delta x} \quad (\text{G.19})$$

$$\text{Backward difference: } \frac{\partial u}{\partial x} = \frac{u_j - u_{j-1}}{\Delta x} \quad (\text{G.20})$$

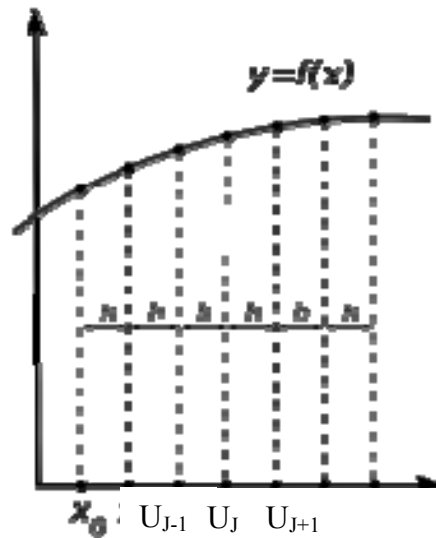


Figure G2. Discretization of differential equation

G.3.2 Discretization in Time

For the unsteady problems, governing equations should also be discretized. Generally, forward difference is used to linearize time dependent term in the governing equation. Three approaches can be used to describe partial differential equation for unsteady problem. They are explicit, implicit and Crank-Nicolson method. These methods are briefly described in below for the following differential equation.

$$\frac{\partial u}{\partial t} = \frac{\partial^2 u}{\partial x^2} \quad (\text{G.21})$$

There are three ways for solving differential equation at every grid points according to the finite difference method. These are explicit method, implicit method and Crank-Nicolson method.

The explicit method concerns a forward difference at time t_n and a second-order central difference for the space at position u_j . For example the one dimensional heat equation can be discretized according to explicit method as follows

$$\frac{u_j^{n+1} - u_j^n}{\Delta t} = \frac{u_{j+1}^n - 2u_j^n + u_{j-1}^n}{h^2} \quad (\text{G.22})$$

The forward point can be found according to backward points as follows

$$u_j^{n+1} = (1 - 2r)u_j^n + r u_{j-1}^n + r u_{j+1}^n \quad (\text{G.23})$$

The explicit method is known to be numerically stable and convergent whenever $r \leq 0.5$.

The implicit method takes in the account backward difference at time t_{n+1} and a second order central difference for the space derivative at u_j . The one dimensional heat equation can be discretized according to implicit method as follows

$$\frac{u_j^{n+1} - u_j^n}{\Delta t} = \frac{u_{j+1}^{n+1} - 2u_j^{n+1} + u_{j-1}^{n+1}}{h^2} \quad (\text{G.24})$$

The u_j^{n+1} can be obtained from solving a system of following linear equations

$$(1 + 2r)u_j^{n+1} - ru_{j-1}^{n+1} - ru_{j+1}^{n+1} = u_j^n \quad (\text{G.25})$$

The scheme is always numerically stable and convergent but usually more numerically intensive than the explicit method as it requires solving a system of numerical equations on each time step.

The Crank-Nicolson method includes the central difference at time $t_{n+1/2}$ and a second-order central difference for the space derivative at position u_j . The one dimensional differential equation can be solved as follows

$$\frac{u_j^{n+1} - u_j^n}{\Delta t} = \frac{1}{2} \left(\frac{u_{j+1}^{n+1} - 2u_j^{n+1} + u_{j-1}^{n+1}}{h^2} + \frac{u_{j+1}^n - 2u_j^n + u_{j-1}^n}{h^2} \right) \quad (\text{G.26})$$

The forward point can be found from following linear equation.

$$(2 + 2r)u_j^{n+1} - ru_{j-1}^{n+1} - ru_{j+1}^{n+1} = (2 - 2r)u_j^n + ru_{j-1}^n + ru_{j+1}^n \quad (\text{G.27})$$

The scheme is always numerically stable and convergent but usually more numerically intensive as it requires solving a system of numerical equations on each time step.

The Crank-Nicolson scheme is the most accurate scheme for small time steps. The explicit scheme is the least accurate and can be unstable, but is also the easiest to implement and the least numerically intensive. The implicit scheme can be employed the best for large time steps.

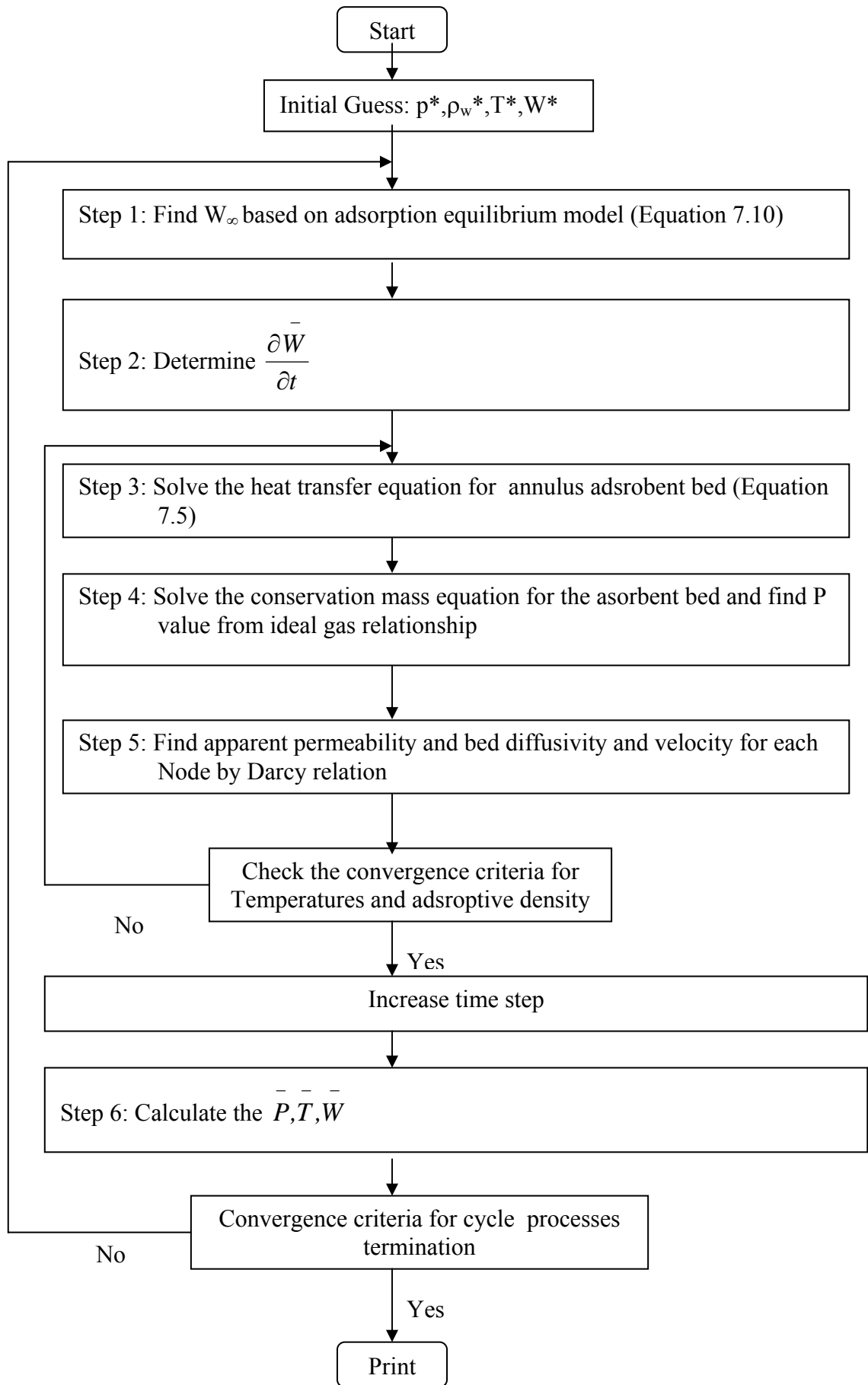


Figure G3. The algorithm of the numerical solution of governing equations for adsorbent bed

VITA

PERSONALITY

Date of Birth : 07-05-1975

Place of Birth : Izmir

EDUCATION

2008 **Philosophy of Doctorate (PhD)** Izmir Institute of Technology, Department of Chemical Engineering

2004 **Master of Science (MSci.)** Izmir Institute of Technology, Department of Chemical Engineering

1999 **Bachelor of Science (BS)** Ege University, Department of Chemical Engineering

PUBLICATIONS

- The use of metal piece additives to enhance heat transfer rate through an unconsolidated adsorbent bed, **Demir H.**, Mobedi M., Ülkü S., *Journal of international refrigeration*, Submitted
- Effects of porosity on heat and mass transfer in a granular adsorbent bed, **Demir H.**, Mobedi M., Ülkü S., *International Communications in Heat and Mass Transfer*, Accepted
- A review on adsorption heat pump: problems and solutions, **Demir H.**, Mobedi M., Ülkü S., *Renewable and Sustainable Energy Reviews*, 12, 2008, 2381-2403

PRESENTATIONS

- An experimental study on silica gel-water intermittent adsorption heat pump, H.Demir, M. Mobedi, S. Ülkü, *International Sorption Heat Pump Conference 2008, 23-26 September, 2008, Seoul, KOREA*
- A numerical study on heat and mass transfer through adsorbent bed of an adsorption heat pump H.Demir, M. Mobedi, S. Ülkü, *VI Minsk International Heat and Mass Transfer Forum, Minsk-Belarus, Minsk, 19 - 23 May, 2008*
- Modeling and Testing of an Intermittent Adsorption Heat Pump H.Demir, M. Mobedi, S. Ülkü, *International Energy, Exergy and Environment symposium, Evora-Portugal, 1-5 July, 2007*